Time Series Analysis of Phenometrics and Long-Term Vegetation Trends for the Flint Hills Ecoregion using Moderate Resolution Satellite Imagery

by

Austin Ray Braget

B.S., University of North Dakota, 2014

A THESIS

submitted in partial fulfillment of the requirements for the degree

MASTER OF ARTS

Department of Geography
College of Arts and Sciences

KANSAS STATE UNIVERSITY
Manhattan, Kansas

2017

Approved by:

Major Professor
Dr. J.M. Shawn Hutchinson

Copyright

Abstract

Grasslands of the Flint Hills are often burned as a land management practice. Remote sensing can be used to help better manage prairie landscapes by providing useful information about the long-term trends in grassland vegetation greenness and helping to quantify regional differences in vegetation development. Using MODIS 16-day NDVI composite imagery between the years 2001-10 for the entire Flint Hills ecoregion, BFAST was used to determine trend, seasonal, and noise components of the image time series. To explain the trend, 4 factors were considered including hydrologic soil group, burn frequency, and precipitation deviation from the 30 year normal. In addition, the time series data was processed using TIMESAT to extract eight different phenometrics: Growing season length, start of season, end of season, middle of season, maximum value, small integral, left derivative, and right derivative. Phenometrics were produced for each year of the study and an ANOVA was performed on the means of all eight phenometrics to assess if significant differences existed across the study area. A K-means cluster analysis was also performed by aggregating pixel-level phenometrics at the county level to identify administrative divisions exhibiting similar vegetation development. For the study period, the area of negatively and positively trending grassland were similar (41-43%). Logistic regression showed that the log odds of a pixel experiencing a negative trend were higher in sites with clay soils and higher burning frequencies and lower for pixels having higher than normal precipitation and loam soils. Significant differences existed for all phenometrics when considering the ecoregion as a whole. On a phenometric-by-phenometric basis, unexpected groupings of counties often showed statistically similar values. Similarly, when considering all phenometrics at the same time, counties clustered in surprising patterns. Results suggest that long-term trends in grassland conditions warrant further attention and may rival other sources of grassland change (e.g., conversion, transition to savannah) in importance. Analyses of phenometrics indicates that factors other than natural gradients in temperature and precipitation play a significant role in the annual cycle of grassland vegetation development. Unanticipated, and sometimes geographically disparate, groups of counties were shown to be similar in the context of specific phenology metrics and this may prove useful in future implementations of smoke management plans within the Flint Hills.

Table of Contents

List of Figures

List of Tables

Acknowledgements

I would like to thank my major advisor, Dr. Shawn Hutchinson for all of the support and guidance during my master's program. Your guidance and belief in me was always appreciated. I would also like to thank my committee members, Dr. Douglas Goodin, and Dr. Jida Wang, for their insightful comments and suggestions. In addition, I would like to thank my fellow graduate students for their support and helping to keep me sane during my master's program. Thank you to the Geography Department here at Kansas State University for giving me the chance to pursue a Master's Degree.

Finally, I would like to thank my parents for supporting me and reassuring me that I could do it despite being so far away from middle of nowhere Minnesota. To my brothers, Mike and Mitch, both of whom provided support and humor to keep me afloat on a sea of doubt. So it goes…

Chapter 1 - Introduction

Grasslands have become one of the most changed biomes in the world due to agricultural pressure and woody encroachment. Given that every year an area the size of Kansas is being converted, protecting existing intact grasslands has become a conservation priority (Plowprint Annual Report, 2016). Time-series analysis of remotely sensed imagery may be able to inform grassland management through evaluation of trends over time. Use of vegetation indices from remote sensing satellites yields valuable information on vegetation life cycles and phenology. Moderate Resolution Imaging Spectrometer (MODIS) normalized difference vegetation index (NDVI) images have been frequently used in such work due to its spectral, spatial, and temporal resolution, as well as being a cost-effective means to assess land surface phenology trends (Zhang et al., 2003).

NDVI is frequently used in remote sensing research to measure the annual cycle of vegetation growth and development and is a suitable proxy measure of the amount of aboveground vegetation biomass. It also often correlates well with other biophysical measures such as leaf area index and green vegetation cover (Tucker 1991; An 2009). Despite the development of newer vegetation indices, such as the enhanced vegetation index (EVI), NDVI remains a popular choice among remote sensing researchers.

Land surface phenology has become an important focus in ecological research and is used for both vegetation monitoring and examining vegetation responses to climate change. Phenology is the variation in seasonal patterns of natural phenomena on land surfaces affected by inter-annual and seasonal variation in soil characteristics and meteorological conditions (Cleland et al., 2007). Seasonal characteristics of plant development, such as emergence ("green-up") and senescence ("brown-down"), are driven by weather and climate. Changes in phenological events

may signal important year-to-year climatic variations or even global environmental change (Reed 1994). The phenology of land surfaces can be detected via remote sensing by examining spectral index values. Changes in seasonal timing such as the start and end of season, duration of growing season, and maximum vegetation productivity can have an impact on a wide range of processes that are dependent on natural cycles of vegetation (Ganguly et al, 2010).

Phenometrics can be extracted from time series datasets by combining techniques that first filter (or smooth) raw NDVI data and then extract relevant phenometric estimates using methods such as principal component analysis (Tan et al., 2010), Fourier analysis (Sakomoto et al., 2005), and pixel-above-threshold technique (Cleland et al., 2007). The TIMESAT software program provides several filtering options to smooth raw time series vegetation data and extract phenometric data (Eklundh and Jonsson 2010), and has been used in a variety of studies to examine vegetation phenology (Eklundh and Jonsson 2003), assess satellite and climate data-derived indices of fire risk (Verbesselt et al., 2006), and examine relationships between coniferous forest NDVI and models of conifer tree photosynthetic activity (Eklundh and Jonsson 2010).

Analyzing vegetation trends also requires time series datasets of remotely-sensed images and use of statistical methods (implemented in programs such as R). Past research that analyzed trends in continuous vegetation time series data include quantifying gradual interannual vegetation change due to rainfall variability and drought (Jacquin et al., 2010), assessing temporal decomposition techniques relevant to the study of vegetation seasonality (Jonsson and Eklundh, 2002), and evaluation of abrupt vegetation change at the intraannual time scale caused by disturbances such as deforestation, disease and insect outbreaks, fire, and other activities (Verbesselt et al., 2010a).

Temporal decomposition of data involves separating an original time series dataset into three different components to study each related to vegetation greenness at different time scales (Cleveland and Delvin, 1988). These include seasonal patterns, multi-annual linear or nonlinear trends (with or without breakpoints), and noise or the residual remaining after elimination of the seasonal and trend components.

The Breaks For Additive Seasonal Trend (BFAST) program developed by Jan Verbesselt allows for extraction of seasonal and trend components of time series data to examine the greenness of vegetation. The BFAST method was used because of its ability to account for seasonality and to detect gradual (interannual) and abrupt (intraannual) changes within the linear trend component for the entire time series duration (Verbesselt et al., 2010a). Other methods such as Seasonal-Trend decomposition procedure (STL) based on a Locally wEighted regression Smoother (LOESS) were excluded from consideration due to its ability to detect only gradual changes in the trend component (Cleveland et al., 1990).

This study investigates long-term trends and phenology of grasslands within the Flint Hills of Kansas and Oklahoma. Its purpose is to analyze grassland vegetation trends and key phenometrics in the Flint Hills ecoregion for the period 2001-2015 and to provide insight as to the cause of observed trends in vegetation greenness and a better understanding of the spatial variation in grassland vegetation development within the region. To achieve this, three studies were conducted. The first study uses the BFAST program to estimate the direction and significance of grassland vegetation trends and the number of breaks in that trend (i.e., disturbances) detected over the study period.

The second study uses the BFAST program to determine vegetation trends and number of disturbances over the 2001-2010 study period. In addition, the study uses a subset of burn

frequency data developed by Mohler and Goodin (2012), cumulative differences between annual and normal (1982-2010) precipitation (precipitation deviation), and hydrological soil group data in a logistic regression form of generalized linear model to determine likely factors causing the negative trend of the Flint Hills ecoregion. This study seeks to help land managers and other interested parties to determine if burning practices, as they currently stand, are beneficial to vegetation greenness as well as providing incentives to consider the impact of smoke on the air quality of nearby cities.

The third study uses the TIMESAT program to examine the phenology of the Flint Hills ecoregion. Using ANOVA and Tukey tests to determine the significance of phenometrics across the study area and a K-Means clustering method to spatially examine the Flint Hills study area as a homogenous region.

Chapter 2 - Literature Review

Grasslands

Grasslands and savannas make up more than 40% of the earth's surface and their rapid response to changes in land management and climate can have dramatic ecological and social consequences (Briggs et al., 2005). Grasslands are among the most biodiverse and productive of all the earth's terrestrial biomes but receive low levels of protection (Mark and McLennan, 2005). Since 2009, 53 million acres of grassland, roughly the area of Kansas, have been converted to cropland across the Great Plains alone (Plowprint Annual Report, 2016). Tallgrass prairie has been reduced to ~4% of its historical extent making it one of the most altered ecosystems in North America (Ratajczak et al., 2016). Temperate grasslands are important for both agronomic and ecological purposes and are a key resource for livestock production in North America and around the world (Briggs et al., 2005). Grasslands provide services such as water storage and clean air (Plowprint Annual Print, 2016) and grassland vegetation reduces soil erosion due to it dense root systems and by shielding the soil surface from direct interception of rainfall (Ratajczak et al, 2016). Grasslands also store and retain large amounts of soil carbon and are an important component of the global carbon cycle (Briggs et al., 2005). The estimated values of these, and other, ecosystems services provided by native grasslands has been estimated to be in excess of $5,000 per hectare per year (Dodds et al., 2008).

The conservation status of grasslands is being evaluated by groups including the Landscape Conservation Cooperatives which seeks to identify the greatest threats to grasslands and shrublands across the U.S. and Mexico, areas that are likely to be resilient to climate change and other threats, and areas with high potential for restoration (Glaser, 2014). The state of North American prairies is also being addressed through a tri-national cooperative program involving

Mexico, the USA, and Canada which is attempting to address both sustainable management and conservation needs (Mark and McLennan, 2005). The Flint Hills ecoregion in Kansas and Oklahoma remain one of the last great expanses of intact and native tallgrass prairie in the United States. The creation of the Tallgrass Prairie National Preserve in 1996 allowed for more area of the Flint Hills to retain its native character.

Grasslands have been under threat in the United States as well as throughout the world due to conversion to row-crop agriculture and changing land management coupled with other global change phenomena (Briggs et al., 2005). A majority of the former area of the tallgrass prairie has been replaced with crops such as wheat, corn, and soybeans (Plowprint Annual Print, 2016). The remaining tallgrass prairies of North America are threatened by an increase over time in the abundance of native woody species, such as the red cedar (*Juniperus virginiana)* in the Flint Hills area (Hulbert, 2009). These woody plants originate both from within the ecosystem and from neighboring ecosystems (Briggs et al., 2005), with encroachment altering the structure and function of temperate grassland ecosystems and resulting in a loss of biodiversity and grazing productivity (Ratajczak et al., 2016). The likely drivers of this increase in woody plant abundance are numerous and include change in climate, atmospheric carbon dioxide concentration, nitrogen deposition, grazing pressure, and disturbance regimes (e.g., the frequency and intensity of fire) (Briggs et al., 2005). Transitions to shrubland and woodland in temperate climates are largely attributed to changes in fire management (Ratajczak et al., 2016). Comparisons of the area occupied by forest at the time of settlement, as recorded in the 1856 Land Office, with that in the 1970's showed that on frequently burned prairies woody plants occupied about the same area today as over a century ago. However, on sites not burned for 20 years or longer, forests had invaded on half or more of the unburned areas (Hulbert, 2009).

Fire is an integral component of prairie development and maintenance and for more than 7000 years vegetation patterns have been influenced by anthropogenic burning practices (Towne and Kemp, 2003). Fire has long been recognized as an important factor influencing the development and persistence of the tallgrass prairie ecosystem (Benson and Hartnett 2006). Fire is both an inexpensive and effective way of controlling woody species and shrubs as well as maintaining high quality nutritious forge for grazers, but air pollution from the smoke can negatively impact cities downwind of the fires (Briggs et al., 2005). Prairie fires were suppressed during European settlement with accidental or lightning-caused wildfires being the primary source of burning (Towne and Kemp, 2003). An influx of cattle to the Flint Hills in the late 1800's created an incentive for prairie burning and pastures were burned annually in February or March to improve livestock weight gains (Towne and Kemp, 2003).

Annual or biennial burning, which is currently a common land management practice in tallgrass prairie, homogenizes the canopy over the long term by suppressing invasion by woody species while promoting a variety of C3 forbs amidst a matrix of C4 graminoids (Goodin and Henebry, 1998) (Benson and Hartnett 2006). Warm season grasses have been shown to increase after burning has been conducted (Towne and Kemp, 2003) (Hulbert, 2009) and average peak-season aboveground biomass on annually burned prairie is reported to be nearly twice that of infrequently burned prairie (Benson and Hartnett 2006). Species diversity is lowest with annual late-spring burning and increases with increasing intervals between fires (Hulbert, 2009).

At the Konza Prairie Biological Station, it has been observed that vegetation development starts earlier on plots burned in November than on those burned in March (Hulbert, 2009). This is likely due to higher soil temperatures on burned areas, resulting from greater solar heating as a response to removal of the insulating layer of standing dead vegetation (Hulbert, 2009). A

burning frequency of 3 to 4 years has been thought to be the historical fire frequency before extensive settlement by Europeans (Briggs et al., 2005). Burning once every 4 years has been shown to increase the number of forb and annual species compared to that seen in annually burned sites (Collins et al., 1995). A complete exclusion of fire in tallgrass prairie has been shown to significantly decrease the grass bud bank while increasing the forb bud bank (Dalgleish and Hartnett, 2008). Prairie that is burned at an intermediate fire frequency showed greater year-to-year variability in grass bud bank size and in the probability of emergence from the bud bank than annually burned prairie (Dalgleish and Hartnett, 2008).

Cattle ranchers in the Flint Hills employ frequent spring burns to remove dead litter and enhance palatability, leading to greater and more consistent weight gain in cattle (Ratajczak et al., 2016). These fires help to reduce species such as buckbrush (*Ceanothus cuneatus)* or coralberry (*Symphoricarpos orbiculatus)* (Hulbert, 2009). Annual spring burning is beneficial in stopping woody encroachment but also can homogenize plant and avian communities (Collins et al., 1995) (Ratajczak et al., 2016). In addition, it has been shown that annual burning does not eliminate shrubs and, over time, this buildup of shrubs can lead to areas where woody vegetation becomes established and later spreads (Towne and Kemp, 2003). Fire alone does not stop the invasion of woody plants. The combination of fire, climate, substrate, and topography are what makes the prairie (Hulbert, 2009).

Depending on the definition used for the Flint Hills, the amount and frequency of burning varies on a yearly basis. Mohler and Goodin (2012) showed that as much as 31% of the Flint Hills grasslands were burned in 2005 and the Nebraska Department of Environment and Quality puts the figure at 48% (NDEQ, 2016). In 2007, roughly 10-14% of Flint Hills grasslands were burned. About 8% of the grassland within the Flint Hills was burned once during the 2000-2010

time period while less than 1% were burned ten times during the same period (Mohler and Goodin, 2012).

The Kansas Department of Health and Environment has developed the Flint Hills Smoke Management Plan to combat smoke conditions caused during the burning season. Their website, www.ksfire.org, seeks to inform land managers conducting prescribed burns in the Flint Hills by providing information and access to tools to assist with burn decisions. The Flint Hills Smoke Management Plan began in fall 2013 when air quality monitors in the Kansas City area recorded very high ozone readings on April 12 and April 13 (KDHE, 2010). Three monitors in Kansas City, Missouri recorded readings that exceeded the federal 8-hour ozone standard and states as far away as Tennessee were impacted with poor air quality and high ozone concentrations (KDHE, 2010). In Nebraska, the cities of Omaha and Lincoln have also been impacted by burning in the Flint Hills with several days of violating air quality standards (NDEQ, 2016).

Because the Flint Hills Smoke Management Program is entirely voluntary, there is no way for the states of Kansas or Nebraska (or any other states) to exercise control over prescribed burning (NDEQ, 2016). States that are downwind have no input into prescribed burning activities and only have the ability to react to air quality conditions that result from the Flint Hills fires and issue air quality advisories as conditions dictate.

Remote Sensing

Even before the term "remote sensing" was first coined by Evelyn Pruitt, it has been an integral part of geography studies. Remote sensing replaced the outdated term of "aerial photography" when it became apparent it no longer described the increasing number of new forms of imagery being collected (Campbell and Wynne, 2011). The act of remote sensing measures the energy emitted by the earth's surface with a sensor mounted on an aircraft or

spacecraft platform (Richards and Jia, 2006). The energy being measured can be from the sun, the earth itself, or from an artificial energy source such as radar or lasers. Remote sensing using artificial energy sources, radar or lasers, is known as active remote sensing while remote sensing using the energy produced by the sun or earth is known as passive remote sensing. The data collected by these sensors is done without direct physical contact with the emitting or reflecting surfaces.

Remote sensors record emitted or reflected electromagnetic radiation (EMR) and changes in the amount or properties of EMR can be analyzed to interpret important properties of vegetation (Kennedy et al., 2009). Due to the physical and chemical properties of a material causing it to absorb, reflect, and emit energy differentially in various parts of the EMR spectrum, the energy measured in different spectral bands can be used to infer information about the character of the object being observed (Kennedy et al., 2009). The data is readily available in digital format and can be processed using computers for machine-assisted information extraction or to enhance its visual qualities to make it more interpretable by a human analyst (Richards and Jia, 2006). Remote sensing has become such a widely used technique in part due to its ability to examine large areal extents, varying degrees of temporal dynamics, and due to the large number of remote sensing platforms allowing for many different types of problems to utilize remote sensing systems (DeFries, 2008).

Remote sensing can be applied to studies of ecological indicators at a variety of spatial and temporal scales (Willis, 2015). Many of these remote sensing platforms are space-based and were specifically designed for environmental monitoring. These include, but are not limited to, Landsat, AVHRR, MODIS, Spot, and MISR (Campbell and Wynne, 2011). Not all of the previously mentioned satellites yield images appropriate for every problem. Landsat and Spot

are high resolution with Landsat at 30m and Spot at 6m which are good for problems that require finer spatial resolutions. Landsat and Spot, however, have a repeat image interval in the 16-day range, making them unsuitable for studying problems or processes at fine temporal resolutions. MODIS, AVHRR, and MISR produce much coarser spatial resolution images at 500m for MODIS, 1km for AVHRR, and up to 1.92km for MISR (Campbell and Wynne, 2011). While these remote sensing systems may have coarser spatial resolution, they are able to collect data daily, making them well suited to study fast changing systems. Remote sensing systems such as these allow for earth systems experiments to be conducted much more efficiently than ever before and are particularly good for examining vegetation processes (DeFries, 2008). In addition, satellite-based remote sensing is particularly well-suited for the study of disturbed areas because remote sensing does not increase the amount of disturbances on the ground in sensitive areas (Willis, 2015).

Satellite remote sensing has been used as a means of detecting and classifying changes in land surface conditions over time (Verbesselt et al., 2010a). For a resource manager or land manager, satellite remote sensing technology is particularly attractive due to its ability to provide consistent and repeatable measurements of landscape condition, allowing detection of abrupt changes and slow trends over time (Kennedy et al., 2009). These satellite observations are also acquired at spatial scales appropriate for capturing the effects of many processes that cause change, including natural (e.g. fires, insect attacks) and anthropogenic (e.g. deforestation, urbanization, farming) disturbances (Vervesselt et al., 2010a).

Remote Sensing of Vegetation

Remote sensing of the environment involves recording and interpreting images produced from a satellite. Spectral reflectance curves can be created by examining the visible and near infrared regions of the electromagnetic spectrum (Jensen 1983). These spectral signatures are not constant for a given feature and depend on interactions between the satellite sensor and atmospheric properties (Slater 1980). Chlorophyll in plant tissue creates a distinct spectral reflectance curve as it absorbs visible energy for photosynthesis in the blue and red regions of the electromagnetic spectrum (An 2009). The red region of the electromagnetic spectrum is highly chlorophyll absorptive and dependent on chlorophyll content (Figure 2.1) and can be seen in green, or active, vegetation (Wardlow 2005).

Figure 2-1. The spectral reflectance curve for healthy, green vegetation at the 0.35 – 2.6 um wavelengths of the electromagnetic spectrum, as well as the dominant factors regulating leaf reflectance and absorption (Jensen 1983).

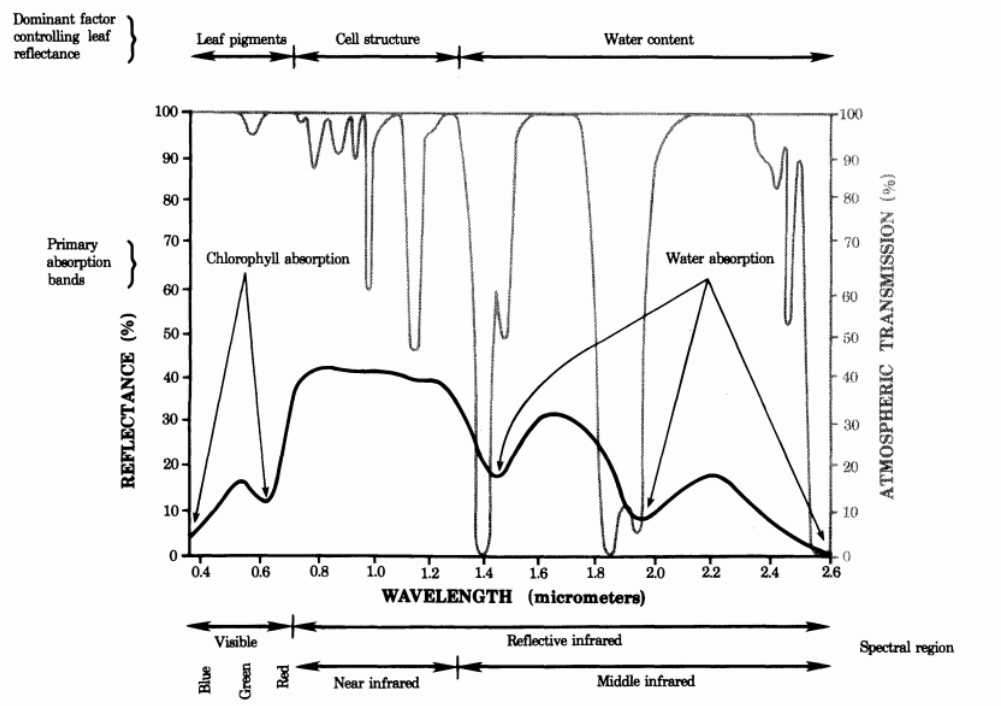

The near-infrared (NIR) spectrum between 0.74 – 0.90 um is the optimal region for estimating vegetation biomass (Tucker 1979). Healthy green vegetation reflecting NIR is

dependent on plant water content in mesophyll cells in vegetation (Jensen 1983). Plant pigments do not absorb NIR, rather it passes through the plant and interacts with the mesophyll cells. Healthy plants with sufficient water will reflect more NIR than plants containing less water.

Satellite remote sensing has been an invaluable asset for examining regional environmental change by post-classification analysis of land cover change to examine separate, abrupt anthropogenic impacts on the land surface, such as deforestation and urbanization. Accompanying satellite remote sensing is a variety of spectral vegetation indices, such as NDVI which can be calculated from satellite image data to quantify the spatial and temporal variation in vegetation growth and activity (Linderholm 2006). NDVI and other indices have been used to successfully assess vegetation phenology (Wright et al., 2012).

Remote sensing indices are mathematical combinations of surface reflectance at two or more wavelengths to emphasize vegetation properties. Vegetation indices are based on the reflectance properties of plant foliage, such as leaves and other green materials which can vary greatly in composition. Vegetation indices correlate with several biophysical parameters such as leaf area index (LAI), fraction of photosynthetically active radiation (FPAR), and green aboveground biomass (Wardlow 2005). Components that have the most effect on leaf spectral response are pigments, water, carbon, and nitrogen (Zhang et al., 2007). Vegetation indices provide insight into basic composition of leaves and how they change in different environmental conditions to determine the general greenness of vegetation, biomass, and land cover, to estimate net productivity (Tucker et al., 1991).

Estimates of vegetation biomass are dependent on the ratio of soil surface-vegetation spectral reflectance making some wavelengths better to use than others (Colwell 1974). The ideal vegetation index would be sensitive to vegetation, insensitive to background soils, and

minimally influenced by atmospheric path radiance (Lunetta el al., 2006). Examples of frequently used vegetation indexes include the IR/red ratio (Colwell 1973), the perpendicular vegetation index (PVI) (Richardson and Weigand 1977), the soil-adjusted vegetation index (SAVI) (Guete 1988), the Kauth-Thomas transformation (tasseled cap or -T) (Kauth and Thomas 1976), the enhanced vegetation index (EVI) (Zhang et al., 2007), and the normalized difference vegetation index (NDVI) (Lunetta et al., 2006).

NDVI is calculated as the ratio of the difference between near-infrared and red over the sum of near-infrared and red (Lunetta et al., 2006) and varies between values of -1 to 1 (Equation 2.1). Red and near-infrared bands are related to chlorophyll content and cell structure and with the spectral response of these two bands, the change in NDVI value over time is a good way to measure the vegetation growth and development (Zhang et al., 2007).

$$NDVI = (NIR - red) / (NIR + red) \quad \textbf{Equation 2.1}$$

where:
NDVI = normalized difference vegetation index
NIR = reflectance in the near – infrared spectrum
Red = reflectance in the red spectrum

NDVI correlates well with total primary production (An 2009) and the amount of photosynthetic biomass (Zhou et al., 2001), which dominates both photosynthesis and transpiration processes. During a normal year, NDVI increases rapidly in the spring and then levels off until the end of August (Verbesselt et al., 2010). Therefore, changes in NDVI suggest changes in vegetation that coincide with absorption of radiation (Sellers 1985). Higher NDVI values are associated with healthier vegetation while degraded vegetation is associated with lower NDVI values.

NDVI has shown consistent correlation with vegetation biomass and dynamics in various ecosystems worldwide. NDVI provides information about the spatial and temporal distribution

of vegetation communities, vegetation biomass, CO_2 fluxes, vegetation quality for herbivores, and the extent of land degradation in various ecosystems (Pettorelli et al., 2005). NDVI has been shown to report consistent negative correlations between fire probabilities and standardized NDVI levels (Pettorelli et al., 2005). While NDVI has been proven to be a very useful application for vegetation production, there are some limitations. The relationship between NDVI and vegetation can be biased in sparsely vegetated areas, such as arid to semiarid areas, and dense canopies, such as the Amazonian Rain Forest (Pettorelli et al., 2005). Due to NDVI being ratio-based, non-linear, lower ratio values tend to be enhanced and higher ratio values condensed causing values to saturate over high biomass conditions (Carlson and Ripley 1997). This may cause areas with high biomass density to have larger NDVI values than areas with lower densities, even if the health conditions of the vegetation were identical. NDVI is also unable to differentiate dominant species within forests due to assemblages of plant species producing similar NDVI values or similar NDVI temporal trends (Pettorelli et al., 2005).

The visible and NIR bands of the spectrum cannot penetrate cloud cover causing satellite images to suffer from cloud contamination and yield lower NDVI values that do not accurately reflect surface conditions unless preprocessing filtering and smoothing is applied to the raw data. The NIR band also include a strong water absorption region, which can reduce the reliability of NDVI calculations (Wardlow 2005). Most vegetation indices are also limited by inter-satellite sensor differences, satellite drift, calibration uncertainties, and atmospheric pat radiance (Zhou et al., 2001).

Phenometrics

Phenology has become an important focus in ecological research for its use in vegetation monitoring and in examining issues related to climate change. Phenology is the variation in

seasonal patterns of natural phenomena on land surfaces affected by inter-annual and seasonal variation in soil characteristics and meteorological conditions (Cleland et al., 2007). Seasonal characteristics of plants, such as emergence and senescence, are closely related to climate and changes in phenological events may signal important year-to-year weather and climate variations or even global environmental change (Reed 1994). The phenology of land surfaces can be detected using remote sensing by examining the spectral index values of the land surface. Changes in the seasonal timing such as the start and end of season, duration of growing season, and maximum productivity can have an impact on a wide range of processes that are dependent on natural cycles of vegetation (Ganguly et al, 2010). However, changes in phenology are part of a complex system and can be influenced by outside forces other than long-term climate change, such as precipitation or fire (Willis, 2015). In order to detect changes in phenology, remotely sensed datasets must have high temporal resolution to capture any sudden changes in the landscape. MODIS-derived indices are ideal for monitoring phenology in vegetation because it support a wide variety of phenology-related data products (i.e., NDVI, EVI, Leaf Area Index (LAI, Albedo) and MODIS images are acquired on a daily basis and are also composited into 8 and 16 day products (Willis, 2015).

Most phenology research has ecosystem monitoring as it ultimate goal while the phenology of entire ecosystems has rarely been studied (Reed 1994). Field-based ecological studies have demonstrated that vegetation phenology tends to follow relatively well-defined temporal patterns (Zhang et al., 2003). When looking at deciduous vegetation and many crops, leaf emergence tends to be followed by a period of rapid growth, and then is followed by a stable period of maximum leaf area (Sakamoto et al., 2005). At the regional and larger scales, variations in community composition, micro and regional climate models, soils, and land

management result in a complex spatio-temporal variation in the phenology of the vegetation (Zhang et al., 2003). In some cases, some vegetation types exhibit multiple modes of growth within a single annual cycle. A profile view of a single annual vegetation cycle (Figure 2.2) illustrates key measures, or phenometrics, often used in such studies, including the onset and end of greenness (start and end of season, respectively), maximum NDVI, the rate of green-up and senescence, growing season length, and accumulated NDVI.

Figure 2-2. An example of a vegetation phenology curve and associated phenometrics (from Reed et al., 1994).

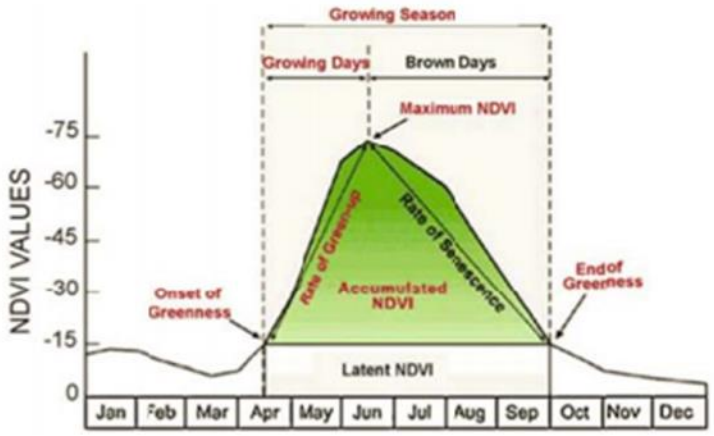

Time Series Analysis and Decomposition

A time series is an ordered sequence of variable values recorded at equally-spaced time intervals. Time series analysis methods can be used to determine if data has internal structure such as trend, seasonal variation, or autocorrelation (Eklundh and Jonsson 2010). In a remote sensing context, time series analysis consists of a series of satellite images which allow comparisons of the same scene, biophysical measure, or vegetation index over a long time period to reveal structure variables of interest. When vegetation indices are used as the basis of the time series, shifts in vegetation properties and dynamics may be revealed (Heumann et al., 2007). Information extracted from time series vegetation index (VI) data has been shown to successfully

characterize vegetation phenology (Reed et al., 1994) and has been used to measure vegetation activity (Zhang et al., 2003).

The MODIS sensor is carried onboard NASA's Terra and Aqua satellites and acquires images at a global scale and at a high (daily) temporal resolution. MODIS possesses seven spectral bands that are designed for land applications with spatial resolutions ranging from 250 m to 1 km (Zhang et al., 2003). MODIS VI products are designed to provide consistent spatial and temporal comparisons of global vegetation conditions that can be used to monitor photosynthetic activity (Huete et al., 2002) and those acquired at the 250m resolution are well suited for application in the U.S. Central Great Plains (Wardlow and Egbert, 2008).

A time series can be decomposed into three parts: Seasonal (systematic, calendar related movements), trend (long-term direction), and irregular (unsystematic, short term fluctuations) (Verbesselt et al., 2009). The seasonal component shows the general vegetation phenology for an area and illustrates the timing and magnitude of the vegetation growing season. Changes from year to year in the seasonal component of the time series suggest weather conditions were variable during that time or that there were changes in dominant land cover types (Verbesselt et al., 2009). The trend component, which is often shown as a linear trend from the beginning to the end of the time series, shows the direction and magnitude of vegetation change, either positive or negative (Jacquin et al., 2009). The irregular component is treated as signal noise or background static caused by external sources.

Before raw data can be used, signal decomposition must be performed to identify the time series signal from the noise. The raw data is first put through a series of filtering, compositing, smoothing, or screening procedures to isolate the signal from the noise. The

preprocessing of raw data is based on a smoothing of distinct sequences of temporally adjacent data points (Jonsson and Eklundh 2004).

Time series analysis techniques used to filter raw NDVI data and extraction of phenometrics can be accomplished using several methods such as principal component analysis (Tan et al., 2010), Fourier analysis (Sakomoto et al., 2005), and pixel-above-threshold technique (Cleland et al., 2007). The TIMESAT software program also provides several filtering options to smooth raw time series vegetation data and extract phenometric data (Eklundh and Jonsson 2010). TIMESAT has been used in a variety of studies to examine vegetation phenology (Eklundh and Jonsson 2003), assess satellite and climate data-derived indices of fire risk (Verbesselt et al., 2006), and examine relationships between coniferous forest NDVI and models of conifer tree photosynthetic activity (Eklundh and Jonsson 2010).

Chapter 3 - Study Areas

The study area for this project includes the 26 counties of Kansas and Oklahoma which comprise the Flint Hills ecological region of eastern Kansas and northern Oklahoma (Figure 3.1). The Flint Hills encompasses an area of 1.6 million hectares and contains the largest area of unplowed tallgrass prairie in North America (Hutchinson et al., 2015). The World Wildlife Fund's Terrestrial Ecoregions of the United States and Canada defines the Flint Hills as the area covering the Flint Hills of Kansas and the Osage Plains of northeastern Oklahoma. The Flint Hills is the smallest grassland ecoregion in North America and can be distinguished from other

Figure 3-1. The Flint Hills study area showing the 26 counties comprising the ecological region in eastern Kansas and north-central Oklahoma.

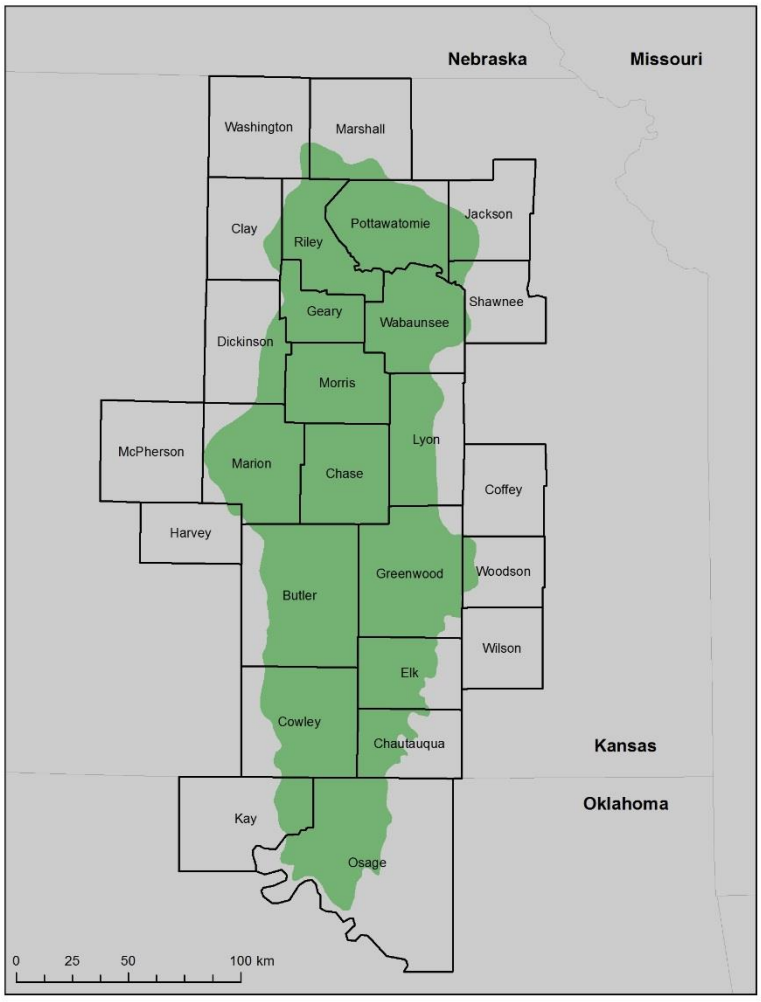

grassland associations by the dominance of tallgrass species and from the Central Tall Grasslands to the north by its lack of biotic variety and a thin soil layer spread over distinct beds of limestone. These flinty beds of limestone, from which the name of this ecoregion is derived, renders most of the area unsuitable for row-crop agriculture, resulting in an unplowed, though heavily grazed, remnant of the original tallgrass prairie (Madson 1993). Unlike many other ecoregion classifications, which are based primarily on biophysical features such as climate and topography, World Wildlife Fund's ecoregions include biogeographic knowledge and therefore reflect the historic events and processes that have shaped biodiversity distributions (McDonald et al., 2005).

The definition for the Flint Hills that will be used in this study is provided by the U.S. Environmental Protection Agency (EPA) which defined ecoregions based on work from Omernik (1987) to serve as a spatial framework for environmental resource management. The map of U.S. ecoregions was compiled based on the premise that ecological regions can be identified through an analysis of the patterns and the composition of biotic and abiotic phenomena that affect or reflect differences in ecosystem quality and integrity (Omernik, 1987). Such phenomena include geology, physiography, vegetation, climate, soils, land use, wildlife, and hydrology. The relative importance of each characteristic varies from one ecological region to another regardless of the hierarchical level (Wilken 1986). The EPA ecoregions use a Roman numeral classification scheme with level I being the coarsest level, dividing North America into 15 ecological regions, level II divides the continent into 52 regions, and levels III and IV further breaking down the ecoregions. The EPA definition of the Flint Hills is identical for level III and IV with Level III boundary used in this study.

Precipitation in the Flint Hills is highly variably from year to year. Based on 30 year normal precipitation (1981-2010) (http://prism.oregonstate.edu (last accessed 02.15.17), the northern and southeastern portions of the Flint Hills receive 720 mm (28 in) and 1120 mm (44 in) of precipitation annually. Much of the precipitation falls during the growing season (approximately 75%), though this, too, varies from year to year (Hayden 1998). Seasonal temperatures are typified by cool winters and hot summers. The City of Manhattan, Kansas, in the northern section of the Flint Hills, averages -1.8 C in January and 26.5 C in July while the southern reaches of the study area experience an average temperature of 1.1 C in January and 27.2 C in July.

Prescribed burning is a common land management practice employed by ranchers within the ecological region (Wilgers and Horne, 2006). Burning tallgrass prairie has been shown to increases plant productivity, decrease aboveground litter, and decrease woody vegetation (Briggs and Knapp, 1995). The frequency of burning in the Flint Hills has changed in recent years. Beginning in the 1980's, a switch in cattle grazing practices prompted land owners to apply controlled burns on an annual basis. However, areas around populated areas often remain unburned for extended periods of time and these different fire regimes may be contributing to recent trends in vegetation, including the encroachment and expansion of woody vegetation (Robbins et al., 2002).

Within the Flint Hills, in addition to tallgrass prairie vegetation, there are several other land cover types. (See Figure 3-2). Croplands are found in the flat floodplains along streams and rivers. Gallery forests can also be found along the streams and rivers. Trees can also be found in upland areas where fire and grazing have been suppressed. Figure 3.3 shows the study area while emphasizing the grassland areas isolated for analysis. The area of the moderate resolution

pixels identified here as grassland consisted of at least 80% grassland cover after rescaling the original higher spatial resolution data provided by the 2011 National Land Cover Database (NLCD) (Homer et al., 2015).

Figure 3-2. Land use/land cover within the counties comprising the Flint Hills ecoregion study area (NLCD 2011).

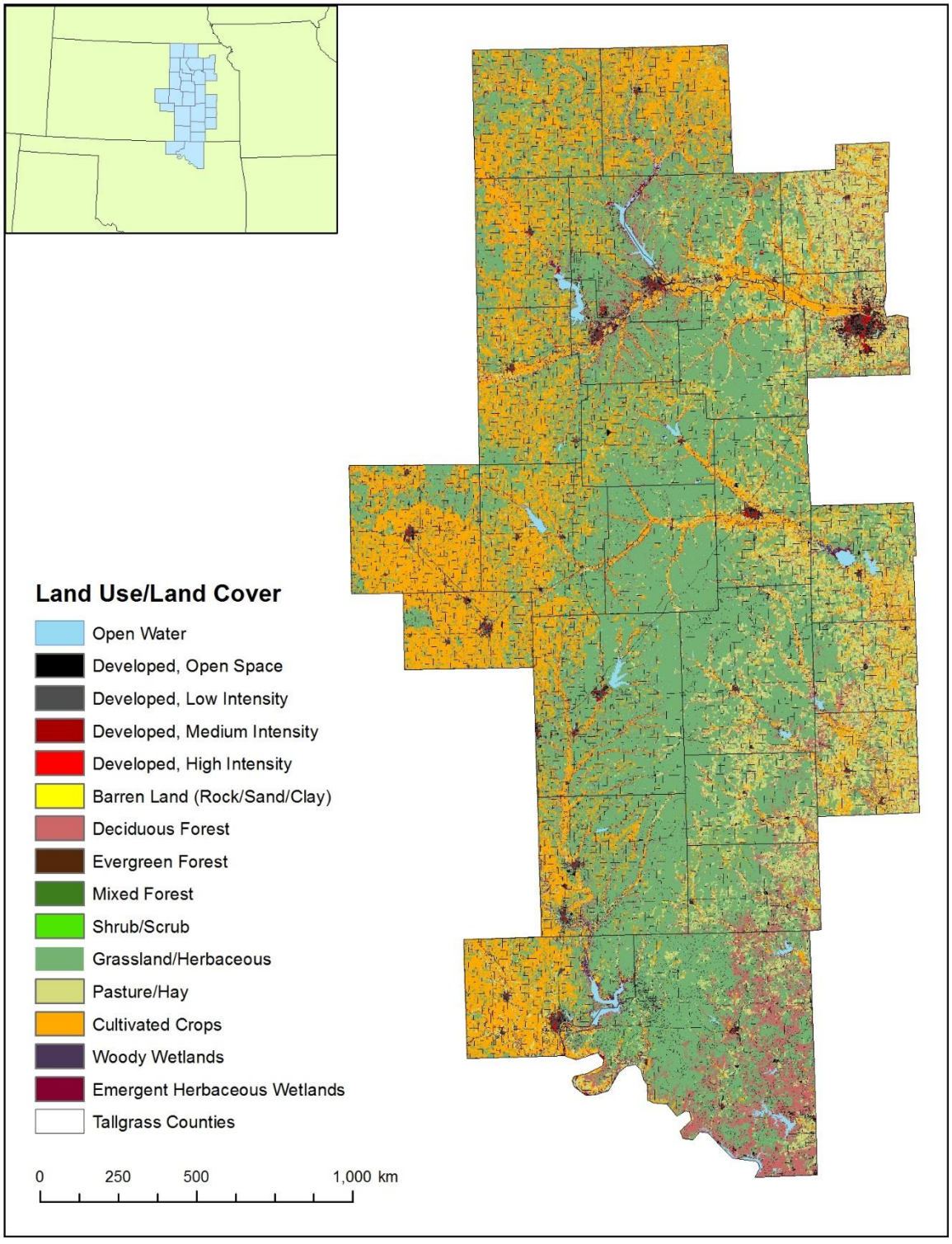

Figure 3-3. The Flint Hills ecoregion study area emphasizing grassland pixels. Each pixel, which correspond to the spatial resolution of the MODIS MOD13Q1 product consists of a minimum of 80% grassland/herbaceous cover according to the 2011 National Land Cover Database.

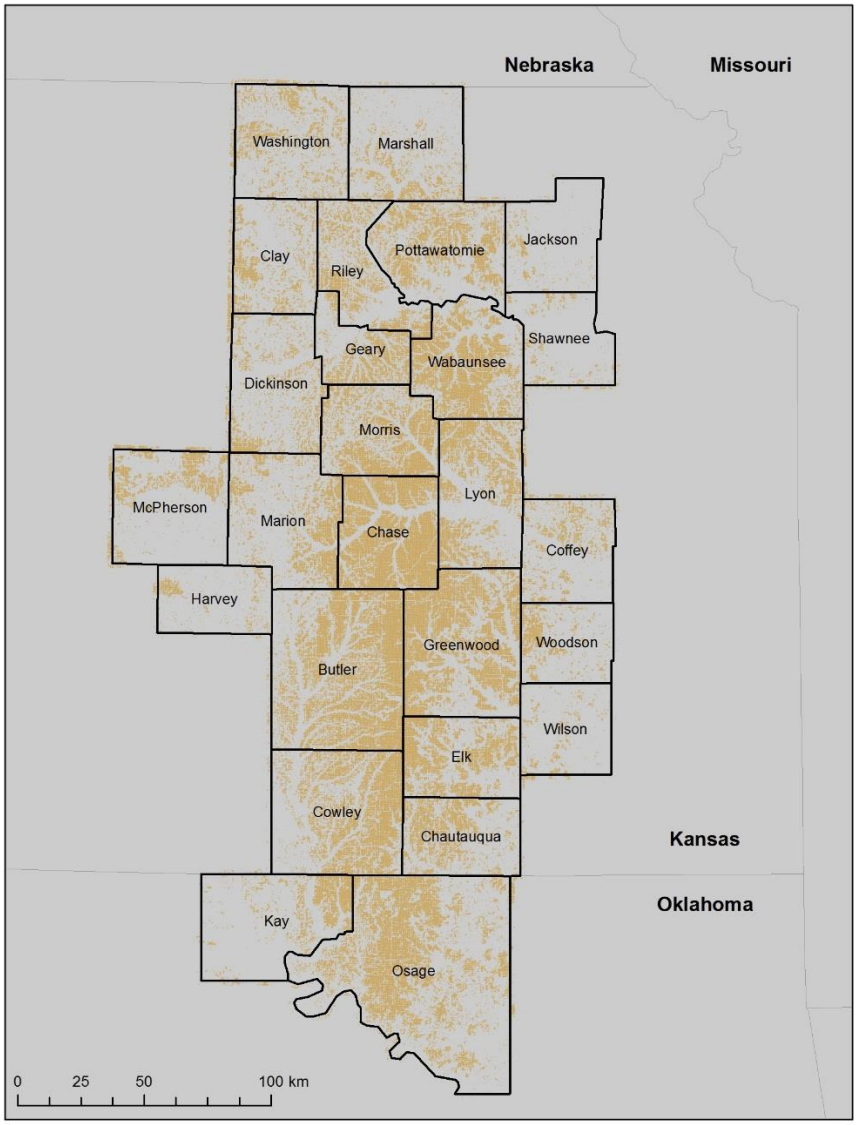

Prescribed burning preserves and sustains the tallgrass prairie ecosystem. Burning is an effective land management practice for stopping woody vegetation from encroaching on grasslands. Tallgrass prairies of North America are threatened by an increase in the abundance of native woody species, such as red cedar (*Juniperus virginiana*) in the Flints Hills area (Hulbert, 2009). These woody plants originate both from within the ecosystem and from

neighboring ecosystems (Briggs et al., 2005). This woody encroachment alters ecosystems structure and functions of temperate grasslands, resulting in a loss of biodiversity and grazing productivity (Ratajczak et al., 2016). There are several likely drivers of the increase in woody plant abundance including change in climate, increasing atmospheric carbon dioxide concentration, nitrogen deposition, grazing pressure, and disturbance regimes (e.g. the frequency and intensity of fire) (Briggs et al., 2005). Transitions to shrubland and woodland in temperate climates are largely attributed to changes in fire management (Ratajczak et al., 2016).

Annual spring burning is beneficial in stopping woody encroachment but also increases homogenization of plant and avian communities (Collins et al., 1995) (Ratajczak et al., 2016). Fire and grazing treatments that promote uniformity cannot maintain biodiversity in tallgrass ecosystems (Fuhlendorf et al. 2006). In addition, it has been shown that annual burns do not eliminate shrub species and that a continued increase in shrubs may lead to areas where woody vegetation may gain a foothold and spread further (Towne and Kemp, 2003). Another negative impact of burning is when large areas are burned, nearby towns and cities suffer from air quality issues related to the particulates released during burning (Dennis et al. 2002). The frequency of burns in the Flint Hills for the period 2001-2010 is shown in Figure 3-4.

Figure 3-4. The frequency of burning within the Flint Hills from 2001-2010. The original data from Mohler and Goodin (2012) was subset to include only the 2001-2010 data.

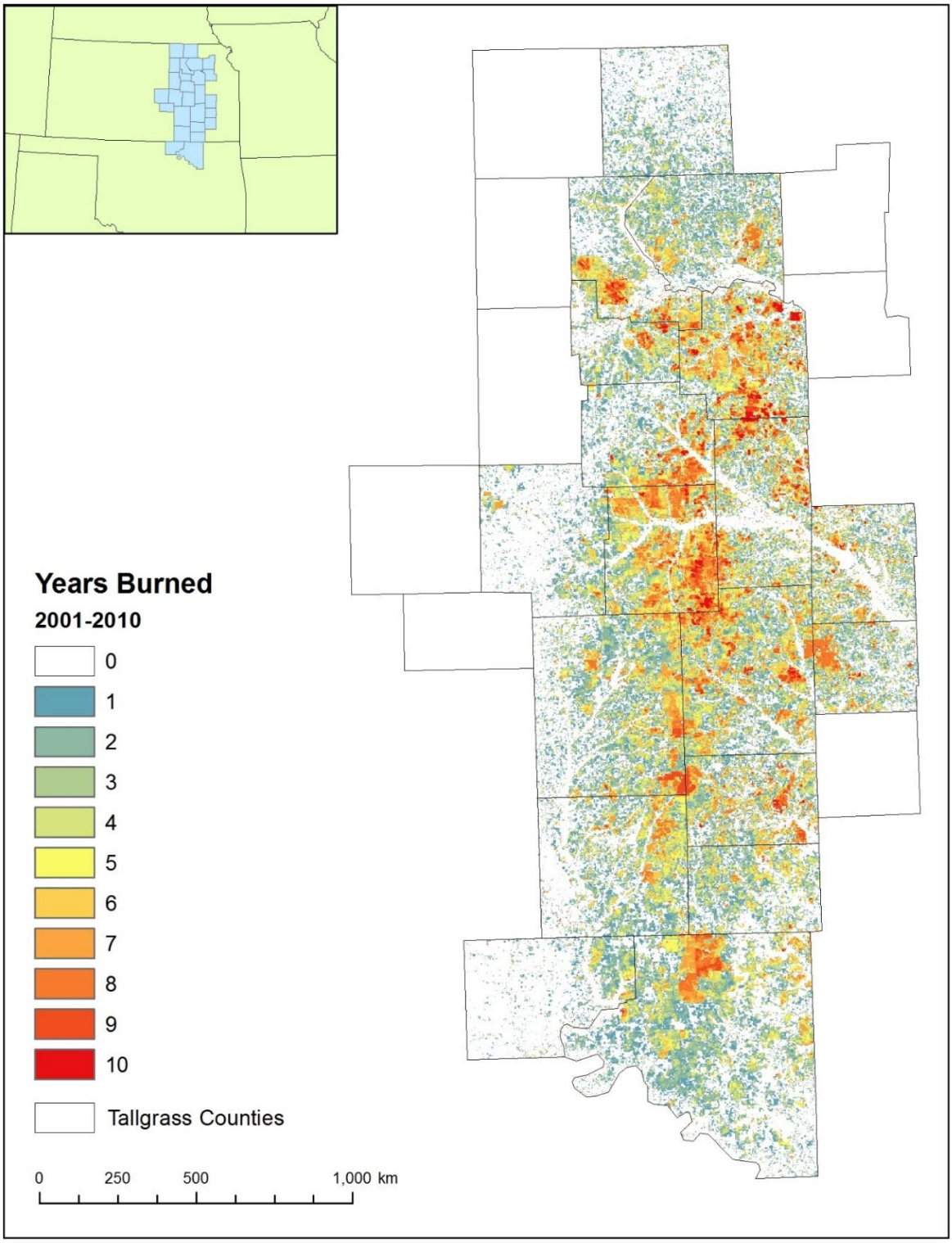

Chapter 4 - Detection of Long-Term Vegetation Trends for the Flint Hills Ecoregion using BFAST and Moderate Resolution Satellite Imagery

Abstract

Grasslands in the Flint Hills are often burned as a land management practice. Remote sensing can be used to help better manage prairie landscapes by providing useful information about the long-term trends in grassland vegetation greenness and help quantifying regional differences in vegetation development. Using MODIS 16-day NDVI composite imagery between the years 2001-15 for the entire Flint Hills ecoregion, BFAST was used to determine trend, seasonal, and noise components of the image time series. For the study period, the area of negatively and positively trending grassland were 52% and 21%, respectfully. 38% of the study area experienced zero breaks during the study period and about 30% experienced only a single break. However, BFAST-derived breaks in trend do not compare favorably with the burn frequency analysis of Mohler and Goodin (2012) and may not be a good proxy for identifying burned areas within the Flint Hills. Results suggest that long-term trends in grassland conditions warrant further attention and may rival other sources of grassland change (e.g., conversion, transition to savannah) in importance.

Introduction

Grasslands and savannas make up more than 40% of the earth's surface and their rapid response to changes in land management and climate can have dramatic ecological and social consequences (Briggs et al., 2005). Grasslands are among the most biodiverse and productive of all the earth's terrestrial biomes but receive low levels of protection (Mark and McLennan, 2005). Since 2009, 53 million acres of grassland, roughly the area of Kansas, have been

converted to cropland across the Great Plains alone (Plowprint Annual Report, 2016). Tallgrass prairie has been reduced to ~4% of its historical extent making it one of the most altered ecosystems in North America (Ratajczak et al., 2016). Temperate grasslands are important for both agronomic and ecological purposes and are a key resource for livestock production in North America and around the world (Briggs et al., 2005). Grasslands provide services such as water storage and clean air (Plowprint Annual Print, 2016) and grassland vegetation reduces soil erosion due to it dense root systems and by shielding the soil surface from direct interception of rainfall (Ratajczak et al, 2016). Grasslands also store and retain large amounts of soil carbon and are an important component of the global carbon cycle (Briggs et al., 2005). The estimated values of theses, and other, ecosystems services provided by native grasslands has been estimated to be in excess of $5,000 per hectare per year (Dodds et al., 2008).

The conservation status of grasslands is being evaluated by groups including the Landscape Conservation Cooperatives which seeks to identify the greatest threats to grasslands and shrublands across the U.S. and Mexico, areas that are likely to be resilient to climate change and other threats, and areas with high potential for restoration (Glaser, 2014). The state of North American prairies is also being addressed through a tri-national cooperative program involving Mexico, the USA, and Canada which is attempting to address both sustainable management and conservation needs (Mark and McLennan, 2005). The Flint Hills ecoregion in Kansas and Oklahoma remain one of the last great expanses of intact and native tallgrass prairie in the United States. The creation of the Tallgrass Prairie National Preserve in 1996 allowed for more area of the Flint Hills to retain its native character.

Grasslands have been under threat in the United States as well as throughout the world due to conversion to row-crop agriculture and changing land management coupled with other

global change phenomena (Briggs et al., 2005). A majority of the former area of the tallgrass prairie has been replaced with crops such as wheat, corn, and soybeans (Plowprint Annual Print, 2016). The remaining tallgrass prairies of North America are threatened by an increase over time in the abundance of native woody species, such as the red cedar (*Juniperus virginiana)* in the Flints Hills area (Hulbert, 2009). These woody plants originate both from within the ecosystem and from neighboring ecosystems (Briggs et al., 2005), with encroachment altering the structure and function of temperate grassland ecosystems and resulting in a loss of biodiversity and grazing productivity (Ratajczak et al., 2016). The likely drivers of this increase in woody plant abundance are numerous and include change in climate, atmospheric carbon dioxide concentration, nitrogen deposition, grazing pressure, and disturbance regimes (e.g., the frequency and intensity of fire) (Briggs et al., 2005). Transitions to shrubland and woodland in temperate climates are largely attributed to changes in fire management (Ratajczak et al., 2016). Comparisons of the area occupied by forest at the time of settlement, as recorded in the 1856 Land Office, with that in the 1970's showed that on frequently burned prairies woody plants occupied about the same area today as over a century ago. However, on sites not burned for 20 years or longer, forests had invaded on half or more of the unburned areas (Hulbert, 2009).

Healthy vegetation in the Flint Hills is essential for cattle ranchers and the overall health of the Flint Hills ecoregion. Degradation of vegetation health results from gradual or abrupt changes in the amount of vegetation activity over time which can be monitored by collecting and analyzing time-series Normalized Difference Vegetation Index (NDVI) data from medium or course spatial resolution satellites (Verbesselt et al., 2010a). Time series datasets using NDVI products from the Moderate Resolution Imaging Spectrometer (MODIS) sensor have been used to successfully quantify vegetation activity and vegetation dynamics (Zhang et al., 2003).

Past methods used for analyzing trends in continuous vegetation time series data include gradual interannual vegetation change due to rainfall variability and drought (Jacquin et al., 2010), temporal decomposition techniques which have been shown relevant to the study of vegetation seasonality (Jonsson and Eklundh, 2002), and abrupt vegetation change seen at the intraannual time scale caused by disturbances such as deforestation, disease and insect outbreaks, fire, and other activities (Verbesselt et al., 2010a).

Temporal decomposition of data involves separating an original time series dataset into three different components in order to study each related to vegetation greenness at different time scales (Cleveland and Delvin, 1988). These include seasonal, trend, and remainder, residual remaining after elimination of the trend and the seasonal components.

Two categories of methods exist to extract the trend component from a time series. In the first category, the trend component takes the shape of a known function and a regression model is fitted to the data using the least squares approach. This method may result in a model that may not reflect reality as trends could exhibit changes over time (Slayback et al., 2003). The second category of methods, the trend component is not assumed to follow a shape and cannot be modeled using a predefined function. Instead, the trend component is obtained via local smoothing using different techniques (Hutchinson et al., 2015). This approach is better adapted to data with one or more slope changes, or breaks, in the trend component over time. After extracting the trend component from time series datasets, information can be derived that identifies and characterized changes in the trend, including the length of the time series, the magnitude of the slope value indicating amplitude of change, and the sign of the slope signifying the direction of change (Verbesselt et al., 2010a).

This study builds off previous work on the military training grounds of Fort Riley, Kansas where Breaks For Additive Seasonal and Trend (BFAST) was used to examine seasonal trends of vegetation (Hutchinson et al., 2015). The BFAST method was used because of its ability to account for seasonality and to detect gradual (interannual) and abrupt (intraannual) changes within the trend component (Verbesselt et al., 2010a). Other methods such as Seasonal-Trend decomposition procedure (STL) based on a Locally wEighted regression Smoother (LOESS) were excluded from consideration due to its ability to detect only gradual changes in the trend component (Cleveland et al., 1990).

This study investigates the use of BFAST and a MODIS NDVI image time series to examine gradual and abrupt changes in the Flint Hills ecoregion of Kansas and Oklahoma. This work helps to extend the application of BFAST to the grassland ecosystem.

Study Area

The study area for this project includes the 26 counties of Kansas and Oklahoma which comprise the Flint Hills ecological region of eastern Kansas and northern Oklahoma (Figure 4-1). The Flint Hills encompasses an area of 1.6 million hectares and contains the largest area of unplowed tallgrass prairie in North America (Hutchinson et al., 2015). The World Wildlife Fund's Terrestrial Ecoregions of the United States and Canada defines the Flint Hills as the area covering the Flint Hills of Kansas and the Osage Plains of northeastern Oklahoma. The Flint Hills is the smallest grassland ecoregion in North America and can be distinguished from other grassland associations by the dominance of tallgrass species and from the Central Tall Grasslands to the north by its lack of biotic variety and a thin soil layer spread over distinct beds of limestone. These flinty beds of limestone, from which the name of this ecoregion is derived,

renders most of the area unsuitable for row-crop agriculture, resulting in an unplowed, though heavily grazed, remnant of the original tallgrass prairie (Madson 1993).

Unlike many other ecoregion classifications, which are based primarily on biophysical features such as climate and topography, World Wildlife Fund's ecoregions include biogeographic knowledge and therefore reflect the historic events and processes that have shaped biodiversity distributions (McDonald et al., 2005).

The definition for the Flint Hills that will be used in this study is provided by the U.S. Environmental Protection Agency (EPA) which defined ecoregions based on work from

Figure 4-1. The Flint Hills study area showing the 26 counties comprising the ecological region in eastern Kansas and north-central Oklahoma.

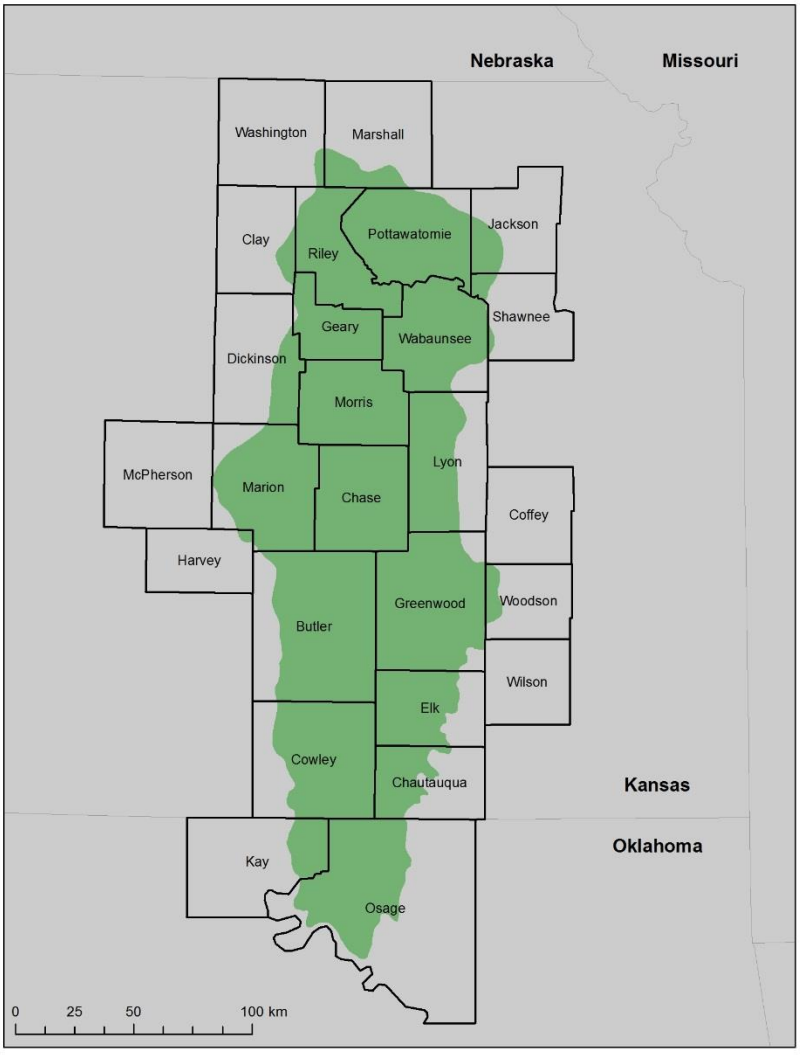

Omernik (1987) to serve as a spatial framework for environmental resource management. The map of U.S. ecoregions was compiled based on the premise that ecological regions can be identified through an analysis of the patterns and the composition of biotic and abiotic phenomena that affect or reflect differences in ecosystem quality and integrity (Omernik, 1987). Such phenomena include geology, physiography, vegetation, climate, soils, land use, wildlife, and hydrology. The relative importance of each characteristic varies from one ecological region to another regardless of the hierarchical level (Wilken 1986). The EPA ecoregions use a Roman numeral classification scheme with level I being the coarsest level, dividing North America into 15 ecological regions, level II divides the continent into 52 regions, and levels III and IV further breaking down the ecoregions. The EPA definition of the Flint Hills is identical for level III and IV with Level III boundary used in this study.

Precipitation in the Flint Hills is highly variably from year to year. Based on 30 year normal precipitation (1981-2010) (http://prism.oregonstate.edu (last accessed 02.15.17), the northern and southeastern portions of the Flint Hills receive 720 mm (28 in) and 1120 mm (44 in) of precipitation annually. Much of the precipitation falls during the growing season (approximately 75%), though this, too, varies from year to year (Hayden 1998). Seasonal temperatures are typified by cool winters and hot summers. The City of Manhattan, Kansas, in the northern section of the Flint Hills, averages -1.8 C in January and 26.5 C in July while the southern reaches of the study area experience an average temperature of 1.1 C in January and 27.2 C in July.

Prescribed burning is a common land management practice employed by ranchers within the ecological region (Wilgers and Horne, 2006). Burning tallgrass prairie has been shown to increases plant productivity, decrease aboveground litter, and decrease woody vegetation (Briggs

and Knapp, 1995). The frequency of burning in the Flint Hills has changed in recent years. Beginning in the 1980's, a switch in cattle grazing practices prompted land owners to apply controlled burns on an annual basis. However, areas around populated areas often remain unburned for extended periods of time and these different fire regimes may be contributing to recent trends in vegetation, including the encroachment and expansion of woody vegetation (Robbins et al., 2002).

In addition to tallgrass prairie vegetation, several other land cover types in the Flint Hills (See figure 4-2). Croplands are found in the flat floodplains along streams and rivers. Gallery forests can also be found along the streams and rivers. Trees can also be found in upland areas where fire and grazing have been suppressed. Figure 4-3 shows the study area while emphasizing the grassland areas isolated for analysis. The area of the moderate resolution pixels

Figure 4-2. Land use/land cover within the counties comprising the Flint Hills ecoregion study area (NLCD 2011).

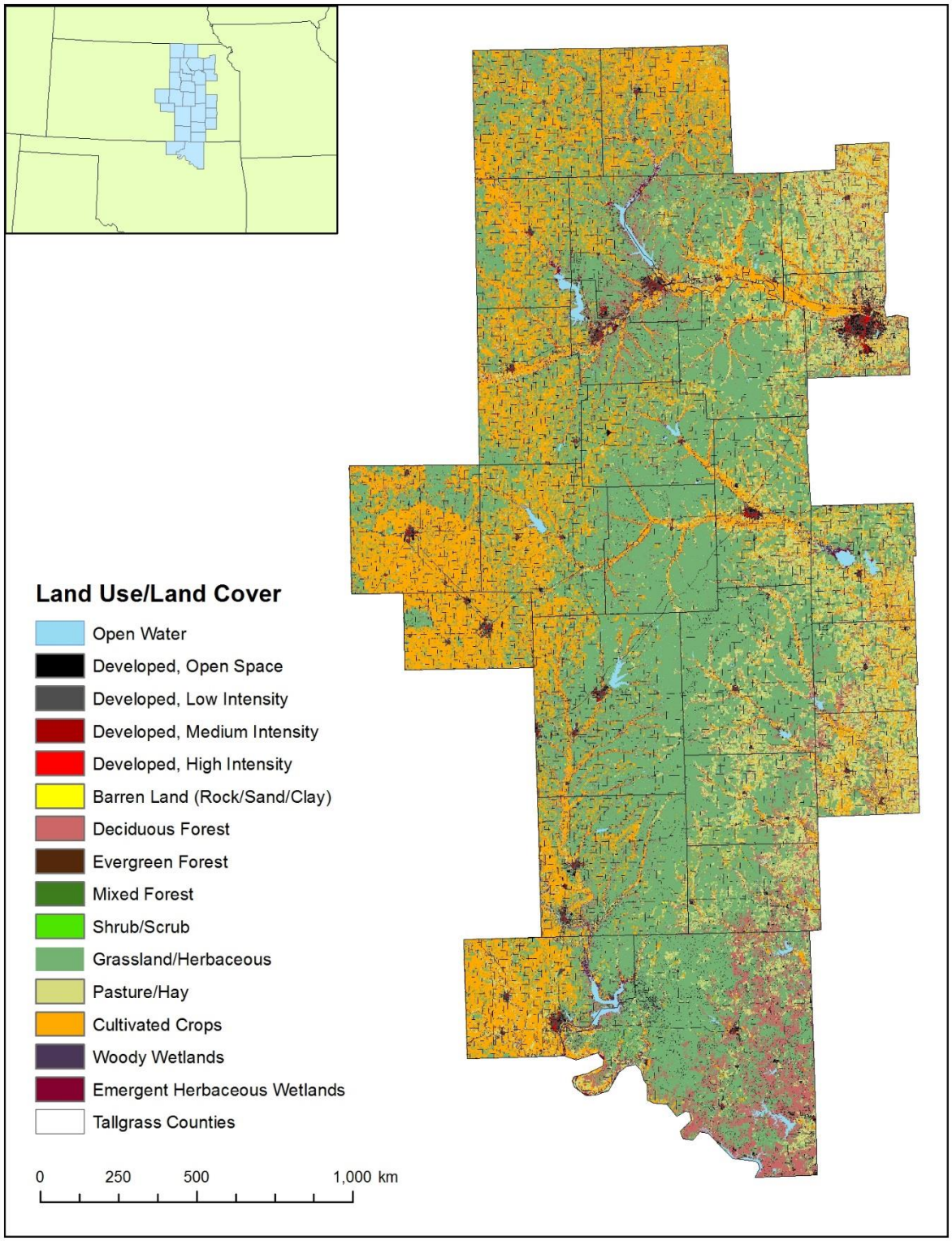

identified here as grassland consisted of at least 80% grassland cover after rescaling the original higher spatial resolution data provided by the 2011 National Land Cover Database (NLCD) (Homer et al., 2015).

Figure 4-3. The Flint Hills ecoregion study area emphasizing grassland pixels. Each pixel corresponds to the spatial resolution of the MODIS MOD13Q1 product and consists of a minimum of 80% grassland/herbaceous cover.

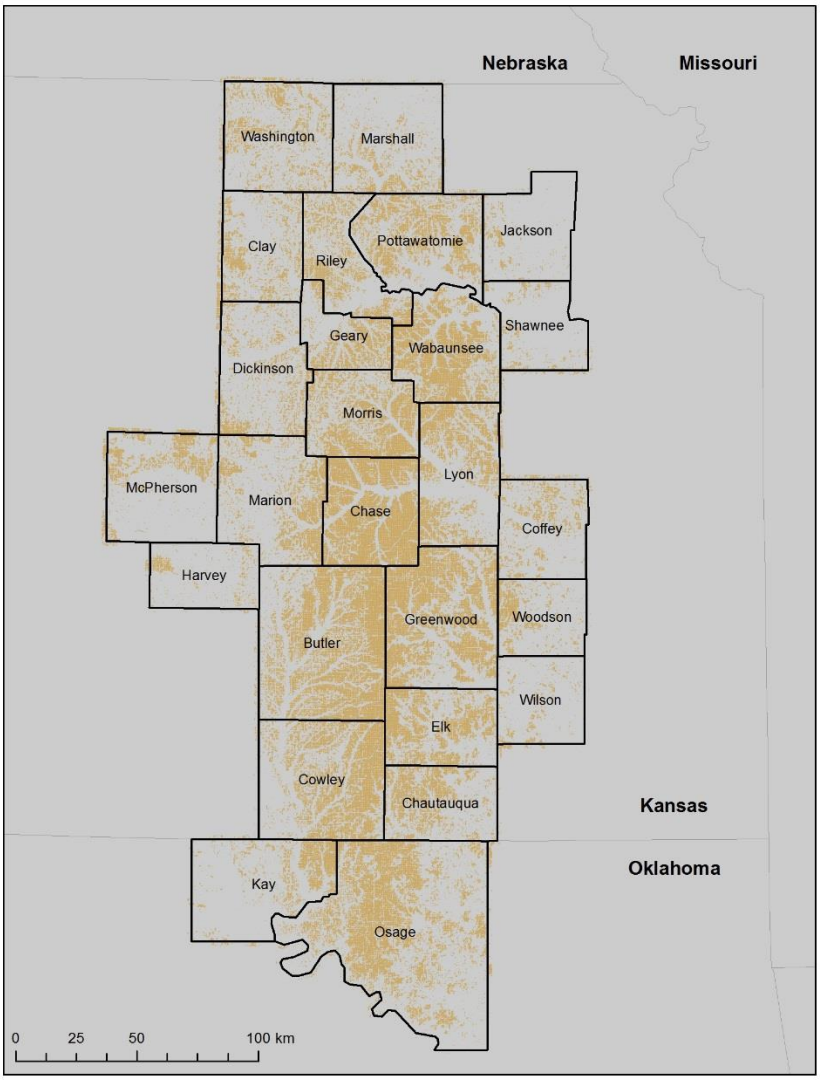

Prescribed burning preserves and sustains the tallgrass prairie ecosystem. Burning is an effective land management practice for stopping woody vegetation from encroaching on grasslands. Tallgrass prairies of North America are threatened by an increase in the abundance of native woody species, such as red cedar (*Juniperus virginiana*) in the Flints Hills area

(Hulbert, 2009). These woody plants originate both from within the ecosystem and from neighboring ecosystems (Briggs et al., 2005). This woody encroachment alters ecosystems structure and functions of temperate grasslands, resulting in a loss of biodiversity and grazing productivity (Ratajczak et al., 2016). There are several likely drivers of the increase in woody plant abundance including change in climate, increasing atmospheric carbon dioxide concentration, nitrogen deposition, grazing pressure, and disturbance regimes (e.g. the frequency and intensity of fire) (Briggs et al., 2005). Transitions to shrubland and woodland in temperate climates are largely attributed to changes in fire management (Ratajczak et al., 2016).

Annual spring burning is beneficial in stopping woody encroachment but also increases homogenization of plant and avian communities (Collins et al., 1995) (Ratajczak et al., 2016). Fire and grazing treatments that promote uniformity cannot maintain biodiversity in tallgrass ecosystems (Fuhlendorf et al. 2006). In addition, it has been shown that annual burns do not eliminate shrub species and that a continued increase in shrubs may lead to areas where woody vegetation may gain a foothold and spread further (Towne and Kemp, 2003). Another negative impact of burning is when large areas are burned, nearby towns and cities suffer from air quality issues related to the particulates released during burning (Dennis et al. 2002).

Data and Methods

The remote sensing data used for analysis were MODIS MOD13Q1 16-day maximum composite NDVI value image products for the period 2001-2015. A total of 23 composite images are produced each year, resulting in a total number of 345 images for the study period. MODIS MOD13Q1 images are a gridded level 3 product delivered in a sinusoidal projection and have a 250 meter spatial resolution. The images acquired came in calibrated and geolocated form based on grid and angular data, masked from cloud, land/water, perceptible water and

aerosol products, incorporate spectral reflectance, and undergo quality assurance flags associated with atmospheric correction products (Huete et al., 2002).

Images were downloaded from the Earth Observing System Data and Information System (EOSDIS) and saved as an 8-bit unsigned integer grid. Due to the nature of the sensor and the curvature of the Earth, the MOD13Q1 spatial resolution for the study area was 231.656 meters. After download, all images were clipped to the spatial extent of the 26 county study area and reprojected into the UTM Zone 14N NAD 83 spatial reference (940 Columns, 1840 Rows).

For this study, only grassland areas were analyzed. Using the 2011 NLCD product, pixels of the "grassland/herbaceous" class were extracted from the original dataset which was produced using Landsat data and has a 30 meter spatial resolution. This 30 meter resolution grassland data was then rescaled to match the spatial resolution of the MOD13Q1 image. Only rescaled pixels comprised of a minimum of 80% of the original NLCD grassland/herbaceous class were retained for further analysis (see Figure 4-3). Once the rescaled grassland "dominant" grid was constructed, the 8-bit NDVI values for the entire MOD13Q1 time series was extracted (Figure 4-4) and stored in a text (CSV) file, resulting in a matrix of values consisting of approximately 311,000 pixels by 345 (2001-2015) NDVI data points.

Figure 4-4. Shows a point shapefile overlaid on MODIS NDVI values.

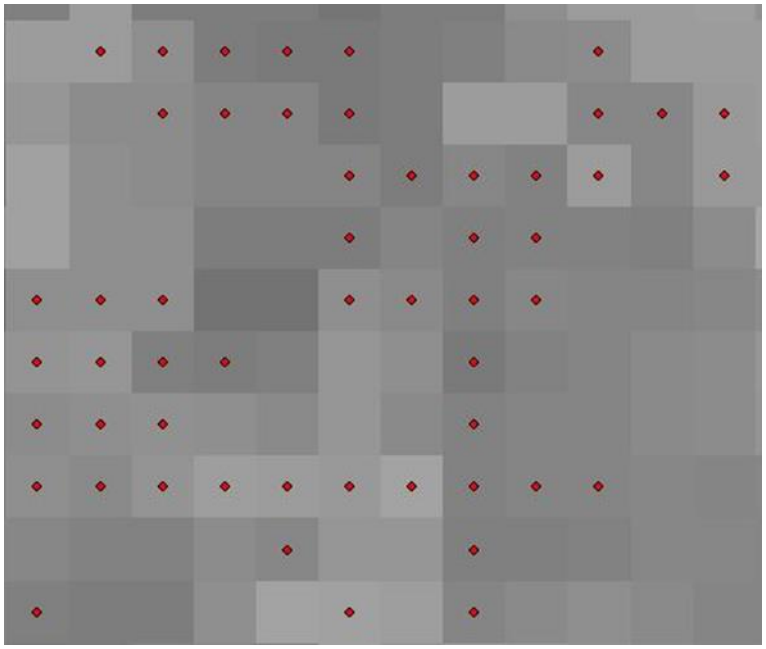

The extracted NDVI data matrix for each of the study periods were then input into the R software package and analyzed using the Breaks for Additive Seasonal and Trend (BFAST) package using a custom script (Appendix B). The temporal decomposition used by BFAST is based on a LOESS driven STL temporal decomposition developed by Verbesselt et al. (2010a). BFAST operates effectively with missing data within a time series to produce reliable estimations of seasonal and trend components, is flexible and easy to implement, and can efficiently process large volumes of data (Hutchinson et al. 2015). BFAST also can model the trend component using either linear or nonlinear regression which permits detection of breakpoints, identify when a breakpoint occurs, and quantifying the magnitude of change associated with each abrupt change (Verbesselt et al., 2010a).

The parameters defined for BFAST include the length of the time series represented by the total number of images available, the length of the season or the number of images encompassing the complete vegetation cycle, the season model, a value (h) corresponding to the minimum time interval between potential breakpoints in the seasonal trend components or the

number of images in one vegetation cycle divided by the total number of images in the time series, and the maximum number of breakpoints (Verbesselt et al., 2010a). The h value chosen for this study was fixed at 0.1, meaning that one break point per year could be detected for a possible maximum of 15 breakpoints in the time series. The complete BFAST script, including all parameters, used in the R implementation can be found in Appendix B.

BFAST decomposed the original MOD13Q1 time series datasets into season, trend, and remainder components (Verbesselt et al., 2010a). An example of BFAST graphical output is shown in Figure 4-5. The unique contribution of BFAST to temporal decomposition is the ability to examine both long-term (interannual) linear trends and to detect abrupt intrannual changes each growing season (maximum of one significant break per season). Additional tabular output from BFAST include output values for the linear trend, the magnitude and timing of significant breaks in the trend component, and the total number of breaks for each pixel during the study period.

Figure 4-5. Example BFAST graphical ouptut showing the seasonal, trend, and noise components from the decomposed time series data. The trend component for image on the left shows a significant negative trend over time with three abrupt intrannual breaks in that trend. The trend for the image on the right show a "null" trend with a slope not significantly different from 0.

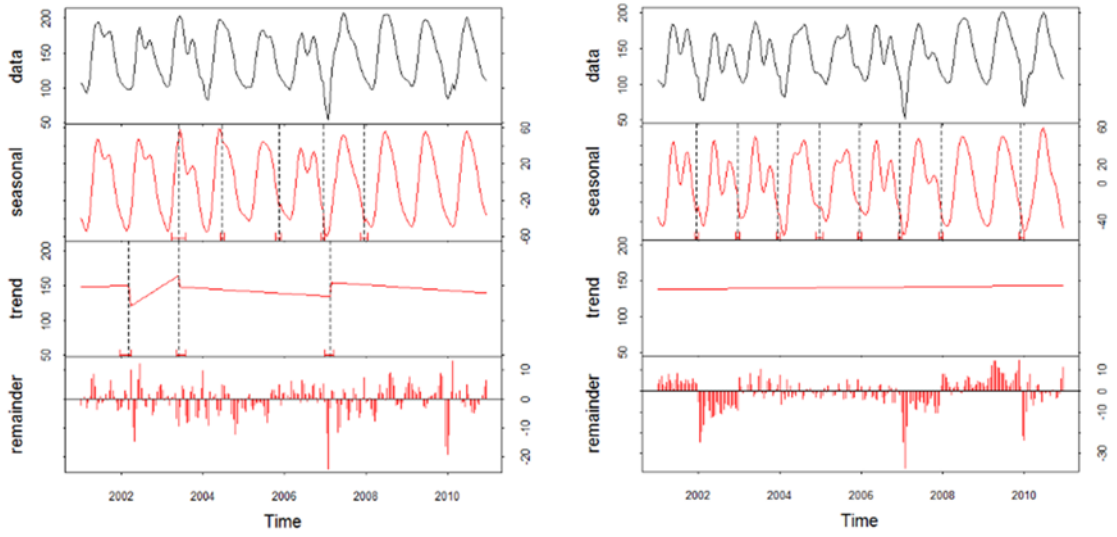

Three indicators for each pixel were calculated from the BFAST trend component. The first describes the gradual interannual vegetation greenness change and corresponds to the linear slope of the trend component across the fifteen-year study period. A statistical analysis was performed on the slope of the linear trend to test its significance against a null slope using a Student's t-test (Equation 1) where, for a given pixel, a_n is the slope of the trend, a_0 is the slope of a null trend (equal to 0), n is the number of images into the time series, x represents the time series NDVI value, and $\bar{x}$ is the mean NDVI value of the time series. Based on the statistical significance (p-value <= 0.05) and sign of the slope, all pixels were placed into three classes to interpret gradual interannual change. The remaining indicator characterizes abrupt intraannual changes as the number of significant breaks contained within the overall linear trend component.

$$t = \frac{a_n - a_0}{\frac{\sqrt{\frac{1}{n-1}\sum(x-\bar{x})^2}}{\sqrt{n-2}}} \qquad \text{Equation 1}$$

Results

The gradual interannual vegetation change classes for 2001-2015 are shown in Figure 4-6. Areas with significant directional trends are shown in green (significant positive slope) and red (significant negative slope). Areas without a significant trend (null slope) are shown in gray. Land managers looking at this picture would be able to assess the overall long-term direction of vegetation greenness across the Flint Hills region in a spatially explicit way. Areas with a positive trend in greenness are interpreted here as having vegetation that experienced improvements in greenness, health, or amount as suggested by NDVI. Conversely, those areas with negative trend declined in quality. For the Flint Hills ecoregion as a whole, 52.47% of the area experienced a negative trend in vegetation activity and greenness during the 2001-2015 period, 21.52% of the area saw increases in vegetation activity and greenness, and 26.01%

experienced no change or was stable during the same time (Table 4-1). Table 4-2 shows the amount of interannual classes each counties experienced during the study period.

Figure 4-6. Gradual interannual change classes for the Flint Hills study area derived from statistical analysis of the BFAST computed trend component for the period 2001-2015.

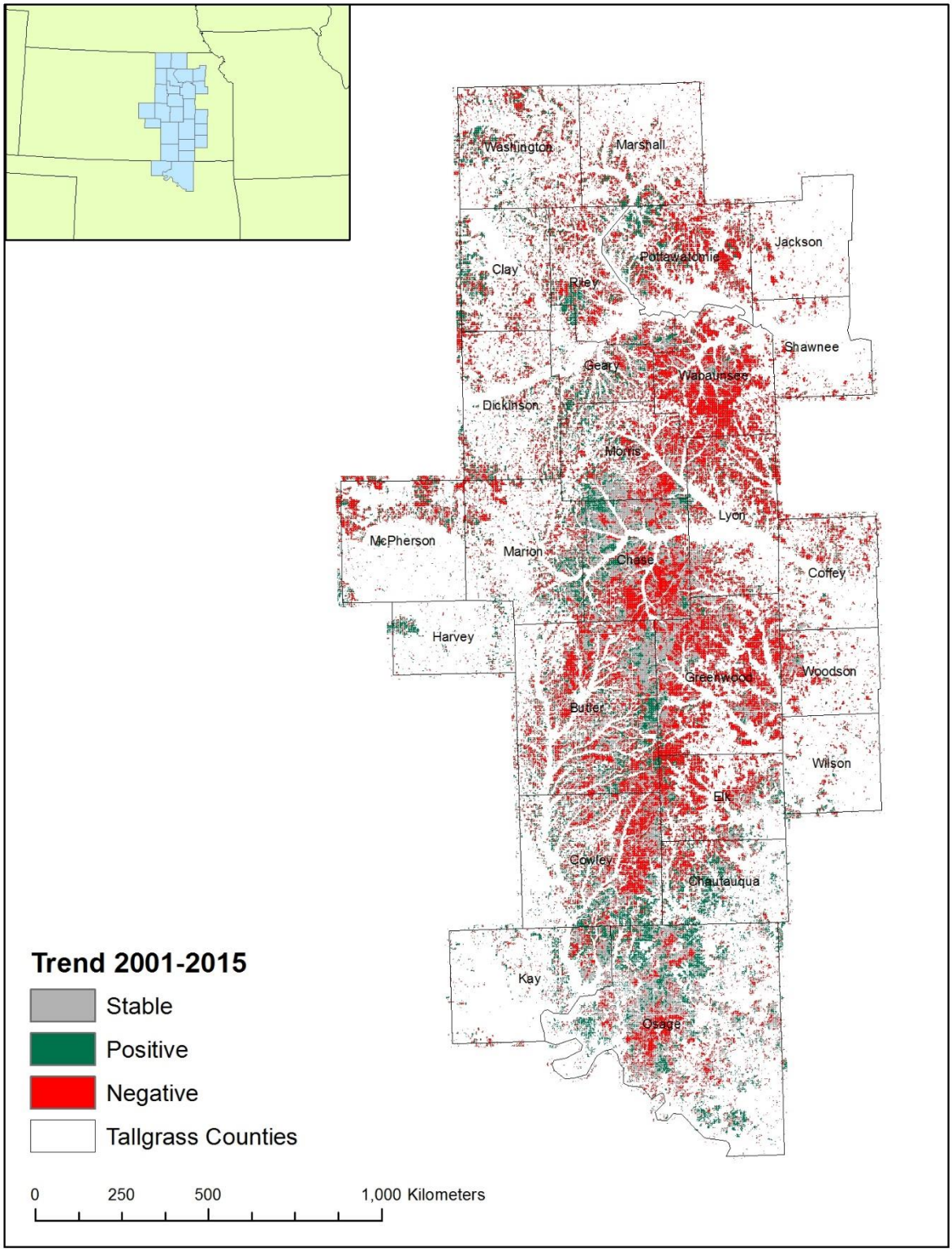

Table 4-1. Summary results for the gradual interannual trend classes for the period 2001-2015 for the Flint Hills study area based on BFAST trend component analysis.

Vegetation Gradual Interannual Change Classes			
	Negative Trend (Browning)	Positive Trend (Greening)	No Change (Stable)
No. Pixels	163,250	66,956	80,917
Area (ha)	876,075.71	359,317.15	434,238.40
% Total Area	52.47%	21.52%	26.01%

Table 4-2. Summary results for the gradual interannual trend classes for the period 2001-2015 for the Flint Hills Counties based on BFAST trend component analysis. Bold number in a trend category indicate a maximum value within the county.

NAME	Stable	Positive	Negative	Sum	% Stable	% Positive	% Negative
Butler	10972	6594	15401	32967	33.28%	20.00%	**46.72%**
Chase	10792	3679	10025	24496	**44.06%**	15.02%	40.93%
Chautauqua	2205	3604	3124	8933	24.68%	**40.34%**	34.97%
Clay	642	2548	3390	6580	9.76%	38.72%	**51.52%**
Coffey	1212	712	3106	5030	24.10%	14.16%	**61.75%**
Cowley	6088	5004	9963	21055	28.91%	23.77%	**47.32%**
Dickinson	1187	2151	4408	7746	15.32%	27.77%	**56.91%**
Elk	2863	1818	7617	12298	23.28%	14.78%	**61.94%**
Geary	1660	2077	3127	6864	24.18%	30.26%	**45.56%**
Greenwood	7197	2007	17674	26878	26.78%	7.47%	**65.76%**
Harvey	357	1032	482	1871	19.08%	**55.16%**	25.76%
Jackson	75	126	1386	1587	4.73%	7.94%	**87.33%**
Kay	2664	2185	1656	6505	**40.95%**	33.59%	25.46%
Lyon	2869	1661	9778	14308	20.05%	11.61%	**68.34%**
Marion	3006	3303	4656	10965	27.41%	30.12%	**42.46%**
Marshall	250	1369	4187	5806	4.31%	23.58%	**72.12%**
McPherson	804	1576	3717	6097	13.19%	25.85%	**60.96%**
Morris	4340	3303	7426	15069	28.80%	21.92%	**49.28%**
Osage	13929	9807	9281	33017	**42.19%**	29.70%	28.11%
Pottawatomie	957	3193	9151	13301	7.19%	24.01%	**68.80%**
Riley	940	2425	5626	8991	10.45%	26.97%	**62.57%**
Shawnee	199	170	1434	1803	11.04%	9.43%	**79.53%**
Wabaunsee	2531	778	14607	17916	14.13%	4.34%	**81.53%**
Washington	503	2897	5020	8420	5.97%	34.41%	**59.62%**
Wilson	384	487	863	1734	22.15%	28.09%	**49.77%**
Woodson	1266	360	2493	4119	30.74%	8.74%	**60.52%**

The number of significant breaks in the trend component can serve as an indicator of both the number and frequency of disturbances and might be related to fire regime. Figure 4-7 shows

the Flint Hills region with the number of significant breaks for each of the pixels. Each pixel could only have a maximum of one break for each year of the study period. Within the ecoregion, 37.86% of the area experienced zero breaks during the study period and about 30% experienced only a single break. The maximum number of breaks experienced by a pixel was seven but only 2 pixels of 311,000 had that many breaks. Figure 4-7 shows the percentage of the study area that experienced the number of breaks in trend and figure 4-8 shows a map of the breaks.

Figure 4-7. The percentage of the Flint Hills study area that experienced a different number of significant breaks within the linear trend for the 2001-2015 study period.

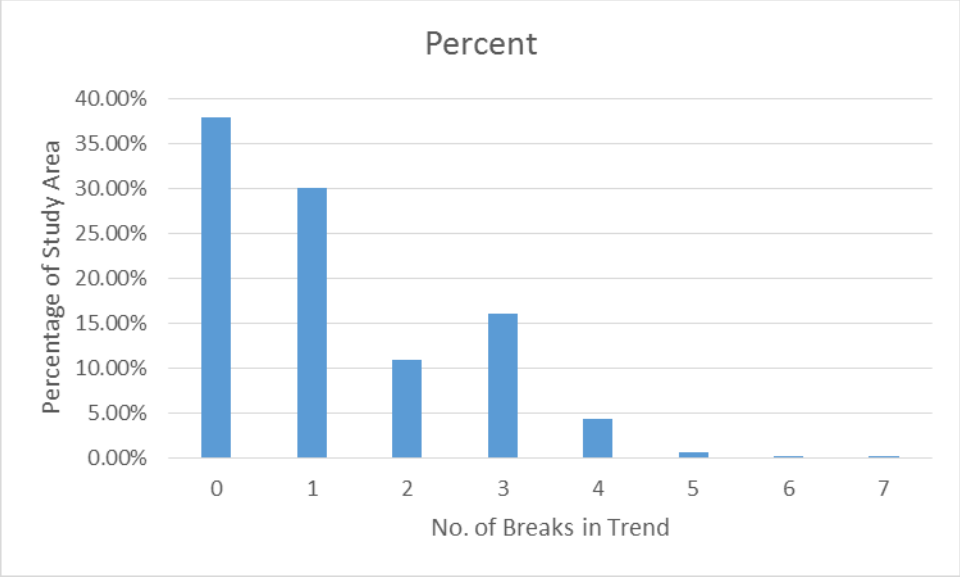

Figure 4-8**.** Shows the number of breaks for each pixel over the study period of 2001-2015. Each pixel could have one break for each year.

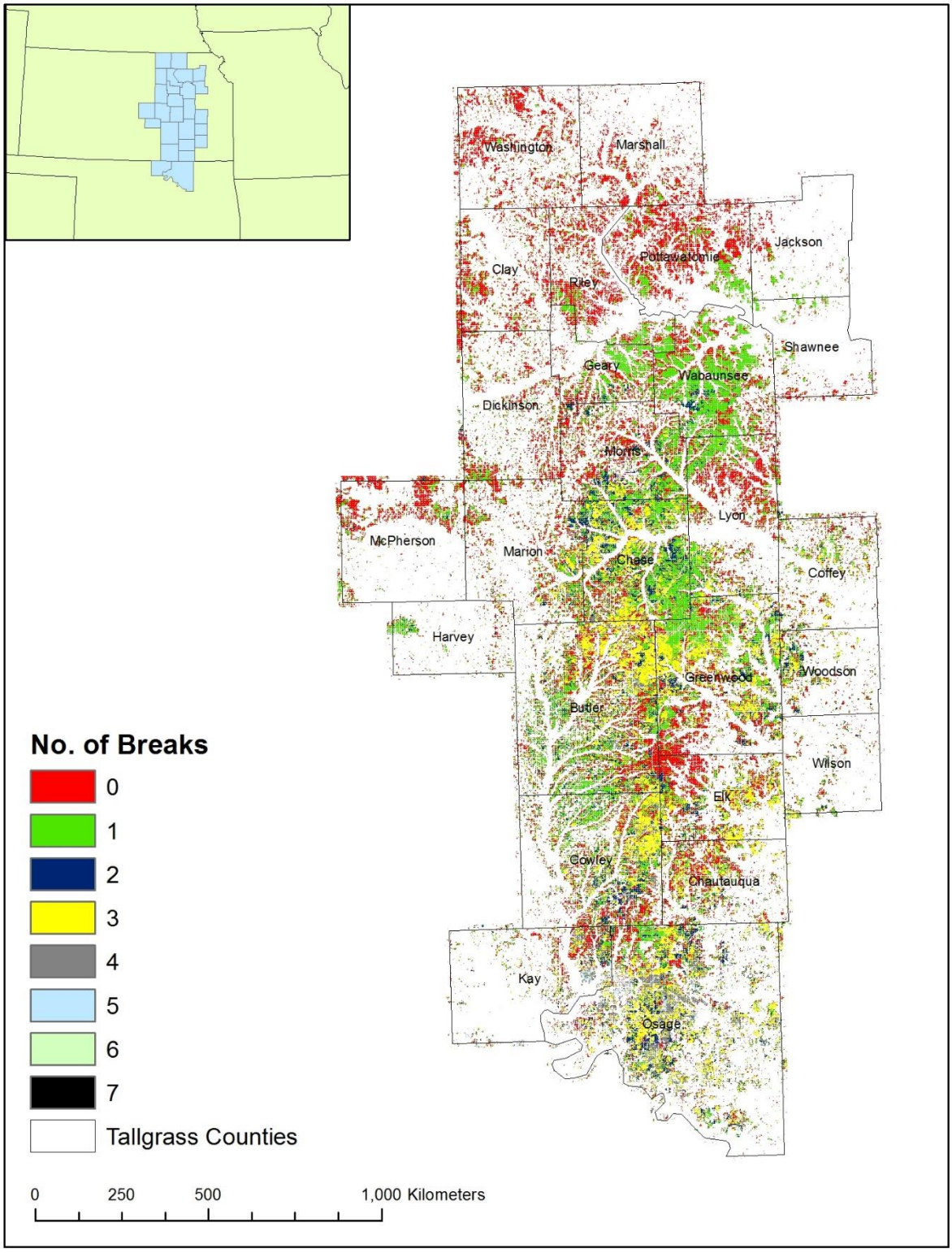

Discussion and Conclusions

Examining results from the BFAST procedure provides an interesting synoptic view of vegetation dynamics within the Flint Hills that should be of interest to land managers and land owners within the ecoregion. For the study period 2001-2015, a majority of the Flint Hills (52%) experienced a significant decline in greenness. The spatial distribution of this "browning" occurs throughout the region with no obvious spatial pattern. Counties in the central part of the Flint Hills - Greenwood, Butler, Wabaunsee, and Chase – each contained over 10,000 negative trending pixels and accounted for 36% of all negative trend pixels in the study area. Positive trending pixels comprised 22% of the study area, with Osage and Butler counties having 25% of all "greening" pixels. These counties lie in the southern area of the Flint Hills. The remaining 26% of the study area were stable (i.e., no significant negative or positive trend) and were distributed throughout the area with Osage, Butler, and Chase counties having 45% of all stable pixels in the study area.

That the majority of the Flint Hills experienced a negative trend is surprising given the burning frequencies and precipitation observed during the study period. As burning is an important and common practice in the Flint Hills to combat woody encroachment and improve forage conditions, more frequent burning was expected to correlate with areas having a positive trend. Comparing estimated trends to burn frequency data for the Flint Hills (Figure 3-4), no clear relationship appears with areas having higher burning frequencies experiencing both positive and negative trends in greenness. A closer examination of the effects of fire may be needed to explain the large percentage of the Flint Hills having a negative trend. A detailed statistical approach could be applied to evaluate the relationship between fire frequency, precipitation, and other important factors such as soils.

Examining the number of significant breaks in trend shows that 38% of the Flint Hills experienced zero disturbances. The remaining 62% of the study area had at least one break in trend during the study period. A qualitative comparison of burn maps for the Flint Hills (Figure 3-4) to BFAST-estimated breaks in trend reveals little agreement. In other words, breaks in trend do not appear to be related to disturbances caused by prescribed burning. This relationship, or lack thereof, should be explored quantitatively.

One limitation related to the use of the MOD13Q1 product is the 16-day compositing period. The timing of a fire combined with the selection of the maximum NDVI value within the 16-day interval may not be sufficient to capture the burning disturbance. If a disturbance is noted, the post-disturbance response could be manifested as both a short-term increase or decrease in trend (Hutchinson et al., 2015). For example, within the timeframe of a 16-day composite image, the warm season grasses of the Flint Hills burned in spring have sufficient time to green up. This would result in a detection of a significant positive break. Other imagery, such as daily or 8-day NDVI composite images may observe and provide better results in these circumstances.

Using MODIS images to create a vegetation index time series and utilizing BFAST with its ability to detect breaks and trend of vegetation greenness allows for consistent assessment of the grassland vegetation of the Flint Hills. Grassland managers across the Flint Hills would benefit from knowing the current greenness of their grasslands and whether that greenness is improving or declining over time. The BFAST trend analysis allows for an interesting method to characterize long-term vegetation trends as well as when and where significant breaks occur in detected trends. However, exactly what is being detected as a break in trend remains unclear.

Chapter 5 - Drivers of Long-Term Vegetation Trends for the Flint Hills Ecoregion as Detected using BFAST and Moderate Resolution Satellite Imagery

Abstract

Grasslands in the Flint Hills are often burned as a land management practice. Remote sensing can be used to help better manage prairie landscapes by providing useful information about the long-term trends in grassland vegetation greenness and help quantifying regional differences in vegetation development. Using MODIS 16-day NDVI composite imagery between the years 2001-10 for the entire Flint Hills ecoregion, BFAST was used to determine trend, seasonal, and noise components of the image time series. To help explain the trend, four factors were considered including hydrologic soil group, burn frequency, and cumulative differences between annual and normal (1982-2010) precipitation (precipitation deviation). For the study period, the area of negatively and positively trending grassland were similar (41-43%). Logistic regression showed that the log odds of a pixel experiencing a negative trend were higher in sites with clay soils and higher burning frequencies and lower for pixels having higher than normal precipitation and loam soils.

Introduction

Grasslands and savannas make up more than 40% of the earth's surface and their rapid response to changes in land management and climate can have dramatic ecological and social consequences (Briggs et al., 2005). Grasslands are among the most biodiverse and productive of all the earth's terrestrial biomes but receive low levels of protection (Mark and McLennan, 2005). Since 2009, 53 million acres of grassland, roughly the area of Kansas, have been converted to cropland across the Great Plains alone (Plowprint Annual Report, 2016). Tallgrass

prairie has been reduced to ~4% of its historical extent making it one of the most altered ecosystems in North America (Ratajczak et al., 2016). Temperate grasslands are important for both agronomic and ecological purposes and are a key resource for livestock production in North America and around the world (Briggs et al., 2005). Grasslands provide services such as water storage and clean air (Plowprint Annual Print, 2016) and grassland vegetation reduces soil erosion due to it dense root systems and by shielding the soil surface from direct interception of rainfall (Ratajczak et al, 2016). Grasslands also store and retain large amounts of soil carbon and are an important component of the global carbon cycle (Briggs et al., 2005). The estimated values of theses, and other, ecosystems services provided by native grasslands has been estimated to be in excess of $5,000 per hectare per year (Dodds et al., 2008).

The conservation status of grasslands is being evaluated by groups including the Landscape Conservation Cooperatives which seeks to identify the greatest threats to grasslands and shrublands across the U.S. and Mexico, areas that are likely to be resilient to climate change and other threats, and areas with high potential for restoration (Glaser, 2014). The state of North American prairies is also being addressed through a tri-national cooperative program involving Mexico, the USA, and Canada which is attempting to address both sustainable management and conservation needs (Mark and McLennan, 2005). The Flint Hills ecoregion in Kansas and Oklahoma remain one of the last great expanses of intact and native tallgrass prairie in the United States. The creation of the Tallgrass Prairie National Preserve in 1996 allowed for more area of the Flint Hills to retain its native character.

Grasslands have been under threat in the United States as well as throughout the world due to conversion to row-crop agriculture and changing land management coupled with other global change phenomena (Briggs et al., 2005). A majority of the former area of the tallgrass

prairie has been replaced with crops such as wheat, corn, and soybeans (Plowprint Annual Print, 2016). The remaining tallgrass prairies of North America are threatened by an increase over time in the abundance of native woody species, such as the red cedar (*Juniperus virginiana)* in the Flints Hills area (Hulbert, 2009). These woody plants originate both from within the ecosystem and from neighboring ecosystems (Briggs et al., 2005), with encroachment altering the structure and function of temperate grassland ecosystems and resulting in a loss of biodiversity and grazing productivity (Ratajczak et al., 2016). The likely drivers of this increase in woody plant abundance are numerous and include change in climate, atmospheric carbon dioxide concentration, nitrogen deposition, grazing pressure, and disturbance regimes (e.g., the frequency and intensity of fire) (Briggs et al., 2005). Transitions to shrubland and woodland in temperate climates are largely attributed to changes in fire management (Ratajczak et al., 2016). Comparisons of the area occupied by forest at the time of settlement, as recorded in the 1856 Land Office, with that in the 1970's showed that on frequently burned prairies woody plants occupied about the same area today as over a century ago. However, on sites not burned for 20 years or longer, forests had invaded on half or more of the unburned areas (Hulbert, 2009).

Fire is an integral component of prairie development and maintenance and for more than 7000 years vegetation patterns have been influenced by anthropogenic burning practices (Towne and Kemp, 2003). Fire has long been recognized as an important factor influencing the development and persistence of the tallgrass prairie ecosystem (Benson and Hartnett 2006). Fire is both an inexpensive and effective way of controlling woody species and shrubs as well as maintaining high quality nutritious forge for grazers, but air pollution from the smoke can negatively impact cities downwind of the fires (Briggs et al., 2005). Prairie fires were suppressed during European settlement with accidental or lightning-caused wildfires being the

primary source of burning (Towne and Kemp, 2003). An influx of cattle to the Flint Hills in the late 1800's created an incentive for prairie burning and pastures were burned annually in February or March to improve livestock weight gains (Towne and Kemp, 2003).

Annual or biennial burning, which is currently a common land management practice in tallgrass prairie, homogenizes the canopy over the long term by suppressing invasion by woody species while promoting a variety of C3 forbs amidst a matrix of C4 graminoids (Goodin and Henebry, 1998) (Benson and Hartnett 2006). Warm season grasses have been shown to increase after burning has been conducted (Towne and Kemp, 2003) (Hulbert, 2009) and average peak-season aboveground biomass on annually burned prairie is reported to be nearly twice that of infrequently burned prairie (Benson and Hartnett 2006). Species diversity is lowest with annual late-spring burning and increases with increasing intervals between fires (Hulbert, 2009).

At the Konza Prairie Biological Station, it has been observed that vegetation development starts earlier on plots burned in November than on those burned in March (Hulbert, 2009). This is likely due to higher soil temperatures on burned areas, resulting from greater solar heating as a response to removal of the insulating layer of standing dead vegetation (Hulbert, 2009). A burning frequency of 3 to 4 years has been thought to be the historical fire frequency before extensive settlement by Europeans (Briggs et al., 2005). Burning once every 4 years has been shown to increase the number of forb and annual species compared to that seen in annually burned sites (Collins et al., 1995). A complete exclusion of fire in tallgrass prairie has been shown to significantly decrease the grass bud bank while increasing the forb bud bank (Dalgleish and Hartnett, 2008). Prairie that is burned at an intermediate fire frequency showed greater year-to-year variability in grass bud bank size and in the probability of emergence from the bud bank than annually burned prairie (Dalgleish and Hartnett, 2008).

Cattle ranchers in the Flint Hills employ frequent spring burns to remove dead litter and enhance palatability, leading to greater and more consistent weight gain in cattle (Ratajczak et al., 2016). These fires help to reduce species such as buckbrush (*Ceanothus cuneatus)* or coralberry (*Symphoricarpos orbiculatus)* (Hulbert, 2009). Annual spring burning is beneficial in stopping woody encroachment but also can homogenize plant and avian communities (Collins et al., 1995) (Ratajczak et al., 2016). In addition, it has been shown that annual burning does not eliminate shrubs and, over time, this buildup of shrubs can lead to areas where woody vegetation becomes established and later spreads (Towne and Kemp, 2003). Fire alone does not stop the invasion of woody plants. The combination of fire, climate, substrate, and topography are what makes the prairie (Hulbert, 2009).

Depending on the definition used for the Flint Hills, the amount and frequency of burning varies on a yearly basis. Mohler and Goodin (2012) showed that as much as 31% of the Flint Hills grasslands were burned in 2005 and the Nebraska Department of Environment and Quality puts the figure at 48%. (NDEQ, 2016). In 2007, roughly 10-14% of Flint Hills grasslands were burned. About 8% of the grassland within the Flint Hills was burned once during the 2000-2010 time period while less than 1% were burned ten times during the same period (Mohler and Goodin, 2012).

The Kansas Department of Health and Environment has developed the Flint Hills Smoke Management Plan to combat smoke conditions caused during the burning season. Their website, www.ksfire.org, seeks to inform land managers conducting prescribed burns in the Flint Hills by providing information and access to tools to assist with burn decisions. The Flint Hills Smoke Management Plan began in fall 2013when air quality monitors in the Kansas City area recorded very high ozone readings on April 12 and April 13 (KDHE, 2010). Three monitors in Kansas

City, Missouri recorded readings that exceeded the federal 8-hour ozone standard and states as far away as Tennessee were impacted with poor air quality and high ozone concentrations (KDHE, 2010). In Nebraska, the cities of Omaha and Lincoln have also been impacted by burning in the Flint Hills with several days of violating air quality standards (NDEQ, 2016).

Because the Flint Hills Smoke Management Program is entirely voluntary, there is no way for the states of Kansas or Nebraska (or any other states) to exercise control over prescribed burning (NDEQ, 2016). States that are downwind have no input into prescribed burning activities and only have the ability to react to air quality conditions that result from the Flint Hills fires and issue air quality advisories as conditions dictate.

Healthy vegetation in the Flint Hills is essential for cattle ranchers and the overall health of the Flint Hills ecoregion. Degradation of vegetation greenness results from gradual or abrupt changes in the amount of vegetation activity over time which can be monitored by collecting and analyzing time-series Normalized Difference Vegetation Index (NDVI) data from medium or course spatial resolution satellites (Verbesselt et al., 2010a). Time series datasets using NDVI products from the Moderate Resolution Imaging Spectrometer (MODIS) sensor have been used to successfully quantify vegetation activity and vegetation dynamics (Zhang et al., 2003).

Past methods used for analyzing trends in continuous vegetation time series data include gradual interannual vegetation change due to rainfall variability and drought (Jacquin et al., 2010), temporal decomposition techniques which have been shown relevant to the study of vegetation seasonality (Jonsson and Eklundh, 2002), and abrupt vegetation change seen at the intraannual time scale caused by disturbances such as deforestation, disease and insect outbreaks, fire, and other activities (Verbesselt et al., 2010a).

Temporal decomposition of data involves separating an original time series dataset into three different components in order to study each related to vegetation greenness at different time scales (Cleveland and Delvin, 1988). These include seasonal, trend, and remainder, residual remaining after elimination of the trend and the seasonal components.

Two categories of methods exist to extract the trend component from a time series. In the first category, the trend component takes the shape of a known function and a regression model is fitted to the data using the least squares approach. This method may result in a model that may not reflect reality as trends cold exhibit changes over time (Slayback et al., 2003). The second category of methods, the trend component is not assumed to follow a shape and cannot be modeled using a predefined function. Instead, the trend component is obtained via local smoothing using different techniques (Hutchinson et al., 2015). This approach is better adapted to data with one or more slope changes, or breaks, in the trend component over time. After extracting the trend component from time series datasets, information can be derived that identifies and characterized changes in the trend, including the length of the time series, the magnitude of the slope value indicating amplitude of change, and the sign of the slope signifying the direction of change (Verbesselt et al., 2010a).

This study builds from the previous success of studies done on military training ground at Fort Riley Kansas where Breaks For Additive Seasonal and Trend (BFAST) was used to examine seasonal trends of vegetation (Hutchinson et al., 2015). The BFAST method was used because of its ability to account for seasonality and to detect gradual (interannual) and abrupt (intraannual) changes within the trend component (Verbesselt et al., 2010a). Other methods such as Seasonal-Trend decomposition procedure (STL) based on a Locally wEighted regression

Smoother (LOESS) were excluded from consideration due to its ability to detect only gradual changes in the trend component (Cleveland et al., 1990).

Tests for statistical significance have been performed to determine how multiple factors influence the trend of vegetation greenness. Generalized linear models (GLM) have been used to explain trends by fire regime and stratification (Jacquin et al., 2016). GLMs are a generalization of linear regression models, allowing various distributions for the response and error terms in models (Augustin et al., 2001). A logistic regression form of GLM can be fitted to a model to determine the significance of different variables.

This study investigates the use of BFAST and a MODIS NDVI image time series to examine gradual and abrupt changes in the Flint Hills ecoregion of Kansas and Oklahoma. This work helps to extend the application of BFAST to the grassland ecosystem as well as seek to explain the trend patterns observed in the Flint Hills ecoregion using burn frequency, precipitation deviation, and hydrological groups.

Study Area

The study area for this project is the 26 counties of Kansas and Oklahoma containing the Flint Hills eco-region of eastern Kansas and north Oklahoma (Figure 5-1). The Flint Hills encompass an area of 1.6 million hectares and contain the largest area of unplowed tallgrass prairie in North America (Hutchinson et al., 2015). The World Wildlife Fund's Terrestrial Ecoregions of the United States and Canada defines the Flint Hills as the area covering the Flint Hills of Kansas and the Osage Plains of northeastern Oklahoma. The Flint Hills is the smallest grassland ecoregion in North America and can be distinguished from other grassland associations by the dominance of tallgrass species and from the Central Tall Grasslands to the north by its

lack of variety of biota and a thin soil layer spread over distinct beds of limestone. These Flinty beds of limestone, from which the name of this ecoregion is derived, rendered large area unsuitable for corn or wheat farming, resulting in an unplowed, though heavily grazed, remnant of the tallgrass prairie (Madson 1993). Unlike many other ecoregion classifications, which are based primarily on biophysical features such as climate and topography, World Wildlife Fund's ecoregions include biogeographic knowledge and therefore reflect the historic events and processes that have shaped biodiversity distribution (McDonald et al., 2005).

Figure 5-1. The Flint Hills study area showing the 26 counties comprising the ecological region in eastern Kansas and north-central Oklahoma.

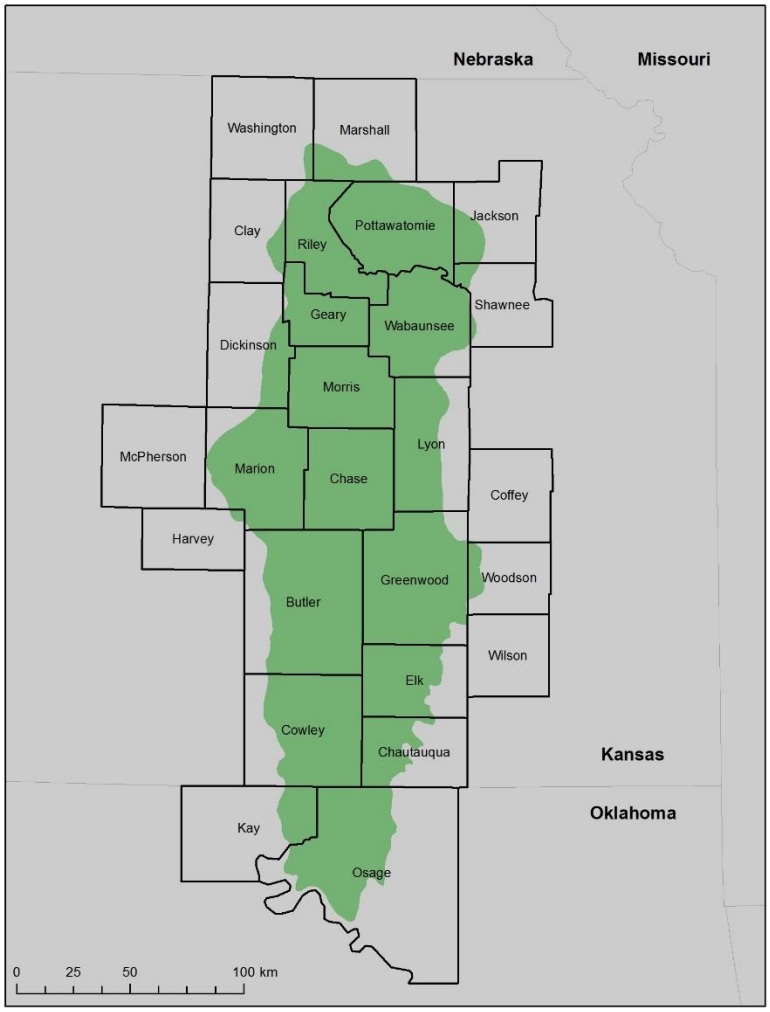

The definition for the Flint Hills that will be used in this study is provided by the U.S. Environmental Protection Agency (EPA) which defined ecoregions based on work derived from Omernik (1987) which seeks to serve as a spatial framework for environmental resource management. The map of U.S. ecoregions was compile based on the premise that ecological regions can be identified through the analysis of the patterns and the composition of biotic and abiotic phenomena that affect or reflect difference in ecosystem quality and integrity (Omernik, 1987). Such phenomena include geology, physiography, vegetation, climate, soils, land use, wildlife, and hydrology. The relative importance of each characteristic varies from one ecological region to another regardless of the hierarchical level (Wilken 1986). The EPA ecoregions use a Roman numeral classification scheme with level I being the coarsest level, dividing North America into 15 ecological regions, level II divides the continent into 52 regions and level III and IV further breaking down the ecoregions. The EPA definition of the Flint Hills is the same for level III and IV with Level III being used for the purposes of this study.

Precipitation for the Flint Hills region is highly variably from year to year. Based on 30 year normal precipitation (1981-2010) (http://prism.oregonstate.edu), the northern parts of the Flint Hills receives 720 mm (28 in) of precipitation and the southeastern parts receive 1120 mm (44 in) of precipitation. Much of the precipitation falls during the growing season (approximately 75%), though this varies from year to year (Hayden 1998). Temperature varies within the region throughout the year with cool winters and hot summers. The City of Manhattan, Kansas in the northern section of the Flint Hills, averages -1.8 C in January and 26.5 C in July while the southern sections of the study area experience an average temperature of 1.1 C in January and 27.2 C in July.

Ranching is commonly practiced within the Flint Hills and these ranchers will periodically burn there land in a land management method called prescribed burning (Wilgers and Horne, 2006). Burning of the tallgrass prairie has been shown to increases plant productivity, decrease aboveground litter, and decrease woody vegetation (Briggs and Knapp, 1995). The frequency of burning in the Flint Hills has changed in recent years. Beginning in the 1980's, a switch in cattle grazing practices caused the rangelands to be annually burned while areas around populated areas often remained unburned for extended periods of time (Robbins et al., 2002). These different fire regimes may contribute to trends in vegetation.

In addition to the tallgrass prairie, several other land cover types can be found in the Flint Hills (See figure 5-2). Croplands are found in the flat floodplains along the streams and rivers. Gallery forests can also be found along the streams and rivers. Trees can be found in the upland areas where fire and grazing have been suppressed. Figure 5.3 shows the study area with only the grassland areas examined. The pixels were determined to be grassland if they contained over80% grassland land cover based on the 2010 national land cover database.

Figure 5-2. Land use/land cover within the counties comprising the Flint Hills ecoregion study area (NLCD 2011).

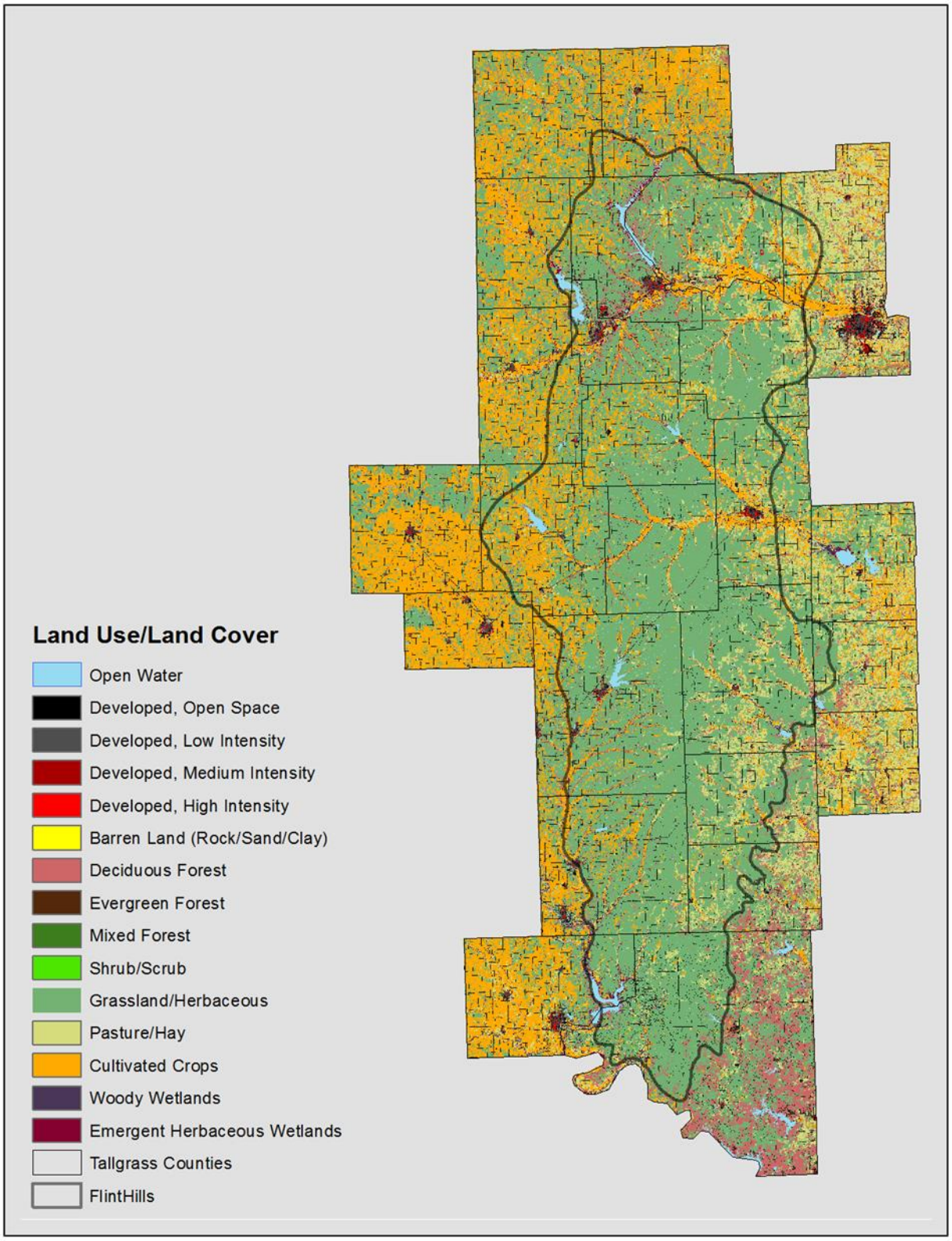

Figure 5-3. The Flint Hills ecoregion study area emphasizing grassland pixels. Each pixel corresponds to the spatial resolution of the MODIS MOD13Q1 product and consists of a minimum of 80% grassland/herbaceous cover.

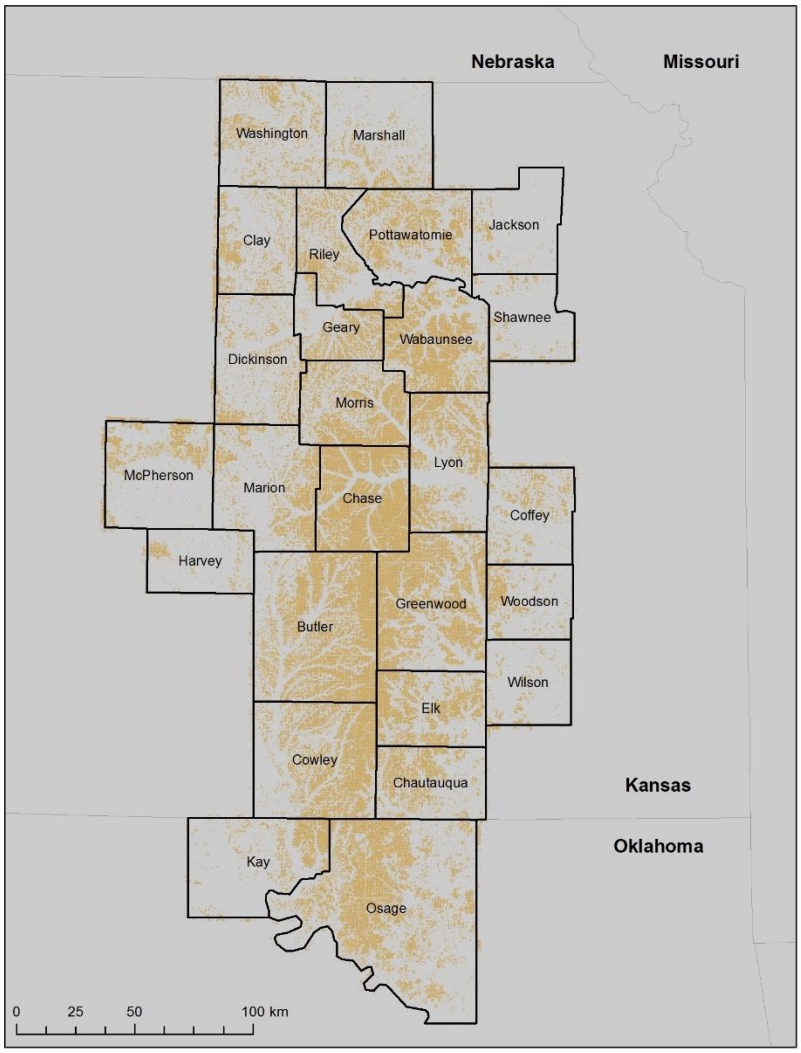

Prescribed burning preserves and sustains the tallgrass prairie ecosystem. Burning is an effective land management practice for stopping woody vegetation from encroaching on grasslands. Tallgrass prairies of North America are threatened by an increase in the abundance of native woody species, such as the Red Ceder in the Flints Hills area (Hulbert, 2009). These woody plants originate both from within the ecosystem and from neighboring ecosystems (Briggs et al., 2005). This woody encroachment alters ecosystems structure and functions of

temperate grasslands, resulting in a loss of biodiversity and grazing productivity (Ratajczak et al., 2016). The likely drives of the increase in woody plant abundance are numerous and include change in climate, atmospheric carbon dioxide concentration, nitrogen deposition, grazing pressure, and disturbance regimes (e.g. the frequency and intensity of fire) (Briggs et al., 2005). Transitions to shrub land and woodland in temperate climates are largely attributed to changes in fire management (Ratajczak et al., 2016).

Annual spring burning is beneficial in stopping woody encroachment but also can homogenize plant and avian communities (Collins et al., 1995) (Ratajczak et al., 2016). Fire and grazing treatments that promote uniformity cannot maintain biodiversity in tallgrass ecosystems (Fuhlendorf et al. 2006). In addition, it has been shown that annual burns do not eliminate shrub species and a buildup of shrubs may lead to areas where woody vegetation may gain a foothold and spread (Towne and Kemp, 2003). Another negative impact of burning is when large areas are burned, nearby towns and cities suffer air quality issues from particulates released during burning (Dennis et al. 2002).

Figure 5-4. The frequency of burning within the Flint Hills from 2001-2010. The original data from Mohler and Goodin (2012) was subset to include only the 2001-2010 data.

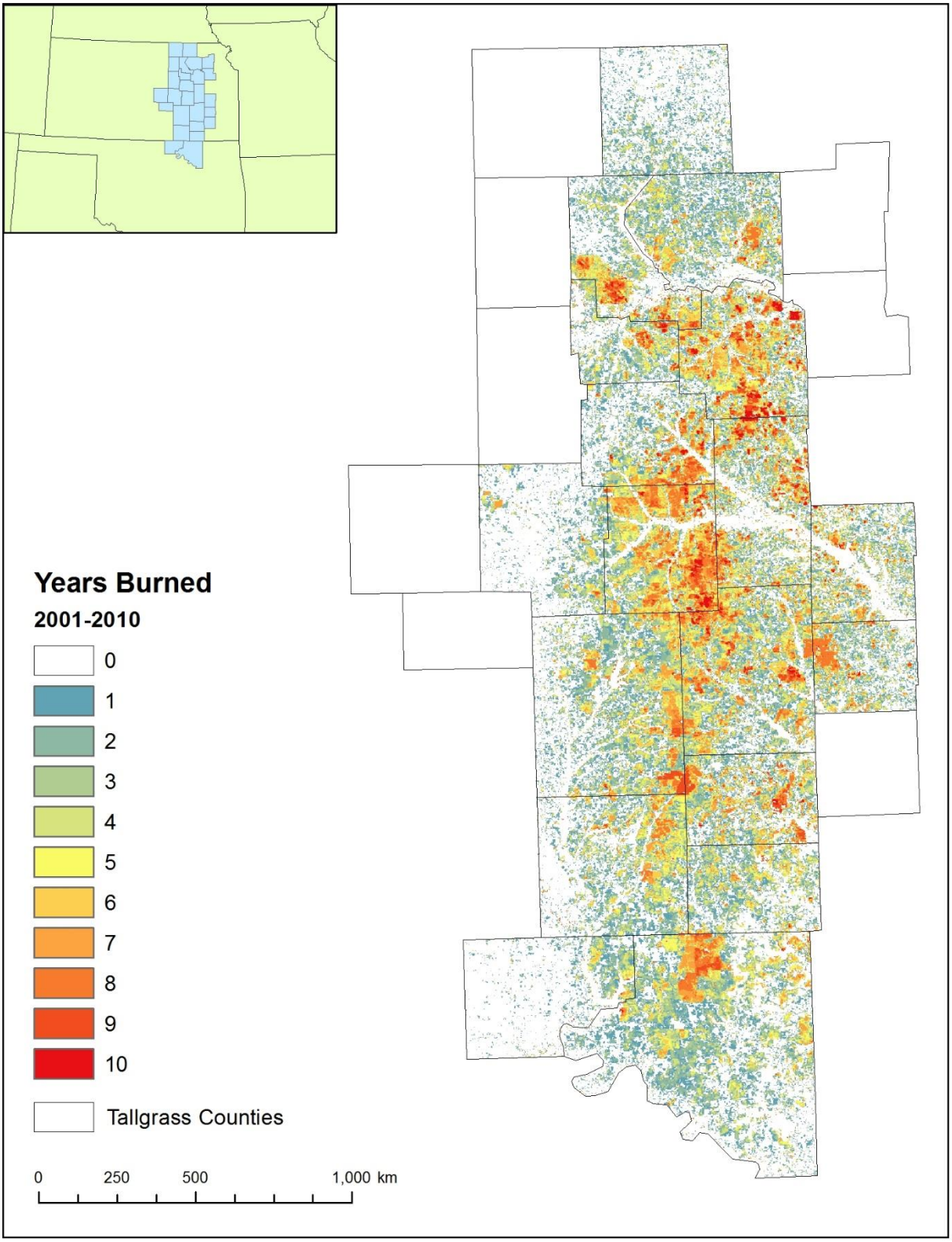

Data and Methods

The remote sensing data used for analysis were MODIS MOD13Q1 16-day maximum composite NDVI value image products for the period 2001-2015. A total of 23 composite images produced each year, resulting in a total number of 345 images for the study period. MODIS MOD13Q1 images are a gridded level 3 product delivered in a sinusoidal projection and have a 250 meter spatial resolution. The images acquired came in calibrated and geolocated form based on grid and angular data, masked from cloud, land/water, perceptible water and aerosol products, incorporate spectral reflectance, and undergo quality assurance flags associated with atmospheric correction products (Huete et al., 2002).

Images were downloaded from the Earth Observing System Data and Information System (EOSDIS) and saved as an 8-bit unsigned integer grid. Due to the nature of the sensor and the curvature of the Earth, the MOD13Q1 spatial resolution for the study area was 231.656 meters. After download, all images were clipped to the spatial extent of the 26 county study area and reprojected into the UTM Zone 14N NAD 83 spatial reference (940 Columns, 1840 Rows).

For this study, only grassland areas were analyzed. Using the 2011 NLCD product, pixels of the "grassland/herbaceous" class were extracted from the original dataset which was produced using Landsat data and has a 30 meter spatial resolution. This 30 meter resolution grassland data was then rescaled to match the spatial resolution of the MOD13Q1 image. Only rescaled pixels comprised of a minimum of 80% of the original NLCD grassland/herbaceous class were retained for further analysis (see Figure 5-3). Once the rescaled grassland "dominant" grid was constructed, the 8-bit NDVI values for the entire MOD13Q1 time series was extracted (Figure 5-5) and stored in a text (CSV) file, resulting in a matrix of values consisting of approximately 311,000 pixels by 230 (2001-2010) NDVI data points.

Figure 5-5. Shows a point shapefile overlaid on MODIS NDVI values.

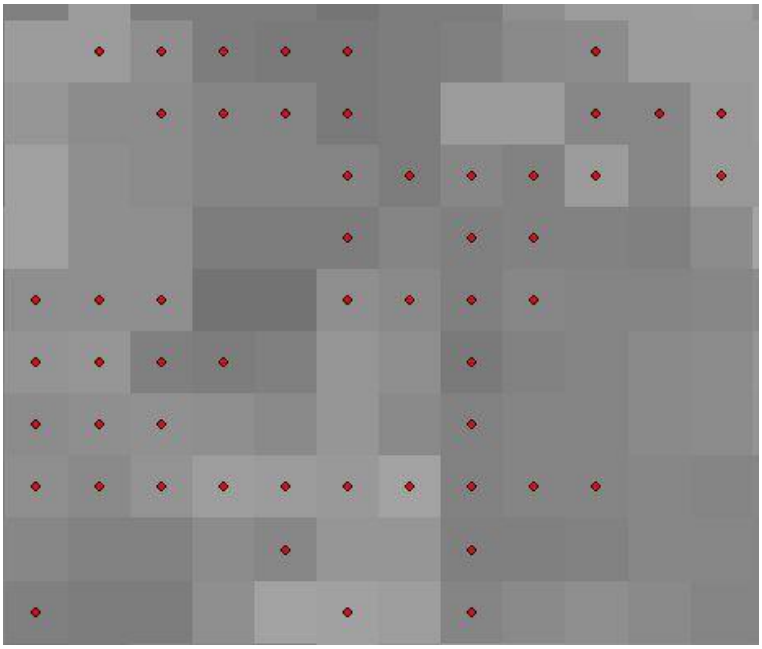

The extracted NDVI data matrix for each of the study periods were then input into the R software package and analyzed using the Breaks for Additive Seasonal and Trend (BFAST) package using a custom script (Appendix B). The temporal decomposition used by BFAST is based on a LOESS driven STL temporal decomposition developed by Verbesselt et al. (2010a). BFAST operates effectively with missing data within a time series to produce reliable estimations of seasonal and trend components, is flexible and easy to implement, and can efficiently process large volumes of data (Hutchinson et al. 2015). BFAST also can model the trend component using either linear or nonlinear regression which permits detection of breakpoints, identify when a breakpoint occurs, and quantifying the magnitude of change associated with each abrupt change (Verbesselt et al., 2010a).

The parameters defined for BFAST include the length of the time series represented by the total number of images available, the length of the season or the number of images encompassing the complete vegetation cycle, the season model, a value (h) corresponding to the minimum time interval between potential breakpoints in the seasonal trend components or the

number of images in one vegetation cycle divided by the total number of images in the time series, and the maximum number of breakpoints (Verbesselt et al., 2010a). The h value chosen for this study was fixed at 0.1, meaning that one break point per year could be detected for a possible maximum of 10 breakpoints in the time series. The complete BFAST script, including all parameters, used in the R implementation can be found in Appendix B.

BFAST decomposed the original MOD13Q1 time series datasets into season, trend, and remainder components (Verbesselt et al., 2010a). An example of BFAST graphical output is shown in Figure 5-6. The unique contribution of BFAST to temporal decomposition is the ability to examine both long-term (interannual) linear trends and to detect abrupt intrannual changes each growing season (maximum of one significant break per season). Additional tabular output from BFAST include output values for the linear trend, the magnitude and timing of significant breaks in the trend component, and the total number of breaks for each pixel during the study period.

Figure 5-6. Example BFAST graphical output showing the seasonal, trend, and noise components from the decomposed time series data. The trend component for image on the left shows a significant negative trend over time with three abrupt intrannual breaks in that trend. The trend for the image on the right show a "null" trend with a slope not significantly different from 0.

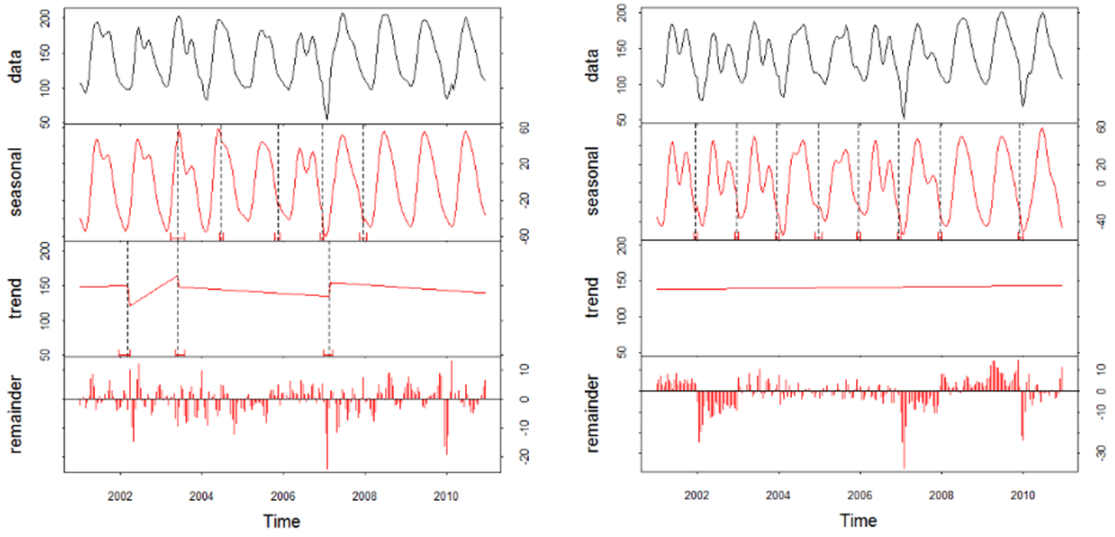

Three indicators for each pixel were calculated from the BFAST trend component. The first describes the gradual interannual vegetation greenness change and corresponds to the linear slope of the trend component across the fifteen-year study period. A statistical analysis was performed on the slope of the linear trend to test its significance against a null slope using a Student's t-test (Equation 1) where, for a given pixel, an is the slope of the trend, a0 is the slope of a null trend (equal to 0), n is the number of images into the time series, x represents the time series NDVI value, and $\bar{x}$ is the mean NDVI value of the time series. . Based on the statistical significance (p-value <= 0.05) and sign of the slope, all pixels were placed into three classes to interpret gradual interannual change. The remaining indicator characterizes abrupt intraannual changes as the number of significant breaks contained within the overall linear trend component.

$$t = \frac{a_n - a_0}{\frac{\sqrt{\frac{1}{n-1}\sum(x - \bar{x})^2}}{\sqrt{n-2}}}$$ Equation 1

To help explain the trends in vegetation greenness over the study period, precipitation deviation, soil hydrologic group, and burn frequency were used as explanatory variables in a logistic regression model.

Average annual precipitation for the most recent climate normal period (1981-2010) was obtained from the PRISM Climate Group (http://www.prism.oregonstate.edu) (Figure 5-7). Annual precipitation for each individual year from 2001-2010 were also acquired from PRISM. Annual precipitation for each year was subtracted from the normal to calculate a measure of precipitation deviation from normal. Annual deviations from normal were then summed to obtain a single precipitation deviation map for the Flint Hills study area over the study period (Figure 5-8).

Figure 5-7. Annual normal precipitation for the Flint Hills study area for the period 1981-2010 (PRISM Climate Group, http://www.prism.oregonstate.edu).

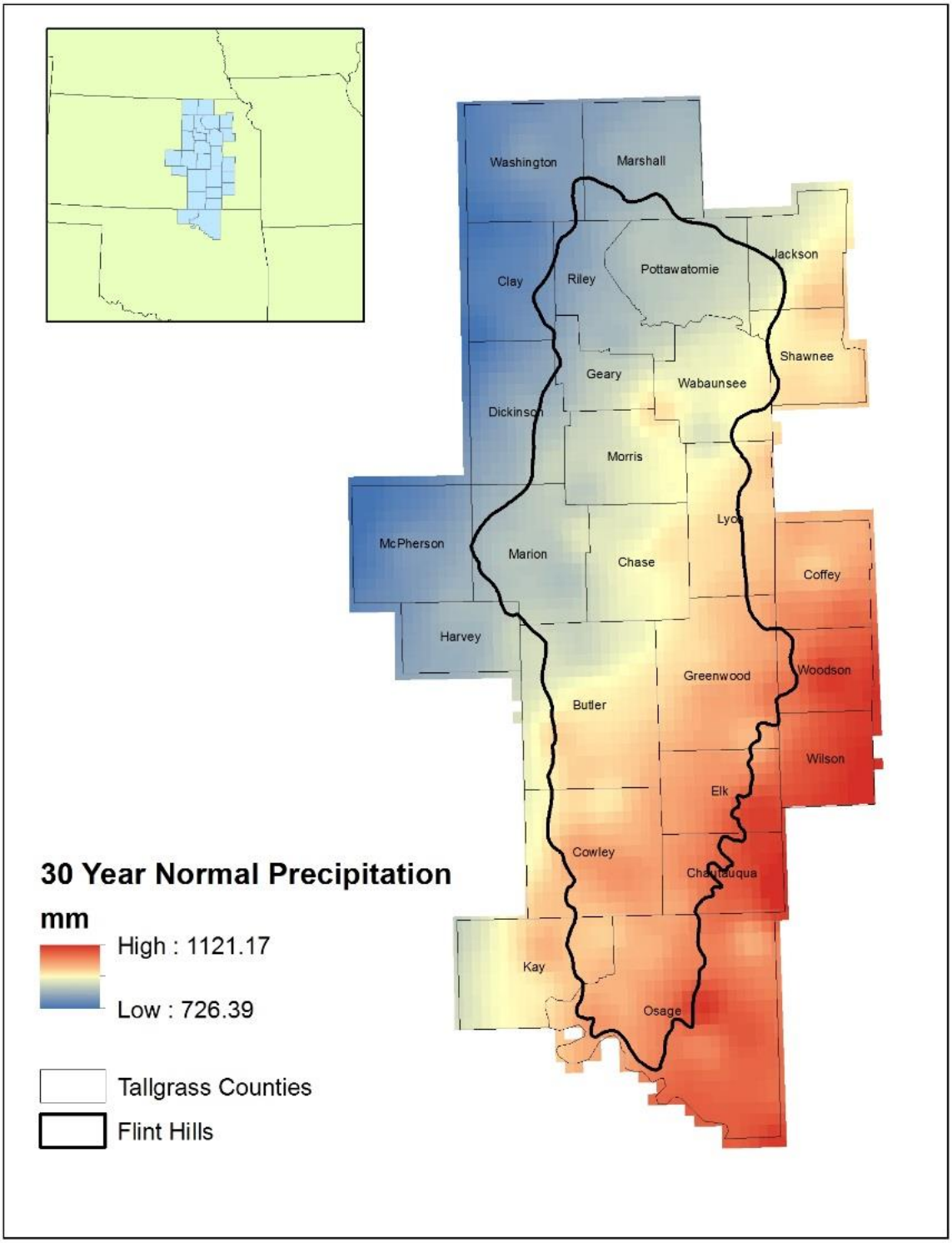

Figure 5-8. Cumulative differences between annual and normal (1981-2010) precipitation (precipitation deviation) for the 2001-2015 period.

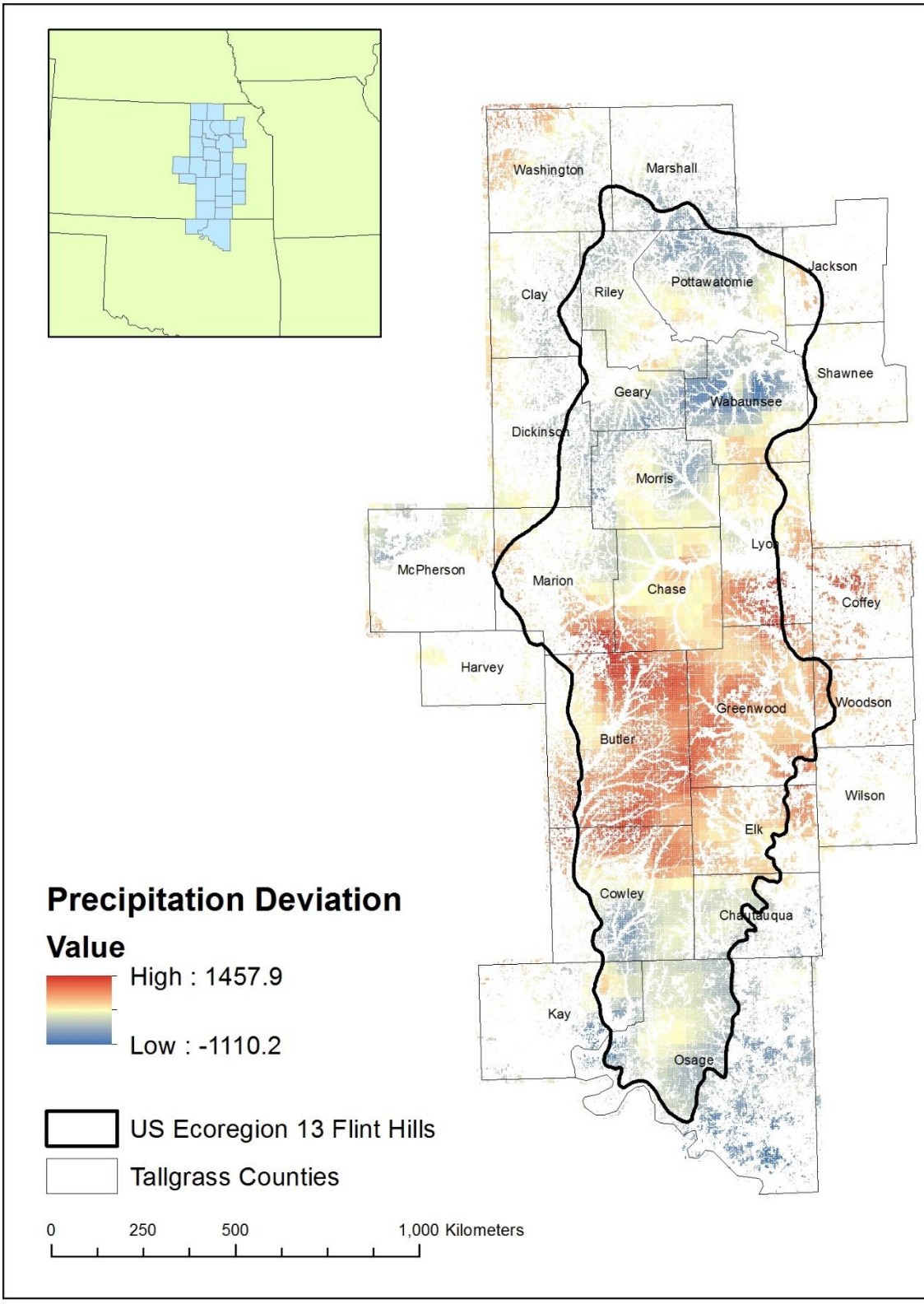
Washington
Marshall
Clay
Riley
Pottawatomie
Jackson
Shawnee
Geary
Wabaunsee
Dickinson
Morris
Lyon
McPherson
Marion
Chase
Coffey
Harvey
Greenwood
Woodson
Butler
Wilson
Elk
Cowley
Chautauqua
Kay
Osage
Precipitation Deviation
Value
High : 1457.9
Low : -1110.2
US Ecoregion 13 Flint Hills
Tallgrass Counties
0
250
500
1,000 Kilometers

Hydrologic soil group data was obtained from the U.S. Department of Agriculture (USDA) Natural Resources Conservation Service (NRCS) using the Digital General Soil Map of the United States, or STATSGO2, inventory of soils and non-soil areas that can be mapped at a scale of 1:250,000 (STATSGO2 metadata) STATSGO2 was released in July 2006 and differs from the original STATSGO in that individual state legends were merged into a single national legend, line-join issues at state boundaries were resolved, and some attribute updates and area updates were made.

Hydrologic soil group classes are used to help compute surface water runoff using the NRCS Curve Number Method. Soil classes (e.g., A, B, C, and D) are based on the minimum annual steady ponded infiltration rate for a bare ground surface (STATSGO2 metadata). Figure 5-9 shows the types of soils by texture comprising each class. Dominant hydrologic soil groups within the Flint Hills are the C and D classes (Figure 5-10).

Figure 5-9. Soil types by texture comprising each hydrologic soil group.

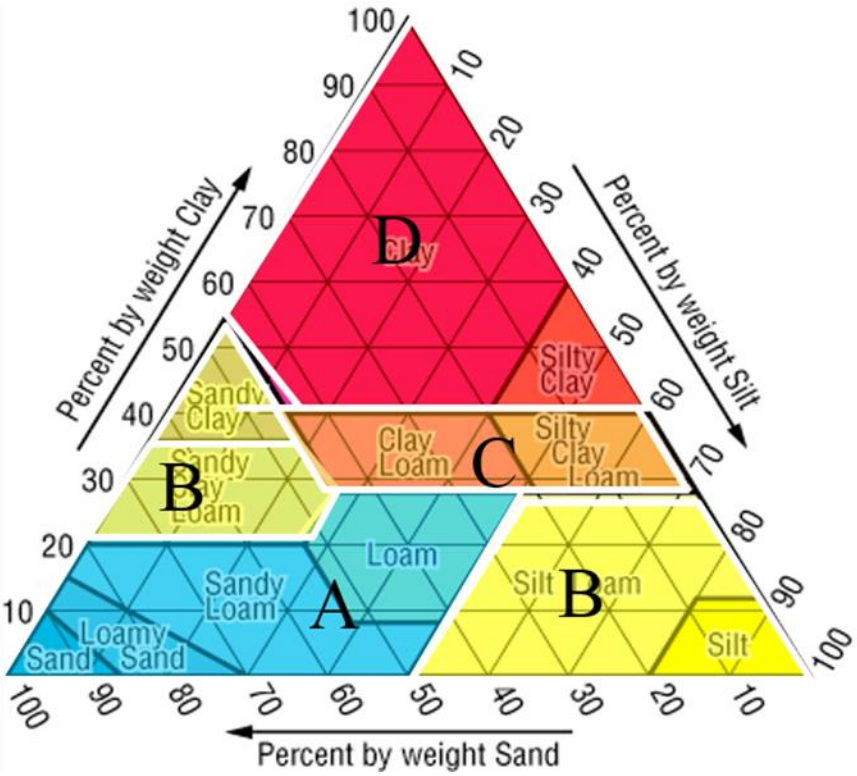

Figure 5-10. Hydrological groups for soils in the Flint Hills study area.

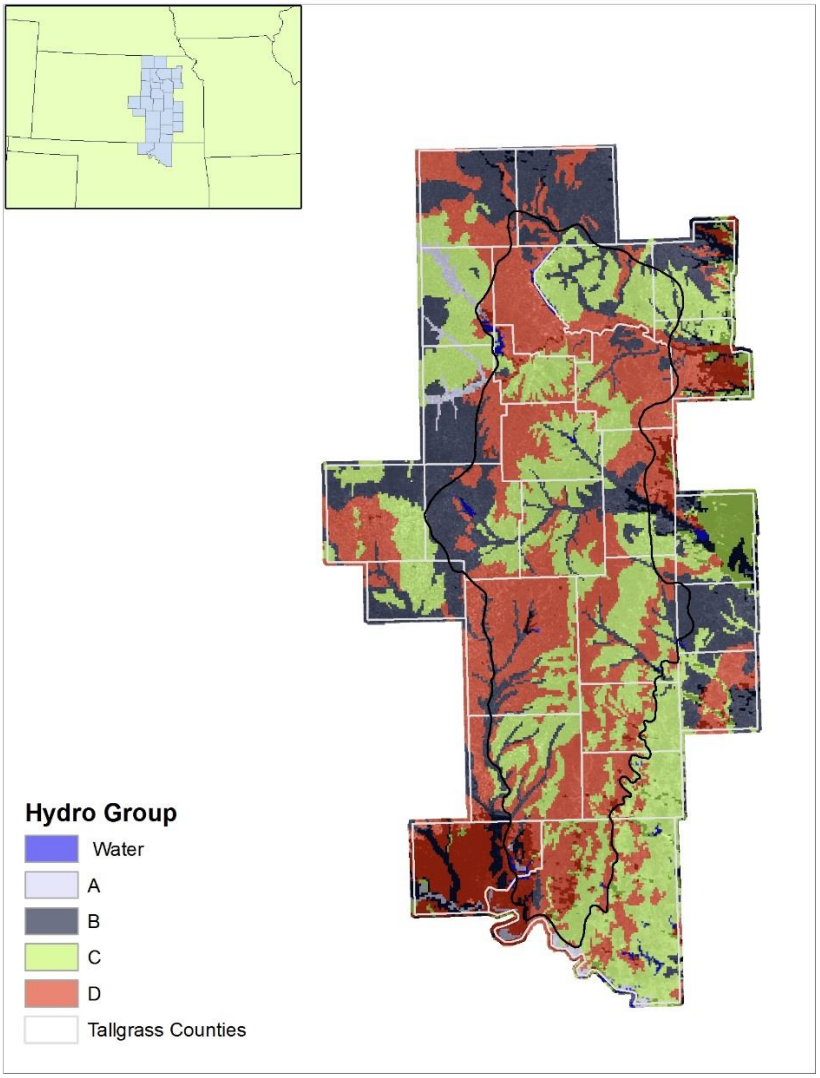

Burn Data

The burn frequency data was obtained from previous work done by Mohler and Goodin (2012) and shows the number of times a pixel has been burned during the study period (Figure 5-11). Mohler and Goodin (2012) used MODIS images acquired between March 1 and May 10 each year from 2000 to 2010. Images in which cloud cover obscured the entire study are were not used and a mask was used to only examine grassland pixels. Burned pixels were classified using the red and near-infarred bands of 250m MODIS images using a minimum distance

classification technique. The classification accuracy of burns was approximately 90% so long as the age of the burned area was two weeks old or less.

Burn data was in the form of raster files for each year between 2000 and 2010. In this study, only the 2001 through 2010 images were used. Raster images of the burns for each year were summed to estimate total burn frequency for the 2001-2010 study period.

Figure 5-11. Burn frequency for the Flint Hills study area for the period 2001-2010. Original data from Mohler and Goodin 2012.

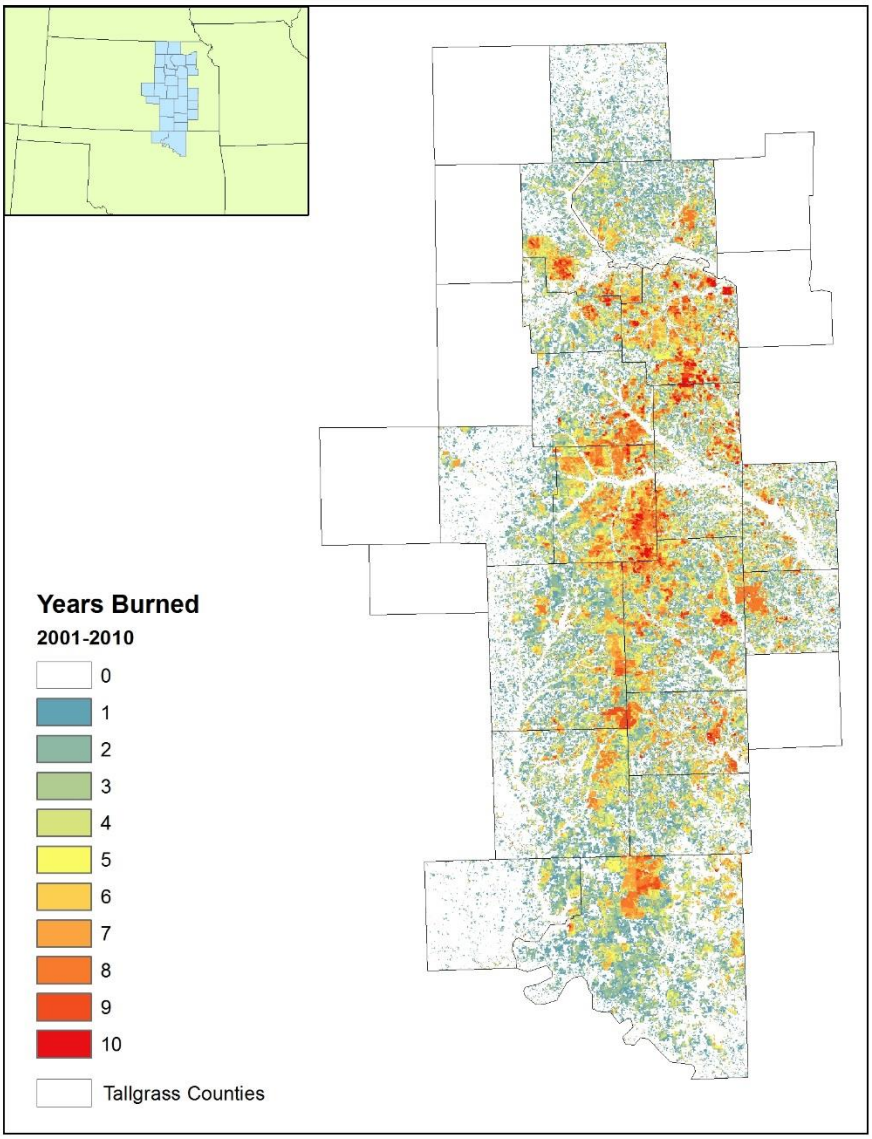

Logistic Regression Model

Logistic regression, a form of generalized linear models (GLM), was used to assess the influence on trend by the independent variables burn frequency, precipitation deviation, and hydrological soil group. The R software program was used to perform the analysis (see appendix B) at the pixel level using vegetation trends from 2001-2010 as a binary dependent variable. A

negative trend was used as the reference and given a value of 0 while the stable and positive trend classes were coded as 1. Hydrologic soil group was treated as a categorical variable with class A soils serving as the reference condition. Input data were continuous for the variables precipitation deviation and burn frequency. Model output included the coefficients for each independent variable which allowed the influence of each on trend to be assessed. For this analysis, no interaction terms were included. An analysis of deviance table was also constructed and a McFadden score was calculated to assess the overall model fit.

Results

The gradual interannual vegetation change classes for 2001-2010 are shown in Figure 5-12. Areas with significant directional trends are shown in green (significant positive slope) and red (significant negative slope). Areas without a significant trend (null slope) are shown in gray. Land managers looking at this picture would be able to assess the overall long-term direction of vegetation greenness across the Flint Hills region in a spatially explicit way. Areas with a positive trend in greenness are interpreted here as having vegetation that experienced improvements in greenness, health, or amount as suggested by NDVI. Conversely, those areas with negative trend declined in quality. For the Flint Hills ecoregion as a whole, approximately 41% of the area experienced a negative trend in vegetation activity and greenness during the 2001-2010 period, 43% of the area saw increases in vegetation activity and greenness, and 16% experienced no change or was stable during the same time (Table 5-1).

Table 5-1. Summary results for the gradual interannual trend classes for the period 2001-2010 for the Flint Hills study area based on BFAST trend component analysis.

	Vegetation Gradual Interannual Change Classes		
	Negative Trend (Browning)	Positive Trend (Greening)	No Change (Stable)
No. Pixels	127,492	132,921	51,332

Area (ha)	684,181.59	713,316.14	275,471.48
% Total Area	40.9%	42.6%	16.5%

Table 5-2. Summary results for the gradual interannual trend classes for the period 2001-2010 for the Flint Hills Counties based on BFAST trend component analysis. Bold number in a trend category indicate a maximum value within the county.

NAME	Stable	Positive	Negative	Sum	%Stable	%Positive	%Negative
Butler	8262	11773	12932	32967	25.06%	**35.71%**	39.23%
Chase	5823	5927	12746	24496	23.77%	24.20%	**52.03%**
Chautauqua	1593	2960	4380	8933	17.83%	33.14%	**49.03%**
Clay	327	3246	3007	6580	4.97%	**49.33%**	45.70%
Coffey	747	3492	791	5030	14.85%	**69.42%**	15.73%
Cowley	4175	6844	10036	21055	19.83%	32.51%	**47.67%**
Dickinson	649	3876	3221	7746	8.38%	**50.04%**	41.58%
Elk	2184	7411	2703	12298	17.76%	**60.26%**	21.98%
Geary	264	1967	4633	6864	3.85%	28.66%	**67.50%**
Greenwood	6278	15183	5417	26878	23.36%	**56.49%**	20.15%
Harvey	193	469	1209	1871	10.32%	25.07%	**64.62%**
Jackson	31	1241	315	1587	1.95%	**78.20%**	19.85%
Kay	1817	1468	3220	6505	27.93%	22.57%	**49.50%**
Lyon	1018	8279	5011	14308	7.11%	**57.86%**	35.02%
Marion	1337	4103	5525	10965	12.19%	37.42%	**50.39%**
Marshall	225	3940	1641	5806	3.88%	**67.86%**	28.26%
McPherson	335	3270	2492	6097	5.49%	**53.63%**	40.87%
Morris	1921	6092	7056	15069	12.75%	40.43%	**46.82%**
Osage	8983	6510	17524	33017	27.21%	19.72%	**53.08%**
Pottawatomie	423	7823	5055	13301	3.18%	**58.82%**	38.00%
Riley	306	4970	3715	8991	3.40%	**55.28%**	41.32%
Shawnee	53	1295	455	1803	2.94%	**71.82%**	25.24%
Wabaunsee	730	9591	7595	17916	4.07%	**53.53%**	42.39%
Washington	388	4849	3183	8420	4.61%	**57.59%**	37.80%
Wilson	383	831	520	1734	22.09%	**47.92%**	29.99%
Woodson	1505	2061	553	4119	36.54%	**50.04%**	13.43%

Figure 5-12. Gradual interannual change classes for the Flint Hills study area derived from statistical analysis of the BFAST computed trend component for the period 2001-2010.

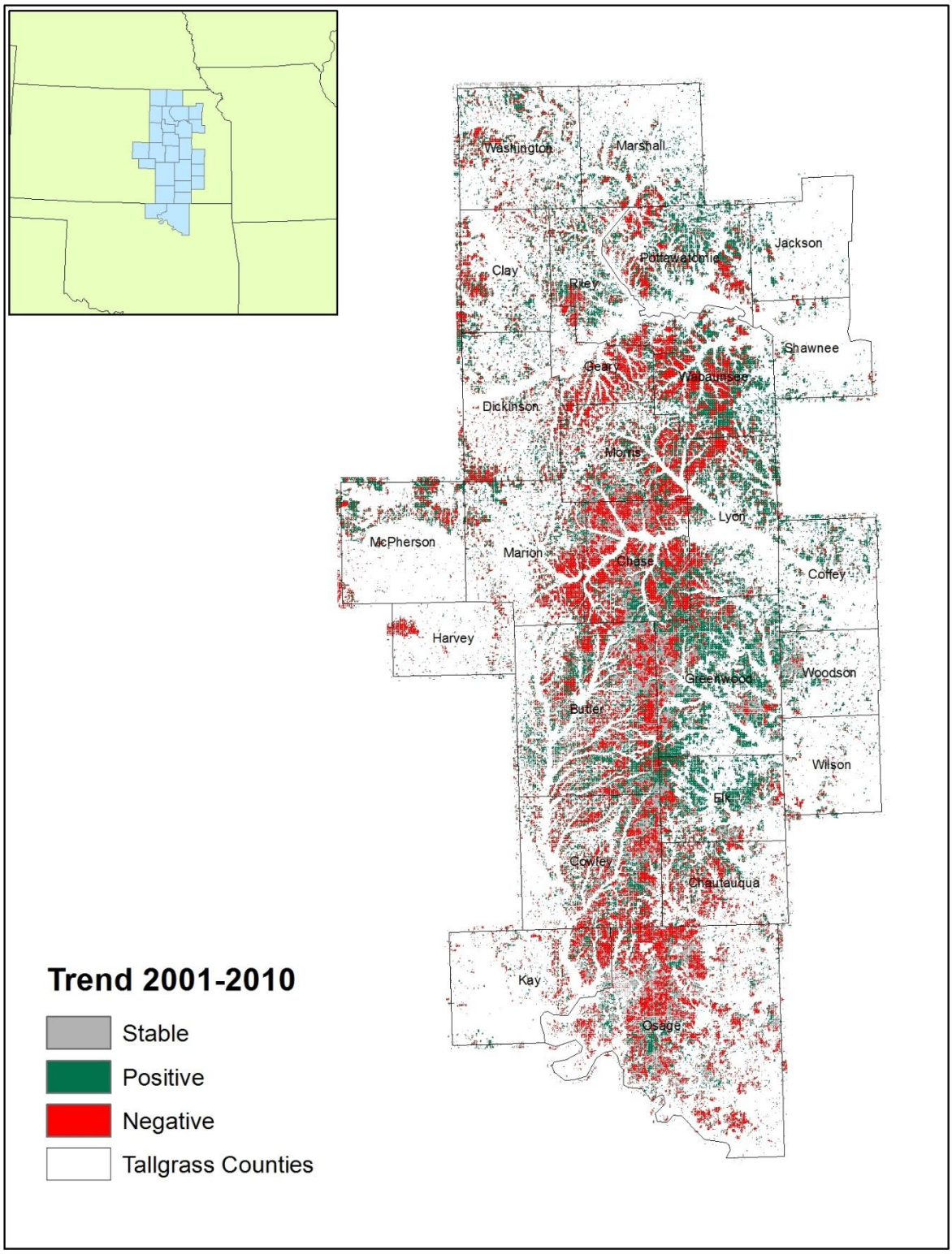
Washington
Marshall
Jackson
Pottawatomie
Clay
Riley
Shawnee
Geary
Wabaunsee
Dickinson
Morris
Lyon
McPherson
Marion
Chase
Coffey
Harvey
Woodson
Greenwood
Butler
Wilson
Elk
Cowley
Chautauqua
Kay
Osage
Trend 2001-2010
Stable
Positive
Negative
Tallgrass Counties

The number of significant breaks in the trend component can serve as an indicator for the intensity of disturbance and could be linked to fire regime. Figure 5-14 shows the Flint Hills region with the number of significant breaks for each of the pixels. Each pixel could only have a maximum of one break for each year of the study period. Approximately 51% of the Flint Hills experienced zero breaks during the study period and about 27% experienced only a single break (Figure 5-13). The maximum number of breaks experienced by a pixel was seven but only 3 pixels of 311,000 had that many breaks.

Figure 5-13. The percentage of the Flint Hills study area that experienced a different number of significant breaks within the linear trend for the 2001-2010 study period.

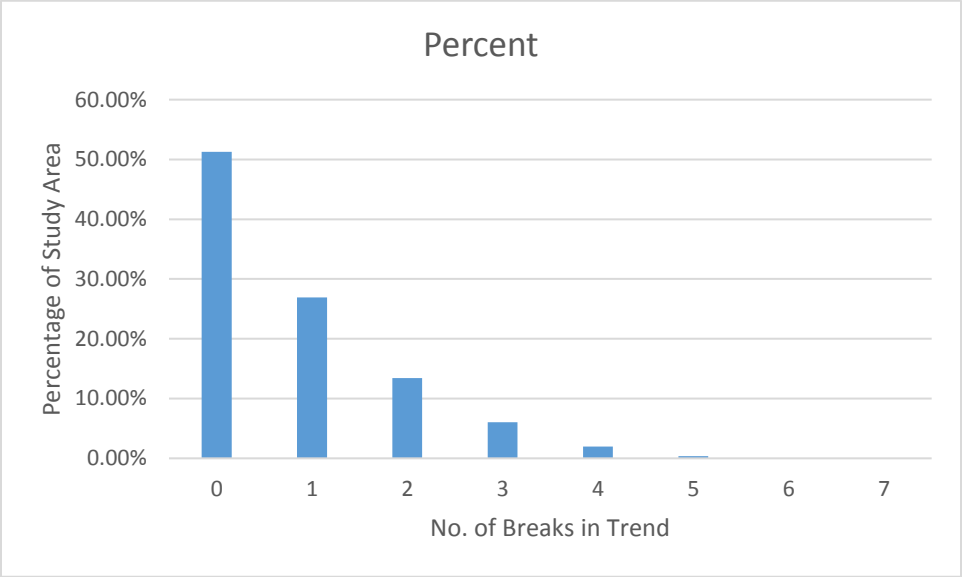

Figure 5-14. Shows the number of breaks for each pixel during the 2001-2010 study period. Each pixel could only have one break per year.

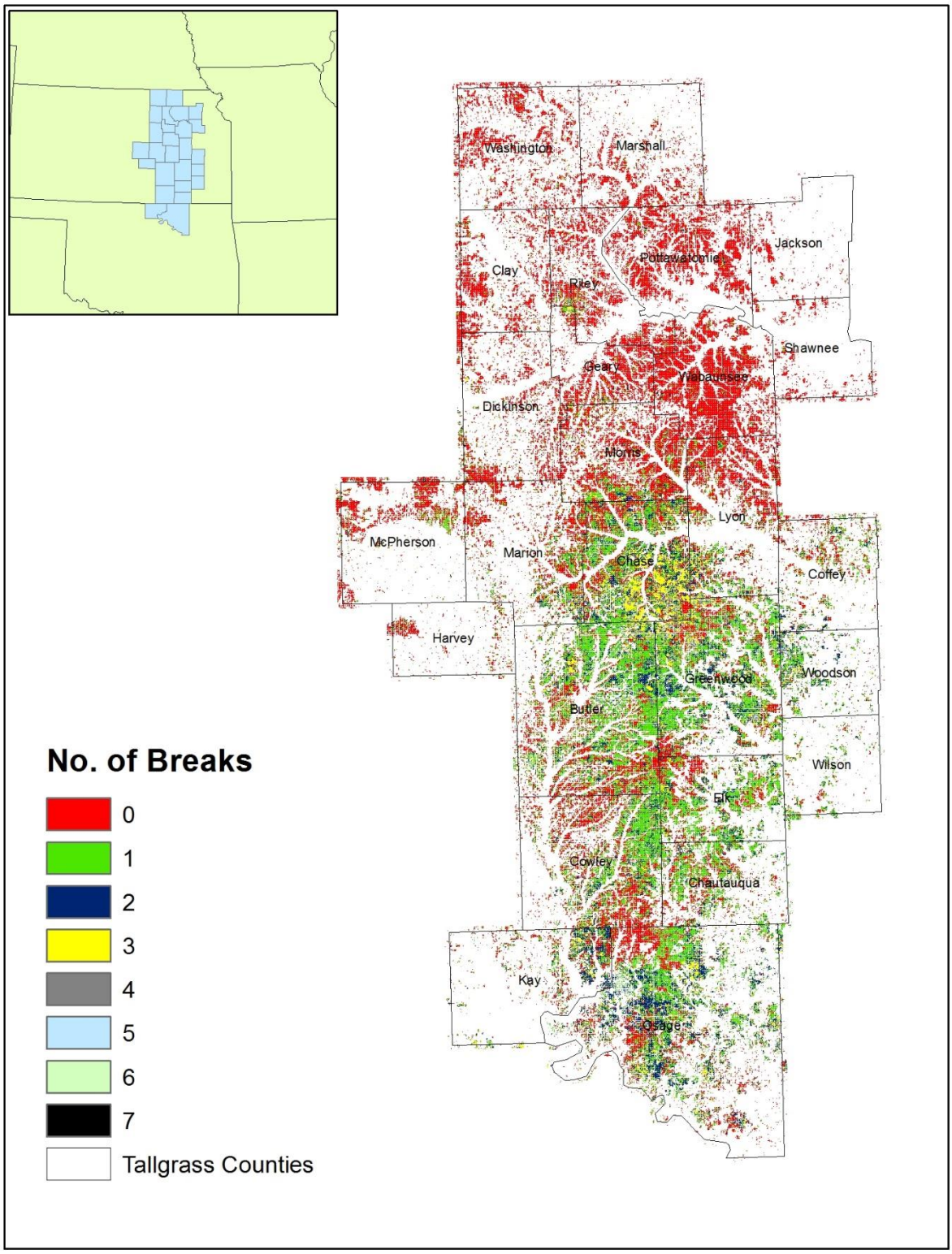
Washington
Marshall
Jackson
Pottawatomie
Clay
Riley
Shawnee
Geary
Wabaunsee
Dickinson
Morris
Lyon
McPherson
Marion
Chase
Coffey
Harvey
Greenwood
Woodson
Butler
Wilson
Elk
Cowley
Chautauqua
Kay
Osage
No. of Breaks
0
1
2
3
4
5
6
7
Tallgrass Counties

Results from the logistic regression model suggests each independent variable is statistically significant (see Figure 5-15) compared to the null model. The positive coefficients for hydrologic soil groups C and D and for burn frequency indicate that, all other variables being equal, each increase the log odds of a negative trend. In other words, negative trends for vegetation appear are more likely when a pixel has a higher burning frequency or for those areas having soils with higher clay contents. Conversely, the log odds of having a negative vegetation trend are reduced at sites having loam soils and wetter than normal conditions over the study period.

Figure 5-15. Results from the logistic regression module based on negative trend as the dependent variable.

```
#Deviance Residuals:
#    Min      1Q  Median      3Q     Max
#-1.584  -1.289   0.950   1.042   1.376
#
#Coefficients:
#              Estimate Std. Error z value Pr(>|z|)
#(Intercept)  1.126e-01  8.476e-02   1.329  0.18387
#HYDROGP1B   -2.597e-01  8.531e-02  -3.045  0.00233 **
#HYDROGP1C    1.958e-01  8.507e-02   2.301  0.02137 *
#HYDROGP1D    1.778e-01  8.504e-02   2.091  0.03650 *
#PDEV        -2.275e-04  7.501e-06 -30.326  < 2e-16 ***
#BURNFREQ     4.275e-02  1.342e-03  31.850  < 2e-16 ***
#---
#Signif. codes:  0 ‘***’ 0.001 ‘**’ 0.01 ‘*’ 0.05 ‘.’ 0.1 ‘ ’ 1
#
#(Dispersion parameter for binomial family taken to be 1)
#
#    Null deviance: 424682  on 311135  degrees of freedom
#Residual deviance: 420376  on 311130  degrees of freedom
#AIC: 420388
#
#Number of Fisher Scoring iterations: 4
```

An ANOVA function was run on the model to analyze the table of deviance, specifically the difference between the residual deviance between the null (intercept only) model and that for each independent variable (Figure 5-16). The difference in residual deviance between the null and subsequent models is an indicator of model performance with larger difference suggesting improved performance. The addition of each independent variable to the model results in a slightly larger difference between residual deviance and indicates that each new term, when

added sequentially, is explaining more overall variance. This, coupled with the significance of all independent variables ($p < 0.000$) suggest each is important. The McFadden R^2, or pseudo R^2, value of approximately 0.01, however, is slightly below what is normally considered to be very satisfactory (0.2-0.4) (Figure 5-16).

Figure 5-16 Table of deviance for the logistic regression model and including the McFadden R^2 value.

```
#          Df Deviance Resid. Df Resid. Dev  Pr(>Chi)
#NULL                     311135     424682
#HYDROGP1  3  2598.35     311132     422084 < 2.2e-16 ***
#PDEV      1   686.64     311131     421397 < 2.2e-16 ***
#BURNFREQ  1  1020.97     311130     420376 < 2.2e-16 ***
#---
#Signif. codes:  0 '***' 0.001 '**' 0.01 '*' 0.05 '.' 0.1 ' ' 1

#run the McFadden R2 index to assess model fit
library(pscl)
pR2(model)

#          llh       llhNull            G2      McFadden          r2ML
#-2.101879e+05 -2.123409e+05  4.305964e+03  1.013927e-02  1.374417e-02
#          r2CU
# 1.845836e-02
```

Discussion and Conclusions

Examining results from the BFAST procedure provides an interesting synoptic view of vegetation dynamics within the Flint Hills that should be of interest to land managers and land owners within the ecoregion. For the study period of 2001-2010, 41% of the Flint Hills experienced a significant decline in greenness. The spatial distribution of this "browning" occurs throughout the region with no obvious spatial pattern. Osage, Butler, Chase, and Cowley counties all contained over 10,000 negative trending pixels and accounted for 42.6% of all pixels having a negative trend. These counties lie in the middle and southern sections of the study area. Approximately 43% of the Flint Hills had a positive trend in greenness during the study period, with Greenwood and Butler counties having 20.7% of all positive trending pixels. These counties lie in the central area of the Flint Hills. The remaining 16% of pixels were stable pixels

and were distributed throughout the area with Osage and Butler counties having 34.5% of all stable trending pixels in the study area.

That such a large percentage of the Flint Hills ecoregion experienced a negative trend during the study period was surprising. As burning is an important and common practice in the Flint Hills to combat woody encroachment and improve forage conditions, more frequent burning was expected to correlate with areas having a positive trend.

A comparison of estimated trends in greenness (Figure 5-12) to burn frequency data (Figure 5-11) for the Flint Hills, suggests that areas with higher burn frequencies tend to also have negative trends in greenness. This qualitative conclusion is supported by logistic regression results where a unit increase in burn frequency was shown to increase the log odds of a negative trend by 4.23. Previous research has shown a burning frequency of burning once every 4 years yields more robust vegetation (Collins el al., 1995) and that perhaps a frequency of approximately one burn every two to three years is sufficient to maintain grasslands (Ratajczak et al., 2016). The results here seem to support these conclusions.

Also not surprising was the logistic regression result indicating that the likelihood of having a negative vegetation trend was reduced when conditions were wet (high positive deviation from normal precipitation). However, this relationship was more difficult to visualize when comparing maps of these variables.

Other findings from the logistic regression model included soils in group B, with significant silt and sand components, reduced the log odds of a negative trend by 2.60. The positive coefficients of group C and D soils, dominated largely by larger fractions of clay and lower infiltration rates, increase the log odds of a negative trend by 1.96 and 1.78, respectively. This result makes some intuitive sense, as soils with lower infiltration rates might limit water

availability in the root zone to support plant growth. It is also interesting that group D soils (minimum 55% clay content) increase the chances of a negative trend slightly less that soils in hydrologic group C (clay loam and silty clay loams soils) despite having a lower rate of infiltration. One speculative reason for this might be that water that is able to enter the root zone in group D soils is more tightly held in the soil matrix with at least some available to plants over a longer time period than in C soils.

Using MODIS images to create a vegetation index time series and utilizing BFAST with its ability to detect breaks and trend of vegetation greenness allows for consistent assessment of the grassland vegetation of the Flint Hills. Grassland managers across the Flint Hills would benefit from knowing the greenness of their grassland and be able to develop better ways to preserve their land. The BFAST trend analysis allows for an interesting method to characterize long-term vegetation trends as well as when and where significant breaks occur in detected trends. With the statistical results from the GLM, it is possible to determine the impact of yearly burning as a negative impact on the vegetation of the Flint Hills ecoregion. Certain soils are beneficial for vegetation while others are not and increasing the amount of precipitation allows for healthy vegetation, and therefore produces positive trending vegetation.

Chapter 6 - Time Series Analysis of Phenometrics for the Flint Hills Ecoregion using Moderate Resolution Satellite Imagery

Abstract

Grasslands of the Flint Hills are often burned as a land management practice. Remote sensing can be used to help better manage prairie landscapes by providing useful information about the long-term trends in grassland vegetation greenness and help quantifying regional differences in vegetation development. Using MODIS 16-day NDVI composite imagery between the years 2001-15 for the entire Flint Hills ecoregion, TIMESAT was used to examine phenometrics of the image time series. Specific phenometrics included: Growing season length, start of season, end of season, middle of season, maximum value, small integral, left derivative, and right derivative. Phenometrics were produced for each year of the study and an ANOVA was performed on the means of all eight phenometrics to assess if significant differences existed across the study area. A K-means cluster analysis was also performed by aggregating pixel-level phenometrics at the county level to identify administrative divisions exhibiting similar vegetation development. Significant differences existed for all phenometrics when considering the ecoregion as a whole. Results suggest that factors other than natural gradients in temperature and precipitation play a significant role in the annual cycle of grassland vegetation development. Unanticipated, and sometimes geographically disparate, groups of counties were shown to be similar in the context of specific phenology metrics and this may prove useful in future implementations of smoke management plans within the Flint Hills.

Introduction

Grasslands and savannas make up more than 40% of the earth's surface and their rapid response to changes in land management and climate can have dramatic ecological and social consequences (Briggs et al., 2005). Grasslands are among the most biodiverse and productive of all the earth's terrestrial biomes but receive low levels of protection (Mark and McLennan, 2005). Since 2009, 53 million acres of grassland, roughly the area of Kansas, have been converted to cropland across the Great Plains alone (Plowprint Annual Report, 2016). Tallgrass prairie has been reduced to ~4% of its historical extent making it one of the most altered ecosystems in North America (Ratajczak et al., 2016). Temperate grasslands are important for both agronomic and ecological purposes and are a key resource for livestock production in North America and around the world (Briggs et al., 2005). Grasslands provide services such as water storage and clean air (Plowprint Annual Print, 2016) and grassland vegetation reduces soil erosion due to it dense root systems and by shielding the soil surface from direct interception of rainfall (Ratajczak et al, 2016). Grasslands also store and retain large amounts of soil carbon and are an important component of the global carbon cycle (Briggs et al., 2005). The estimated values of theses, and other, ecosystems services provided by native grasslands has been estimated to be in excess of $5,000 per hectare per year (Dodds et al., 2008).

The conservation status of grasslands is being evaluated by groups including the Landscape Conservation Cooperatives which seeks to identify the greatest threats to grasslands and shrublands across the U.S. and Mexico, areas that are likely to be resilient to climate change and other threats, and areas with high potential for restoration (Glaser, 2014). The state of North American prairies is also being addressed through a tri-national cooperative program involving Mexico, the USA, and Canada which is attempting to address both sustainable management and

conservation needs (Mark and McLennan, 2005). The Flint Hills ecoregion in Kansas and Oklahoma remain one of the last great expanses of intact and native tallgrass prairie in the United States. The creation of the Tallgrass Prairie National Preserve in 1996 allowed for more area of the Flint Hills to retain its native character.

Grasslands have been under threat in the United States as well as throughout the world due to conversion to row-crop agriculture and changing land management coupled with other global change phenomena (Briggs et al., 2005). A majority of the former area of the tallgrass prairie has been replaced with crops such as wheat, corn, and soybeans (Plowprint Annual Print, 2016). The remaining tallgrass prairies of North America are threatened by an increase over time in the abundance of native woody species, such as the red cedar (*Juniperus virginiana)* in the Flints Hills area (Hulbert, 2009). These woody plants originate both from within the ecosystem and from neighboring ecosystems (Briggs et al., 2005), with encroachment altering the structure and function of temperate grassland ecosystems and resulting in a loss of biodiversity and grazing productivity (Ratajczak et al., 2016). The likely drivers of this increase in woody plant abundance are numerous and include change in climate, atmospheric carbon dioxide concentration, nitrogen deposition, grazing pressure, and disturbance regimes (e.g., the frequency and intensity of fire) (Briggs et al., 2005). Transitions to shrubland and woodland in temperate climates are largely attributed to changes in fire management (Ratajczak et al., 2016). Comparisons of the area occupied by forest at the time of settlement, as recorded in the 1856 Land Office, with that in the 1970's showed that on frequently burned prairies woody plants occupied about the same area today as over a century ago. However, on sites not burned for 20 years or longer, forests had invaded on half or more of the unburned areas (Hulbert, 2009).

Fire is an integral component of prairie development and maintenance and for more than 7000 years vegetation patterns have been influenced by anthropogenic burning practices (Towne and Kemp, 2003). Fire has long been recognized as an important factor influencing the development and persistence of the tallgrass prairie ecosystem (Benson and Hartnett 2006). Fire is both an inexpensive and effective way of controlling woody species and shrubs as well as maintaining high quality nutritious forge for grazers, but air pollution from the smoke can negatively impact cities downwind of the fires (Briggs et al., 2005). Prairie fires were suppressed during European settlement with accidental or lightning-caused wildfires being the primary source of burning (Towne and Kemp, 2003). An influx of cattle to the Flint Hills in the late 1800's created an incentive for prairie burning and pastures were burned annually in February or March to improve livestock weight gains (Towne and Kemp, 2003).

Annual or biennial burning, which is currently a common land management practice in tallgrass prairie, homogenizes the canopy over the long term by suppressing invasion by woody species while promoting a variety of C3 forbs amidst a matrix of C4 gramminoids (Goodin and Henebry, 1998) (Benson and Hartnett 2006). Warm season grasses have been shown to increase after burning has been conducted (Towne and Kemp, 2003) (Hulbert, 2009) and average peak-season aboveground biomass on annually burned prairie is reported to be nearly twice that of infrequently burned prairie (Benson and Hartnett 2006). Species diversity is lowest with annual late-spring burning and increases with increasing intervals between fires (Hulbert, 2009).

At the Konza Prairie Biological Station, it has been observed that vegetation development starts earlier on plots burned in November than on those burned in March (Hulbert, 2009). This is likely due to higher soil temperatures on burned areas, resulting from greater solar heating as a response to removal of the insulating layer of standing dead vegetation (Hulbert, 2009). A

burning frequency of 3 to 4 years has been thought to be the historical fire frequency before extensive settlement by Europeans (Briggs et al., 2005). Burning once every 4 years has been shown to increase the number of forb and annual species compared to that seen in annually burned sites (Collins et al., 1995). A complete exclusion of fire in tallgrass prairie has been shown to significantly decrease the grass bud bank while increasing the forb bud bank (Dalgleish and Hartnett, 2008). Prairie that is burned at an intermediate fire frequency showed greater year-to-year variability in grass bud bank size and in the probability of emergence from the bud bank than annually burned prairie (Dalgleish and Hartnett, 2008).

Cattle ranchers in the Flint Hills employ frequent spring burns to remove dead litter and enhance palatability, leading to greater and more consistent weight gain in cattle (Ratajczak et al., 2016). These fires help to reduce species such as buckbrush (*Ceanothus cuneatus)* or coralberry (*Symphoricarpos orbiculatus)* (Hulbert, 2009). Annual spring burning is beneficial in stopping woody encroachment but also can homogenize plant and avian communities (Collins et al., 1995) (Ratajczak et al., 2016). In addition, it has been shown that annual burning does not eliminate shrubs and, over time, this buildup of shrubs can lead to areas where woody vegetation becomes established and later spreads (Towne and Kemp, 2003). Fire alone does not stop the invasion of woody plants. The combination of fire, climate, substrate, and topography are what makes the prairie (Hulbert, 2009).

Satellite remote sensing has been an invaluable asset for examining regional environmental change by post-classification analysis of land cover change to examine separate, abrupt anthropogenic impacts on the land surface, such as deforestation and urbanization. Accompanying satellite remote sensing is a variety of spectral vegetation indices, such as NDVI which can be calculated from satellite image data to quantify the spatial and temporal variation

in vegetation growth and activity (Linderholm 2006). NDVI and other indices have been used to successfully assess vegetation phenology (Wright et al., 2012).

Remote sensing indices are mathematical combinations of surface reflectance at two or more wavelengths to emphasize vegetation properties. Vegetation indices are based on the reflectance properties of plant foliage, such as leaves and other green materials which can vary greatly in composition. Vegetation indices correlate with several biophysical parameters such as leaf area index (LAI), fraction of photosynthetically active radiation (FPAR), and green aboveground biomass (Wardlow 2005). Components that have the most effect on leaf spectral response are pigments, water, carbon, and nitrogen (Zhang et al., 2007). Vegetation indices provide insight into basic composition of leaves and how they change in different environmental conditions to determine the general greeness of vegetation, biomass, and land cover, to estimate net productivity (Tucker et al., 1991).

Estimates of vegetation biomass are dependent on the ratio of soil surface-vegetation spectral reflectance making some wavelengths better to use than others (Colwell 1974). The ideal vegetation index would be sensitive to vegetation, insensitive to background soils, and minimally influenced by atmospheric path radiance (Lunetta el al., 2006). Examples of frequently used vegetation indexes include the IR/red ratio (Colwell 1973), the perpendicular vegetation index (PVI) (Richardson and Weigand 1977), the soil-adjusted vegetation index (SAVI) (Guete 1988), the Kauth-Thomas transformation (tasseled cap or -T) (Kauth and Thomas 1976), the enhanced vegetation index (EVI) (Zhang et al., 2007), and the normalized difference vegetation index (NDVI) (Lunetta et al., 2006).

NDVI is calculated as the ratio of the difference between near-infrared and red over the sum of near-infrared and red (Lunetta et al., 2006) and varies between values of -1 to 1 (Equation

2.1). Red and near-infrared bands are related to chlorophyll content and cell structure and with the spectral response of these two bands, the change in NDVI value over time is a good way to measure the vegetation growth and development (Zhang et al., 2007).

$$NDVI = (NIR - red) / (NIR + red) \quad \textbf{Equation 6.1}$$

where:
NDVI = normalized difference vegetation index
NIR = reflectance in the near – infrared spectrum
Red = reflectance in the red spectrum

NDVI correlates well with total primary production (An 2009) and the amount of photosynthetic biomass (Zhou et al., 2001), which dominates both photosynthesis and transpiration processes. During a normal year, NDVI increases rapidly in the spring and then levels off until the end of August (Verbesselt et al., 2010). Therefore, changes in NDVI suggest changes in vegetation that coincide with absorption of radiation (Sellers 1985). Higher NDVI values are associated with healthier vegetation while degraded vegetation is associated with lower NDVI values.

NDVI has shown consistent correlation with vegetation biomass and dynamics in various ecosystems worldwide. NDVI provides information about the spatial and temporal distribution of vegetation communities, vegetation biomass, CO_2 fluxes, vegetation quality for herbivores, and the extent of land degradation in various ecosystems (Pettorelli et al., 2005). NDVI has been shown to report consistent negative correlations between fire probabilities and standardized NDVI levels (Pettorelli et al., 2005). While NDVI has been proven to be a very useful application for vegetation production, there are some limitations. The relationship between NDVI and vegetation can be biased in sparsely vegetated areas, such as arid to semiarid areas, and dense canopies, such as the Amazonian Rain Forest (Pettorelli et al., 2005). Due to NDVI being ratio-based, non-linear, lower ratio values tend to be enhanced and higher ratio values

condensed causing values to saturate over high biomass conditions (Carlson and Ripley 1997). This may cause areas with high biomass density to have larger NDVI values than areas with lower densities, even if the health conditions of the vegetation were identical. NDVI is also unable to differentiate dominant species within forests due to assemblages of plant species producing similar NDVI values or similar NDVI temporal trends (Pettorelli et al., 2005).

The visible and NIR bands of the spectrum cannot penetrate cloud cover causing satellite images to suffer from cloud contamination and yield lower NDVI values that do not accurately reflect surface conditions unless preprocessing filtering and smoothing is applied to the raw data. The NIR band also include a strong water absorption region, which can reduce the reliability of NDVI calculations (Wardlow 2005). Most vegetation indices are also limited by inter-satellite sensor differences, satellite drift, calibration uncertainties, and atmospheric pat radiance (Zhou et al., 2001).

Phenology has become an important focus in ecological research for its use in vegetation monitoring and examining issues related to climate change. Phenology is the variation in seasonal patterns of natural phenomena on land surfaces affected by inter-annual and seasonal variation in soil characteristics and meteorological conditions (Cleland et al., 2007). Seasonal characteristics of plants, such as emergence and senescence, are closely related to climate and changes in phenological events may signal important year-to-year weather and climate variations or even global environmental change (Reed 1994). The phenology of land surfaces can be detected using remote sensing by examining the spectral index values of the land surface. Changes in the seasonal timing such as the start and end of season, duration of growing season, and maximum productivity can have an impact on a wide range of processes that are dependent on natural cycles of vegetation (Ganguly et al, 2010). However, changes in phenology are part

of a complex system and can be influenced by outside forces other than long-term climate change, such as precipitation or fire (Willis, 2015). In order to detect changes in phenology, remotely sensed datasets must have high temporal resolution to capture any sudden changes in the landscape. MODIS-derived indices are ideal for monitoring phenology in vegetation because it support a wide variety of phenology-related data products (i.e., NDVI, EVI, Leaf Area Index (LAI, Albedo) and MODIS images are acquired on a daily basis and are also composited into 8 and 16 day products (Willis, 2015).

Most phenology research has ecosystem monitoring as its ultimate goal while the phenology of entire ecosystems has rarely been studied (Reed 1994). Field-based ecological studies have demonstrated that vegetation phenology tends to follow relatively well-defined temporal patterns (Zhang et al., 2003). When looking at deciduous vegetation and many crops, leaf emergence tends to be followed by a period of rapid growth, and then is followed by a stable period of maximum leaf area (Sakamoto et al., 2005). At the regional and larger scales, variations in community composition, micro and regional climate models, soils, and land management result in a complex spatio-temporal variation in the phenology of the vegetation (Zhang et al., 2003). In some cases, some vegetation types exhibit multiple modes of growth within a single annual cycle. A profile view of a single annual vegetation cycle (Figure 6-1) illustrates key measures, or phenometrics, often used in such studies, including the onset and end of greenness (start and end of season, respectively), maximum NDVI, the rate of green-up and senescence, growing season length, and accumulated NDVI.

Figure 6-1. An example of a vegetation phenology curve and associated phenometrics (Reed et al., 1994)

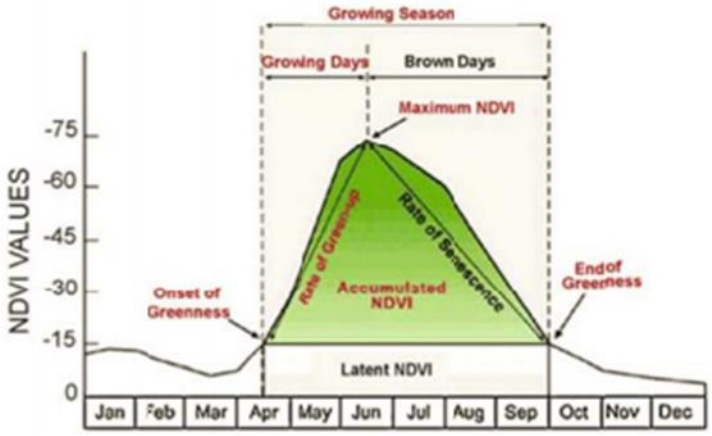

A time series is an ordered sequence of variable values recorded at equally-spaced time intervals. Time series analysis methods can be used to determine if data has internal structure such as trend, seasonal variation, or autocorrelation (Eklundh and Jonsson 2010). In a remote sensing context, time series analysis consists of a series of satellite images which allow comparisons of the same scene, biophysical measure, or vegetation index over a long time period to reveal structure in variables of interest. When vegetation indices are used as the basis of the time series, shifts in vegetation properties and dynamics may be revealed (Heumann et al., 2007). Information extracted from time series vegetation index (VI) data has been shown to successfully characterize vegetation phenology (Reed et al., 1994) and has been used to measure vegetation activity (Zhang et al., 2003).

The MODIS sensor is carried onboard NASA's Terra and Aqua satellites and acquires images at a global scale and at a high (daily) temporal resolution. MODIS possesses seven spectral bands that are designed for land applications with spatial resolutions ranging from 250 m to 1 km (Zhang et al., 2003). MODIS VI products are designed to provide consistent spatial and temporal comparisons of global vegetation conditions that can be used to monitor photosynthetic

activity (Huete et al., 2002) and those acquired at the 250m resolution are well suited for application in the U.S. Central Great Plains (Wardlow and Egbert, 2008).

Before satellite data can be used to study land surface phenology, the raw image data is first put through a series of filtering, compositing, smoothing, or screening procedures to isolate the signal from the noise. The preprocessing of raw data is based on a smoothing of distinct sequences of temporally adjacent data points (Jonsson and Eklundh 2004). Phenometrics can be extracted from time series datasets by combining techniques that first filter (or smooth) raw NDVI data and then extract relevant phenometric estimates using methods such as principal component analysis (Tan et al., 2010), Fourier analysis (Sakomoto et al., 2005), and pixel-above-threshold technique (Cleland et al., 2007). The TIMESAT software program provides several filtering options to smooth raw time series vegetation data and extract phenometric data (Eklundh and Jonsson 2010), and has been used in a variety of studies to examine vegetation phenology (Eklundh and Jonsson 2003), assess satellite and climate data-derived indices of fire risk (Verbesselt et al., 2006), and examine relationships between coniferous forest NDVI and models of conifer tree photosynthetic activity (Eklundh and Jonsson 2010).

For this study, TIMESAT is used to derive various phenometrics from across the entire Flint Hills ecoregion. The ANOVA and Tukey tests are employed to determine the significance of phenometrics across the study area and a K-Means clustering method applied to spatially examine the Flint Hills study area as a homogenous region.

Analysis of variance (ANOVA) can be used to analyze the differences among group means. ANOVA provides a statistical test of whether the means of several groups are equal and are useful for comparing three or more means for statistical significance. The Tukey's Honestly Signficant Differences (HSD) test is often done in conjunction with ANOVA to find specific

groups that are significantly different from each other by comparing all possible pairs of groups means.

K-means cluster analysis has been used in a variety of studies due to its ease of implementation, simplicity, efficiency, and empirical success (Jain 2009). K-means clustering seeks to place all features into set classes in which each observation belongs to the cluster with the nearest mean. To determine the optimum number of clusters, different values of K are run in an algorithm and the best value of K is then chosen based on a predefined criterion (Fiqueiredo and Jain, 2002). An optimal number of clusters assumes that when dividing data into an optimal number of clusters, the resulting partition is most resilient to the random perturbations (Jain 2009).

Study Area

The study area for this project includes the 26 counties of Kansas and Oklahoma which comprise the Flint Hills ecological region of eastern Kansas and northern Oklahoma (Figure 6-2). The Flint Hills encompasses an area of 1.6 million hectares and contains the largest area of unplowed tallgrass prairie in North America (Hutchinson et al., 2015). The World Wildlife Fund's Terrestrial Ecoregions of the United States and Canada defines the Flint Hills as the area covering the Flint Hills of Kansas and the Osage Plains of northeastern Oklahoma.

The Flint Hills is the smallest grassland ecoregion in North America and can be distinguished from other grassland associations by the dominance of tallgrass species and from the Central Tall Grasslands to the north by its lack of biotic variety and a thin soil layer spread over distinct beds of limestone. These flinty beds of limestone, from which the name of this ecoregion is derived, renders most of the area unsuitable for row-crop agriculture, resulting in an unplowed, though heavily grazed, remnant of the original tallgrass prairie (Madson 1993).

Unlike many other ecoregion classifications, which are based primarily on biophysical features such as climate and topography, World Wildlife Fund's ecoregions include biogeographic knowledge and therefore reflect the historic events and processes that have shaped biodiversity distributions (McDonald et al., 2005).

The definition for the Flint Hills that will be used in this study is provided by the U.S. Environmental Protection Agency (EPA) which defined ecoregions based on work from Omernik (1987) to serve as a spatial framework for environmental resource management. The map of U.S. ecoregions was compiled based on the premise that ecological regions can be

Figure 6-2. The Flint Hills study area showing the 26 counties comprising the ecological region in eastern Kansas and north-central Oklahoma.

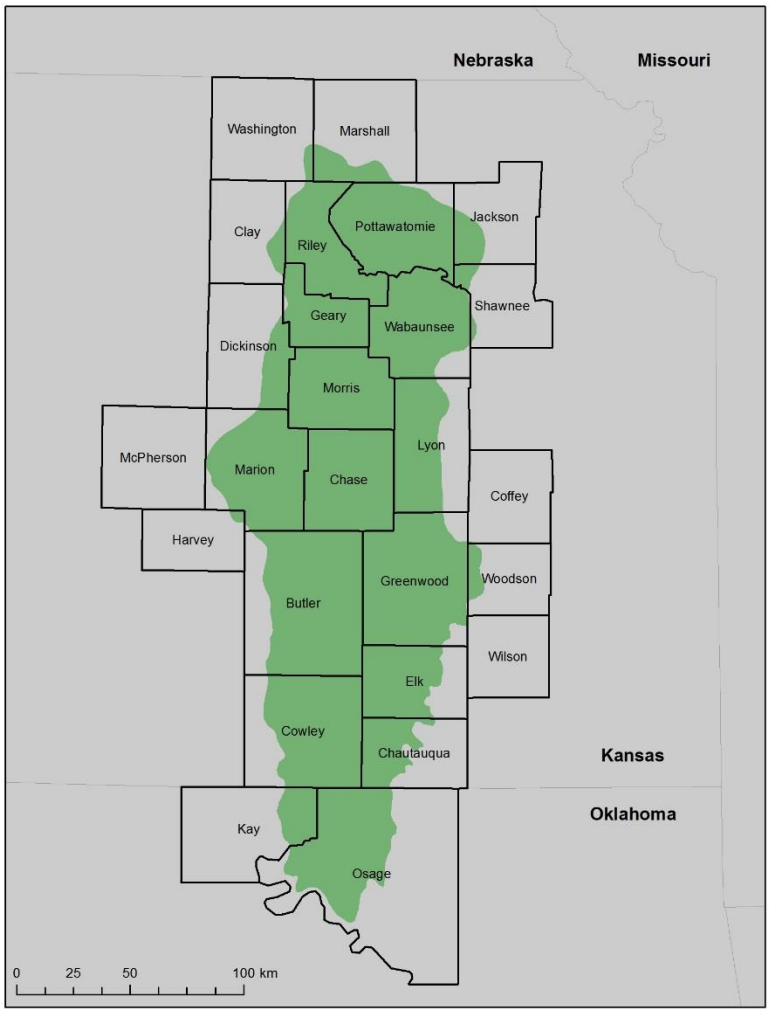

identified through an analysis of the patterns and the composition of biotic and abiotic phenomena that affect or reflect differences in ecosystem quality and integrity (Omernik, 1987). Such phenomena include geology, physiography, vegetation, climate, soils, land use, wildlife, and hydrology. The relative importance of each characteristic varies from one ecological region to another regardless of the hierarchical level (Wilken 1986). The EPA ecoregions use a Roman numeral classification scheme with level I being the coarsest level, dividing North America into 15 ecological regions, level II divides the continent into 52 regions, and levels III and IV further breaking down the ecoregions. The EPA definition of the Flint Hills is identical for level III and IV with Level III boundary used in this study.

Precipitation in the Flint Hills is highly variably from year to year. Based on 30 year normal precipitation (1981-2010) (http://prism.oregonstate.edu, last accessed 02.15.17), the northern and southeastern portions of the Flint Hills receive 720 mm (28 in) and 1120 mm (44 in) of precipitation annually. Much of the precipitation falls during the growing season (approximately 75%), though this, too, varies from year to year (Hayden 1998). Seasonal temperatures are typified by cool winters and hot summers. The City of Manhattan, Kansas, in the northern section of the Flint Hills, averages -1.8 C in January and 26.5 C in July while the southern reaches of the study area experience an average temperature of 1.1 C in January and 27.2 C in July.

Prescribed burning is a common land management practice employed by ranchers within the ecological region (Wilgers and Horne, 2006). Burning tallgrass prairie has been shown to increases plant productivity, decrease aboveground litter, and decrease woody vegetation (Briggs and Knapp, 1995). The frequency of burning in the Flint Hills has changed in recent years. Beginning in the 1980's, a switch in cattle grazing practices prompted land owners to apply

controlled burns on an annual basis. However, areas around populated areas often remain unburned for extended periods of time and these different fire regimes may be contributing to recent trends in vegetation, including the encroachment and expansion of woody vegetation (Robbins et al., 2002).

In addition to tallgrass prairie vegetation, several other land cover types in the Flint Hills (See Figure 6-3). Croplands are found in the flat floodplains along streams and rivers. Gallery forests can also be found along the streams and rivers. Trees can also be found in upland areas where fire and grazing have been suppressed. Figure 6-4 shows the study area while emphasizing the grassland areas isolated for analysis. The area of the moderate resolution pixels identified here as grassland consisted of at least 80% grassland cover after rescaling the original higher spatial resolution data provided by the 2011 National Land Cover Database (NLCD)(Homer et al., 2015).

Figure 6-3. Land use/land cover within the counties comprising the Flint Hills ecoregion study area (NLCD 2011).

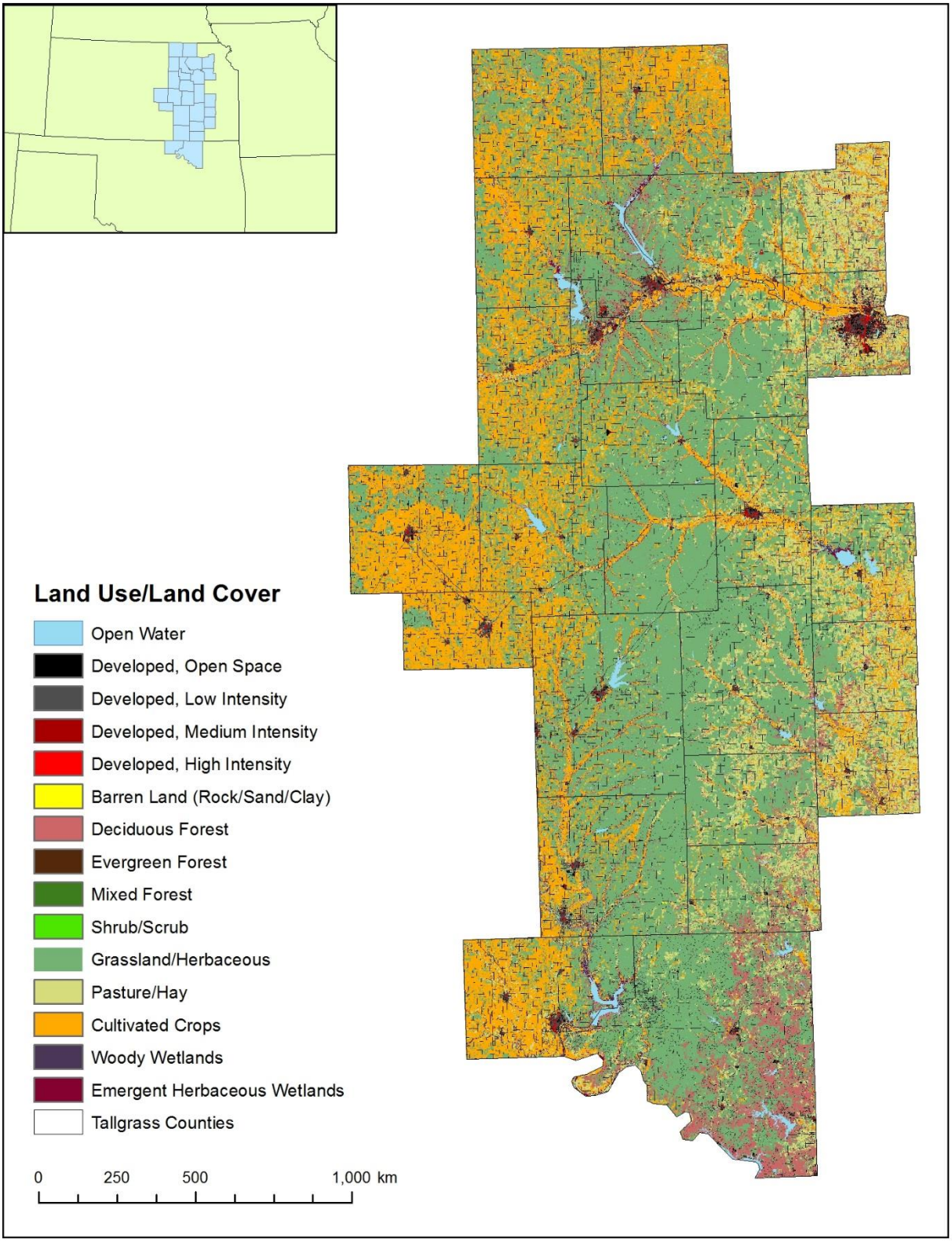

Figure 6-4. The Flint Hills ecoregion study area emphasizing grassland pixels. Each pixel corresponds to the spatial resolution of the MODIS MOD13Q1 product and consists of a minimum of 80% grassland/herbaceous cover.

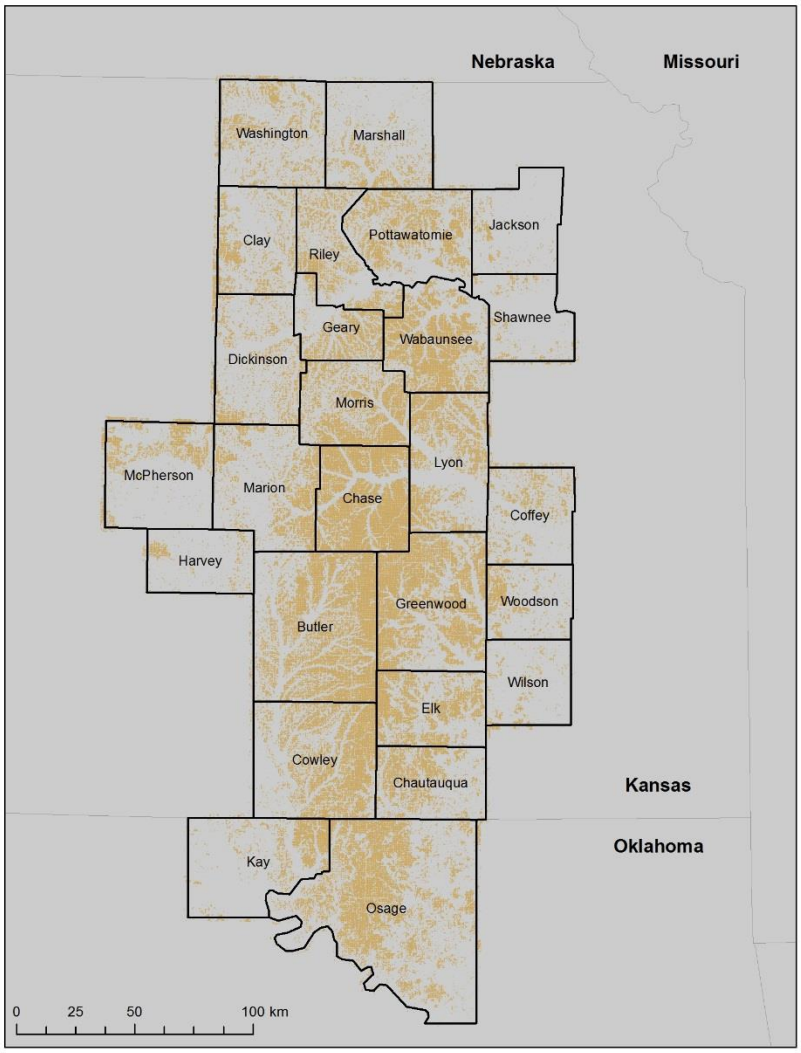

Prescribed burning preserves and sustains the tallgrass prairie ecosystem. Burning is an effective land management practice for stopping woody vegetation from encroaching on grasslands. Tallgrass prairies of North America are threatened by an increase in the abundance of native woody species, such as red cedar (*Juniperus virginiana*) in the Flints Hills area (Hulbert, 2009). These woody plants originate both from within the ecosystem and from neighboring ecosystems (Briggs et al., 2005). This woody encroachment alters ecosystems

structure and functions of temperate grasslands, resulting in a loss of biodiversity and grazing productivity (Ratajczak et al., 2016). There are several likely drivers of the increase in woody plant abundance including change in climate, increasing atmospheric carbon dioxide concentration, nitrogen deposition, grazing pressure, and disturbance regimes (e.g. the frequency and intensity of fire) (Briggs et al., 2005). Transitions to shrubland and woodland in temperate climates are largely attributed to changes in fire management (Ratajczak et al., 2016).

Annual spring burning is beneficial in stopping woody encroachment but also increases homogenization of plant and avian communities (Collins et al., 1995) (Ratajczak et al., 2016). Fire and grazing treatments that promote uniformity cannot maintain biodiversity in tallgrass ecosystems (Fuhlendorf et al. 2006). In addition, it has been shown that annual burns do not eliminate shrub species and that a continued increase in shrubs may lead to areas where woody vegetation may gain a foothold and spread further (Towne and Kemp, 2003). Another negative impact of burning is when large areas are burned, nearby towns and cities suffer from air quality issues related to the particulates released during burning (Dennis et al. 2002). The frequency of burns in the Flint Hills for the period 2001-2010 is shown in Figure 6-5.

Figure 6-5. The frequency of burning within the Flint Hills from 2001-2010. The original data from Mohler and Goodin (2012) was subset to include only the 2001-2010 data.

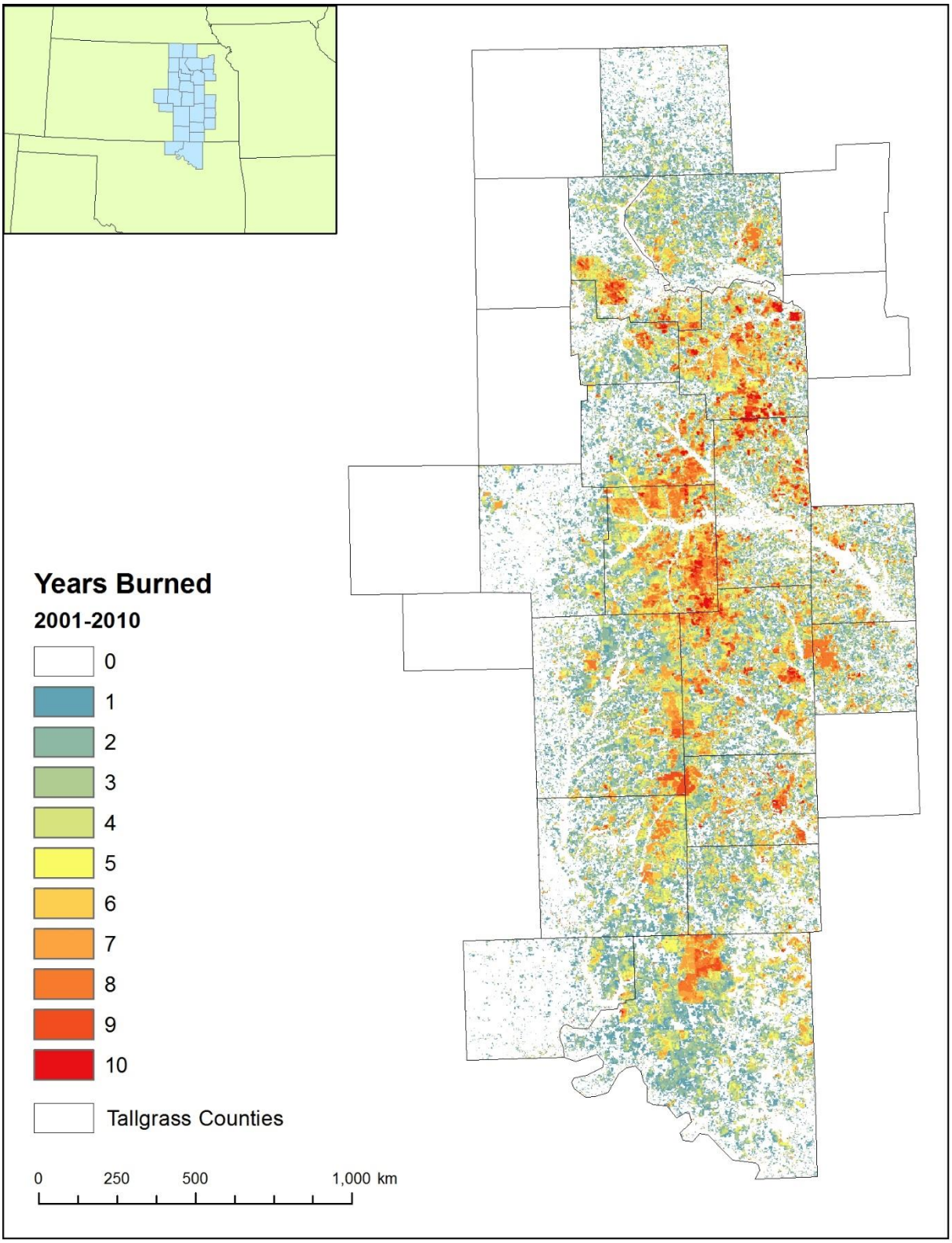

Data and Methods

Data Acquisition

The image data used for this analysis were MODIS MOD13Q1 product images. These were 16 day maximum value NDVI composite images with a 250 meter spatial resolution. MODIS MOD13Q1 images are a gridded level 3 product delivered in a sinusoidal projection. The images calibrated and geolocated based on grid and angular data, masked from cloud, land/water, perceptible water and aerosol products, incorporate spectral reflectance, and undergo quality assurance flags associated with atmospheric correction products (Huete et al., 2002).

Images were downloaded from the Earth Observing System Data and Information System and saved as an 8-bit unsigned integer grid. Due to the nature of the sensor and the curvature of the Earth, the cell resolution for the study area was 231.656 meters. Images were clipped to the study area of 26 counties (940 Columns, 1840 Rows). Images were saved as .dat files to meet the TIMESAT input requirement of headerless binary files. Saved images were placed in the same file directory for later processing in TIMESAT.

Images were collect for the period of January 2001 through December 2015. TIMESAT only analyzes for n -1 centermost season, the results of this study will be for 14 years and exclude the 2015 season. Each calendar year include 23 MODIS images with this study using 345 total images (23 x 15).

Data Processing in TIMESAT

After image data collection and preprocessing was complete, a text file of all NDVI time series dataset was constructed for input into TIMESAT processing (Appendix A). The first row of the input file indicated how many images were to be used in the study (n=345), while the

second and subsequent rows show the full path and filename of each MOD13Q1 image in the complete series.

TIMESAT reads each image file in the time series, as well as any optional quality indicators, preprocesses the images using optional quality indicators, smooth's the time series data using a number of possible filter types and user-defined parameter settings, and extracts seasonality parameters, known as phenometrics, to a file based on the selected smoothing function. Pixel reliability for images can be used to weight each pixel in the time series. A value of 0 (good data), had full weight (1.0), values 1-2 (marginal data, snow/ice) had half weight (0.5) and value 3 (cloudy) had low weight (0.1).

The TIMESAT graphical user interface (GUI) displays the controls for selecting the smoothing function and parameter settings, and provides a graphical view of the raw and smoothed curves for one pixel as well as that pixels associated phenometrics (Figure 6-6). The TIMESAT interface is composed of three sections, data plotting, common settings, and class-specific settings. Each of these sections allow for the selecting of a smoothing function and related parameter settings. A discussion of each section follows.

Figure 6-6. The TIMESAT graphical user interface showing the raw data of the MODIS image cell in blue and the fitted phenology curves in brown during the study period. The start of season (left) and end of season (right) phenometrics can be seen as brown points on the curves.

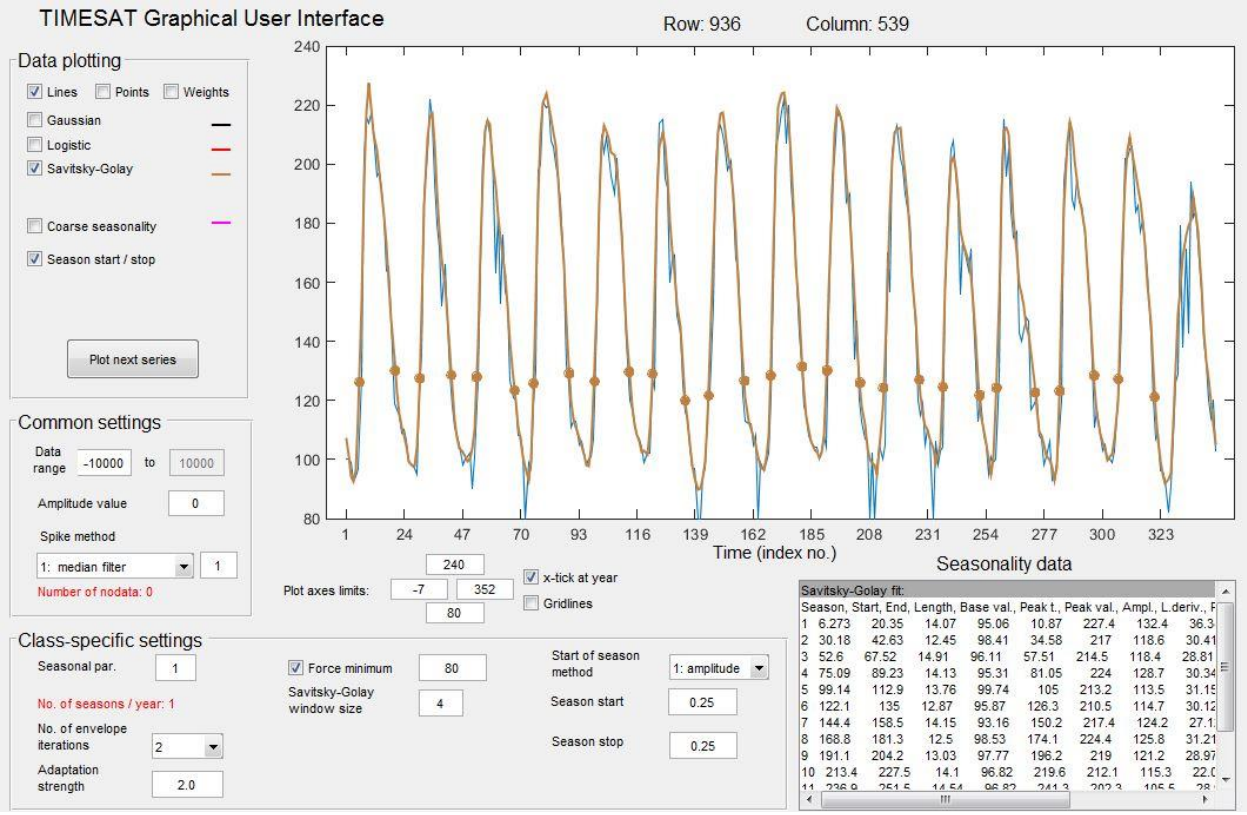

Data Plotting

TIMESAT ha three different filters, or smoothing functions, including Gaussian, Logistic, and Savitzky-Golay. The Gaussian filter is an asymmetric function fitting method that determines the positon of the maximum or the minimum value in a time series while accounting for the independent time variable (Jonsson and Eklundh 2002). The disadvantage with Gaussian filtering is in the difficulty associated with identifying a reasonable and consistent set of maxima and minima which determine the local functions used to fit to the raw data (Jonsson and Eklundh 2002). This could make it difficult to determine between the maxima and minima that could be due to seasonal variation, and that which is due to disturbances or noise (Jonsson and Eklundh 2010). The double logistic filter that is included with TIMESAT has been found to preserve

NDVI values but has shown no major difference with the Saviszky-Golay filter (Jonsson et al., 2010).

The Savizky-Golay filter is a simplified least-squares-fit convolution for extracting derivatives and smoothing a spectrum of consecutive values (Jonsson and Eklundh, 2002). It is a weighted moving average filter based on a polynomial where the polynomial order dictates the convolution. When the weight coefficients are applied to a signal, a polynomial least squares fit will be applied to the filter window. This procedure is done to maintain peak times within the data and reduce bias noise from the data (Chen et al., 2004). It is also intended to preserve the area and mean position of a seasonal peak, but alters both the height and width. The Savitzky-Golay filter is sensitive to local variations in vegetation index values, which proves useful when comparing different regions (Jonsson et al., 2010). The result is a smoothed curve adapted to the upper envelope, or peak values, of the value in a time-series.

Common Settings

The common settings section in TIMESAT affect all pixels in the image time series. Within the common settings, there are three different spike methods: STL original, STL replace, and median filter method. The STL method, which stand for seasonal trend LOESS, performs seasonal smoothing and decomposes time series data by using a LOESS smoother (locally weighted regression smoother) based on a weight system (Verbesselt et al., 2009). The STL decomposition take the full time-series and partitions it into a seasonal and trend component, and low weights are assigned to the values that do not fit these patterns (Cleveland et al., 1990).

For this project's analysis, the median spike method was used because unlike the two STL options, the median spike method retains all raw data values. Values in the time series that

are significantly different from neighboring values and from the median in a window are classified as outliers and are assigned a zero weight value (Eklundh and Jonsson 2010).

The median filter method also incorporates a spike value. The spike value is used to determine significant differences in adjacent values in the time series. Data values that differ from the median by more than the product of the spike value and standard deviation of the time-series, and that are different from the values neighbors are removed (Eklundh and Jonsson 2010). A spike value of 2 was used in this analysis due to the TIMESAT manual suggesting that a spike value below 2 will remove more data value from an analysis.

Class-specific Settings

TIMESAT class-specific settings apply to individual land classes such as different landuse/landcover categories. Eight different class–specific settings can be applied. The seasonality parameter defines the number of growing season per year. A value of 1 will force the program to treat all data as if there is one season per year. This study uses a value of 1 as there is one season per year. Areas that experience dual seasons should use a parameter value of 0.

The number of envelope iterations makes the function fit and approach the upper envelope of the time-series in an iterative procedure. A value of 1, 2, or 3 can be set for this parameter. Specifying 1 means there is only one fit to the data and no adaption to the envelope. Specifying 2 or 3 there are, respectively, one and two additional fits where the weights of the values below the fitted curve is decreased forcing the fitted function toward the upper envelope (Eklundh and Jonsson 2010). A value of 2 was selected for this parameter as it has been determined to better fit the raw data values within the Flint Hills ecoregion (Pockrandt 2014).

The adaption strength parameter varies between 1 and 10. It indicates the strength of the upper envelope adaption with 10 being the strongest adaption to the upper envelope and 1 being

no adaption. Having too strong of an adaption may put too much emphasis on single high data values leading to poor results. The adaption strength needs to be fine-tuned for given data, but a normal adaption value is around 2 or 3. A value of 2 was used in this study.

Force minimum removes extremely low value in the time series and replaces them with the value entered. This parameter is useful in eliminating low NDVI values that are recorded during winter when the snow covers the land surface. By forcing the low values into something approaching the mean winter minima, it helps preserve the true seasonal curves generated by the fitted function. The Flint Hills do experience extended winter periods with snow on the ground, so a value of 80 was set for this parameter.

The window size for Savitzky-Golay is the width, or half-window, of the moving window used by the Savizky-Golay filter during smoothing. The width of the moving window helps to determine the amount of smoothing that takes place and impacts the ability to capture rapid change in the NDVI time-series. A large value of the window gives a high degree of smoothing, but affects the possibility to follow a rapid change in data in the beginning of the growth season (Eklundh and Jonsson, 2010). The TIMESAT manual suggests a starting window size value of floor (nptsperyear/4). A window size of 4 was set as it was determined by previous work that it was the optimal setting for the data.

The start of season method parameter offers two choices: amplitude and absolute value. This parameter works with the season start and season stop values. When using the amplitude method, the season start and stop value are entered as percentages of the growing season maximum value. For example, a season start value of 0.25 will identify the time when 25% of the maximum growing season amplitude is reached. Using the absolute method will find the time each season when that specific value is reached.

As previously mentioned, the season start and season stop are parameters in TIMESAT that can either be set as amplitude or absolute values. Using amplitude as the start of season method, values for season start and season stop will range between 0 and 1. These values represent the proportion of the seasonal amplitude reached each season. A season start value of 0.25, for example, establishes the season start where the fitted curve reaches 25% of its maximum value each growing season. Although season start and season stop are two separate settings, they are typically assigned the same values. Selecting low value for the season start and season stop may place the values too early or late in the season in portions of the fitted curve dominated by atmospheric and calibration noise. High values may incorrectly label as the season start and season stop date periods well inside the actual growing season instead of its true beginning and end.

Phenometric Extraction

In TIMESAT, a parameter settings file was created for phenometric extraction. The parameters discussed in the previous section can be seen in Figure 6-7 with the values for each of the parameters filled in. With a valid parameter file, the time-series data was processed using TIMESAT TSF_process (TIMESAT Fortran process) which applied a Savitzky-Golay filter to the raw NDVI data. Seasonality data was extracted from the smoothed curves and output to a TPA file and processed by the TIMESAT TSM_printseasons to generate numerical phenometric data. The TIMESAT seasonality files contain 11 total phenometrics for each pixel for a maximum of n-1 years in a time series.

Each MODIS NDVI image had 1847 rows and 940 columns of pixels which is more than 1.7 Million data values per phenometric per season. Most of these values were null values with only 311,000 data values examined. Eight of the 11 phenometrics were examined in this study

including, start of season, end of season, middle of season, left derivative, right derivative, growing season length, maximum value, and small integral. Table 6-1 shows a more complete list of phenometrics as well as providing a definition and explanation of biological significance.

Figure 6-7. Settings interface in TIMESAT with values filled in for the parameters

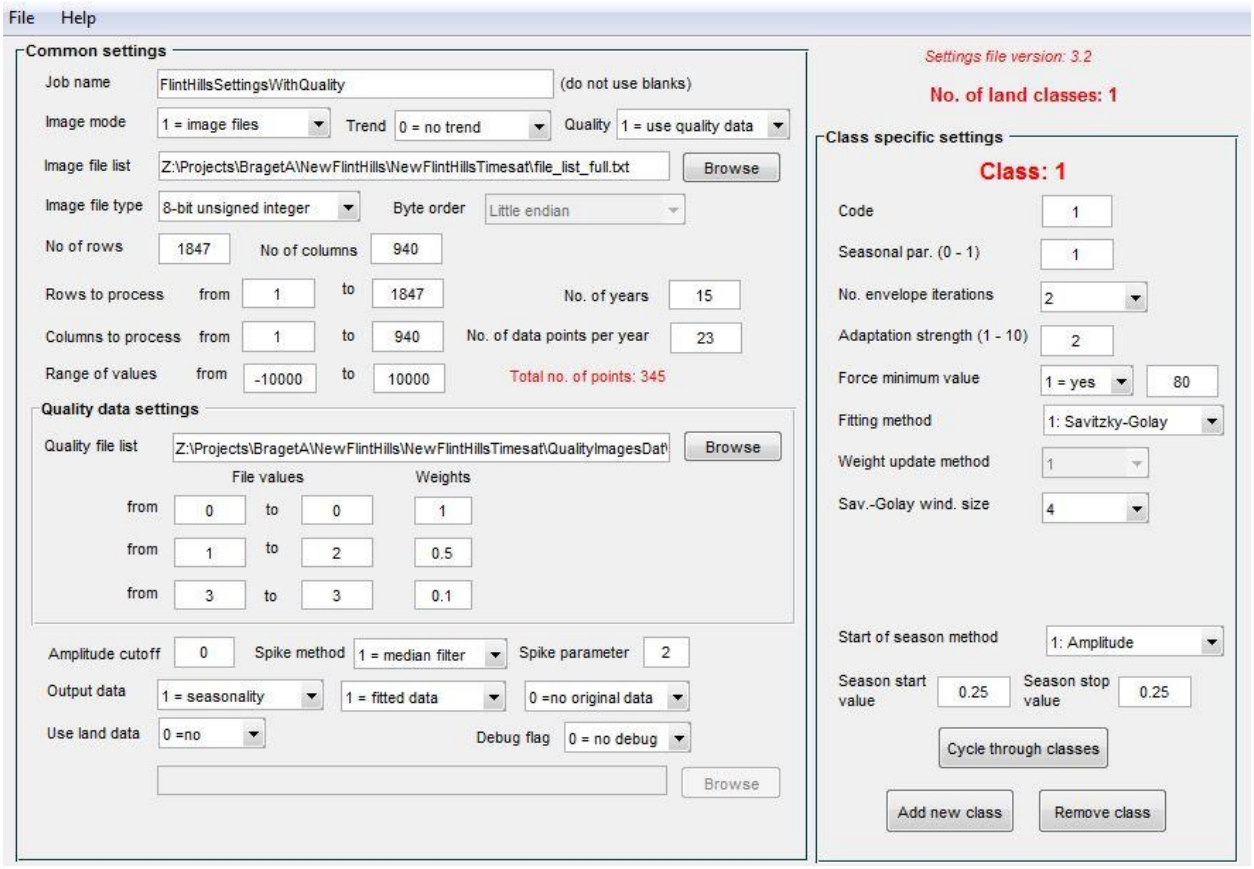

Table 6-1. Phenometrics output in TIMESAT. Grayed ones were examined in this thesis.

Phenometric	Definition	Biological Significance
Start of Season	Time for which the left edge has increased to a user defined level measured from the left minimum level	Time of initial vegetation green up
End of Season	Time for which the right edge has decreased to a user defined level measured from the right minimum level	Time of initial vegetation senescence
Season Length	Time from the start to the end of the season	Length of growing season from green up to senescence
Base Level	The average of the left and right minimum values	Baseline for the seasonal phenology curve
Middle of Season	Mean value of the times for which the left edge has increased to the 80% level and the right edge has decreased to the 80% level	Time of the middle of the growing season
Maximum Value	Largest data value for the fitted function during the season	The highest NDVI value of the season
Seasonal Amplitude	Difference between the maximum value and the base level	Used for referenced start and end of season thresholds
Rate of Increase at Beginning of Season	Ration of the difference between the left 20% and 80% levels and the corresponding time difference	Rate of vegetation green up
Rate of Decrease at the End of Season	Absolute value of the ratio of the difference between the right 20% and 80% levels and the corresponding time difference	Rate of vegetation senescence
Large Seasonal Integral	Integral of the function describing the season from season start to season end	Proxy for the relative amount of vegetation biomass without regarding minimum values
Small Seasonal Integral	Integral of the difference between the function describing the season and the base level from season start to season end	Proxy for the relative amount of vegetation biomass while regarding minimum values

Using the TSF_seas2img function in TIMESAT, each of the eight selected phenometrics were output to an image file for each available year in the study period (n=14). Figure 6-8 shows a map of the "end of season" phenometric for the 2002 season as generated by TIMESAT. The end of season, middle of season, and start of season phenometrics were given values, by

TIMESAT, which corresponded to their image number in the series. For the first season, this value corresponded directly to day of year (DOY). However, in subsequent seasons image numbers were converted to appropriate DOY values. For example, the second MOD13Q1 image in year two and three would have image numbers of 25 and 48, respectively. The individual phenometric images for each year were also used to calculate mean and standard deviation images for the 2001-2014 period.

Figure 6-8. The end of season phenometric for the Flint Hills ecoregion in 2002 as estimated by TIMESAT.

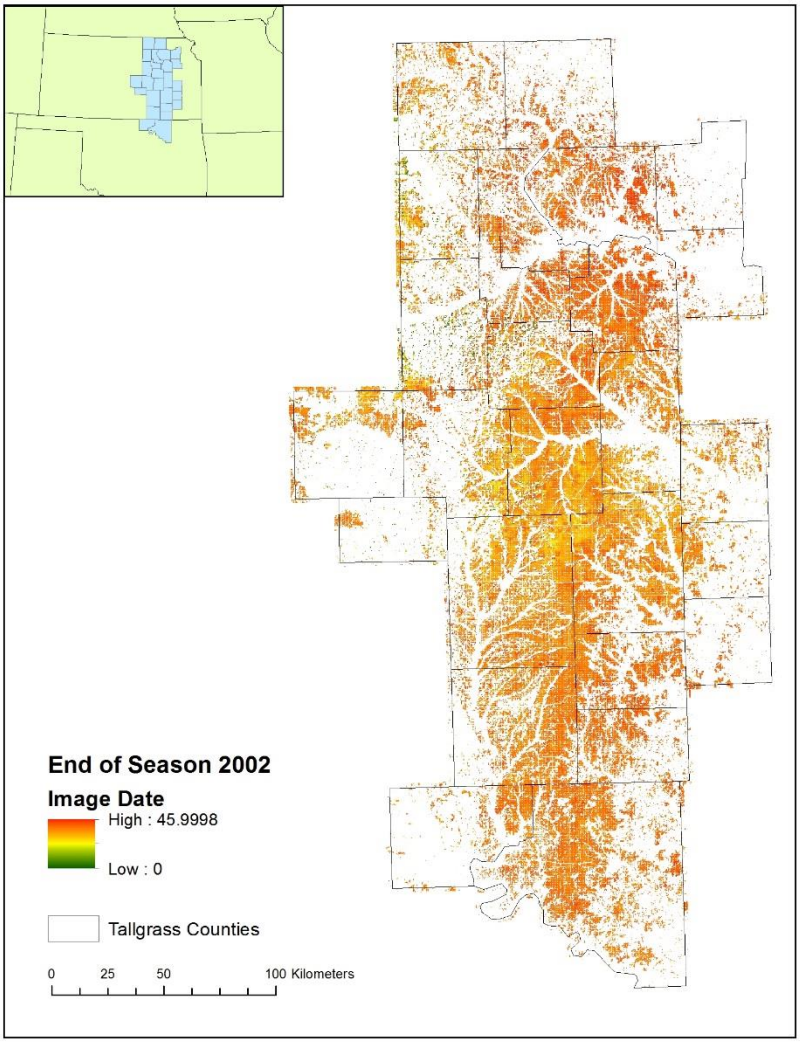

ANOVA and Tukey HSD Analysis

An ANOVA was performed in R (Appendix B) on the mean values for each pixel and each phenometric. In addition, pixel-scale phenometrics were aggregated at the county level which later served as treatments in statistical analyses. Each of the eight phenometrics was also subjected to a Tukey HSD to determine if significant differences between treatments (counties) were present and to identify groups of treatments with similar phenometric means. Prior to running the ANOVA and Tukey HSD tests, the phenometric mean data values were evaluated for normality using histograms and measurements of skewness and kurtosis (Figure 6-9 and Appendix C).

The Tukey's HSD test is a single step multiple comparison procedure and statistical test often performed in conjunction with ANOVA to find means that are significantly different from each other. The Tukey HSD test was performed on each of the eight phenometrics mean values, which were divided into the 26 counties of the study area. This created a mean value of the phenometric mean values for each county, which can be seen in Figure 6-12 for the end of season. Each county has been assigned a group number, shown under the M column. Counties with the same letter belong in the same group while counties that contain multiple letters share characteristics of additional counties but retains a unique identity. The output of the Tukey HSD was incorporated into a GIS for mapping and visualization. Figure 6-11 shows the ANVOA result for the end of season phenometric.

Figure 6-9. Histogram for the end of season phenometric illustrating the approximate normality common to all phenometrics evaluated.

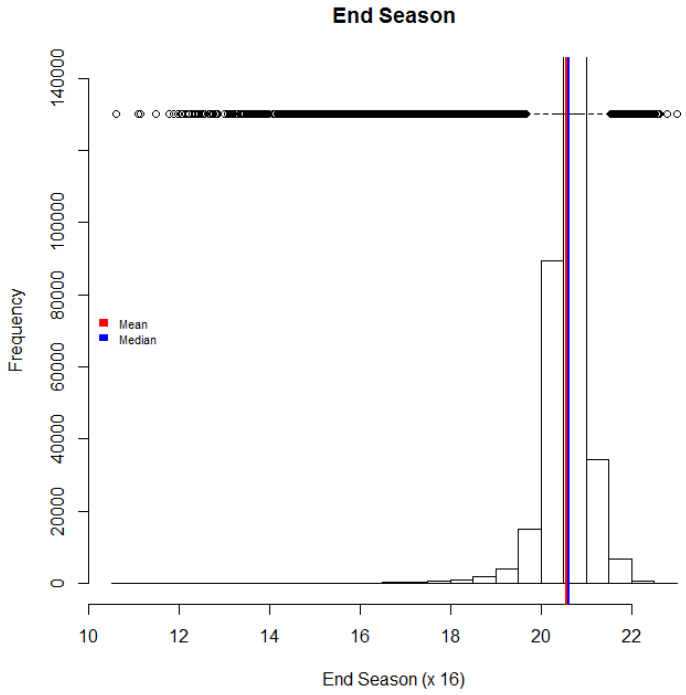

Figure 6-10. Data summary for end of season phenometric. A good indication that a data set is normally distributed is when the mean and median values are similar.

	vars	n	mean	sd	median	trimmed	mad	min	max	range	skew	kurtosis	se
X1	1	304386	20.57	0.57	20.61	20.61	0.35	10.61	23	12.39	-3.15	27.23	0

Figure 6-11. ANOVA result for the end of season phenometric.

```
Analysis of Variance Table

Response: pheno
               Df Sum Sq Mean Sq F value    Pr(>F)
data$County    25   6869 274.755  922.27 < 2.2e-16 ***
Residuals   304360  90673   0.298
---
Signif. codes:  0 '***' 0.001 '**' 0.01 '*' 0.05 '.' 0.1 ' ' 1
```

Figure 6-12. Tukey HSD test results with a mean value calculated for the end of season phenometric. Each county has been assigned a group number, shown under the M column. Counties with the same letter belong in the same group while counties that contain multiple letters share characteristics of additional counties but retain a unique identity.

$groups

	trt	means	M
1	Jackson	21.12229	a
2	Shawnee	21.08074	a
3	Pottawatomie	20.78606	b
4	Wabaunsee	20.77811	bc
5	Coffey	20.74865	c
6	Elk	20.70999	d
7	Woodson	20.69907	de
8	Lyon	20.69387	de
9	Chautauqua	20.67094	ef
10	Riley	20.65785	f
11	Wilson	20.65695	fg
12	Washington	20.65037	fg
13	Geary	20.64714	fg
14	Morris	20.60727	gh
15	Marshall	20.57955	hi
16	Greenwood	20.57770	i
17	Butler	20.53282	j
18	Chase	20.52469	j
19	Marion	20.48944	k
20	Cowley	20.47771	k
21	Osage	20.45622	l
22	Clay	20.44302	l
23	Kay	20.26886	m
24	Dickinson	20.22807	n
25	McPherson	20.22234	n
26	Harvey	20.09495	o

A K-Means clustering analysis was also performed using the R software package (see Appendix B for the script used in this study) to determine which groups of counties were similar. The K-Means clustering is a method of vector quantization that aims to partition the data in a set number of clusters in which each observation belongs to a cluster with the nearest mean. The optimal number of clusters was determined to be 6 based on a range of clusters examined in R. Figure 6-13 shows the graph where the optimum number of clusters is at the "elbow" of the curve signifying that many clusters are sufficient to group the data. The 6 clusters divided the 26 counties based on their means for each phenometrics (Figure 6-14).

Figure 6-13. Elbow curve graph indicating the optimum number of clusters is at the "elbow" of the curve, or a value of 6.

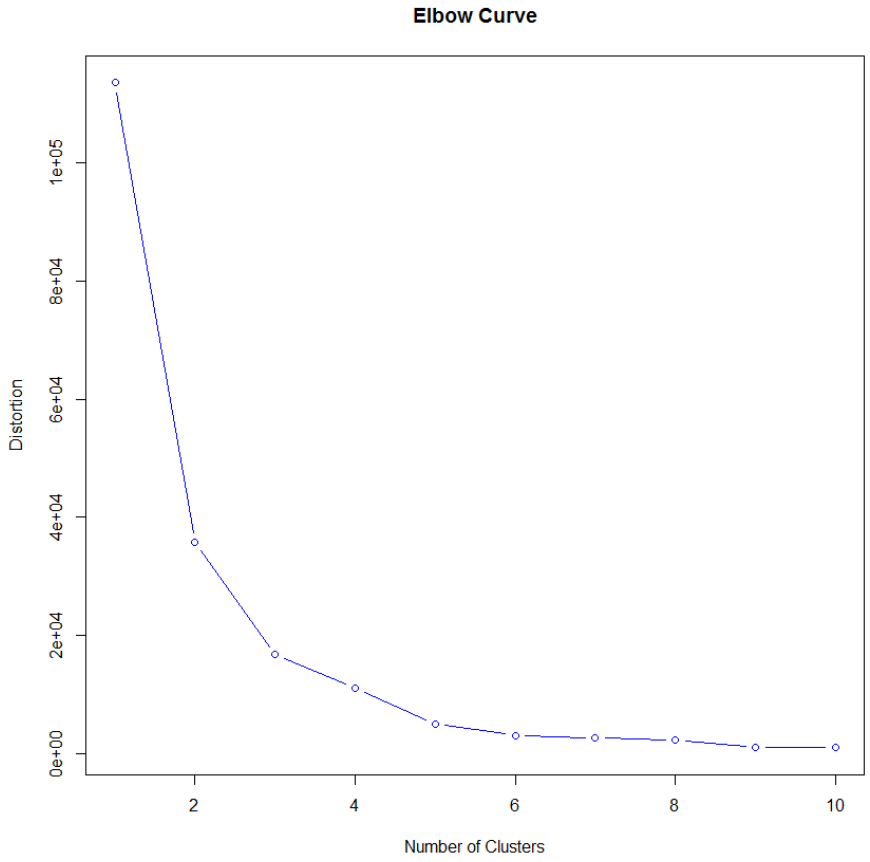

Figure 6-14 Cluster means resulting from K-Means clustering.

```
K-means clustering with 6 clusters of sizes 2, 6, 3, 10, 1, 4

Cluster means:
   ESMeans GSLMeans  LDMeans MaxMeans MidSMeans  RDMeans SmIntMeans StSeaMeans
1 20.22521 14.13018 19.16784 193.0662  11.96855 11.07009   920.3748   6.095021
2 20.56356 14.13124 21.39716 199.3223  12.21450 11.49978  1017.0288   6.432321
3 20.40044 14.17138 19.57742 193.9935  12.17032 11.29242   953.7208   6.229061
4 20.66016 14.08714 22.62604 201.5990  12.30481 11.82576  1054.5798   6.573029
5 20.09495 13.86538 16.71786 191.1949  12.36334 11.57381   855.2643   6.229570
6 20.91875 14.40500 23.31951 205.5751  12.36520 11.92707  1116.7053   6.513747

Clustering vector:
 [1] 2 4 4 3 4 2 1 4 4 4 5 6 3 6 3 4 1 2 2 4 4 6 6 2 2 4

Within cluster sum of squares by cluster:
[1]   20.50301  949.64490  333.83129 1899.70103    0.00000 1122.93679
 (between_SS / total_SS =  96.2 %)
```

Results

The ANOVA test performed on each of the eight phenometrics indicated all phenometrics exhibited significant differences across the Flint Hills study area. The ANOVA test performed on the end of season phenometric showed that of the 26 Flint Hills counties, 25 were highly significant with only Chase county being of little significance (see Figure 6-15). The ANOVA test shows that most counties differed from the intercept (Butler County) with only Chase being similar to Butler County.

Figure 6-15. ANOVA test for the end of season phenometric with all counties being highly significant (p > 0.99) except for Chase County (p = 0.95).

```
Call:
lm(formula = pheno ~ data$County)

Residuals:
    Min      1Q  Median      3Q     Max
-9.4866 -0.2134  0.0270  0.2736  2.4169

Coefficients:
                          Estimate Std. Error  t value Pr(>|t|)
(Intercept)             20.532823   0.003008 6826.535  < 2e-16 ***
data$CountyChase        -0.008135   0.004605   -1.766   0.0773 .
data$CountyChautauqua    0.138118   0.006508   21.224  < 2e-16 ***
data$CountyClay         -0.089807   0.007367  -12.190  < 2e-16 ***
data$CountyCoffey        0.215827   0.008255   26.145  < 2e-16 ***
data$CountyCowley       -0.055116   0.004818  -11.439  < 2e-16 ***
data$CountyDickinson    -0.304754   0.006898  -44.183  < 2e-16 ***
data$CountyElk           0.177169   0.005764   30.735  < 2e-16 ***
data$CountyGeary         0.114319   0.007247   15.774  < 2e-16 ***
data$CountyGreenwood     0.044872   0.004487   10.001  < 2e-16 ***
data$CountyHarvey       -0.437872   0.012956  -33.798  < 2e-16 ***
data$CountyJackson       0.589470   0.014011   42.073  < 2e-16 ***
data$CountyKay          -0.263964   0.007412  -35.611  < 2e-16 ***
data$CountyLyon          0.161044   0.005464   29.474  < 2e-16 ***
data$CountyMarion       -0.043379   0.006022   -7.203 5.91e-13 ***
data$CountyMarshall      0.046723   0.007768    6.015 1.80e-09 ***
data$CountyMcPherson    -0.310483   0.007605  -40.826  < 2e-16 ***
data$CountyMorris        0.074444   0.005367   13.872  < 2e-16 ***
data$CountyOsage        -0.076603   0.004250  -18.022  < 2e-16 ***
data$CountyPottawatomie  0.253239   0.005608   45.153  < 2e-16 ***
data$CountyRiley         0.125030   0.006487   19.274  < 2e-16 ***
data$CountyShawnee       0.547912   0.013208   41.482  < 2e-16 ***
data$CountyWabaunsee     0.245284   0.005066   48.416  < 2e-16 ***
data$CountyWashington    0.117549   0.006666   17.635  < 2e-16 ***
data$CountyWilson        0.124126   0.013433    9.240  < 2e-16 ***
data$CountyWoodson       0.166244   0.008998   18.475  < 2e-16 ***
---
Signif. codes:  0 '***' 0.001 '**' 0.01 '*' 0.05 '.' 0.1 ' ' 1

Residual standard error: 0.5458 on 304360 degrees of freedom
Multiple R-squared:  0.07042,   Adjusted R-squared:  0.07034
F-statistic: 922.3 on 25 and 304360 DF,  p-value: < 2.2e-16
```

The Tukey HSD test results show the statistical means for each county as well as other statistical relevant information (Figure 6-16). Based on these mean values, the Tukey test grouped the counties into classes (Figure 6-17) and provide a visual representation of the ANOVA analysis (Figure 6-18). Butler and Chase counties are in the same group which represents the ANOVA result of those two counties not being significantly different from each other. Similar results for each of the seven remaining phenometrics can be seen in Appendix D.

Figure 6-16. Tukey HSD test results for the end of season phenometric.

```
$statistics
     Mean       CV   MSerror        HSD r.harmonic
  20.5695 2.653509 0.2979123 0.03782578   5631.982

$parameters
      Df ntr StudentizedRange alpha  test      name.t
  304360  26          5.20085  0.05 Tukey data$County

$means
                pheno       std     r      Min      Max
Butler       20.53282 0.5025619 32930 14.90204 22.27961
Chase        20.52469 0.3299433 24496 17.03443 22.18155
Chautauqua   20.67094 0.3467515  8946 16.95392 22.29539
Clay         20.44302 0.6920198  6587 14.55005 22.79228
Coffey       20.74865 0.5895204  5041 16.66716 22.48851
Cowley       20.47771 0.5199397 21026 13.41788 22.31789
Dickinson    20.22807 1.1799589  7732 11.09398 22.17673
Elk          20.70999 0.3611998 12320 17.80602 22.39068
Geary        20.64714 0.3782002  6852 16.84066 22.18278
Greenwood    20.57770 0.3761509 26873 17.75605 22.33444
Harvey       20.09495 1.3005861  1876 10.60833 22.51105
Jackson      21.12229 0.5254465  1591 18.38652 22.50564
Kay          20.26886 1.0165015  6491 11.48470 22.61635
Lyon         20.69387 0.4718006 14317 18.02468 22.56155
Marion       20.48944 0.8745306 10944 12.27767 22.43974
Marshall     20.57955 0.5945443  5808 16.19783 22.99640
McPherson    20.22234 1.1742971  6106 11.14480 22.29429
Morris       20.60727 0.5058217 15082 16.27977 22.32575
Osage        20.45622 0.3954456 33029 14.40785 22.14817
Pottawatomie 20.78606 0.3381763 13295 18.55215 22.34181
Riley        20.65785 0.3762047  9018 17.61865 22.27008
Shawnee      21.08074 0.5233846  1801 17.90162 22.49718
Wabaunsee    20.77811 0.3343258 17926 18.37093 22.55568
Washington   20.65037 0.5467107  8419 16.43177 22.60207
Wilson       20.65695 0.6492733  1738 16.79889 22.36265
Woodson      20.69907 0.4821074  4142 14.48958 22.29346
```

Figure 6-17. Tukey HSD test groupings for the end of season phenometric. Each of the 26 counties of the Flint Hills was placed into a class based on their mean values. Counties with similar mean values were placed into the same class.

$groups

	trt	means	M
1	Jackson	21.12229	a
2	Shawnee	21.08074	a
3	Pottawatomie	20.78606	b
4	Wabaunsee	20.77811	bc
5	Coffey	20.74865	c
6	Elk	20.70999	d
7	Woodson	20.69907	de
8	Lyon	20.69387	de
9	Chautauqua	20.67094	ef
10	Riley	20.65785	f
11	Wilson	20.65695	fg
12	Washington	20.65037	fg
13	Geary	20.64714	fg
14	Morris	20.60727	gh
15	Marshall	20.57955	hi
16	Greenwood	20.57770	i
17	Butler	20.53282	j
18	Chase	20.52469	j
19	Marion	20.48944	k
20	Cowley	20.47771	k
21	Osage	20.45622	l
22	Clay	20.44302	l
23	Kay	20.26886	m
24	Dickinson	20.22807	n
25	McPherson	20.22234	n
26	Harvey	20.09495	o

Figure 6-18. Map of Tukey HSD county-level groups for the end of season phenometric.

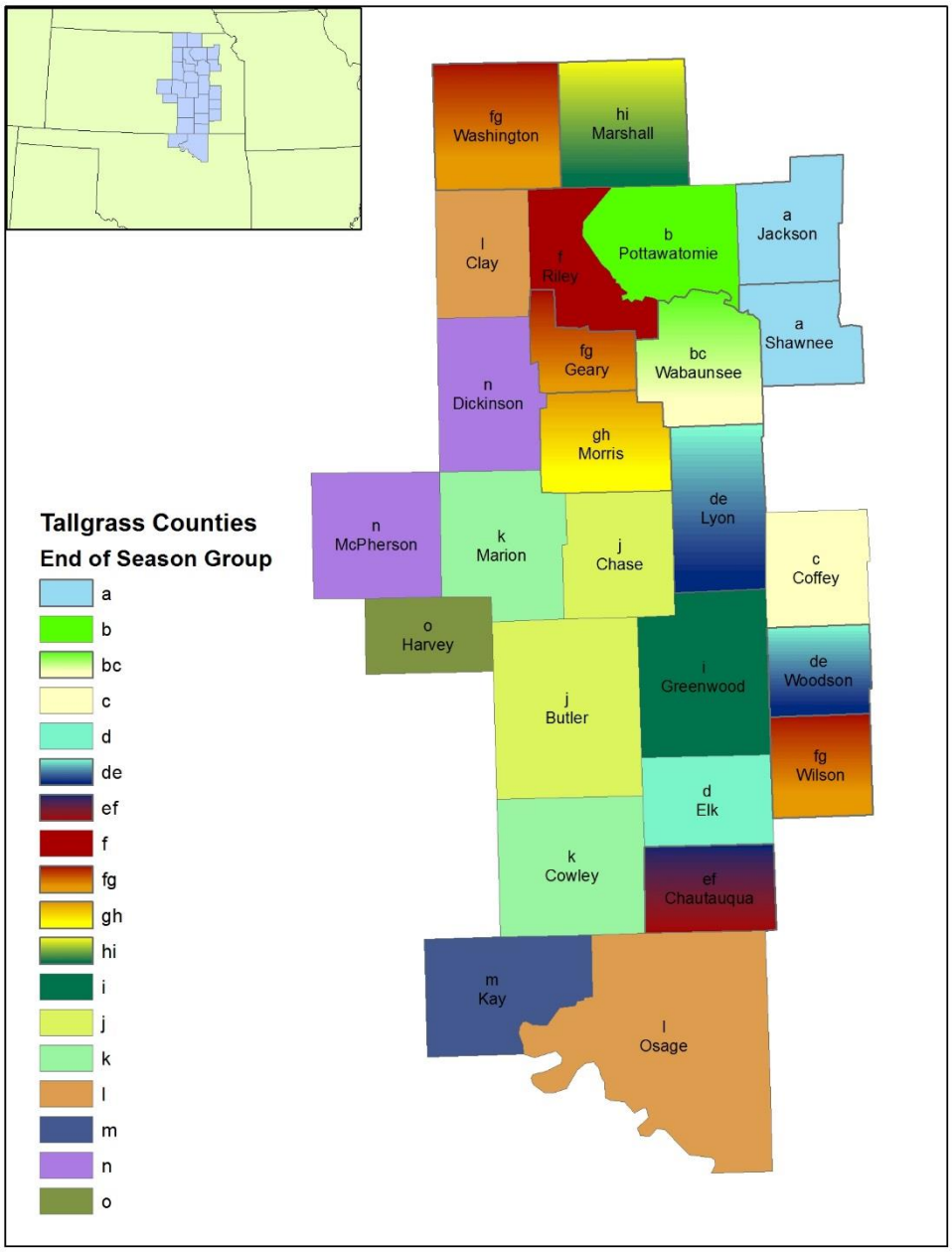

The K-means cluster partitioned the 26 counties into 6 clusters based on the mean values for each county and contained all eight phenometrics (Figure 6-19).

Figure 6-19. K-Means cluster analysis of the study area.

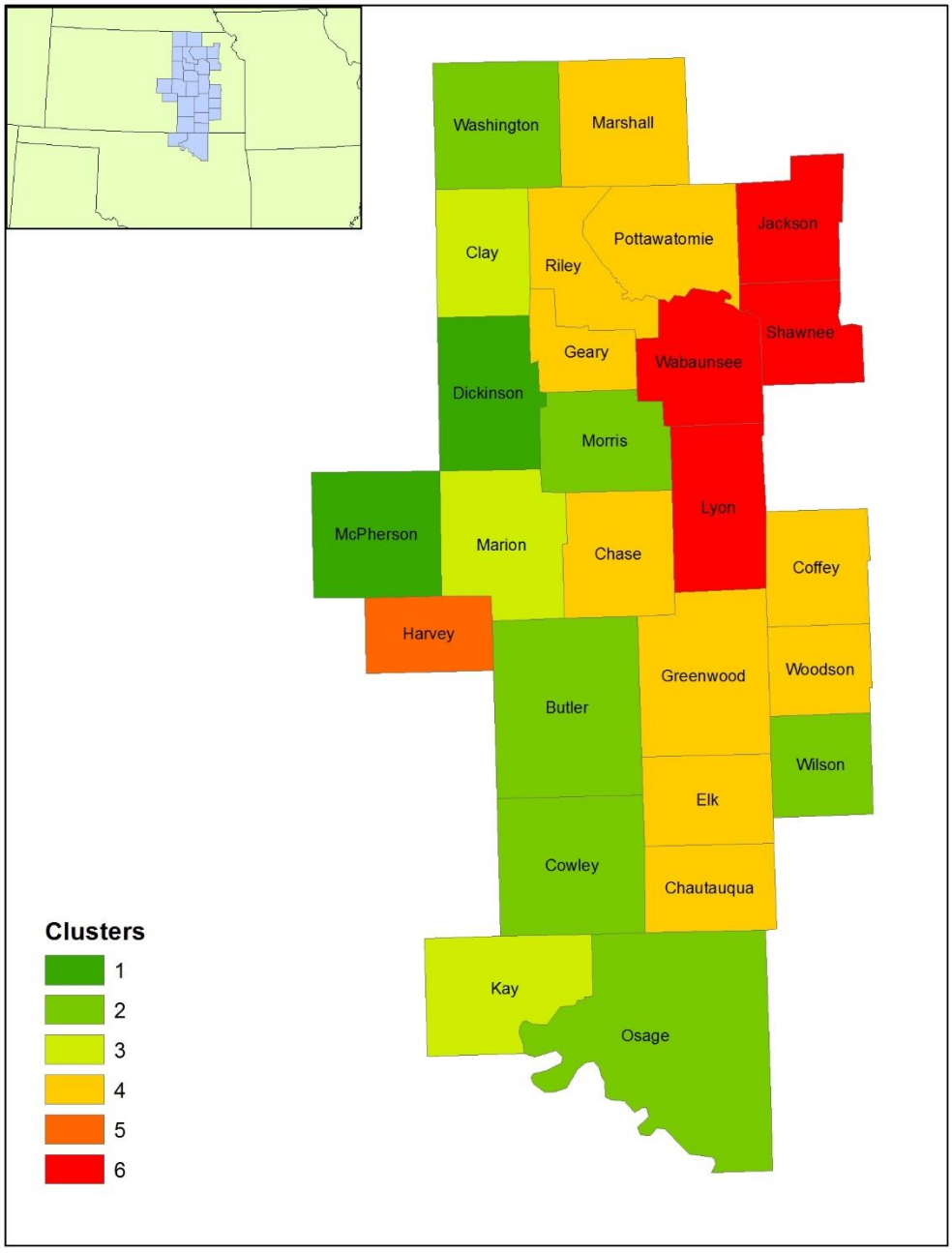

Discussion and Conclusions

The Tukey test resulted in counties being grouped together based on differences in their mean phenometric values. For each of the Tukey test analyses, this grouping could be seen when looking at two counties that the ANOVA test showed where not significantly different than each

other. Looking at the end of season phenometric from the results section confirms that Chase and Butler County were grouped together based on their similar mean values for the end of season phenometric. Similar patterns can be seen in other phenometrics. Counties with similar mean values were put into the same group or into a group that had one letter corresponding to each groups it was similar to.

Each of the K-Means clusters differ based on an evaluation of all eight phenometrics extracted. Cluster one contains the counties of Dickinson and McPherson (Figure 6-15). These counties lie on the western edge of the study area and contained the lowest phenometric values for middle of season, right derivative, and start of season mean value. With the lowest start of season value, vegetation within Dickinson and McPherson begin development earlier than any other county. Cluster two contains the counties of Washington, Morris, Butler, Wilson, Cowley, and Osage. These counties lie in the southern region of the study area except Washington and Morris counties are in the north and middle, respectfully. Morris is odd as it is in the center of the study area and one would think it would share characteristics with Chase or Geary, both of which are in cluster four.

Cluster three contains Clay, Marion, and Kay counties. These counties lie on the western edge of the study area and appear to be in a straight line (North-South) with a county between each of them (See figure 6-15). The maximum NDVI value is similar to cluster one which was also on the western edge. Small integral is similar to cluster one as well. Cluster four contains Marshall, Riley, Pottawatomie, and Geary in the North and Chase, Coffey, Greenwood, Woodson, Elk, and Chautauqua in the south. This cluster is mostly south-north gradient with Morris separating them. This cluster is second highest in all but start of season and middle of season. It contains the highest phenometric value of start of season.

Cluster five contains only the county of Harvey on the western edge of the study area (See figure 6-15) This cluster has the lowest end of season, growing season length, left derivative, maximum, and small integer. After multiple iterations of clustering, Harvey County remained as a single cluster likely due to the small amount of grassland pixels located there. Cluster six contains Jackson, Shawnee, Wabaunsee, and Lyon counties (See figure 6-15). These counties are all in one cluster on the eastern edge of the study area in a north-south distribution. This cluster has the highest in all phenometrics except start of season.

Based on the ANOVA and Tukey's test results, each of the eight phenometrics examined were significant. Each of the eight phenometrics had multiple groupings where all 26 counties of the Flint Hills did not conform into one group. This would suggest that the Flint Hills varies in terms of its phenometric values and is not a homogenous region. The K-means clustering also did not group all study area counties into one cluster but put them into 6 as per the algorithms suggested optimal number of clusters to encapsulate all of the information. Looking at the spatial distribution of clusters there is some semblance of a pattern. Clusters one and six contain counties that are next to each other in small groups. Cluster four and 2 contain counties in a north to south distribution. This can be said about most of the clusters due to the nature of the study area, however it is important to note that the clusters rarely overlap with the north to south groups steadily moving from the west to the east across the study area. It can be speculated that factors such as precipitation may cause the pattern observed due to the increasing amount of precipitation seen when traveling from the western section of the study area to the eastern sections. Further tests must be done to determine what factors may be influencing the observed pattern.

Chapter 7 - Synthesis Conclusion

Using MODIS images to create a vegetation index time series and utilizing BFAST with its ability to detect breaks and trend of vegetation greenness allows for consistent assessment of grassland vegetation in the Flint Hills. Grassland managers across the Flint Hills would benefit from knowing the greenness of their grassland and would be able to develop better ways to preserve their land. The BFAST trend analysis allows for an interesting method to characterize long-term vegetation trends as well as when and where significant breaks occur in detected trends. In addition, TIMESAT allows for the extraction of phenometrics. These phenometrics can tell us valuable information about the vegetation of an area.

This thesis presents a BFAST analysis of the Flint Hills ecoregion for the time period of 2001-2015. This BFAST analysis showed the trending direction of grassland in the area as well as the number of disturbances during the period. The BFAST analysis showed a majority (52%) of the Flint Hills experienced a browning of vegetation during the study period. Only 22% of the Flint Hills experienced positive trending pixels. The remaining 26% were stable pixels. Examining the number of breaks in trend show 38% of the Flint Hills experienced zero disturbances and the remaining 62% had at least one or more breaks in trend. These breaks in vegetation greenness resulted in either an increase or decrease in vegetation greenness. By utilizing BFAST, the location and trend of vegetation can be spatially presented for examination by land managers interested in preserving their land.

To determine the cause of vegetation trend, a second study was performed using BFAST and logistic regression with burn frequency, precipitation deviation, and hydrological soil group data. Due to the limited time frame of the burn frequency data of 2001-2010, the BFAST analysis was run on grassland pixels of the same time frame. During the 2001-2010 study

period, 41% of the Flint Hills experienced browning and 43% experienced positive trend. The remaining 16% of were stable during the study period. Examining the number of breaks in trend show 52% of the Flint Hills experienced zero disturbances while the remaining 48% had at least one or more breaks in trend. The logistic regression showed each of the variables examined in this study as being statistically significant. The negative coefficients of the GLM suggest that precipitation deviation and hydrologic group B are less likely to result in a negative trend. Soils of group B reduce the log odds of a negative trend by 2.60 and a unit increase in precipitation deviation, or an increase in the amount of precipitation vegetation receives, reduces the log odds of a negative trend by 2.28. The soils of group C and D have positive coefficients which means they increase the log odds of a negative trend by 1.96 and 1.78, respectively. For every increase in unit of burn frequency there is an increase in log odds of a negative trend by 4.23.

It is no surprise that increasing the amount of precipitation will result in healthier vegetation. However, in conjunction with precipitation, there needs to be soils capable of capturing this moisture. Hydrologic group B contains loam, silt loam, and silt soils, all of which are able to retain soil moisture to be used by vegetation. Hydrologic groups C and D result in negative trending vegetation because they contain clay and sandy soils which are unable to retain soil moisture. The burn frequency shows burning every year will result in a negative trend in vegetation greenness. Previous research has shown a burning frequency of once every 4 years is healthier for vegetation (Collins et al., 1995).

The analysis of deviance table shows the residual deviance decreasing with each variable input but the individual deviance decreases and then increases with the final input. The difference between the null deviance and the residual deviance shows how the model is doing against the null model, a model with only the intercept. The wider the gap is, the better. With

each variable input, the residual deviation decreased about one thousand. Each of the variables was significant and helped to explain the model. The McFadden R^2 value represents how well the model fits the data. With a McFadden value of 0.01, our model need more strong predictors in order to get an optimum value near 1.

Lastly, this thesis examined the use of TIMESAT to extract important information about the phenology of the Flint Hills. Eight phenometrics were extracted; start of season, end of season, end of season, maximum, left derivative, right derivative, season length, and middle of season. These phenometrics can show us when and where vegetation is greening up and browning down for the year as well as show the amount of vegetation biomass. These phenometrics were examined using ANOVA and the Tukey test to determine if there were significant differences in each phenometric across the entire study area and which subsets of county-level administrative divisions exhibited similarities. The ANOVA test determined that each phenometric was significantly different. The Tukey test groupings resulted in counties being grouped together based on how different their mean phenometric value was compared to other counties mean phenometric value. For each of the Tukey test groupings, this grouping could be seen when looking at two counties that the ANOVA test showed where not significantly different than each other. Looking at the end of season phenometric from the results section confirms that Chase and Butler County were grouped together based on their similar mean values for the end of season phenometric. Similar patterns can be seen in other phenometrics. Counties with similar mean values were put into the same group or into a group that had one letter corresponding to each group it was similar to.

For the K-Means clusters, the clusters were based on the mean value of each phenometric. There were six clusters distributed throughout the study area. These clusters

would suggest that the Flint Hills varies in terms of its phenometric values and is not a homogenous region. Looking at the spatial distribution of clusters there is some semblance of a pattern. Clusters one and six contain counties that are next to each other in small groups. Cluster four and 2 contain counties in a north to south distribution. This can be said about most of the clusters due to the nature of the study area, however it is important to note that the clusters rarely overlap with the north to south groups steadily moving from the west to the east across the study area. It can be speculated that factors such as precipitation may cause the observed pattern due to the increasing amount of precipitation seen when traveling from the western section of the study area to the eastern sections. Using either the k-means clusters of counties or the Tukey test groupings, it may be possible to inform burning practices to burn in different locations at different times to help mitigate excessive smoke.

References

An, N. 2009. Estimating Annual Net Primary Productivity of the Tallgrass Prairie Ecosystem of the Central Great Plains using AVHRR NDVI. University of Kansas.

Augustin, N.H., Cummins, R.P., and French, D.D. 2001. Exploring spatial vegetation dynamics using logistic regression and a multinomial logit model. *Journal of Applied Ecology* 38(5):991-1006.

Benson, E.J., and Hartnett, D.C. 2006. The role of seed and vegetative reproduction in plant recruitment and demography in tallgrass prairie. *Plant Ecology* 187:163-177.

Briggs, J.M. and Knapp, A.K. 1995. Interannual variability in primary production in tallgrass prairie: climate, soil moisture, topographic position, and fire as determinants of above-ground biomass. *American Journal of Botany* 82:1024-1030.

Briggs, J.M., Knapp, A.K., Blair, J.M., Heisler, J.L., Hoch, G.A., Lett, M.S., and McCarron, J.K. 2005. An ecosystem in transition: Causes and consequences of the conversion of mesic grassland to shrubland. *BioScience* 55:3.

Campbell, J.B., and Randolph, H.W. 2011. Introduction to remote sensing. *Guilford Press*.

Carlson, T.N., and David A.R. 1997. On the relation between NDVI, fractional vegetation cover, and leaf area index. *Remote Sensing of Environment* 62 (3): 241-52.

Chen, J., Jönsson, P., Tamura, M., Gu, Z., Matsushita, B., and Eklundh, L. 2004. A simple method for reconstructing a high-quality NDVI time-series data set based on the Savitzky–Golay filter. *Remote Sensing of the Environment* 91: 332–344.

Cleland, E. E., Chuine, I., Menzel, A., Mooney, H.A., and Schwartz, M.D. 2007. Shifting plant phenology in response to global change. *Trends in Ecology & Evolution* 22: 357–365.

Cleveland, W.S., and Devlin, S.J. 1988. Locally weighted regression: An approach to regression analysis by local fitting. *Journal of the American Statistical Association* 83 (403): 596-610.

Cleveland, R.B., Cleveland, W.S., McRae, J.E., and Terpenning, I. 1990. STL: A SeasonalTrend Decomposition Procedure Based on Loess. *Journal of Official Statistics* Vol. 6(1): 3-73.

Collins, S.L., Gleen, S.M., and Gibson, D.J. 1995. Experimental analysis of intermediate disturbance and initial floristic composition: Decoupling cause and effect. *Ecology* 76:486-492.

Colwell, J.E. 1973. Bidirectional spectral reflectance of grass canopies for determination of above ground standing biomass. University of Michigan, Ann Arbor, Michigan.

Colwell, J.E. 1974. Vegetation canopy reflectance. *Remote Sensing of Environment*. 3:175-183

Dalgleish, H.J., and Hartnett, D.C. 2008. The effects of fire frequency and grazing on tallgrass prairie productivity and plant composition are mediated through bud bank demography. *Journal of Plant Ecology* 201:411-420.

DeFries, Ruth. 2008. Terrestrial Vegetation in the Coupled Human-Earth System: Contributions of Remote Sensing. *Annual Review Environment and Resources* 33:369-390.

Dennis, A., Fraser, M., Anderson, S., and Allen, D. 2002. Air pollution emissions associated with forest, grassland, and agricultural burning in Texas. *Atmospheric Environment* 36:3779-96.

Dodds, W.K., K.C. Wilson, R.L. Rehmeier, G.L. Knight, S. Wiggam, J.A. Falke, H.J. Dalgleish, and K.N. Bertrand. 2008. Comparing ecosystem goods and services provided by restored and native lands. *BioScience* 58(9):837-845.

Eklundh, L., and Jönsson, P. 2010. Timesat 3.0 Software Manual. Lund University, Sweden.

Figueiredo, M.A.T., and Jain, A.K. 2002. Unsupervised learning of finite mixture models. *IEEE Transactions on Pattern Analysis and Machine Intelligence* 24 (3):381-396.

Fuhlendorf, S.D., Harrell, W.C., Engle D.M., Hamilton R.G., Davis C.A., and Leslie, D.M. 2006. Should heterogeneity be the basis for conservation? Grassland bird response to fire and grazing. *Ecological Applications* 16 (5): 1706-16.

Ganguly, S., Friedl, M.A., Tan, B., Zhang, X., and Verma, M. 2010. Land surface phenology from MODIS: Characterization of the collection 5 global land cover dynamics product. *Remote Sensing of Environment* 114 (8):1805-1816.

Glaser, A. 2014. America's grasslands: The future of grasslands in a changing landscape. Proceedings of the 2nd biennial conference on the conservation of America's grasslands.

Heumann, B.W., Seaquist, J. W., Eklundh, L., and Jönsson, P. 2007. AVHRR Derived Phenological Change in the Sahel and Soudan, Africa, 1982 - 2005. *Remote Sensing of Environment* 108: 385-392.

Homer, C.G., Dewitz, J.A., Yang, L., Jin, S., Danielson, P., Xian, G., Coulston, J., Herold, N.D., Wickham, J.D., and Megown, K. 2015. Completion of the 2011 National Land Cover Database for the conterminous United States-representing a decade of land cover change information. *Photogrammetric Engineering and Remote Sensing* 81(5):345-354.

Huete, A.R. 1988. A soil-adjusted vegetation index (SAVI). *Remote Sensing of the Environment* 25:295-309.

Huete, A., Didan, K., Miura, T., Rodriguez, E.P., Gao, X., and Ferreira, L.G. 2002. Overview of the radiometric and biophysical performance of the MODIS vegetation indices. *Remote Sensing of Environment* 83:195-213.

Hulbert, L.C. 2009. Fire effects on tallgrass prairie. *Proceedings of the Ninth North American Prairie Conference* 138.

Hutchinson, J.M.S., Jacquin, A., Hutchinson, S.L., and Verbesselt, J. 2015. Monitoring vegetation change and dynamics on U.S. Army training lands using satellite image time series analysis. *Journal of Environmental Management* 150:355-366.

Jacquin, A., Sheeren, D., and Lacombe, J.P. 2010. Vegetation cover degradation assessment in Madagascar savanna based on trend analysis of MODIS NDVI time series. *International Journal of Applied Earth Observation Geoinformation* 12S, S3-S10.

Jacquin, A., Goulard, M., Hutchinson, J.M.S., Devienne, T. and Hutchinson, S.L. 2016. A statistical approach for predicting grassland degradation in disturbance-driven landscapes. *Journal of Environmental Protection* 7:912-925.

Jain, A.K. 2010. Data clustering: 50 years beyond K-means. *Pattern Recognition Letters* 31(8):651-666.

Jensen, A. R. 1983. Biophysical Remote Sensing. *Annals of the Association of American Geographers*, 73(1): 111–132.

Jonsson, P., and Eklundh, L. 2004. TIMESAT – A program for analyzing time-series of satellite sensor data. *Computers & Geosciences* 30(8):833-845.

Jönsson, P., and Eklundh, L. 2002. Seasonality extraction by function fitting to time-series of satellite sensor data. *IEEE Transactions on Geoscience and Remote Sensing* 40(8): 1824–1832.

Jönsson, A.M., Eklundh, L., Hellström, M., Bärring, L., and Jönsson, P. 2010. Annual changes in MODIS vegetation indices of Swedish coniferous forests in relation to snow dynamics and tree phenology. *Remote Sensing of Environment* 114: 2719–2730.

Kansas Department of Health and Environment. 2010. State of Kansas Flint Hills Smoke Management Plan.

Kauth, R.J., and Thomas, G.S. 1976. The Tasseled cap- graphic description of the spectral temporal development of agricultural crops as seen by LANDSAT. *Proceedings of the Symposium Machine Processing of Remote Sensing Data*. LARS, Purdue.

Kennedy, R.E., Townsent, P.A., Gross, J.E., Cohen, W.B., Bolstad, P., Wang, Y.Q., and Adams, P. 2009. Remote sensing change detection tools for natural resource managers: Understanding concepts and tradeoffs in the design of landscape monitoring projects. *Remote Sensing of Environment* 113(7):1382-1396.

Linderholm H.W. 2006. Growing season changes in the last century. *Agricultural and Forest Meteorology*. 137:1-14

Lunetta, R.S., Knight, J.F., Ediriwickrema, J., Lyon, J.G., and Worthy, L.D. 2006. Land-Cover change detection using multi-temporal MODIS NDIV data. *Remote Sensing of Environment* 105:142-154.

Mark, A.F., and McLennan, B. 2005. The conservation status of New Zealand's indigenous grasslands. *New Zealand Journal of Botany* 43(1):245-270.

Mohler, R.L. and D.G. Goodin. 2012. Mapping burned area in the Flint Hills of Kansas and Oklahoma, 2000-2010. *Great Plains Research* 22: 15-25

Nebraska Department of Environment Quality. 2015. State of Nebraska Exceptional Event Demonstration Package.

McDonald, R., McKnight, M., Weiss, D., Selig, E., O'Connor, M., Violin, C., and Moody, A. 2005. Species compositional similarity and ecoregions: Do ecoregion boundaries represent zones of high species turnover: *Biological Conservation* 126(1):24-40.

Omernik, J.M. 1987. Ecoregions of the conterminous United States. Map (scale 1:7,500,000). *Annals of the Association of American Geographers* 77(1):118-125.

Pettorelli, N., Vik, J.O., Mysterud, A., Gaillard, J.M., Tucker, C.J., and Stenseth, N.C. 2005. Using the satellite-derived NDVI to assess ecological response to environmental change. *Trends in Ecology and Evolution* 20:9.

Pockrandt, B. 2014. Amulti-year comparison of vegetation phenology between military training lands and native tallgrass prairie using TIMESAT and moderate-resolution satellite imagery. Unpublished Masters' Thesis, Kansas State University.

PRISM Climate Group, 2012. US 30 year normal. http://prism.oregonstate.edu (last accessed, created 02.15.17).

Ratajczak, Z., Briggs, J.M., Goodin, D.G., Luo, L., Mohler, R.L., Nippert, J.B., and Obermeyer, B. 2016. Assessing the potential for transitions from tallgrass prairie to woodlands: Are we operating beyond critical fire thresholds?. *Rangeland Ecology & Management* 69: 280- 287.

Reed, B. C., Brown, J. F., VanderZee, D., Loveland, T. R., Merchant, J. W., and Ohlen, D. O. 1994. Measuring phenological variability from satellite imagery. *Journal of Vegetation Science* 5: 703-714.

Richards, J.A., and Jia, X. 2006. Remote sensing digital image analysis. Springer-Verlag Berlin Heidelberg.

Richardson, A.J., and Wiegand, C.L. 1977. Distinguishing vegetation from soil background information. *Photogrammetric Engineering & Remote Sensing*. 43:1541-1552.

Robbins, M.B., Peterson, A.T., and Ortega-Huerta, M.A. 2002. Major negative impacts of early intensive cattle stocking on tallgrass prairies: The case of the greater prairie-chicken (tympanuchus cupido). *North American Birds* 56:239-244.

Sakamoto, T., Yokozawa, M., Toritani, H., Shibayama, M., Ishitusuka, N., and Ohno, H. 2005. A crop phenology detection method using time-series MODIS data. *Remote Sensing of Environment* 96(3):366-374.

Sellers, P.J. 1985. Canopy reflectance, photosynthesis and transpiration. *International Journal of Remote Sensing* 6:1335-1372.

Slayback, D.A., Pinzon, J.E., Los, S.O., Tucker, C.J. 2003. Northern hemisphere photosynthetic trends 1982-1999. *Global Change Biology* 9(1):1-15.

Tan, B., Morisette, J.T., Wolfe, R.E., Gao, F., Ederer, G.A., Nightingale, J., and Pedelty, J.A. 2010. An enhanced TIMESAT algorithm for estimating vegetation phenology metrics from MODIS data. *IEEE Journal of Selected Topics in Applied Earth Observations and Remote Sensing*

Towne, E.G., and Kemp, K.E. 2003. Vegetation dynamics from annually burning tallgrass prairie in different seasons. *Journal of Range Management* 56:185-192.

Tucker, C. 1979. Red and photographic infrared linear combinations for monitoring vegetation. *Remote Sensing of Environment* 8(2):127-150.

Tucker, C.J., Newcomb, W.W., Los, S.O., and Prince, S.D. 1991. Mean and inter-year variation of growing season normalized difference vegetation index for the sahel 1981-1989. *International Journal of Remote Sensing* 12(6):1133-5.

U.S. Department of Agriculture, National Resources Conservation Service. 2012. Web Soil Survey. http://websoilsurvey.nrcs.usda.gov/ (last accessed 02.10.17).

Verbesselt, J., Jönsson, P., Lhermitte, S., van Aardt, J., and Coppin, P. 2006. Evaluating satellite and climate data derived indices as fire risk indicators in savanna ecosystems. *IEEE transactions of Geoscience and Remote Sensing* 44: 1622.

Verbesselt, J., Hyndman, R., Newnham, G., Culvenor, D. 2009. Detecting trend and seasonal changes in satellite image time series. *International Journal of Remote Sensing*. 114: 106-115.

Verbesselt, J., Hyndman, R., Newnham, G., Culvenor, D., 2010a. Detecting trend and seasonal changes in satellite image time series. *Remote Sensing of Environment*. 114(1):106-115.

Wardlow, B. D. 2005. An Evaluation of Time-Series MODIS 250-Meter Vegetation Index Data for Crop Mapping in the U.S. Central Great Plains. PhD Dissertation, Department of Geography, University of Kansas, Lawrence, Kansas.

Wardlow, B.D., and Egbert, S.L. 2008. Large-area crop mapping using time-series MODIS 250m NDVI data: An assessment for the US central great plains. *Remote Sensing of Environment* 112(3):1096-1116.

Wilgers, D.J., and Horne, E.A. 2006. Effects of different burn regimes on tallgrass prairie herpetofaunal species diversity and community composition in the flint hills, Kansas. *Journal of Herpetology* 40(1):73-84.

Wilken, D.H., and Allard, S.T. 1986. Intergradation among populations of the ipomopsis aggregate complex in the Colorado front range. *Systematic Botany*:1-13.

Willis, K.S. 2015. Remote sensing change detection for ecological monitoring in united states protected area. *Biological Conservation* 182:233-242.

World Wildlife Fund. Plowprint annual report 2016.

Wright, C. K., de Beurs, K. M., Henebry, G. M., 2012. Combined analysis of land cover change and NDVI trends in the Northern Eurasian wheat belt. *Frontier of Earth Science* 6(2):177–187.

Zhang, X., Friedl, M. A., Schaaf, C.B., Strahler, A.H., Hodges, J. C. F., Gao, F., Reed, B. C., and Huete, A., 2003. Monitoring vegetation phenology using MODIS. *Remote Sensing of Environment* 84: 471-475.

Zhang, X., Tarpley, D., and Sullivan, J.T. 2007. Diverse responses of vegetation phenology to a warming climate. *Geophysical Research Letters* 34(19).

Zhou, L., Tucker, C. J., Kaufmann, R. K., Slayback, D., Shabanov, N. V., Myneni, R. B., 2001. Variations in northern vegetation activity inferred from satellite data of vegetation index during 1981–1999. *Journal of Geophysical Research*. 106: 20069–20083.

Appendix A - TIMESAT Input Text File

345

Z:\Projects\BragetA\FlintHillsTimeSat\mi010101.dat

Z:\Projects\BragetA\FlintHillsTimeSat\mi010117.dat

Z:\Projects\BragetA\FlintHillsTimeSat\mi010202.dat

Z:\Projects\BragetA\FlintHillsTimeSat\mi010218.dat

Z:\Projects\BragetA\FlintHillsTimeSat\mi010306.dat

Z:\Projects\BragetA\FlintHillsTimeSat\mi010322.dat

Z:\Projects\BragetA\FlintHillsTimeSat\mi010407.dat

Z:\Projects\BragetA\FlintHillsTimeSat\mi010423.dat

Z:\Projects\BragetA\FlintHillsTimeSat\mi010509.dat

Z:\Projects\BragetA\FlintHillsTimeSat\mi010525.dat

Z:\Projects\BragetA\FlintHillsTimeSat\mi010610.dat

Z:\Projects\BragetA\FlintHillsTimeSat\mi010626.dat

Z:\Projects\BragetA\FlintHillsTimeSat\mi010712.dat

Z:\Projects\BragetA\FlintHillsTimeSat\mi010728.dat

Z:\Projects\BragetA\FlintHillsTimeSat\mi010813.dat

Z:\Projects\BragetA\FlintHillsTimeSat\mi010829.dat

Z:\Projects\BragetA\FlintHillsTimeSat\mi010914.dat

Z:\Projects\BragetA\FlintHillsTimeSat\mi010930.dat

Z:\Projects\BragetA\FlintHillsTimeSat\mi011016.dat

Z:\Projects\BragetA\FlintHillsTimeSat\mi011101.dat

Z:\Projects\BragetA\FlintHillsTimeSat\mi011117.dat

Z:\Projects\BragetA\FlintHillsTimeSat\mi011203.dat

Z:\Projects\BragetA\FlintHillsTimeSat\mi011219.dat

Z:\Projects\BragetA\FlintHillsTimeSat\mi020101.dat

Z:\Projects\BragetA\FlintHillsTimeSat\mi020117.dat

Z:\Projects\BragetA\FlintHillsTimeSat\mi020202.dat

Z:\Projects\BragetA\FlintHillsTimeSat\mi020218.dat

Z:\Projects\BragetA\FlintHillsTimeSat\mi020306.dat

Z:\Projects\BragetA\FlintHillsTimeSat\mi020322.dat

Z:\Projects\BragetA\FlintHillsTimeSat\mi020407.dat

Z:\Projects\BragetA\FlintHillsTimeSat\mi020423.dat

Z:\Projects\BragetA\FlintHillsTimeSat\mi020509.dat

Z:\Projects\BragetA\FlintHillsTimeSat\mi020525.dat

Z:\Projects\BragetA\FlintHillsTimeSat\mi020610.dat

Z:\Projects\BragetA\FlintHillsTimeSat\mi020626.dat

Z:\Projects\BragetA\FlintHillsTimeSat\mi020712.dat

Z:\Projects\BragetA\FlintHillsTimeSat\mi020728.dat

Z:\Projects\BragetA\FlintHillsTimeSat\mi020813.dat

Z:\Projects\BragetA\FlintHillsTimeSat\mi020829.dat

Z:\Projects\BragetA\FlintHillsTimeSat\mi020914.dat

Z:\Projects\BragetA\FlintHillsTimeSat\mi020930.dat

Z:\Projects\BragetA\FlintHillsTimeSat\mi021016.dat

Z:\Projects\BragetA\FlintHillsTimeSat\mi021101.dat

Z:\Projects\BragetA\FlintHillsTimeSat\mi021117.dat

Z:\Projects\BragetA\FlintHillsTimeSat\mi021203.dat

Z:\Projects\BragetA\FlintHillsTimeSat\mi021219.dat

Z:\Projects\BragetA\FlintHillsTimeSat\mi030101.dat

Z:\Projects\BragetA\FlintHillsTimeSat\mi030117.dat

Z:\Projects\BragetA\FlintHillsTimeSat\mi030202.dat

Z:\Projects\BragetA\FlintHillsTimeSat\mi030218.dat

Z:\Projects\BragetA\FlintHillsTimeSat\mi030306.dat

Z:\Projects\BragetA\FlintHillsTimeSat\mi030322.dat

Z:\Projects\BragetA\FlintHillsTimeSat\mi030407.dat

Z:\Projects\BragetA\FlintHillsTimeSat\mi030423.dat

Z:\Projects\BragetA\FlintHillsTimeSat\mi030509.dat

Z:\Projects\BragetA\FlintHillsTimeSat\mi030525.dat

Z:\Projects\BragetA\FlintHillsTimeSat\mi030610.dat

Z:\Projects\BragetA\FlintHillsTimeSat\mi030626.dat

Z:\Projects\BragetA\FlintHillsTimeSat\mi030712.dat

Z:\Projects\BragetA\FlintHillsTimeSat\mi030728.dat

Z:\Projects\BragetA\FlintHillsTimeSat\mi030813.dat

Z:\Projects\BragetA\FlintHillsTimeSat\mi030829.dat

Z:\Projects\BragetA\FlintHillsTimeSat\mi030914.dat

Z:\Projects\BragetA\FlintHillsTimeSat\mi030930.dat

Z:\Projects\BragetA\FlintHillsTimeSat\mi031016.dat

Z:\Projects\BragetA\FlintHillsTimeSat\mi031101.dat

Z:\Projects\BragetA\FlintHillsTimeSat\mi031117.dat

Z:\Projects\BragetA\FlintHillsTimeSat\mi031203.dat

Z:\Projects\BragetA\FlintHillsTimeSat\mi031219.dat

Z:\Projects\BragetA\FlintHillsTimeSat\mi040101.dat

Z:\Projects\BragetA\FlintHillsTimeSat\mi040117.dat

Z:\Projects\BragetA\FlintHillsTimeSat\mi040202.dat

Z:\Projects\BragetA\FlintHillsTimeSat\mi040218.dat

Z:\Projects\BragetA\FlintHillsTimeSat\mi040306.dat

Z:\Projects\BragetA\FlintHillsTimeSat\mi040322.dat

Z:\Projects\BragetA\FlintHillsTimeSat\mi040407.dat

Z:\Projects\BragetA\FlintHillsTimeSat\mi040423.dat

Z:\Projects\BragetA\FlintHillsTimeSat\mi040509.dat

Z:\Projects\BragetA\FlintHillsTimeSat\mi040525.dat

Z:\Projects\BragetA\FlintHillsTimeSat\mi040610.dat

Z:\Projects\BragetA\FlintHillsTimeSat\mi040626.dat

Z:\Projects\BragetA\FlintHillsTimeSat\mi040712.dat

Z:\Projects\BragetA\FlintHillsTimeSat\mi040728.dat

Z:\Projects\BragetA\FlintHillsTimeSat\mi040813.dat

Z:\Projects\BragetA\FlintHillsTimeSat\mi040829.dat

Z:\Projects\BragetA\FlintHillsTimeSat\mi040914.dat

Z:\Projects\BragetA\FlintHillsTimeSat\mi040930.dat

Z:\Projects\BragetA\FlintHillsTimeSat\mi041016.dat

Z:\Projects\BragetA\FlintHillsTimeSat\mi041101.dat

Z:\Projects\BragetA\FlintHillsTimeSat\mi041117.dat

Z:\Projects\BragetA\FlintHillsTimeSat\mi041203.dat

Z:\Projects\BragetA\FlintHillsTimeSat\mi041219.dat

Z:\Projects\BragetA\FlintHillsTimeSat\mi050101.dat

Z:\Projects\BragetA\FlintHillsTimeSat\mi050117.dat

Z:\Projects\BragetA\FlintHillsTimeSat\mi050202.dat

Z:\Projects\BragetA\FlintHillsTimeSat\mi050218.dat

Z:\Projects\BragetA\FlintHillsTimeSat\mi050306.dat

Z:\Projects\BragetA\FlintHillsTimeSat\mi050322.dat

Z:\Projects\BragetA\FlintHillsTimeSat\mi050407.dat

Z:\Projects\BragetA\FlintHillsTimeSat\mi050423.dat

Z:\Projects\BragetA\FlintHillsTimeSat\mi050509.dat

Z:\Projects\BragetA\FlintHillsTimeSat\mi050525.dat

Z:\Projects\BragetA\FlintHillsTimeSat\mi050610.dat

Z:\Projects\BragetA\FlintHillsTimeSat\mi050626.dat

Z:\Projects\BragetA\FlintHillsTimeSat\mi050712.dat

Z:\Projects\BragetA\FlintHillsTimeSat\mi050728.dat

Z:\Projects\BragetA\FlintHillsTimeSat\mi050813.dat

Z:\Projects\BragetA\FlintHillsTimeSat\mi050829.dat

Z:\Projects\BragetA\FlintHillsTimeSat\mi050914.dat

Z:\Projects\BragetA\FlintHillsTimeSat\mi050930.dat

Z:\Projects\BragetA\FlintHillsTimeSat\mi051016.dat

Z:\Projects\BragetA\FlintHillsTimeSat\mi051101.dat

Z:\Projects\BragetA\FlintHillsTimeSat\mi051117.dat

Z:\Projects\BragetA\FlintHillsTimeSat\mi051203.dat

Z:\Projects\BragetA\FlintHillsTimeSat\mi051219.dat

Z:\Projects\BragetA\FlintHillsTimeSat\mi060101.dat

Z:\Projects\BragetA\FlintHillsTimeSat\mi060117.dat

Z:\Projects\BragetA\FlintHillsTimeSat\mi060202.dat

Z:\Projects\BragetA\FlintHillsTimeSat\mi060218.dat

Z:\Projects\BragetA\FlintHillsTimeSat\mi060306.dat

Z:\Projects\BragetA\FlintHillsTimeSat\mi060322.dat

Z:\Projects\BragetA\FlintHillsTimeSat\mi060407.dat

Z:\Projects\BragetA\FlintHillsTimeSat\mi060423.dat

Z:\Projects\BragetA\FlintHillsTimeSat\mi060509.dat

Z:\Projects\BragetA\FlintHillsTimeSat\mi060525.dat

Z:\Projects\BragetA\FlintHillsTimeSat\mi060610.dat

Z:\Projects\BragetA\FlintHillsTimeSat\mi060626.dat

Z:\Projects\BragetA\FlintHillsTimeSat\mi060712.dat

Z:\Projects\BragetA\FlintHillsTimeSat\mi060728.dat

Z:\Projects\BragetA\FlintHillsTimeSat\mi060813.dat

Z:\Projects\BragetA\FlintHillsTimeSat\mi060829.dat

Z:\Projects\BragetA\FlintHillsTimeSat\mi060914.dat

Z:\Projects\BragetA\FlintHillsTimeSat\mi060930.dat

Z:\Projects\BragetA\FlintHillsTimeSat\mi061016.dat

Z:\Projects\BragetA\FlintHillsTimeSat\mi061101.dat

Z:\Projects\BragetA\FlintHillsTimeSat\mi061117.dat

Z:\Projects\BragetA\FlintHillsTimeSat\mi061203.dat

Z:\Projects\BragetA\FlintHillsTimeSat\mi061219.dat

Z:\Projects\BragetA\FlintHillsTimeSat\mi070101.dat

Z:\Projects\BragetA\FlintHillsTimeSat\mi070117.dat

Z:\Projects\BragetA\FlintHillsTimeSat\mi070202.dat

Z:\Projects\BragetA\FlintHillsTimeSat\mi070218.dat

Z:\Projects\BragetA\FlintHillsTimeSat\mi070306.dat

Z:\Projects\BragetA\FlintHillsTimeSat\mi070322.dat

Z:\Projects\BragetA\FlintHillsTimeSat\mi070407.dat

Z:\Projects\BragetA\FlintHillsTimeSat\mi070423.dat

Z:\Projects\BragetA\FlintHillsTimeSat\mi070509.dat

Z:\Projects\BragetA\FlintHillsTimeSat\mi070525.dat

Z:\Projects\BragetA\FlintHillsTimeSat\mi070610.dat

Z:\Projects\BragetA\FlintHillsTimeSat\mi070626.dat

Z:\Projects\BragetA\FlintHillsTimeSat\mi070712.dat

Z:\Projects\BragetA\FlintHillsTimeSat\mi070728.dat

Z:\Projects\BragetA\FlintHillsTimeSat\mi070813.dat

Z:\Projects\BragetA\FlintHillsTimeSat\mi070829.dat

Z:\Projects\BragetA\FlintHillsTimeSat\mi070914.dat

Z:\Projects\BragetA\FlintHillsTimeSat\mi070930.dat

Z:\Projects\BragetA\FlintHillsTimeSat\mi071016.dat

Z:\Projects\BragetA\FlintHillsTimeSat\mi071101.dat

Z:\Projects\BragetA\FlintHillsTimeSat\mi071117.dat

Z:\Projects\BragetA\FlintHillsTimeSat\mi071203.dat

Z:\Projects\BragetA\FlintHillsTimeSat\mi071219.dat

Z:\Projects\BragetA\FlintHillsTimeSat\mi080101.dat

Z:\Projects\BragetA\FlintHillsTimeSat\mi080117.dat

Z:\Projects\BragetA\FlintHillsTimeSat\mi080202.dat

Z:\Projects\BragetA\FlintHillsTimeSat\mi080218.dat

Z:\Projects\BragetA\FlintHillsTimeSat\mi080306.dat

Z:\Projects\BragetA\FlintHillsTimeSat\mi080322.dat

Z:\Projects\BragetA\FlintHillsTimeSat\mi080407.dat

Z:\Projects\BragetA\FlintHillsTimeSat\mi080423.dat

Z:\Projects\BragetA\FlintHillsTimeSat\mi080509.dat

Z:\Projects\BragetA\FlintHillsTimeSat\mi080525.dat

Z:\Projects\BragetA\FlintHillsTimeSat\mi080610.dat

Z:\Projects\BragetA\FlintHillsTimeSat\mi080626.dat

Z:\Projects\BragetA\FlintHillsTimeSat\mi080712.dat

Z:\Projects\BragetA\FlintHillsTimeSat\mi080728.dat

Z:\Projects\BragetA\FlintHillsTimeSat\mi080813.dat

Z:\Projects\BragetA\FlintHillsTimeSat\mi080829.dat

Z:\Projects\BragetA\FlintHillsTimeSat\mi080914.dat

Z:\Projects\BragetA\FlintHillsTimeSat\mi080930.dat

Z:\Projects\BragetA\FlintHillsTimeSat\mi081016.dat

Z:\Projects\BragetA\FlintHillsTimeSat\mi081101.dat

Z:\Projects\BragetA\FlintHillsTimeSat\mi081117.dat

Z:\Projects\BragetA\FlintHillsTimeSat\mi081203.dat

Z:\Projects\BragetA\FlintHillsTimeSat\mi081219.dat

Z:\Projects\BragetA\FlintHillsTimeSat\mi090101.dat

Z:\Projects\BragetA\FlintHillsTimeSat\mi090117.dat

Z:\Projects\BragetA\FlintHillsTimeSat\mi090202.dat

Z:\Projects\BragetA\FlintHillsTimeSat\mi090218.dat

Z:\Projects\BragetA\FlintHillsTimeSat\mi090306.dat

Z:\Projects\BragetA\FlintHillsTimeSat\mi090322.dat

Z:\Projects\BragetA\FlintHillsTimeSat\mi090407.dat

Z:\Projects\BragetA\FlintHillsTimeSat\mi090423.dat

Z:\Projects\BragetA\FlintHillsTimeSat\mi090509.dat

Z:\Projects\BragetA\FlintHillsTimeSat\mi090525.dat

Z:\Projects\BragetA\FlintHillsTimeSat\mi090610.dat

Z:\Projects\BragetA\FlintHillsTimeSat\mi090626.dat

Z:\Projects\BragetA\FlintHillsTimeSat\mi090712.dat

Z:\Projects\BragetA\FlintHillsTimeSat\mi090728.dat

Z:\Projects\BragetA\FlintHillsTimeSat\mi090813.dat

Z:\Projects\BragetA\FlintHillsTimeSat\mi090829.dat

Z:\Projects\BragetA\FlintHillsTimeSat\mi090914.dat

Z:\Projects\BragetA\FlintHillsTimeSat\mi090930.dat

Z:\Projects\BragetA\FlintHillsTimeSat\mi091016.dat

Z:\Projects\BragetA\FlintHillsTimeSat\mi091101.dat

Z:\Projects\BragetA\FlintHillsTimeSat\mi091117.dat

Z:\Projects\BragetA\FlintHillsTimeSat\mi091203.dat

Z:\Projects\BragetA\FlintHillsTimeSat\mi091219.dat

Z:\Projects\BragetA\FlintHillsTimeSat\mi100101.dat

Z:\Projects\BragetA\FlintHillsTimeSat\mi100117.dat

Z:\Projects\BragetA\FlintHillsTimeSat\mi100202.dat

Z:\Projects\BragetA\FlintHillsTimeSat\mi100218.dat

Z:\Projects\BragetA\FlintHillsTimeSat\mi100306.dat

Z:\Projects\BragetA\FlintHillsTimeSat\mi100322.dat

Z:\Projects\BragetA\FlintHillsTimeSat\mi100407.dat

Z:\Projects\BragetA\FlintHillsTimeSat\mi100423.dat

Z:\Projects\BragetA\FlintHillsTimeSat\mi100509.dat

Z:\Projects\BragetA\FlintHillsTimeSat\mi100525.dat

Z:\Projects\BragetA\FlintHillsTimeSat\mi100610.dat

Z:\Projects\BragetA\FlintHillsTimeSat\mi100626.dat

Z:\Projects\BragetA\FlintHillsTimeSat\mi100712.dat

Z:\Projects\BragetA\FlintHillsTimeSat\mi100728.dat

Z:\Projects\BragetA\FlintHillsTimeSat\mi100813.dat

Z:\Projects\BragetA\FlintHillsTimeSat\mi100829.dat

Z:\Projects\BragetA\FlintHillsTimeSat\mi100914.dat

Z:\Projects\BragetA\FlintHillsTimeSat\mi100930.dat

Z:\Projects\BragetA\FlintHillsTimeSat\mi101016.dat

Z:\Projects\BragetA\FlintHillsTimeSat\mi101101.dat

Z:\Projects\BragetA\FlintHillsTimeSat\mi101117.dat

Z:\Projects\BragetA\FlintHillsTimeSat\mi101203.dat

Z:\Projects\BragetA\FlintHillsTimeSat\mi101219.dat

Z:\Projects\BragetA\FlintHillsTimeSat\mi110101.dat

Z:\Projects\BragetA\FlintHillsTimeSat\mi110117.dat

Z:\Projects\BragetA\FlintHillsTimeSat\mi110202.dat

Z:\Projects\BragetA\FlintHillsTimeSat\mi110218.dat

Z:\Projects\BragetA\FlintHillsTimeSat\mi110306.dat

Z:\Projects\BragetA\FlintHillsTimeSat\mi110322.dat

Z:\Projects\BragetA\FlintHillsTimeSat\mi110407.dat

Z:\Projects\BragetA\FlintHillsTimeSat\mi110423.dat

Z:\Projects\BragetA\FlintHillsTimeSat\mi110509.dat

Z:\Projects\BragetA\FlintHillsTimeSat\mi110525.dat

Z:\Projects\BragetA\FlintHillsTimeSat\mi110610.dat

Z:\Projects\BragetA\FlintHillsTimeSat\mi110626.dat

Z:\Projects\BragetA\FlintHillsTimeSat\mi110712.dat

Z:\Projects\BragetA\FlintHillsTimeSat\mi110728.dat

Z:\Projects\BragetA\FlintHillsTimeSat\mi110813.dat

Z:\Projects\BragetA\FlintHillsTimeSat\mi110829.dat

Z:\Projects\BragetA\FlintHillsTimeSat\mi110914.dat

Z:\Projects\BragetA\FlintHillsTimeSat\mi110930.dat

Z:\Projects\BragetA\FlintHillsTimeSat\mi111016.dat

Z:\Projects\BragetA\FlintHillsTimeSat\mi111101.dat

Z:\Projects\BragetA\FlintHillsTimeSat\mi111117.dat

Z:\Projects\BragetA\FlintHillsTimeSat\mi111203.dat

Z:\Projects\BragetA\FlintHillsTimeSat\mi111219.dat

Z:\Projects\BragetA\FlintHillsTimeSat\mi120101.dat

Z:\Projects\BragetA\FlintHillsTimeSat\mi120117.dat

Z:\Projects\BragetA\FlintHillsTimeSat\mi120202.dat

Z:\Projects\BragetA\FlintHillsTimeSat\mi120218.dat

Z:\Projects\BragetA\FlintHillsTimeSat\mi120306.dat

Z:\Projects\BragetA\FlintHillsTimeSat\mi120322.dat

Z:\Projects\BragetA\FlintHillsTimeSat\mi120407.dat

Z:\Projects\BragetA\FlintHillsTimeSat\mi120423.dat

Z:\Projects\BragetA\FlintHillsTimeSat\mi120509.dat

Z:\Projects\BragetA\FlintHillsTimeSat\mi120525.dat

Z:\Projects\BragetA\FlintHillsTimeSat\mi120610.dat

Z:\Projects\BragetA\FlintHillsTimeSat\mi120626.dat

Z:\Projects\BragetA\FlintHillsTimeSat\mi120712.dat

Z:\Projects\BragetA\FlintHillsTimeSat\mi120728.dat

Z:\Projects\BragetA\FlintHillsTimeSat\mi120813.dat

Z:\Projects\BragetA\FlintHillsTimeSat\mi120829.dat

Z:\Projects\BragetA\FlintHillsTimeSat\mi120914.dat

Z:\Projects\BragetA\FlintHillsTimeSat\mi120930.dat

Z:\Projects\BragetA\FlintHillsTimeSat\mi121016.dat

Z:\Projects\BragetA\FlintHillsTimeSat\mi121101.dat

Z:\Projects\BragetA\FlintHillsTimeSat\mi121117.dat

Z:\Projects\BragetA\FlintHillsTimeSat\mi121203.dat

Z:\Projects\BragetA\FlintHillsTimeSat\mi121219.dat

Z:\Projects\BragetA\FlintHillsTimeSat\mi130101.dat

Z:\Projects\BragetA\FlintHillsTimeSat\mi130117.dat

Z:\Projects\BragetA\FlintHillsTimeSat\mi130202.dat

Z:\Projects\BragetA\FlintHillsTimeSat\mi130218.dat

Z:\Projects\BragetA\FlintHillsTimeSat\mi130306.dat

Z:\Projects\BragetA\FlintHillsTimeSat\mi130322.dat

Z:\Projects\BragetA\FlintHillsTimeSat\mi130407.dat

Z:\Projects\BragetA\FlintHillsTimeSat\mi130423.dat

Z:\Projects\BragetA\FlintHillsTimeSat\mi130509.dat

Z:\Projects\BragetA\FlintHillsTimeSat\mi130525.dat

Z:\Projects\BragetA\FlintHillsTimeSat\mi130610.dat

Z:\Projects\BragetA\FlintHillsTimeSat\mi130626.dat

Z:\Projects\BragetA\FlintHillsTimeSat\mi130712.dat

Z:\Projects\BragetA\FlintHillsTimeSat\mi130728.dat

Z:\Projects\BragetA\FlintHillsTimeSat\mi130813.dat

Z:\Projects\BragetA\FlintHillsTimeSat\mi130829.dat

Z:\Projects\BragetA\FlintHillsTimeSat\mi130914.dat

Z:\Projects\BragetA\FlintHillsTimeSat\mi130930.dat

Z:\Projects\BragetA\FlintHillsTimeSat\mi131016.dat

Z:\Projects\BragetA\FlintHillsTimeSat\mi131101.dat

Z:\Projects\BragetA\FlintHillsTimeSat\mi131117.dat

Z:\Projects\BragetA\FlintHillsTimeSat\mi131203.dat

Z:\Projects\BragetA\FlintHillsTimeSat\mi131219.dat

Z:\Projects\BragetA\FlintHillsTimeSat\mi140101.dat

Z:\Projects\BragetA\FlintHillsTimeSat\mi140117.dat

Z:\Projects\BragetA\FlintHillsTimeSat\mi140202.dat

Z:\Projects\BragetA\FlintHillsTimeSat\mi140218.dat

Z:\Projects\BragetA\FlintHillsTimeSat\mi140306.dat

Z:\Projects\BragetA\FlintHillsTimeSat\mi140322.dat

Z:\Projects\BragetA\FlintHillsTimeSat\mi140407.dat

Z:\Projects\BragetA\FlintHillsTimeSat\mi140423.dat

Z:\Projects\BragetA\FlintHillsTimeSat\mi140509.dat

Z:\Projects\BragetA\FlintHillsTimeSat\mi140525.dat

Z:\Projects\BragetA\FlintHillsTimeSat\mi140610.dat

Z:\Projects\BragetA\FlintHillsTimeSat\mi140626.dat

Z:\Projects\BragetA\FlintHillsTimeSat\mi140712.dat

Z:\Projects\BragetA\FlintHillsTimeSat\mi140728.dat

Z:\Projects\BragetA\FlintHillsTimeSat\mi140813.dat

Z:\Projects\BragetA\FlintHillsTimeSat\mi140829.dat

Z:\Projects\BragetA\FlintHillsTimeSat\mi140914.dat

Z:\Projects\BragetA\FlintHillsTimeSat\mi140930.dat

Z:\Projects\BragetA\FlintHillsTimeSat\mi141016.dat

Z:\Projects\BragetA\FlintHillsTimeSat\mi141101.dat

Z:\Projects\BragetA\FlintHillsTimeSat\mi141117.dat

Z:\Projects\BragetA\FlintHillsTimeSat\mi141203.dat

Z:\Projects\BragetA\FlintHillsTimeSat\mi141219.dat

Z:\Projects\BragetA\FlintHillsTimeSat\mi150101.dat

Z:\Projects\BragetA\FlintHillsTimeSat\mi150117.dat

Z:\Projects\BragetA\FlintHillsTimeSat\mi150202.dat

Z:\Projects\BragetA\FlintHillsTimeSat\mi150218.dat

Z:\Projects\BragetA\FlintHillsTimeSat\mi150306.dat

Z:\Projects\BragetA\FlintHillsTimeSat\mi150322.dat

Z:\Projects\BragetA\FlintHillsTimeSat\mi150407.dat

Z:\Projects\BragetA\FlintHillsTimeSat\mi150423.dat

Z:\Projects\BragetA\FlintHillsTimeSat\mi150509.dat

Z:\Projects\BragetA\FlintHillsTimeSat\mi150525.dat

Z:\Projects\BragetA\FlintHillsTimeSat\mi150610.dat

Z:\Projects\BragetA\FlintHillsTimeSat\mi150626.dat

Z:\Projects\BragetA\FlintHillsTimeSat\mi150712.dat

Z:\Projects\BragetA\FlintHillsTimeSat\mi150728.dat

Z:\Projects\BragetA\FlintHillsTimeSat\mi150813.dat

Z:\Projects\BragetA\FlintHillsTimeSat\mi150829.dat

Z:\Projects\BragetA\FlintHillsTimeSat\mi150914.dat

Z:\Projects\BragetA\FlintHillsTimeSat\mi150930.dat

Z:\Projects\BragetA\FlintHillsTimeSat\mi151016.dat

Z:\Projects\BragetA\FlintHillsTimeSat\mi151101.dat

Z:\Projects\BragetA\FlintHillsTimeSat\mi151117.dat

Z:\Projects\BragetA\FlintHillsTimeSat\mi151203.dat

Z:\Projects\BragetA\FlintHillsTimeSat\mi151219.dat

Appendix B - Scripts

ANOVA and Tukey HSD R Script

```
#read in dataset and explore its structure

library(agricolae)

setwd ("Z:\\Projects\\BragetA\\NewFlintHills\\Scratch\\")

data <- read.csv(file="PhenometricMeans.csv", header=TRUE, sep=",")

str(data)

#Create a variable to store a phenometric name

pheno <- data$Mean.End.Season

#Calculate Means for Treatment "Type"

aggregate(pheno ~ data$County, FUN=mean)

#Run ANOVA and assess whether differences exist between brands and tasters

output1 <- lm(pheno ~ data$County)

summary(output1)

anova(output1)

#Run the Tukey's HSD test to see where differences lie

a1 <- aov(pheno ~ data$County)

posthoc <- TukeyHSD(x=a1, "data$County", conf.level=0.95)

posthoc

#Visualize the confidence intervals for the mean differences

plot(posthoc)

#Run the Tukey's HSD test in alternative fashion

#Yields easier way to visualize groups with similar means

output <- HSD.test(output1, "data$County")

output

#write output to file for mapping

write.csv(output$groups, file="PhenoGroups_StartSeason.csv")
```

K-Means Script

```
#perform a basic k-means analysis

#read in dataset and explore its structure

setwd("Z:\\Projects\\BragetA\\NewFlintHills\\Scratch")

data <- read.csv(file="PhenoGroups_Summary.csv",header=TRUE, sep=",")

str(data)

myvars <- c("LDMeans", "RDMeans", "MaxMeans", "SmIntMeans", “ESMeans”, “”MidMeans”,

“StSeaMeans”, “GSLMeans”)

x <- data[myvars]

str(x)

#perform kmeans cluster analysis (4 clusters) and plot results

#and write output to table

km <- kmeans(x, 4)

str(km)

plot(x, col=km$cluster)

write.table(km$cluster,file="outputClusters.csv",sep=",")

#re-run kmeans using optimal number for k

#write a function to calculate sum of all within sum of squares for clusters

kmeans.wss.k <- function(x, k){

        km = kmeans(x, k)

        km$tot.withinss = sum(km$withinss)

        return (km$tot.withinss)

}

#use function to calculate the sum of withinss for k = 3

kmeans.wss.k(x, 3)

#write a function to extract km$tot.withinss values (distortion) for a range of clusters

kmeans.dis <- function(x, maxk){

        dis=(nrow(x)-1)*sum(apply(x,2,var))
```

```
        dis[2:maxk]=sapply (2:maxk, kmeans.wss.k, x=x)
        return(dis)
}
#populate variable for maximum number of clusters, invoke function, and plot results
maxk = 10
dis = kmeans.dis(x, maxk)
plot(1:maxk, dis, type='b', main="Elbow Curve", xlab="Number of Clusters", ylab="Distortion",
col="blue")
#re-run kmeans with optimal cluster number, view clusters, and add to input data
km <- kmeans(x, 6)
km
plot(x, col = km$cluster)
write.table(km$cluster,file="outputClustersLDRDMXSI.csv",sep=",")
```

BFAST Script

Load these packages in R:

```
library(zoo)
library(sandwich)
library(MASS)
library(quadprog)
library(tseries)
library(strucchange)
library(fracdiff)
library(forecast)
library(iterators)
library(codetools)
library(foreach)
library(bfast)

setwd("Z:/Projects/BragetA/NewFlintHills/NewFlintHillsBFAST")
datafile <- "fh_ndvi.csv"

inidata<-read.table(datafile, header=TRUE, sep = ",", dec = ".") #use only with small files; modify if no labels are in the input

mdata<-as.matrix(inidata)
tpdata<-mdata
vmax<-dim(mdata)
#number of lines
vmax[1]
#number of columns
vmax[2]

for(count in 1:vmax[1])
```

```
{
poly_id<-tpdata[count,1]
ndvi<-tpdata[count,2:vmax[2]]  #highlighted number identifies first column with NDVI data
plot(ndvi)
tsdata<-ts(ndvi,frequency=23,start=c(2001,1))
dim(tsdata)<-NULL
#(rdist<-23/length(tsdata))
fits<-bfast(tsdata,h=0.10,season="harmonic",max.iter=1)
plot(fits)
fits2<-fits$Time
ts_trend_break_time<-t(fits2[1])
fits3<-fits$Magnitude
ts_trend_break_magnitude<-t(fits3[1])
fits4<-fits$output
fits4a<-fits4[[1]]$Vt.bp
fits4adata<-as.matrix(fits4a)
fits4amax<-dim(fits4adata)
ts_trend_nbbreak<-t(fits4amax[1])
results1<-ts_trend_break_time
aLine<-t(c(poly_id,results1))
write.table(aLine,file="fh_trend_breaks_time.txt",append=TRUE,quote=FALSE,sep=",",eol="\n",na="NA",dec=".",row.names=F
ALSE,col.names=FALSE,qmethod=c("escape","double"))
results2<-ts_trend_break_magnitude
aLine<-t(c(poly_id,results2))
write.table(aLine,file="fh_trend_breaks_magnitude.txt",append=TRUE,quote=FALSE,sep=",",eol="\n",na="NA",dec=".",row.na
mes=FALSE,col.names=FALSE,qmethod=c("escape","double"))
results3<-ts_trend_nbbreak
aLine<-t(c(poly_id,results3))
write.table(aLine,file="fh_trend_nbbreaks.txt",append=TRUE,quote=FALSE,sep=",",eol="\n",na="NA",de=".",row.names=FALSE,
col.names=FALSE,qmethod=c("escape","double"))
fits4b<-fits4[[1]]$Tt
results4<-fits4b
aLine<-t(c(poly_id,results4))
write.table(aLine,file="fh_trend_bfast.txt",append=TRUE,quote=FALSE,sep=",",eol="\n",na="NA",dec=".",row.names=FALSE,col
.names=FALSE,qmethod=c("escape","double"))
fits4c<-fits4[[1]]$Wt.bp
fits4cdata<-as.matrix(fits4c)
fits4cmax<-dim(fits4cdata)
ts_season_nbbreak<-t(fits4cmax[1])
results5<-ts_season_nbbreak
aLine<-t(c(poly_id,results5))
write.table(aLine,file="fh_season_nbbreaks.txt",append=TRUE,quote=FALSE,sep=",",eol="\n",na="NA",de=".",row.names=FALS
E,col.names=FALSE,qmethod=c("escape","double"))
ts_season_breaks_time<-t(fits4cdata)
results6<- ts_season_breaks_time
aLine<- t(c(poly_id,results6))
write.table(aLine,file="fh_season_breaks_time.txt",append=TRUE,quote=FALSE,sep=",",eol="\n",na="NA",de=".",row.names=F
ALSE,col.names=FALSE,qmethod=c("escape","double"))
fits4d<-fits4[[1]]$St
results7<-fits4d
aLine<-t(c(poly_id,results7))
write.table(aLine,file="fh_season_bfast.txt",append=TRUE,quote=FALSE,sep=",",eol="\n",na="NA",dec=".",row.names=FALSE,c
ol.names=FALSE,qmethod=c("escape","double"))
}
```

Appendix C - Histograms

Figure C-1. The histogram and summary for the growing season phenometric. The data values appear to be nominally distributed.

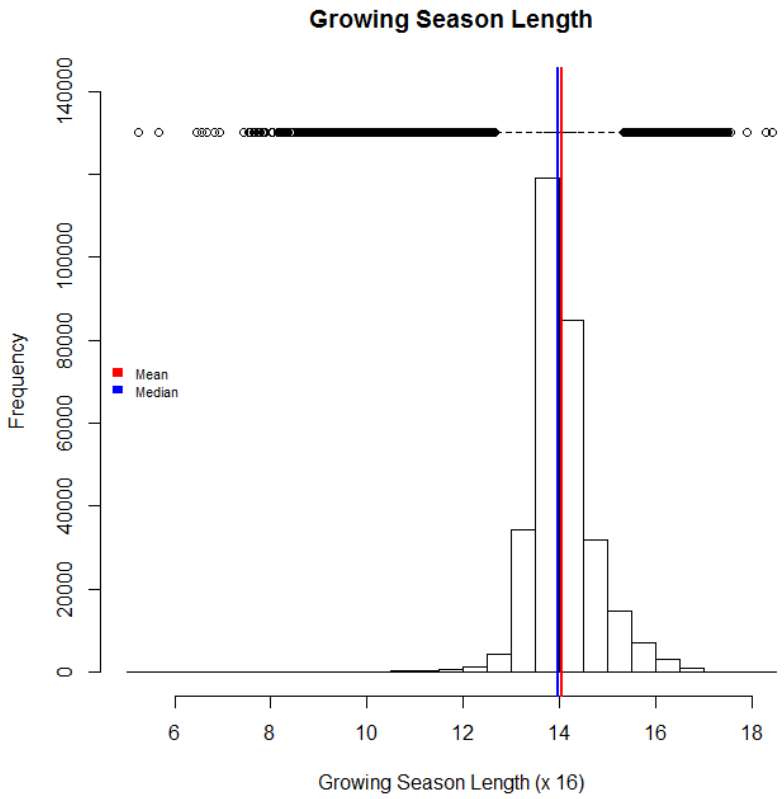

	vars	n	mean	sd	median	trimmed	mad	min	max	range	skew	kurtosis	se
X1	1	304386	14.05	0.7	13.96	14.01	0.48	5.24	18.42	13.18	0.05	5.82	0

Figure C-2. The histogram and summary for the left derivative phenometric. The data values appear to be nominally distributed.

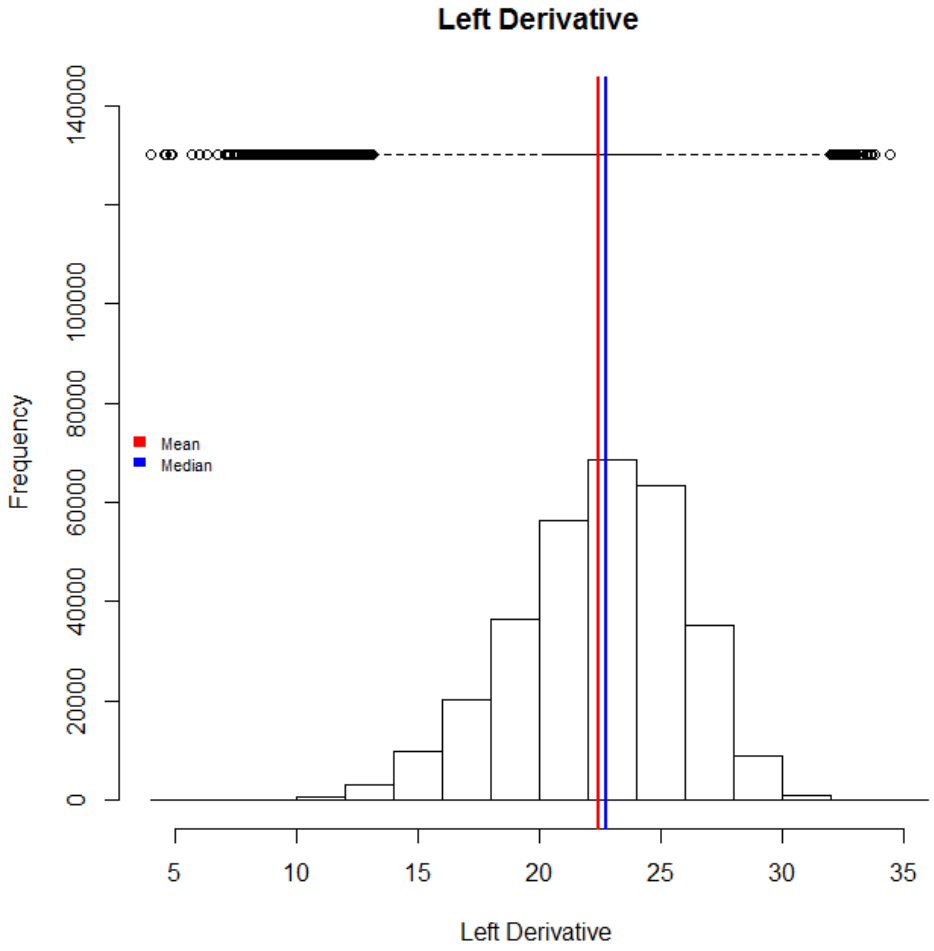

	vars	n	mean	sd	median	trimmed	mad	min	max	range	skew	kurtosis	se
X1	1	304386	22.44	3.45	22.75	22.6	3.47	4.01	34.45	30.44	-0.42	-0.02	0.01

Figure C-3. The histogram and summary for the maximum phenometric. The data values appear to be nominally distributed.

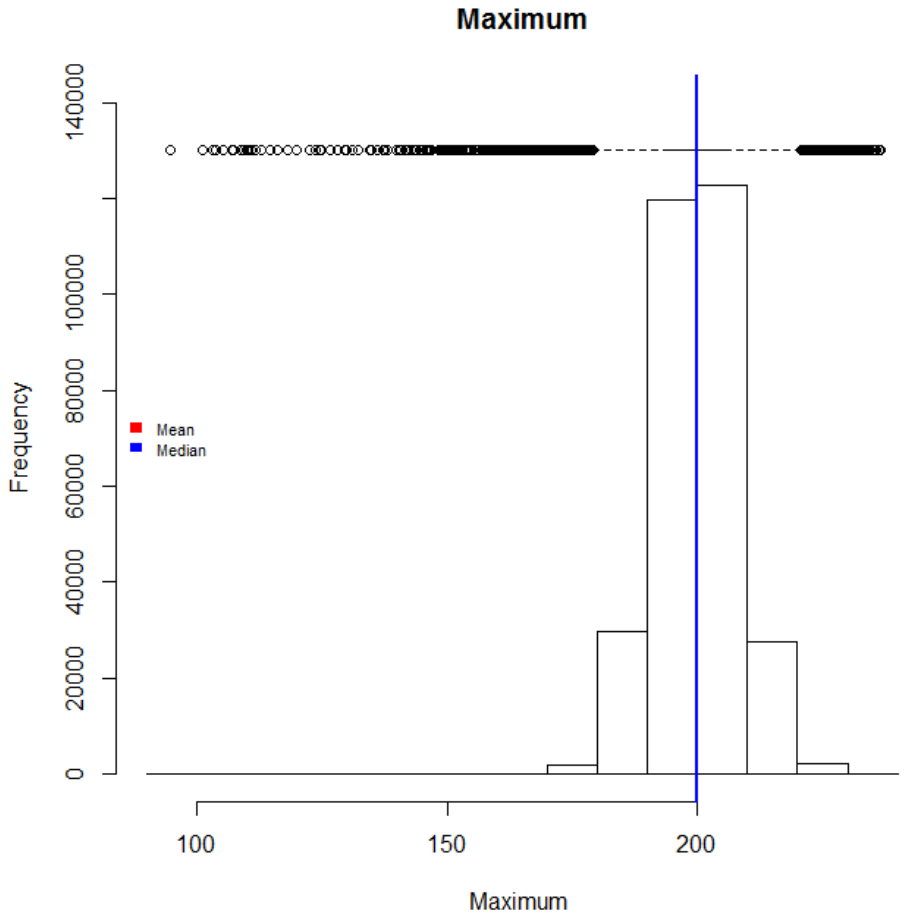

	vars	n	mean	sd	median	trimmed	mad	min	max	range	skew	kurtosis	se
X1	1	304386	199.94	8.07	200.03	199.96	7.75	94.66	236.7	142.05	-0.21	2.12	0.01

Figure C-4. The histogram and summary for the middle season phenometric. The data values appear to be nominally distributed.

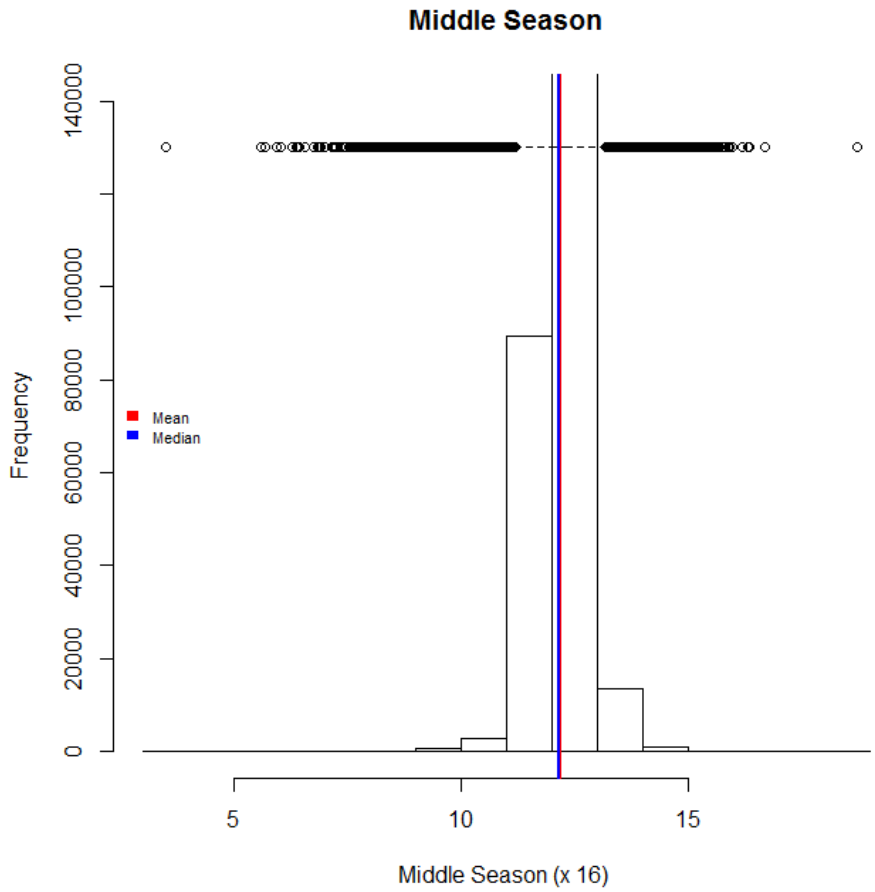

	vars	n	mean	sd	median	trimmed	mad	min	max	range	skew	kurtosis	se
X1	1	304386	12.21	0.49	12.17	12.2	0.37	3.5	18.72	15.22	-0.45	8.75	0

Figure C-5. The histogram and summary for the right derivative phenometric. The data values appear to be nominally distributed.

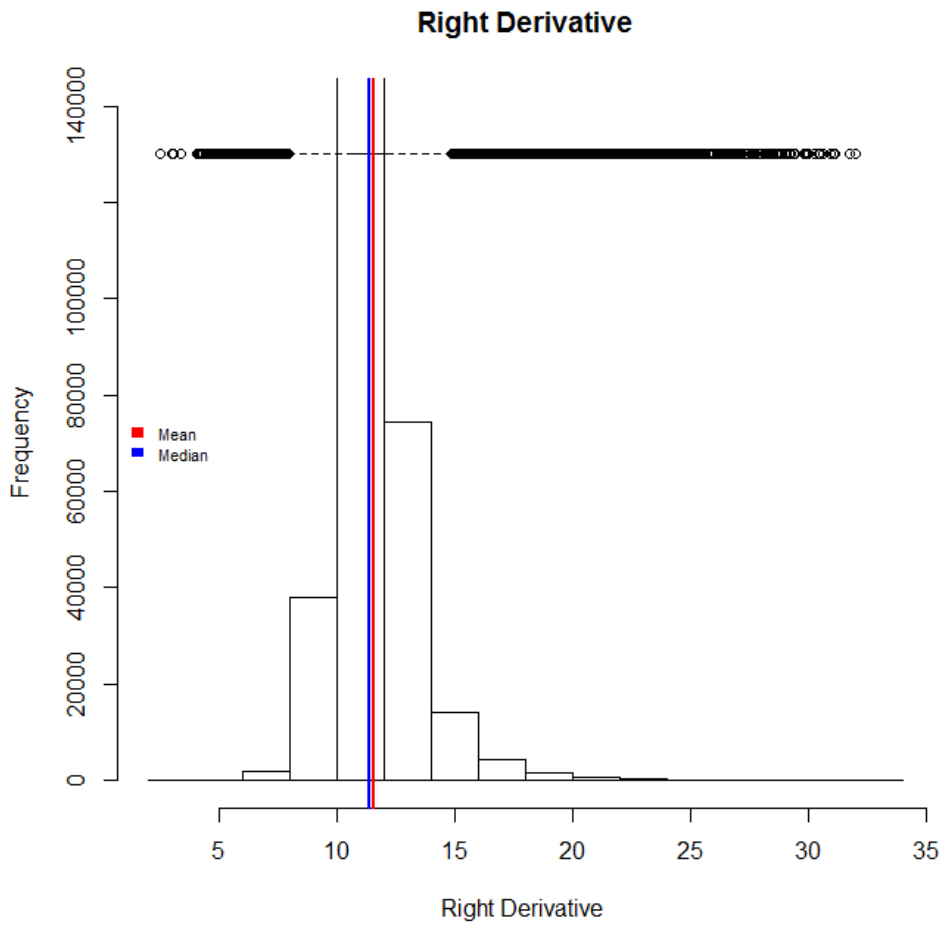

	vars	n	mean	sd	median	trimmed	mad	min	max	range	skew	kurtosis	se
X1	1	304386	11.58	1.77	11.38	11.43	1.27	2.55	32.04	29.49	1.8	8.42	0

Figure C-6. The histogram and summary for the small integral phenometric. The data values appear to be nominally distributed.

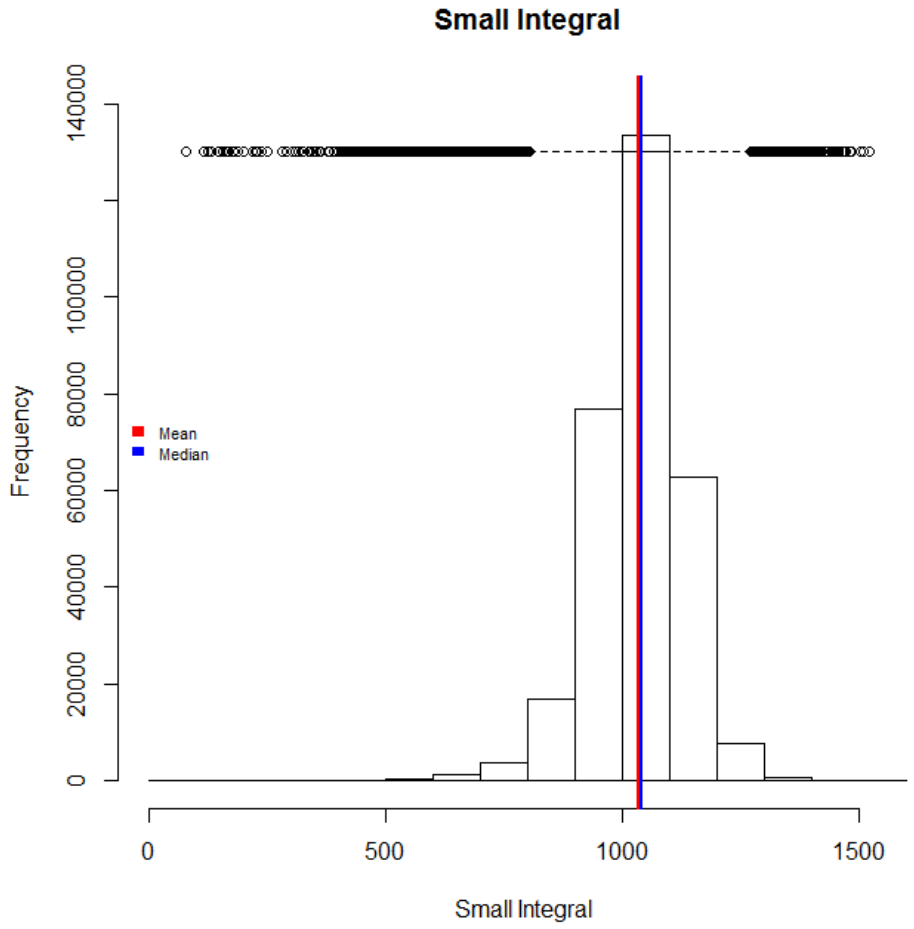

	vars	n	mean	sd	median	trimmed	mad	min	max	range	skew	kurtosis	se
X1	1	304386	1033.81	96.81	1040.04	1037.81	86.46	77.91	1521.78	1443.87	-0.71	2.67	0.18

Figure C-7. The histogram and summary for the start season phenometric. The data values appear to be nominally distributed.

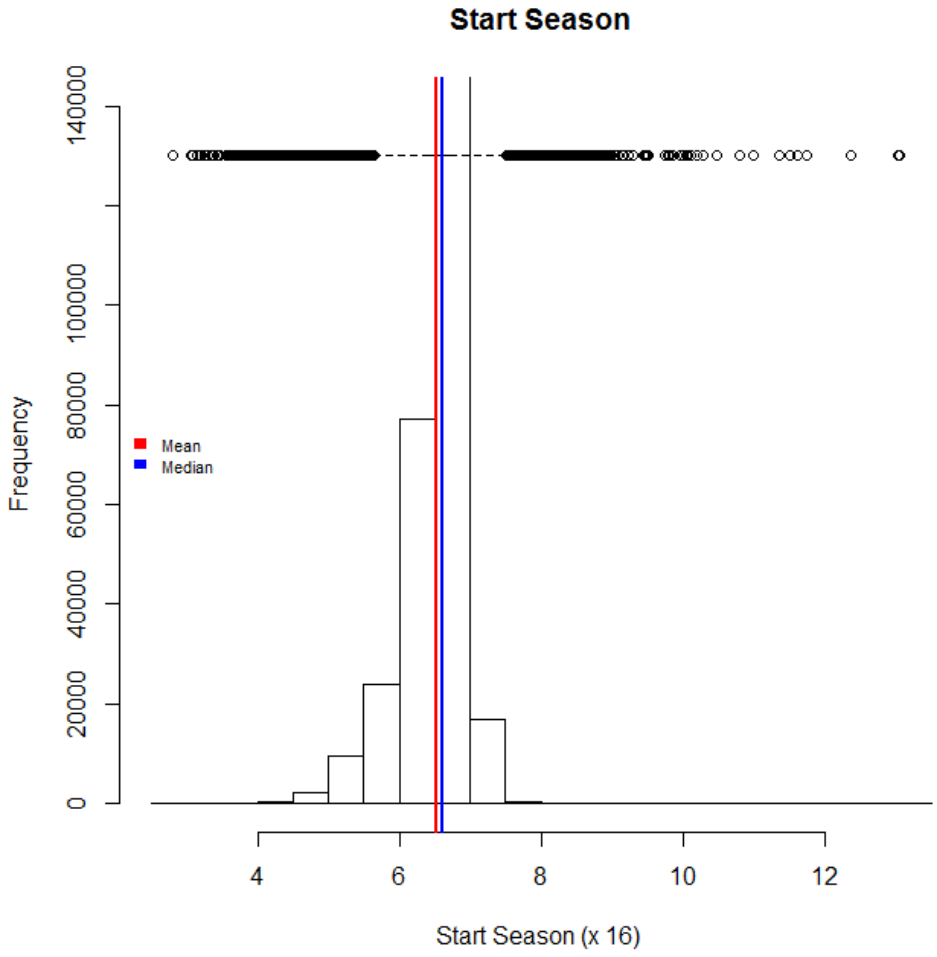

	vars	n	mean	sd	median	trimmed	mad	min	max	range	skew	kurtosis	se
X1	1	304386	6.52	0.45	6.62	6.57	0.32	2.81	13.06	10.26	-1.27	3.82	0

Appendix D - Phenometrics

Figure D-1. ANOVA result for the Growing Season Length phenometric.

```
Analysis of Variance Table

Response: pheno
               Df Sum Sq Mean Sq F value    Pr(>F)
data$County    25   7834 313.355  684.96 < 2.2e-16 ***
Residuals   304360 139238   0.457
---
Signif. codes:  0 '***' 0.001 '**' 0.01 '*' 0.05 '.' 0.1 ' ' 1
```

Figure D-2. ANOVA test for the Growing Season Length phenometric with all counties being highly significant except for Riley county, which was slightly less significant.

```
Call:
lm(formula = pheno ~ data$County)

Residuals:
    Min      1Q  Median      3Q     Max
-9.0491 -0.3564 -0.0739  0.2802  4.3599

Coefficients:
                          Estimate Std. Error  t value Pr(>|t|)
(Intercept)              13.968017   0.003727 3747.536  < 2e-16 ***
data$CountyChase         -0.207229   0.005707  -36.312  < 2e-16 ***
data$CountyChautauqua     0.321347   0.008064   39.849  < 2e-16 ***
data$CountyClay           0.219311   0.009129   24.023  < 2e-16 ***
data$CountyCoffey         0.349379   0.010230   34.154  < 2e-16 ***
data$CountyCowley         0.050278   0.005971    8.421  < 2e-16 ***
data$CountyDickinson      0.257322   0.008547   30.105  < 2e-16 ***
data$CountyElk            0.282148   0.007143   39.499  < 2e-16 ***
data$CountyGeary          0.072444   0.008981    8.066 7.27e-16 ***
data$CountyGreenwood     -0.048365   0.005560   -8.698  < 2e-16 ***
data$CountyHarvey        -0.102635   0.016055   -6.393 1.63e-10 ***
data$CountyJackson        0.895690   0.017362   51.590  < 2e-16 ***
data$CountyKay            0.066213   0.009185    7.209 5.67e-13 ***
data$CountyLyon           0.124766   0.006771   18.427  < 2e-16 ***
data$CountyMarion         0.324562   0.007463   43.490  < 2e-16 ***
data$CountyMarshall       0.096473   0.009626   10.022  < 2e-16 ***
data$CountyMcPherson      0.067012   0.009424    7.111 1.16e-12 ***
data$CountyMorris         0.107968   0.006650   16.235  < 2e-16 ***
data$CountyOsage          0.018625   0.005267    3.536 0.000406 ***
data$CountyPottawatomie   0.150382   0.006950   21.638  < 2e-16 ***
data$CountyRiley          0.021409   0.008039    2.663 0.007739 **
data$CountyShawnee        0.631181   0.016368   38.562  < 2e-16 ***
data$CountyWabaunsee      0.096313   0.006278   15.341  < 2e-16 ***
data$CountyWashington     0.323112   0.008260   39.117  < 2e-16 ***
data$CountyWilson         0.479332   0.016647   28.794  < 2e-16 ***
data$CountyWoodson        0.153195   0.011151   13.738  < 2e-16 ***
---
Signif. codes:  0 '***' 0.001 '**' 0.01 '*' 0.05 '.' 0.1 ' ' 1

Residual standard error: 0.6764 on 304360 degrees of freedom
Multiple R-squared:  0.05327,   Adjusted R-squared:  0.05319
F-statistic:   685 on 25 and 304360 DF,  p-value: < 2.2e-16
```

Figure D-3. Tukey test results for the Growing Season Length phenometric.

```
$statistics
      Mean       CV   MSerror        HSD r.harmonic
  14.05403 4.812647 0.4574774 0.04687362   5631.982

$parameters
      Df ntr StudentizedRange alpha  test      name.t
  304360  26          5.20085  0.05 Tukey data$County

$means
                pheno       std     r       Min      Max
Butler       13.96802 0.7085601 32930  6.445644 17.48388
Chase        13.76079 0.4637339 24496  9.964226 17.36088
Chautauqua   14.28936 0.4526268  8946 10.378637 17.28328
Clay         14.18733 0.8279411  6587  8.754104 18.30494
Coffey       14.31740 0.8667453  5041  6.933385 17.45892
Cowley       14.01830 0.5904968 21026  7.840858 17.20593
Dickinson    14.22534 1.0669844  7732  7.427611 17.56790
Elk          14.25016 0.4963023 12320 11.474356 17.37980
Geary        14.04046 0.5863961  6852  9.926509 17.16519
Greenwood    13.91965 0.5086106 26873  9.806402 17.10492
Harvey       13.86538 1.2565856  1876  6.831343 17.34912
Jackson      14.86371 0.9390673  1591 10.091861 17.25242
Kay          14.03423 0.7696616  6491  7.742138 16.95902
Lyon         14.09278 0.7282924 14317  8.849158 17.46217
Marion       14.29258 0.9942912 10944  5.243522 17.45421
Marshall     14.06449 0.9423723  5808  9.080594 18.42440
McPherson    14.03503 0.9664883  6106  6.454010 17.10866
Morris       14.07598 0.7336778 15082  8.721796 17.45701
Osage        13.98664 0.5019687 33029  5.663491 16.95755
Pottawatomie 14.11840 0.5941106 13295 10.923259 17.08848
Riley        13.98943 0.6205404  9018 10.201431 17.15660
Shawnee      14.59920 0.8403428  1801 10.568074 17.34544
Wabaunsee    14.06433 0.6310406 17926  9.671106 17.51241
Washington   14.29113 0.8306652  8419  9.665363 17.55912
Wilson       14.44735 0.7891891  1738  9.160338 17.35505
Woodson      14.12121 0.5912839  4142  8.554791 16.61619
```

Figure D-4. Tukey test groupings of the Growing Season Length phenometric. Each of the 26 counties of the Flint Hills was placed into a class based on their mean values. Counties with similar mean values were placed into the same class.

$groups

	trt	means	M
1	Jackson	14.86371	a
2	Shawnee	14.59920	b
3	Wilson	14.44735	c
4	Coffey	14.31740	d
5	Marion	14.29258	d
6	Washington	14.29113	d
7	Chautauqua	14.28936	d
8	Elk	14.25016	e
9	Dickinson	14.22534	ef
10	Clay	14.18733	f
11	Woodson	14.12121	g
12	Pottawatomie	14.11840	g
13	Lyon	14.09278	gh
14	Morris	14.07598	hi
15	Marshall	14.06449	hij
16	Wabaunsee	14.06433	ij
17	Geary	14.04046	ijk
18	McPherson	14.03503	jk
19	Kay	14.03423	jk
20	Cowley	14.01830	kl
21	Riley	13.98943	lm
22	Osage	13.98664	m
23	Butler	13.96802	m
24	Greenwood	13.91965	n
25	Harvey	13.86538	n
26	Chase	13.76079	o

Figure D-5. ANOVA result for the Left Derivative phenometric

```
Analysis of Variance Table

Response: pheno
                Df  Sum Sq Mean Sq F value    Pr(>F)
data$County     25 1036527   41461  4876.5 < 2.2e-16 ***
Residuals   304360 2587757       9
---
Signif. codes:  0 '***' 0.001 '**' 0.01 '*' 0.05 '.' 0.1 ' ' 1
> 
```

Figure D-6. ANOVA test for the Left Derivative phenometric with all counties being highly significant except for Morris county, which was slightly less significant, and Riley County, which was not significantly different.

```
Call:
lm(formula = pheno ~ data$County)

Residuals:
     Min       1Q   Median       3Q      Max
-18.8597  -1.7588   0.2115   1.9985  12.7576

Coefficients:
                          Estimate Std. Error  t value Pr(>|t|)
(Intercept)              22.867986   0.016068 1423.167  < 2e-16 ***
data$CountyChase          2.098455   0.024602   85.294  < 2e-16 ***
data$CountyChautauqua    -0.618824   0.034765  -17.800  < 2e-16 ***
data$CountyClay          -4.721550   0.039357 -119.968  < 2e-16 ***
data$CountyCoffey        -1.263896   0.044100  -28.660  < 2e-16 ***
data$CountyCowley        -0.557813   0.025740  -21.671  < 2e-16 ***
data$CountyDickinson     -3.890186   0.036849 -105.572  < 2e-16 ***
data$CountyElk            0.258891   0.030795    8.407  < 2e-16 ***
data$CountyGeary         -0.437224   0.038717  -11.293  < 2e-16 ***
data$CountyGreenwood      1.164431   0.023970   48.578  < 2e-16 ***
data$CountyHarvey        -6.150124   0.069212  -88.859  < 2e-16 ***
data$CountyJackson       -1.484714   0.074848  -19.836  < 2e-16 ***
data$CountyKay           -3.075691   0.039599  -77.672  < 2e-16 ***
data$CountyLyon           1.106612   0.029190   37.911  < 2e-16 ***
data$CountyMarion        -2.074454   0.032173  -64.479  < 2e-16 ***
data$CountyMarshall      -3.361575   0.041498  -81.006  < 2e-16 ***
data$CountyMcPherson     -3.510097   0.040628  -86.396  < 2e-16 ***
data$CountyMorris        -0.074530   0.028669   -2.600  0.00933 **
data$CountyOsage         -1.009646   0.022707  -44.464  < 2e-16 ***
data$CountyPottawatomie  -0.340561   0.029962  -11.367  < 2e-16 ***
data$CountyRiley         -0.634813   0.034656  -18.318  < 2e-16 ***
data$CountyShawnee        0.004898   0.070562    0.069  0.94466
data$CountyWabaunsee      2.179311   0.027065   80.523  < 2e-16 ***
data$CountyWashington    -4.694463   0.035610 -131.829  < 2e-16 ***
data$CountyWilson        -2.488506   0.071765  -34.676  < 2e-16 ***
data$CountyWoodson        0.715656   0.048072   14.887  < 2e-16 ***
---
Signif. codes:  0 '***' 0.001 '**' 0.01 '*' 0.05 '.' 0.1 ' ' 1

Residual standard error: 2.916 on 304360 degrees of freedom
Multiple R-squared:  0.286,     Adjusted R-squared:  0.2859
F-statistic:  4876 on 25 and 304360 DF,  p-value: < 2.2e-16
```

Figure D-7. Tukey test results of the Left Derivative phenometric. Each of the 26 counties of the Flint Hills was placed into a class based on their mean values. Counties with similar mean values were placed into the same class.

```
$statistics
      Mean       CV  MSerror       HSD r.harmonic
  22.44044 12.99381 8.502291 0.2020746   5631.982

$parameters
      Df ntr StudentizedRange alpha  test      name.t
  304360  26          5.20085  0.05 Tukey data$County

$means
                pheno      std     r       Min      Max
Butler       22.86799 3.290084 32930  4.008311 31.06431
Chase        24.96644 2.400248 24496 11.001667 33.70438
Chautauqua   22.24916 2.339394  8946  8.895608 30.12326
Clay         18.14644 2.634924  6587  8.315157 28.11210
Coffey       21.60409 3.612392  5041  8.317553 31.82428
Cowley       22.31017 3.258469 21026  7.898092 31.10186
Dickinson    18.97780 2.827153  7732  7.237340 28.69783
Elk          23.12688 2.353438 12320 11.616822 31.98789
Geary        22.43076 2.810382  6852 10.797576 31.25398
Greenwood    24.03242 2.329168 26873  9.130041 32.20244
Harvey       16.71786 2.989436  1876  8.394395 29.47551
Jackson      21.38327 2.752397  1591 12.463325 29.94089
Kay          19.79230 3.348202  6491  4.614645 28.42497
Lyon         23.97460 3.597707 14317  9.709537 33.46496
Marion       20.79353 3.409912 10944  6.754968 29.58579
Marshall     19.50641 2.878915  5808  9.519110 29.78726
McPherson    19.35789 2.583628  6106  6.032660 26.71807
Morris       22.79346 3.665211 15082  9.493662 31.61494
Osage        21.85834 2.425180 33029  5.710933 30.88369
Pottawatomie 22.52743 2.781040 13295  4.888553 31.47091
Riley        22.23317 3.646893  9018  7.162153 31.44101
Shawnee      22.87288 3.136236  1801 12.461758 31.34134
Wabaunsee    25.04730 2.819379 17926 10.554509 34.44996
Washington   18.17352 2.309066  8419  9.630597 25.97046
Wilson       20.37948 2.916243  1738  9.747136 28.42678
Woodson      23.58364 2.872986  4142 10.774711 30.25011
```

Figure D-8. Tukey test groupings of the Left Derivative phenometric. Each of the 26 counties of the Flint Hills was placed into a class based on their mean values. Counties with similar mean values were placed into the same class.

$groups

	trt	means	M
1	Wabaunsee	25.04730	a
2	Chase	24.96644	a
3	Greenwood	24.03242	b
4	Lyon	23.97460	b
5	Woodson	23.58364	c
6	Elk	23.12688	d
7	Shawnee	22.87288	de
8	Butler	22.86799	e
9	Morris	22.79346	e
10	Pottawatomie	22.52743	f
11	Geary	22.43076	fg
12	Cowley	22.31017	gh
13	Chautauqua	22.24916	h
14	Riley	22.23317	h
15	Osage	21.85834	i
16	Coffey	21.60409	j
17	Jackson	21.38327	j
18	Marion	20.79353	k
19	Wilson	20.37948	l
20	Kay	19.79230	m
21	Marshall	19.50641	n
22	McPherson	19.35789	n
23	Dickinson	18.97780	o
24	Washington	18.17352	p
25	Clay	18.14644	p
26	Harvey	16.71786	q

Figure D-9. ANOVA result for the Maximum NDVI phenometric.

```
Analysis of Variance Table

Response: pheno
                Df   Sum Sq Mean Sq F value    Pr(>F)
data$County     25  3497423  139897    2611 < 2.2e-16 ***
Residuals   304360 16307243      54
---
Signif. codes:  0 '***' 0.001 '**' 0.01 '*' 0.05 '.' 0.1 ' ' 1
> 
```

Figure D-10. ANOVA test for the Maximum NDVI phenometric with all counties being highly significant.

```
Call:
lm(formula = pheno ~ data$County)

Residuals:
     Min       1Q   Median       3Q      Max
-104.270   -4.676   -0.142    4.518   42.007

Coefficients:
                        Estimate Std. Error  t value Pr(>|t|)
(Intercept)             198.92663    0.04034 4931.651  < 2e-16 ***
data$CountyChase          1.36490    0.06176   22.100  < 2e-16 ***
data$CountyChautauqua     2.89481    0.08727   33.170  < 2e-16 ***
data$CountyClay          -5.07661    0.09880  -51.384  < 2e-16 ***
data$CountyCoffey         5.44562    0.11071   49.190  < 2e-16 ***
data$CountyCowley        -0.25669    0.06462   -3.973 7.11e-05 ***
data$CountyDickinson     -5.45265    0.09250  -58.947  < 2e-16 ***
data$CountyElk            3.94839    0.07730   51.076  < 2e-16 ***
data$CountyGeary          0.48258    0.09719    4.965 6.87e-07 ***
data$CountyGreenwood      2.35143    0.06017   39.078  < 2e-16 ***
data$CountyHarvey        -7.73176    0.17374  -44.501  < 2e-16 ***
data$CountyJackson        4.85289    0.18789   25.828  < 2e-16 ***
data$CountyKay           -6.31576    0.09941  -63.536  < 2e-16 ***
data$CountyLyon           6.44646    0.07328   87.975  < 2e-16 ***
data$CountyMarion        -3.40699    0.08076  -42.185  < 2e-16 ***
data$CountyMarshall       1.19511    0.10417   11.472  < 2e-16 ***
data$CountyMcPherson     -6.26815    0.10199  -61.459  < 2e-16 ***
data$CountyMorris         1.00654    0.07197   13.986  < 2e-16 ***
data$CountyOsage          0.54561    0.05700    9.572  < 2e-16 ***
data$CountyPottawatomie   1.58270    0.07521   21.043  < 2e-16 ***
data$CountyRiley          1.06367    0.08700   12.227  < 2e-16 ***
data$CountyShawnee        8.17329    0.17713   46.142  < 2e-16 ***
data$CountyWabaunsee      7.12117    0.06794  104.815  < 2e-16 ***
data$CountyWashington    -3.61278    0.08939  -40.415  < 2e-16 ***
data$CountyWilson         4.69143    0.18015   26.041  < 2e-16 ***
data$CountyWoodson        6.39434    0.12068   52.988  < 2e-16 ***
---
Signif. codes:  0 '***' 0.001 '**' 0.01 '*' 0.05 '.' 0.1 ' ' 1

Residual standard error: 7.32 on 304360 degrees of freedom
Multiple R-squared:  0.1766,    Adjusted R-squared:  0.1765
F-statistic:  2611 on 25 and 304360 DF,  p-value: < 2.2e-16
```

Figure D-11. Tukey test results of the Maximum NDVI phenometric. Each of the 26 counties of the Flint Hills was placed into a class based on their mean values. Counties with similar mean values were placed into the same class.

```
$statistics
      Mean       CV MSerror       HSD r.harmonic
  199.9361 3.661047 53.5788 0.5072711   5631.982

$parameters
      Df ntr StudentizedRange alpha  test      name.t
  304360  26          5.20085  0.05 Tukey data$County

$means
                pheno      std     r       Min      Max
Butler       198.9266 7.614700 32930  94.65656 227.5182
Chase        200.2915 6.758079 24496 139.84321 227.2118
Chautauqua   201.8214 7.420164  8946 174.24843 234.6327
Clay         193.8500 7.895476  6587 154.07000 228.2603
Coffey       204.3723 6.506633  5041 105.20892 231.4833
Cowley       198.6699 8.136994 21026 111.72204 235.3748
Dickinson    193.4740 7.833715  7732 131.09355 229.3958
Elk          202.8750 7.391918 12320 156.82138 236.1958
Geary        199.4092 7.820540  6852 152.78473 231.7408
Greenwood    201.2781 6.593789 26873 129.77135 233.8134
Harvey       191.1949 9.188119  1876 162.52015 233.2015
Jackson      203.7795 7.813444  1591 179.77279 230.5526
Kay          192.6109 8.061498  6491 141.56238 228.5995
Lyon         205.3731 6.521632 14317 146.01093 230.0791
Marion       195.5196 7.000375 10944 108.80908 223.0283
Marshall     200.1217 7.758874  5808 158.21040 236.7035
McPherson    192.6585 6.973354  6106 136.15018 226.5310
Morris       199.9332 7.296399 15082 134.80120 227.5634
Osage        199.4722 7.267549 33029 101.08533 234.1906
Pottawatomie 200.5093 7.615737 13295 103.40301 233.1560
Riley        199.9903 8.837748  9018 144.05729 235.2152
Shawnee      207.0999 6.833469  1801 163.27086 235.2879
Wabaunsee    206.0478 6.541713 17926 167.03557 233.9271
Washington   195.3139 7.639613  8419 145.00400 227.9364
Wilson       203.6181 7.056199  1738 177.91028 229.3886
Woodson      205.3210 5.280120  4142 157.06923 231.5064
```

Figure D-12. Tukey test groupings of the Maximum NDVI phenometric. Each of the 26 counties of the Flint Hills was placed into a class based on their mean values. Counties with similar mean values were placed into the same class.

$groups

	trt	means	M
1	Shawnee	207.0999	a
2	Wabaunsee	206.0478	b
3	Lyon	205.3731	c
4	Woodson	205.3210	c
5	Coffey	204.3723	d
6	Jackson	203.7795	de
7	Wilson	203.6181	e
8	Elk	202.8750	f
9	Chautauqua	201.8214	g
10	Greenwood	201.2781	h
11	Pottawatomie	200.5093	i
12	Chase	200.2915	ij
13	Marshall	200.1217	ijk
14	Riley	199.9903	jk
15	Morris	199.9332	k
16	Osage	199.4722	l
17	Geary	199.4092	l
18	Butler	198.9266	m
19	Cowley	198.6699	n
20	Marion	195.5196	o
21	Washington	195.3139	o
22	Clay	193.8500	p
23	Dickinson	193.4740	p
24	McPherson	192.6585	q
25	Kay	192.6109	q
26	Harvey	191.1949	r

Figure D-13. ANOVA result for the Middle of Season phenometric.

```
Analysis of Variance Table

Response: pheno
                Df Sum Sq Mean Sq F value    Pr(>F)
data$County     25  13434  537.34  2787.5 < 2.2e-16 ***
Residuals   304360  58672    0.19
---
Signif. codes:  0 '***' 0.001 '**' 0.01 '*' 0.05 '.' 0.1 ' ' 1
> |
```

Figure D-14. ANOVA test for the Maximum Phenometric with all counties being highly significant except Kay county.

```
Call:
lm(formula = pheno ~ data$County)

Residuals:
    Min      1Q  Median      3Q     Max
-8.5825 -0.2202 -0.0156  0.2148  6.6375

Coefficients:
                          Estimate Std. Error  t value Pr(>|t|)
(Intercept)              12.084055   0.002419 4994.449  < 2e-16 ***
data$CountyChase         -0.027933   0.003705   -7.540 4.70e-14 ***
data$CountyChautauqua    -0.055714   0.005235  -10.643  < 2e-16 ***
data$CountyClay           0.496815   0.005926   83.834  < 2e-16 ***
data$CountyCoffey         0.242305   0.006640   36.490  < 2e-16 ***
data$CountyCowley        -0.036767   0.003876   -9.486  < 2e-16 ***
data$CountyDickinson     -0.088874   0.005548  -16.018  < 2e-16 ***
data$CountyElk            0.022071   0.004637    4.760 1.94e-06 ***
data$CountyGeary          0.275746   0.005830   47.299  < 2e-16 ***
data$CountyGreenwood      0.055496   0.003609   15.376  < 2e-16 ***
data$CountyHarvey         0.279282   0.010422   26.798  < 2e-16 ***
data$CountyJackson        0.414840   0.011270   36.809  < 2e-16 ***
data$CountyKay            0.002839   0.005963    0.476    0.634
data$CountyLyon           0.095714   0.004395   21.777  < 2e-16 ***
data$CountyMarion        -0.240856   0.004844  -49.718  < 2e-16 ***
data$CountyMarshall       0.682148   0.006249  109.169  < 2e-16 ***
data$CountyMcPherson     -0.142135   0.006118  -23.234  < 2e-16 ***
data$CountyMorris         0.049245   0.004317   11.407  < 2e-16 ***
data$CountyOsage          0.191032   0.003419   55.872  < 2e-16 ***
data$CountyPottawatomie   0.469292   0.004511  104.022  < 2e-16 ***
data$CountyRiley          0.458122   0.005218   87.792  < 2e-16 ***
data$CountyShawnee        0.360303   0.010625   33.911  < 2e-16 ***
data$CountyWabaunsee      0.253731   0.004075   62.261  < 2e-16 ***
data$CountyWashington     0.667459   0.005362  124.479  < 2e-16 ***
data$CountyWilson        -0.088329   0.010806   -8.174 2.99e-16 ***
data$CountyWoodson        0.085992   0.007238   11.880  < 2e-16 ***
---
Signif. codes:  0 '***' 0.001 '**' 0.01 '*' 0.05 '.' 0.1 ' ' 1

Residual standard error: 0.4391 on 304360 degrees of freedom
Multiple R-squared:  0.1863,    Adjusted R-squared:  0.1862
F-statistic:  2787 on 25 and 304360 DF,  p-value: < 2.2e-16
```

Figure D-15. Tukey test results of the Middle of Season phenometric. Each of the 26 counties of the Flint Hills was placed into a class based on their mean values. Counties with similar mean values were placed into the same class.

```
$statistics
      Mean       CV   MSerror        HSD r.harmonic
  12.20553 3.597197 0.1927711 0.03042739   5631.982

$parameters
      Df ntr StudentizedRange alpha  test      name.t
  304360  26          5.20085  0.05 Tukey data$County

$means
                pheno       std     r     Min     Max
Butler       12.08405 0.3770688 32930  8.3670 18.7216
Chase        12.05612 0.3067073 24496  9.3985 14.5374
Chautauqua   12.02834 0.3373573  8946  9.8728 15.4475
Clay         12.58087 0.6252196  6587  8.4321 15.9727
Coffey       12.32636 0.5107065  5041 10.6226 15.2123
Cowley       12.04729 0.4072411 21026  6.2801 16.7007
Dickinson    11.99518 0.8538928  7732  6.4299 16.3370
Elk          12.10613 0.3199607 12320 10.3768 13.7617
Geary        12.35980 0.4377035  6852  8.7256 14.5250
Greenwood    12.13955 0.3001627 26873 10.6811 14.3225
Harvey       12.36334 0.9697519  1876  5.6072 15.3833
Jackson      12.49889 0.5033518  1591  9.3008 14.3781
Kay          12.08689 0.7240771  6491  3.5044 14.9344
Lyon         12.17977 0.3975498 14317 10.2868 15.1227
Marion       11.84320 0.5973647 10944  7.4224 15.7092
Marshall     12.76620 0.4825181  5808 10.2093 15.2266
McPherson    11.94192 0.8346573  6106  5.7060 15.5203
Morris       12.13330 0.4411735 15082  9.4122 15.5584
Osage        12.27509 0.3241377 33029  9.4564 16.3498
Pottawatomie 12.55335 0.3479343 13295  9.7835 14.7161
Riley        12.54218 0.4611179  9018 10.1810 15.3756
Shawnee      12.44436 0.3957442  1801 10.7990 14.3104
Wabaunsee    12.33779 0.3313906 17926  9.8434 14.6047
Washington   12.75151 0.5171427  8419  9.5545 15.5970
Wilson       11.99573 0.4775466  1738 10.2767 15.5476
Woodson      12.17005 0.3435886  4142  9.3314 15.0560
```

Figure D-16. Tukey test groupings of the Middle of Season phenometric. Each of the 26 counties of the Flint Hills was placed into a class based on their mean values. Counties with similar mean values were placed into the same class.

$groups

	trt	means	M
1	Marshall	12.76620	a
2	Washington	12.75151	a
3	Clay	12.58087	b
4	Pottawatomie	12.55335	c
5	Riley	12.54218	cd
6	Jackson	12.49889	de
7	Shawnee	12.44436	e
8	Harvey	12.36334	f
9	Geary	12.35980	f
10	Wabaunsee	12.33779	f
11	Coffey	12.32636	f
12	Osage	12.27509	g
13	Lyon	12.17977	h
14	Woodson	12.17005	h
15	Greenwood	12.13955	i
16	Morris	12.13330	i
17	Elk	12.10613	j
18	Kay	12.08689	jk
19	Butler	12.08405	k
20	Chase	12.05612	l
21	Cowley	12.04729	lm
22	Chautauqua	12.02834	mn
23	Wilson	11.99573	no
24	Dickinson	11.99518	o
25	McPherson	11.94192	p
26	Marion	11.84320	q

Figure D-17. ANOVA result for the Right Derivative phenometric.

```
Analysis of Variance Table

Response: pheno
               Df Sum Sq Mean Sq F value    Pr(>F)
data$County    25  92304  3692.2  1303.2 < 2.2e-16 ***
Residuals   304360 862293     2.8
---
Signif. codes:  0 '***' 0.001 '**' 0.01 '*' 0.05 '.' 0.1 ' ' 1
>
```

Figure D-18. ANOVA test for the Maximum Phenometric with all counties being highly significant except Dickinson being slightly less significant and Kay not significantly different.

```
Call:
lm(formula = pheno ~ data$County)

Residuals:
    Min      1Q  Median      3Q     Max
-9.7935 -0.9628 -0.1617  0.6720 20.4628

Coefficients:
                          Estimate Std. Error  t value Pr(>|t|)
(Intercept)              11.169593   0.009276 1204.203  < 2e-16 ***
data$CountyChase          0.095018   0.014202    6.691 2.23e-11 ***
data$CountyChautauqua    -0.068205   0.020068   -3.399 0.000677 ***
data$CountyClay           1.165672   0.022719   51.309  < 2e-16 ***
data$CountyCoffey         0.757802   0.025457   29.768  < 2e-16 ***
data$CountyCowley        -0.006480   0.014859   -0.436 0.662749
data$CountyDickinson      0.063233   0.021271    2.973 0.002952 **
data$CountyElk            0.255689   0.017776   14.384  < 2e-16 ***
data$CountyGeary          0.759056   0.022350   33.963  < 2e-16 ***
data$CountyGreenwood      0.286019   0.013837   20.671  < 2e-16 ***
data$CountyHarvey         0.404219   0.039953   10.117  < 2e-16 ***
data$CountyJackson        0.815399   0.043206   18.872  < 2e-16 ***
data$CountyKay            0.024249   0.022858    1.061 0.288763
data$CountyLyon           0.458131   0.016850   27.189  < 2e-16 ***
data$CountyMarion        -0.821455   0.018572  -44.231  < 2e-16 ***
data$CountyMarshall       2.126918   0.023955   88.789  < 2e-16 ***
data$CountyMcPherson     -0.262236   0.023453  -11.182  < 2e-16 ***
data$CountyMorris         0.118135   0.016549    7.138 9.47e-13 ***
data$CountyOsage          0.868857   0.013108   66.286  < 2e-16 ***
data$CountyPottawatomie   0.916828   0.017295   53.010  < 2e-16 ***
data$CountyRiley          1.170243   0.020005   58.498  < 2e-16 ***
data$CountyShawnee        0.686491   0.040732   16.854  < 2e-16 ***
data$CountyWabaunsee      1.069890   0.015623   68.481  < 2e-16 ***
data$CountyWashington     1.388597   0.020556   67.552  < 2e-16 ***
data$CountyWilson        -0.387972   0.041426   -9.365  < 2e-16 ***
data$CountyWoodson        0.262261   0.027750    9.451  < 2e-16 ***
---
Signif. codes:  0 '***' 0.001 '**' 0.01 '*' 0.05 '.' 0.1 ' ' 1

Residual standard error: 1.683 on 304360 degrees of freedom
Multiple R-squared:  0.09669,   Adjusted R-squared:  0.09662
F-statistic:  1303 on 25 and 304360 DF,  p-value: < 2.2e-16
```

Figure D-19. Tukey test results of the Right Derivative phenometric. Each of the 26 counties of the Flint Hills was placed into a class based on their mean values. Counties with similar mean values were placed into the same class.

```
$statistics
      Mean       CV  MSerror      HSD r.harmonic
  11.58314 14.53139 2.833134 0.116648   5631.982

$parameters
      Df ntr StudentizedRange alpha  test      name.t
  304360  26          5.20085  0.05 Tukey data$County

$means
                pheno      std     r      Min      Max
Butler       11.16959 1.605177 32930 4.056843 27.71576
Chase        11.26461 1.059563 24496 7.009601 25.28710
Chautauqua   11.10139 1.347085  8946 3.000685 23.43872
Clay         12.33527 2.671821  6587 5.899312 28.27171
Coffey       11.92740 2.286711  5041 6.907932 27.79957
Cowley       11.16311 1.444194 21026 3.076590 29.44696
Dickinson    11.23283 2.527014  7732 4.911003 30.01708
Elk          11.42528 1.247020 12320 6.558435 21.70855
Geary        11.92865 1.679221  6852 6.897736 26.90026
Greenwood    11.45561 1.102888 26873 6.892670 26.60777
Harvey       11.57381 3.417907  1876 5.227039 32.03657
Jackson      11.98499 2.074833  1591 6.872783 27.36791
Kay          11.19384 1.640621  6491 4.322425 30.26735
Lyon         11.62772 1.613296 14317 7.138898 28.40939
Marion       10.34814 1.790495 10944 4.977984 26.92675
Marshall     13.29651 2.942146  5808 6.078669 31.16141
McPherson    10.90736 2.037743  6106 4.444560 28.31856
Morris       11.28773 1.813930 15082 6.161345 28.89308
Osage        12.03845 1.386196 33029 3.373764 31.05060
Pottawatomie 12.08642 1.520126 13295 4.218688 23.11583
Riley        12.33984 2.008879  9018 2.546382 25.05080
Shawnee      11.85608 1.768245  1801 6.819227 24.98825
Wabaunsee    12.23948 1.385314 17926 7.475453 25.28205
Washington   12.55819 2.722399  8419 6.435235 28.61367
Wilson       10.78162 2.437121  1738 5.756518 30.52411
Woodson      11.43185 1.462646  4142 7.572346 26.68941
```

Figure D-20. Tukey test groupings of the Right Derivative phenometric. Each of the 26 counties of the Flint Hills was placed into a class based on their mean values. Counties with similar mean values were placed into the same class.

$groups

	trt	means	M
1	Marshall	13.29651	a
2	Washington	12.55819	b
3	Riley	12.33984	c
4	Clay	12.33527	c
5	Wabaunsee	12.23948	d
6	Pottawatomie	12.08642	e
7	Osage	12.03845	e
8	Jackson	11.98499	ef
9	Geary	11.92865	f
10	Coffey	11.92740	f
11	Shawnee	11.85608	f
12	Lyon	11.62772	g
13	Harvey	11.57381	gh
14	Greenwood	11.45561	h
15	Woodson	11.43185	h
16	Elk	11.42528	h
17	Morris	11.28773	i
18	Chase	11.26461	ij
19	Dickinson	11.23283	ijk
20	Kay	11.19384	jkl
21	Butler	11.16959	kl
22	Cowley	11.16311	kl
23	Chautauqua	11.10139	l
24	McPherson	10.90736	m
25	Wilson	10.78162	m
26	Marion	10.34814	n

Figure D-21. ANOVA result for the Small Integral phenometric.

```
Analysis of Variance Table

Response: pheno
               Df     Sum Sq  Mean Sq F value    Pr(>F)
data$County    25  696493616 27859745  3932.4 < 2.2e-16 ***
Residuals   304360 2156270868     7085
---
Signif. codes:  0 '***' 0.001 '**' 0.01 '*' 0.05 '.' 0.1 ' ' 1
> |
```

Figure D-22. ANOVA test for the Small Integral Phenometric with all counties being highly significant except Osage being slightly less significant.

```
Call:
lm(formula = pheno ~ data$County)

Residuals:
    Min      1Q  Median      3Q     Max
-947.92  -48.11    2.11   52.09  499.37

Coefficients:
                        Estimate Std. Error  t value Pr(>|t|)
(Intercept)             1025.8267     0.4638 2211.628  < 2e-16 ***
data$CountyChase          18.9836     0.7102   26.731  < 2e-16 ***
data$CountyChautauqua     16.3796     1.0035   16.322  < 2e-16 ***
data$CountyClay          -75.0532     1.1361  -66.063  < 2e-16 ***
data$CountyCoffey         41.4763     1.2730   32.581  < 2e-16 ***
data$CountyCowley        -10.9476     0.7430  -14.734  < 2e-16 ***
data$CountyDickinson    -102.2889     1.0637  -96.165  < 2e-16 ***
data$CountyElk            46.6089     0.8889   52.433  < 2e-16 ***
data$CountyGeary          14.0883     1.1176   12.606  < 2e-16 ***
data$CountyGreenwood      31.1123     0.6919   44.964  < 2e-16 ***
data$CountyHarvey       -170.5624     1.9979  -85.371  < 2e-16 ***
data$CountyJackson        93.4760     2.1606   43.264  < 2e-16 ***
data$CountyKay           -83.0948     1.1431  -72.695  < 2e-16 ***
data$CountyLyon           63.2451     0.8426   75.059  < 2e-16 ***
data$CountyMarion        -58.1696     0.9287  -62.635  < 2e-16 ***
data$CountyMarshall       15.6286     1.1979   13.047  < 2e-16 ***
data$CountyMcPherson    -108.6149     1.1728  -92.613  < 2e-16 ***
data$CountyMorris          7.7518     0.8276    9.367  < 2e-16 ***
data$CountyOsage          -1.7925     0.6555   -2.735  0.00625 **
data$CountyPottawatomie   39.4866     0.8649   45.656  < 2e-16 ***
data$CountyRiley          14.8186     1.0004   14.813  < 2e-16 ***
data$CountyShawnee       106.9340     2.0369   52.499  < 2e-16 ***
data$CountyWabaunsee      99.8595     0.7813  127.820  < 2e-16 ***
data$CountyWashington    -27.9950     1.0279  -27.234  < 2e-16 ***
data$CountyWilson        -19.8043     2.0716   -9.560  < 2e-16 ***
data$CountyWoodson        48.9479     1.3877   35.274  < 2e-16 ***
---
Signif. codes:  0 '***' 0.001 '**' 0.01 '*' 0.05 '.' 0.1 ' ' 1

Residual standard error: 84.17 on 304360 degrees of freedom
Multiple R-squared:  0.2441,    Adjusted R-squared:  0.2441
F-statistic:  3932 on 25 and 304360 DF,  p-value: < 2.2e-16
```

Figure D-23. Tukey test results of the Small Integral phenometric. Each of the 26 counties of the Flint Hills was placed into a class based on their mean values. Counties with similar mean values were placed into the same class.

```
$statistics
      Mean       CV  MSerror      HSD r.harmonic
  1033.808 8.141753 7084.607 5.833128   5631.982

$parameters
      Df ntr StudentizedRange alpha  test      name.t
  304360  26          5.20085  0.05 Tukey data$County

$means
                pheno       std     r       Min      Max
Butler       1025.8267  92.81451 32930  77.90963 1394.669
Chase        1044.8103  64.15957 24496 483.49471 1448.612
Chautauqua   1042.2063  76.22105  8946 349.20967 1401.714
Clay          950.7735  83.40483  6587 577.50323 1450.143
Coffey       1067.3030  82.03283  5041 133.59736 1345.348
Cowley       1014.8791  97.28524 21026 220.28452 1332.752
Dickinson     923.5378 111.58204  7732 417.37563 1375.001
Elk          1072.4356  69.61416 12320 652.65521 1341.311
Geary        1039.9150  87.14558  6852 660.14337 1521.777
Greenwood    1056.9390  62.12351 26873 362.29343 1413.531
Harvey        855.2643 116.04561  1876 382.61835 1267.062
Jackson      1119.3027  98.34530  1591 846.55389 1469.369
Kay           942.7319 123.68213  6491 354.62160 1275.009
Lyon         1089.0718  77.39502 14317 513.24586 1472.732
Marion        967.6571 104.32310 10944 115.11976 1394.286
Marshall     1041.4553  83.82449  5808 587.26188 1482.852
McPherson     917.2118 110.05322  6106 360.60520 1362.796
Morris       1033.5785  86.33651 15082 338.87310 1418.967
Osage        1024.0342  80.28481 33029 148.48211 1338.614
Pottawatomie 1065.3133  79.08053 13295 165.80688 1445.047
Riley        1040.6453  91.17172  9018 317.07099 1447.470
Shawnee      1132.7607  75.91086  1801 730.69535 1385.520
Wabaunsee    1125.6862  68.99229 17926 785.46315 1484.006
Washington    997.8317  78.18499  8419 657.58322 1470.297
Wilson       1006.0224 102.67619  1738 602.92077 1369.240
Woodson      1074.7746  71.27363  4142 569.52518 1370.099
```

Figure D-24. Tukey test groupings of the Small Integral phenometric. Each of the 26 counties of the Flint Hills was placed into a class based on their mean values. Counties with similar mean values were placed into the same class.

$groups

	trt	means	M
1	Shawnee	1132.7607	a
2	Wabaunsee	1125.6862	ab
3	Jackson	1119.3027	b
4	Lyon	1089.0718	c
5	Woodson	1074.7746	d
6	Elk	1072.4356	de
7	Coffey	1067.3030	ef
8	Pottawatomie	1065.3133	f
9	Greenwood	1056.9390	g
10	Chase	1044.8103	h
11	Chautauqua	1042.2063	hi
12	Marshall	1041.4553	hi
13	Riley	1040.6453	i
14	Geary	1039.9150	i
15	Morris	1033.5785	j
16	Butler	1025.8267	k
17	Osage	1024.0342	k
18	Cowley	1014.8791	l
19	Wilson	1006.0224	m
20	Washington	997.8317	n
21	Marion	967.6571	o
22	Clay	950.7735	p
23	Kay	942.7319	q
24	Dickinson	923.5378	r
25	McPherson	917.2118	s
26	Harvey	855.2643	t

Figure D-25. ANOVA result for the Start of Season phenometric.

```
Analysis of Variance Table

Response: pheno
               Df Sum Sq Mean Sq F value    Pr(>F)
data$County    25   9300  372.00  2220.8 < 2.2e-16 ***
Residuals   304360  50982    0.17
---
Signif. codes:  0 '***' 0.001 '**' 0.01 '*' 0.05 '.' 0.1 ' ' 1
> |
```

Figure D-26. ANOVA test for the Start of Season Phenometric with all counties being highly significant except Woodson being insignificant.

```
Call:
lm(formula = pheno ~ data$County)

Residuals:
    Min      1Q  Median      3Q     Max
-3.4262 -0.1519  0.0756  0.2463  6.8679

Coefficients:
                          Estimate Std. Error  t value Pr(>|t|)
(Intercept)               6.564807   0.002255 2910.732  < 2e-16 ***
data$CountyChase          0.199094   0.003453   57.654  < 2e-16 ***
data$CountyChautauqua    -0.183228   0.004880  -37.550  < 2e-16 ***
data$CountyClay          -0.309119   0.005524  -55.957  < 2e-16 ***
data$CountyCoffey        -0.133552   0.006190  -21.576  < 2e-16 ***
data$CountyCowley        -0.105395   0.003613  -29.171  < 2e-16 ***
data$CountyDickinson     -0.562076   0.005172 -108.674  < 2e-16 ***
data$CountyElk           -0.104979   0.004322  -24.287  < 2e-16 ***
data$CountyGeary          0.041875   0.005434    7.706 1.31e-14 ***
data$CountyGreenwood      0.093237   0.003365   27.712  < 2e-16 ***
data$CountyHarvey        -0.335236   0.009715  -34.508  < 2e-16 ***
data$CountyJackson       -0.306220   0.010506  -29.148  < 2e-16 ***
data$CountyKay           -0.330177   0.005558  -59.404  < 2e-16 ***
data$CountyLyon           0.036278   0.004097    8.854  < 2e-16 ***
data$CountyMarion        -0.367941   0.004516  -81.478  < 2e-16 ***
data$CountyMarshall      -0.049750   0.005825   -8.541  < 2e-16 ***
data$CountyMcPherson     -0.377495   0.005703  -66.197  < 2e-16 ***
data$CountyMorris        -0.033523   0.004024   -8.331  < 2e-16 ***
data$CountyOsage         -0.095228   0.003187  -29.878  < 2e-16 ***
data$CountyPottawatomie   0.102857   0.004205   24.458  < 2e-16 ***
data$CountyRiley          0.103621   0.004864   21.302  < 2e-16 ***
data$CountyShawnee       -0.083269   0.009904   -8.407  < 2e-16 ***
data$CountyWabaunsee      0.148972   0.003799   39.215  < 2e-16 ***
data$CountyWashington    -0.205563   0.004998  -41.127  < 2e-16 ***
data$CountyWilson        -0.355206   0.010073  -35.263  < 2e-16 ***
data$CountyWoodson        0.013049   0.006747    1.934   0.0531 .
---
Signif. codes:  0 '***' 0.001 '**' 0.01 '*' 0.05 '.' 0.1 ' ' 1

Residual standard error: 0.4093 on 304360 degrees of freedom
Multiple R-squared:  0.1543,    Adjusted R-squared:  0.1542
F-statistic:  2221 on 25 and 304360 DF,  p-value: < 2.2e-16
```

Figure D-27. Tukey test results of the Start of Season phenometric. Each of the 26 counties of the Flint Hills was placed into a class based on their mean values. Counties with similar mean values were placed into the same class.

```
$statistics
     Mean       CV   MSerror        HSD r.harmonic
  6.51547 6.281594 0.1675063 0.02836346   5631.982

$parameters
      Df ntr StudentizedRange alpha  test      name.t
  304360  26          5.20085  0.05 Tukey data$County

$means
                pheno       std     r      Min       Max
Butler       6.564807 0.4429321 32930 3.885877 13.044519
Chase        6.763901 0.2910200 24496 4.567910  8.489144
Chautauqua   6.381578 0.2520413  8946 4.625424  7.588196
Clay         6.255688 0.5042489  6587 4.148270  8.753369
Coffey       6.431255 0.4602725  5041 4.705388 11.749465
Cowley       6.459412 0.4245571 21026 3.571987 10.985880
Dickinson    6.002731 0.6138784  7732 3.424426  9.962678
Elk          6.459828 0.2741466 12320 4.673813  7.284623
Geary        6.606682 0.4097339  6852 4.447737  8.395436
Greenwood    6.658044 0.2595881 26873 4.345804  8.486741
Harvey       6.229570 0.7450526  1876 3.776980 10.048451
Jackson      6.258587 0.4894424  1591 4.780184  8.387917
Kay          6.234630 0.5947300  6491 2.808480  8.652156
Lyon         6.601084 0.3760729 14317 4.579052  9.175522
Marion       6.196866 0.6187852 10944 4.149261 13.064723
Marshall     6.515057 0.4903162  5808 4.572010  8.934332
McPherson    6.187312 0.6308219  6106 3.559100  8.025413
Morris       6.531283 0.4766549 15082 4.541725 10.469757
Osage        6.469578 0.2947752 33029 4.230126 12.359054
Pottawatomie 6.667663 0.3437569 13295 4.809442  8.032917
Riley        6.668427 0.4076835  9018 4.680184  8.899599
Shawnee      6.481538 0.4033374  1801 4.769576  7.948748
Wabaunsee    6.713779 0.3785204 17926 4.665219  8.730512
Washington   6.359244 0.4639739  8419 4.652044  8.983021
Wilson       6.209601 0.4076977  1738 4.798688  9.796845
Woodson      6.577856 0.3338601  4142 4.732240  9.457639
```

Figure D-28. Tukey test groupings of the Start of Season phenometric. Each of the 26 counties of the Flint Hills was placed into a class based on their mean values. Counties with similar mean values were placed into the same class.

$groups

	trt	means	M
1	Chase	6.763901	a
2	Wabaunsee	6.713779	b
3	Riley	6.668427	c
4	Pottawatomie	6.667663	c
5	Greenwood	6.658044	c
6	Geary	6.606682	d
7	Lyon	6.601084	d
8	Woodson	6.577856	de
9	Butler	6.564807	e
10	Morris	6.531283	f
11	Marshall	6.515057	fg
12	Shawnee	6.481538	gh
13	Osage	6.469578	h
14	Elk	6.459828	h
15	Cowley	6.459412	h
16	Coffey	6.431255	i
17	Chautauqua	6.381578	j
18	Washington	6.359244	j
19	Jackson	6.258587	k
20	Clay	6.255688	k
21	Kay	6.234630	k
22	Harvey	6.229570	kl
23	Wilson	6.209601	klm
24	Marion	6.196866	lm
25	McPherson	6.187312	m
26	Dickinson	6.002731	n

Figure D-29. Start of Season Phenometric mean value for each cell for the 2001-2015 study period.

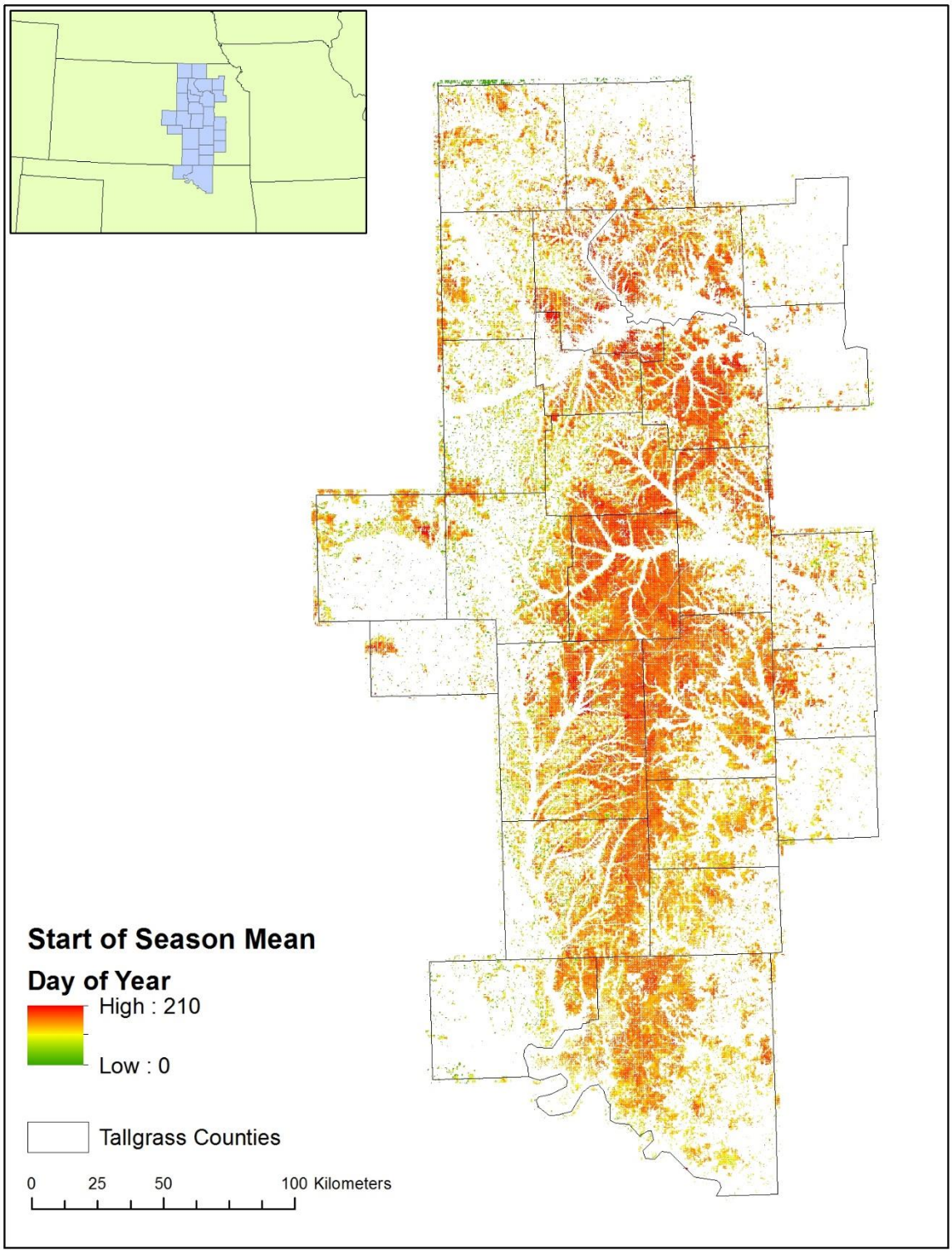

Figure D-30. Small Integral Phenometric mean value for each cell for the 2001-2015 study period.

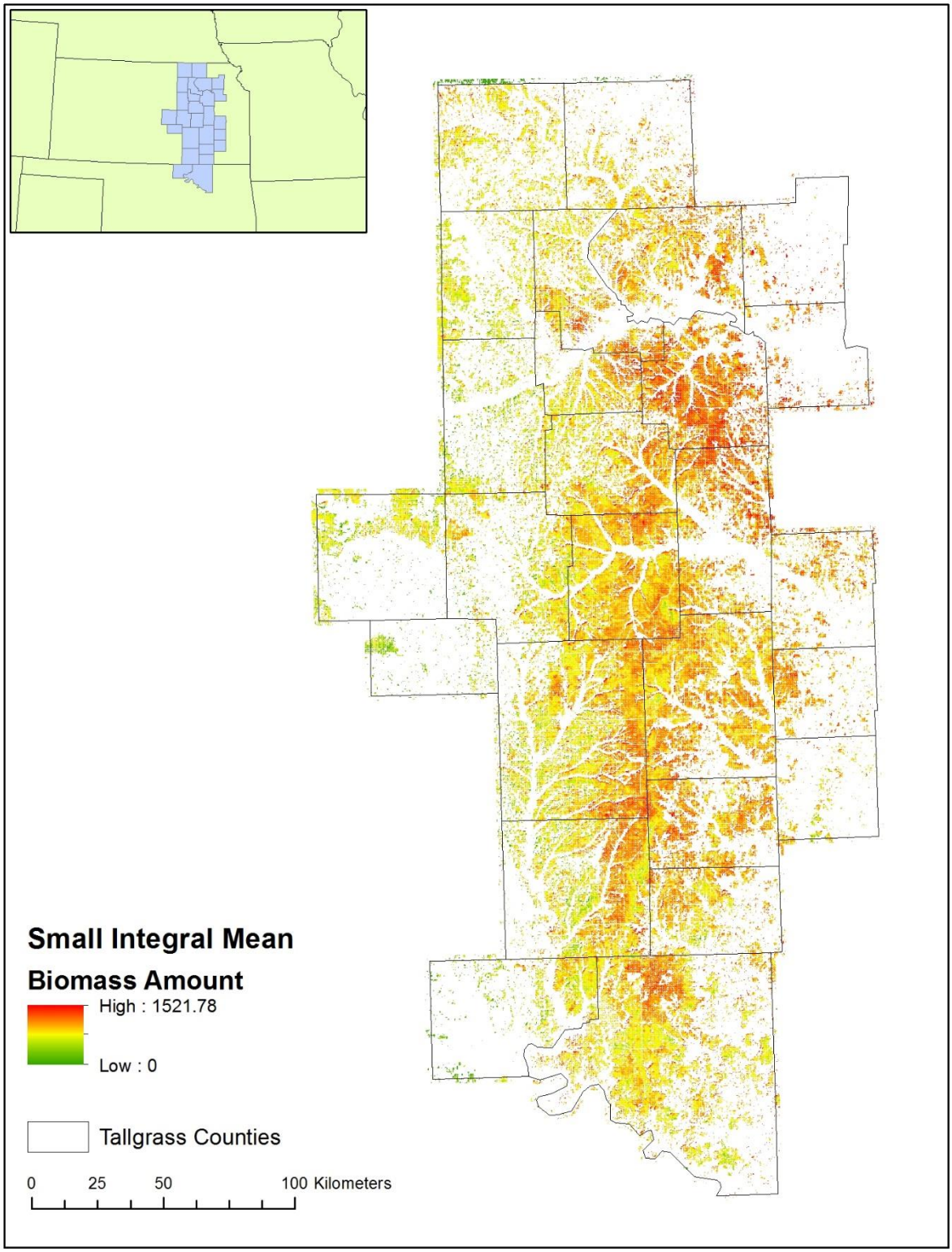

Figure D-31. Season Length Phenometric mean value for each cell in the 2001-2015 study period.

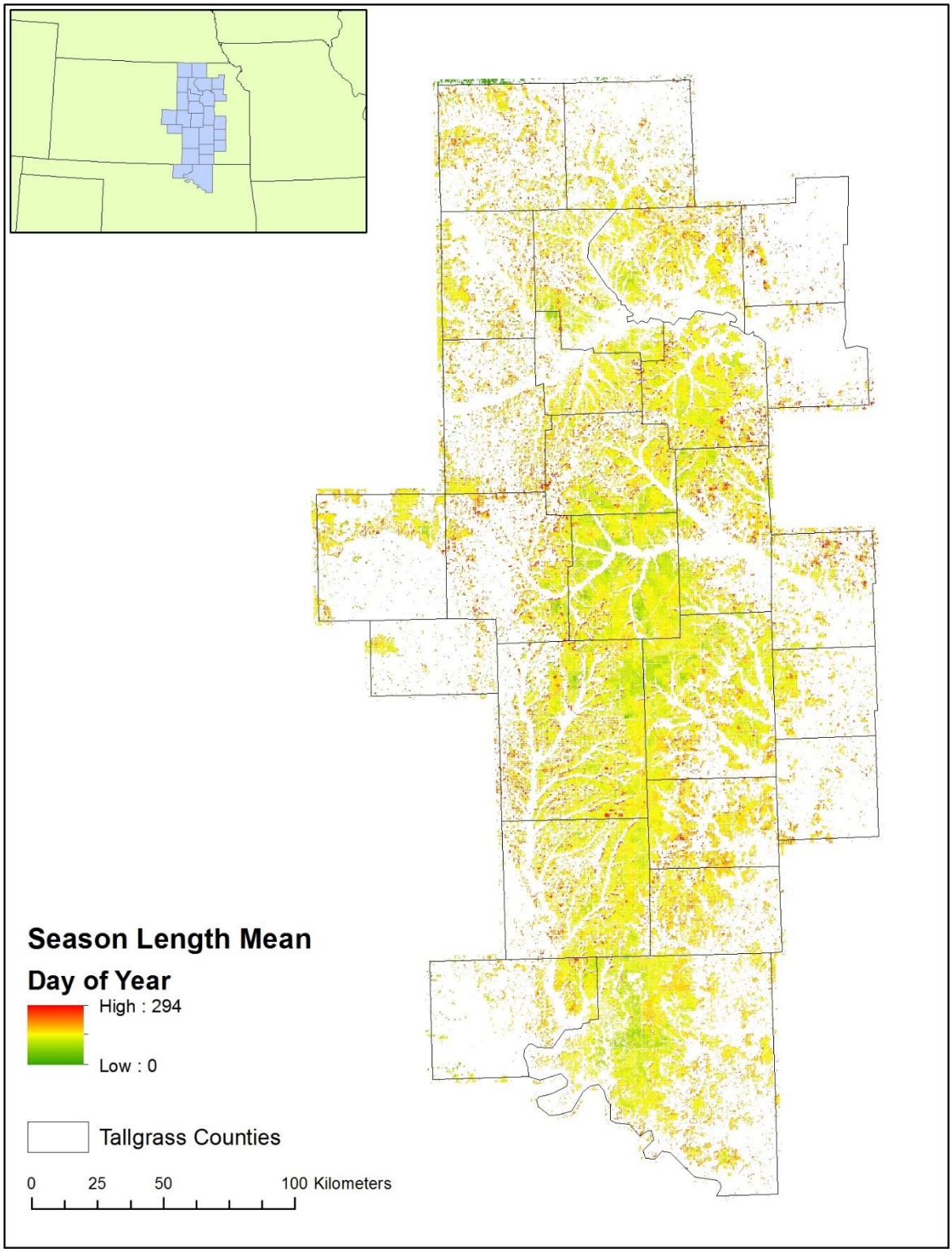

Figure D-32. Right Derivative phenometric mean value for each cell in the 2001-2015 study period.

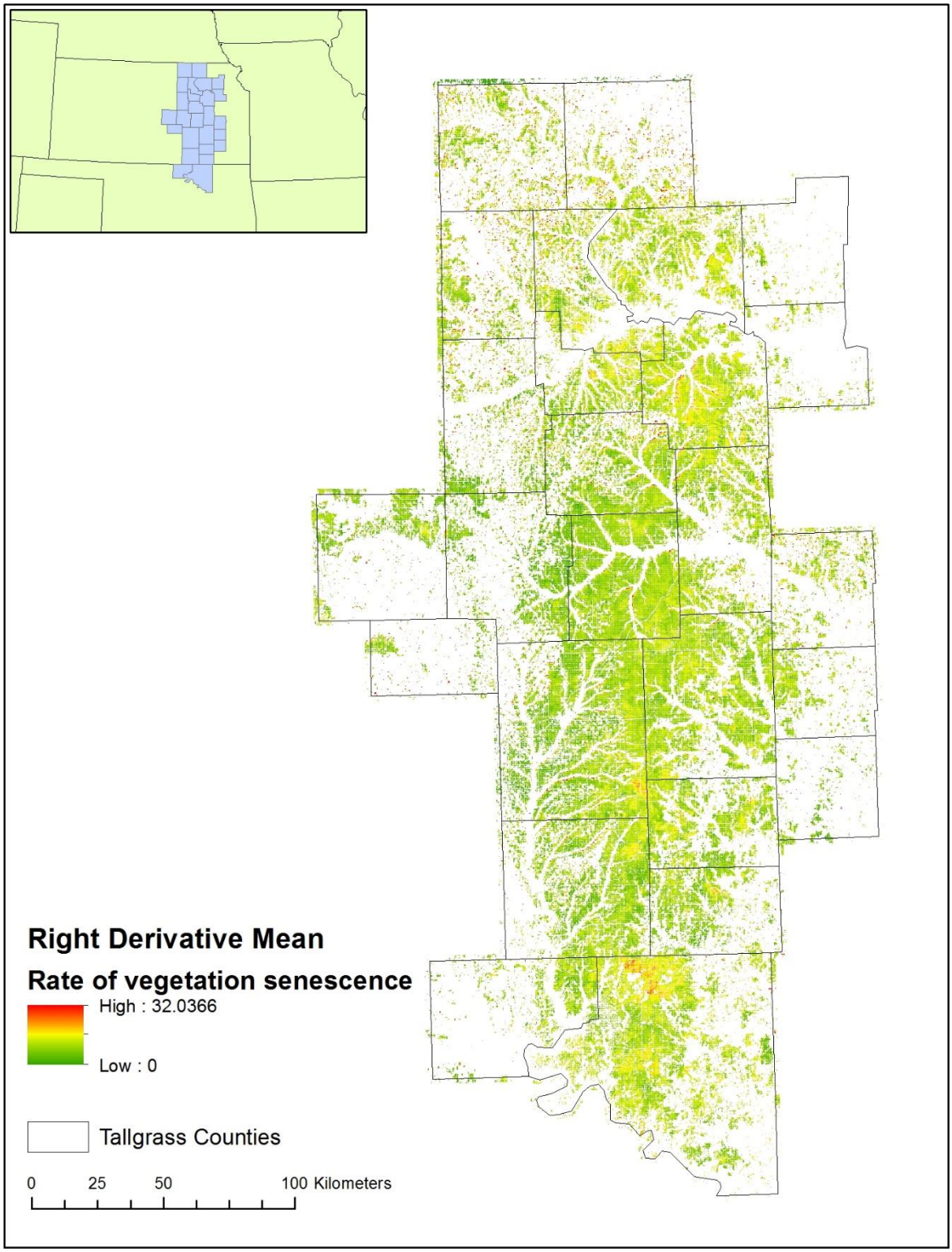

Figure D-33. Middle of Season phenometric mean value for each cell in the 2001-2015 study period.

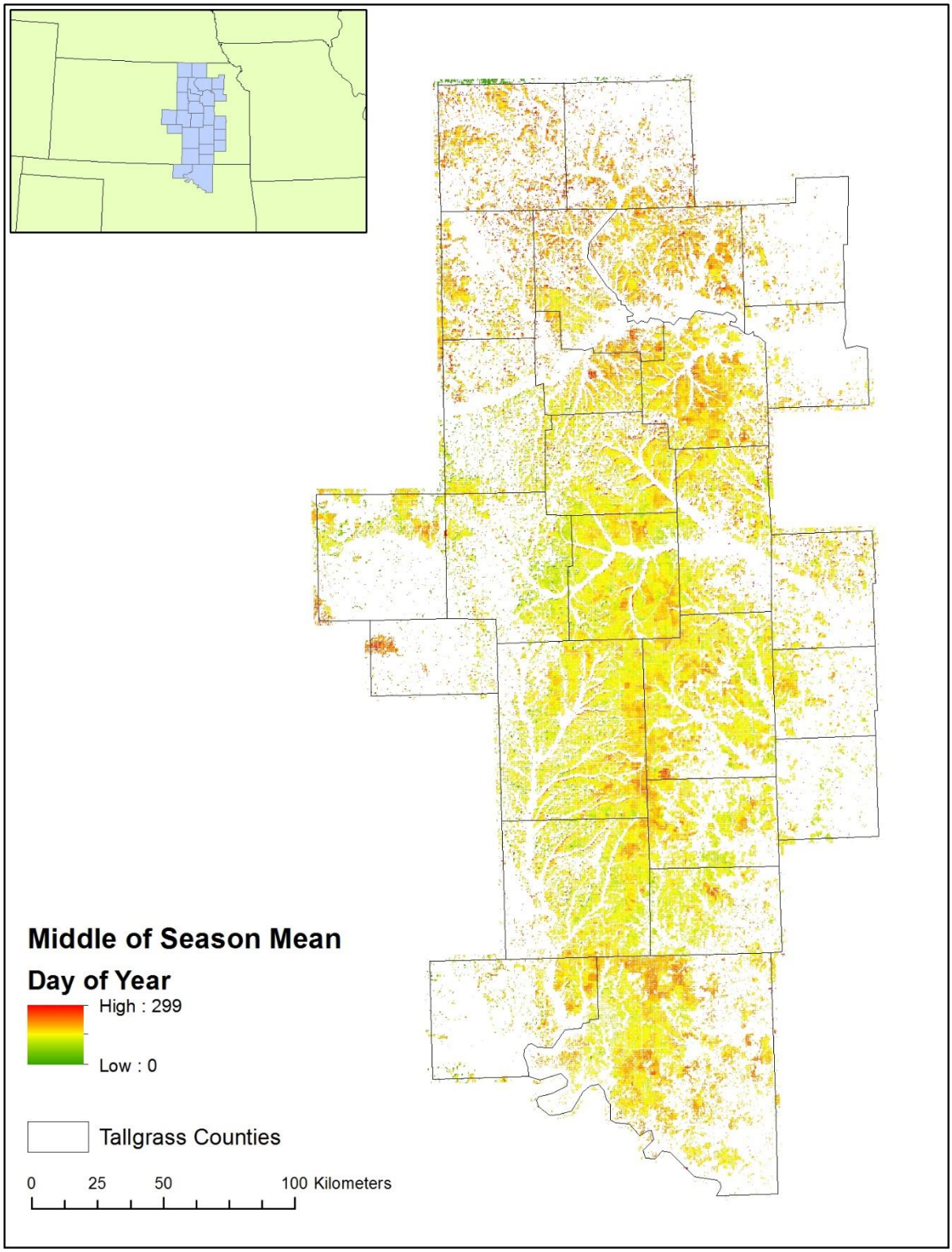

Figure D-34. Maximum NDVI phenometric mean value for each cell in the 2001-2015 study period.

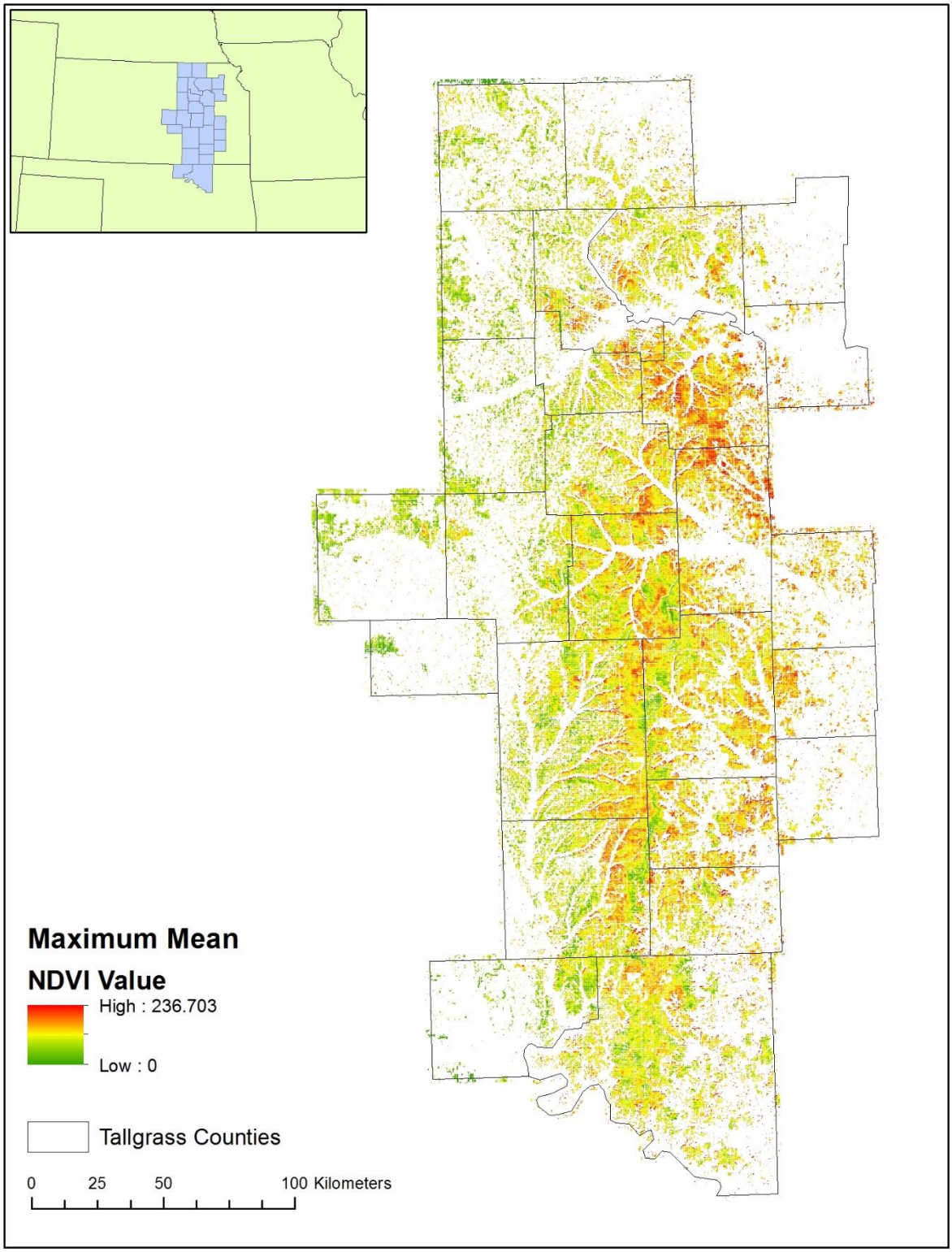

Figure D-35. Left Derivative phenometric mean value for each cell in the 2001-2015 study period.

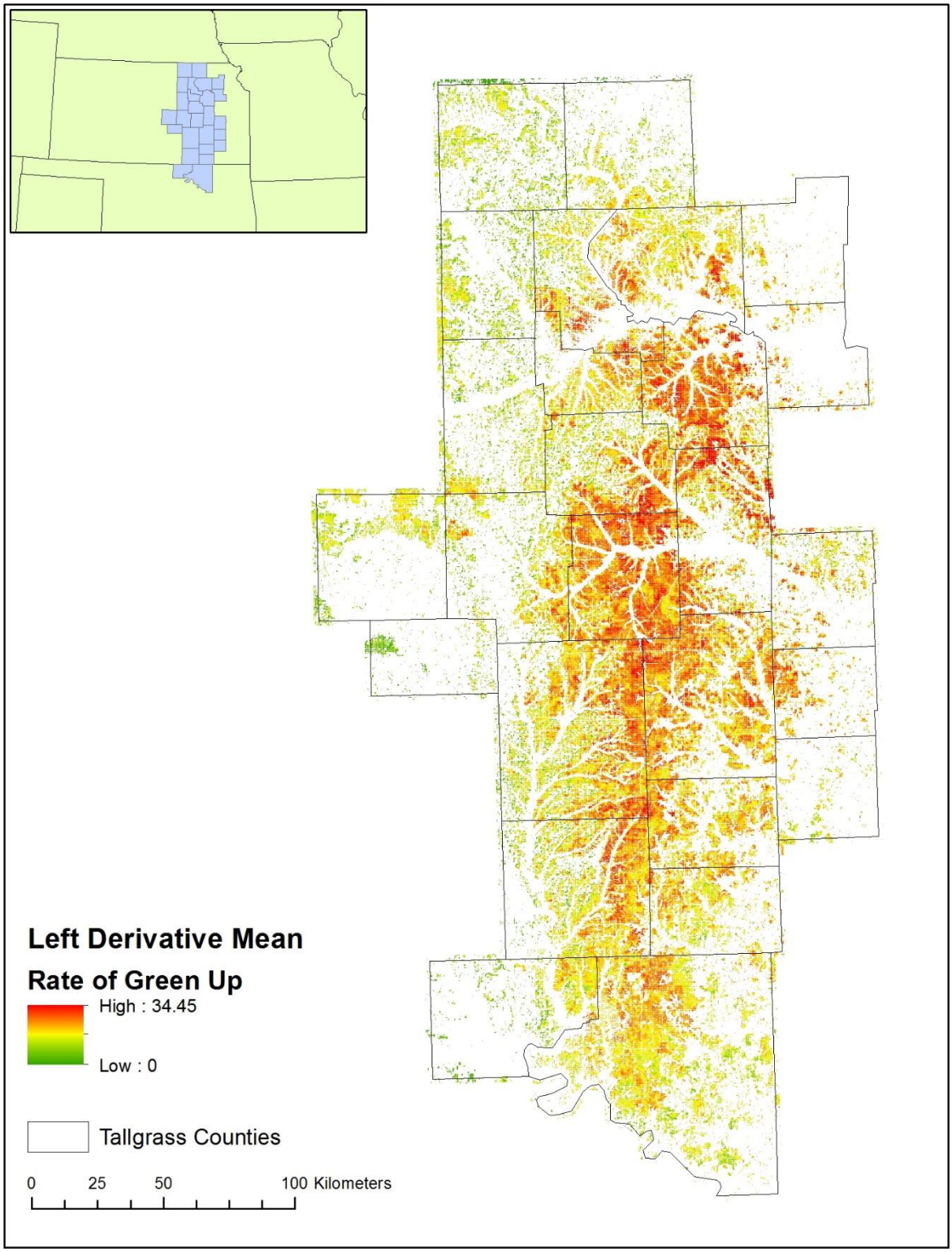

Figure D-36. End of Season phenometric mean value for each cell in the 2001-2015 study period.

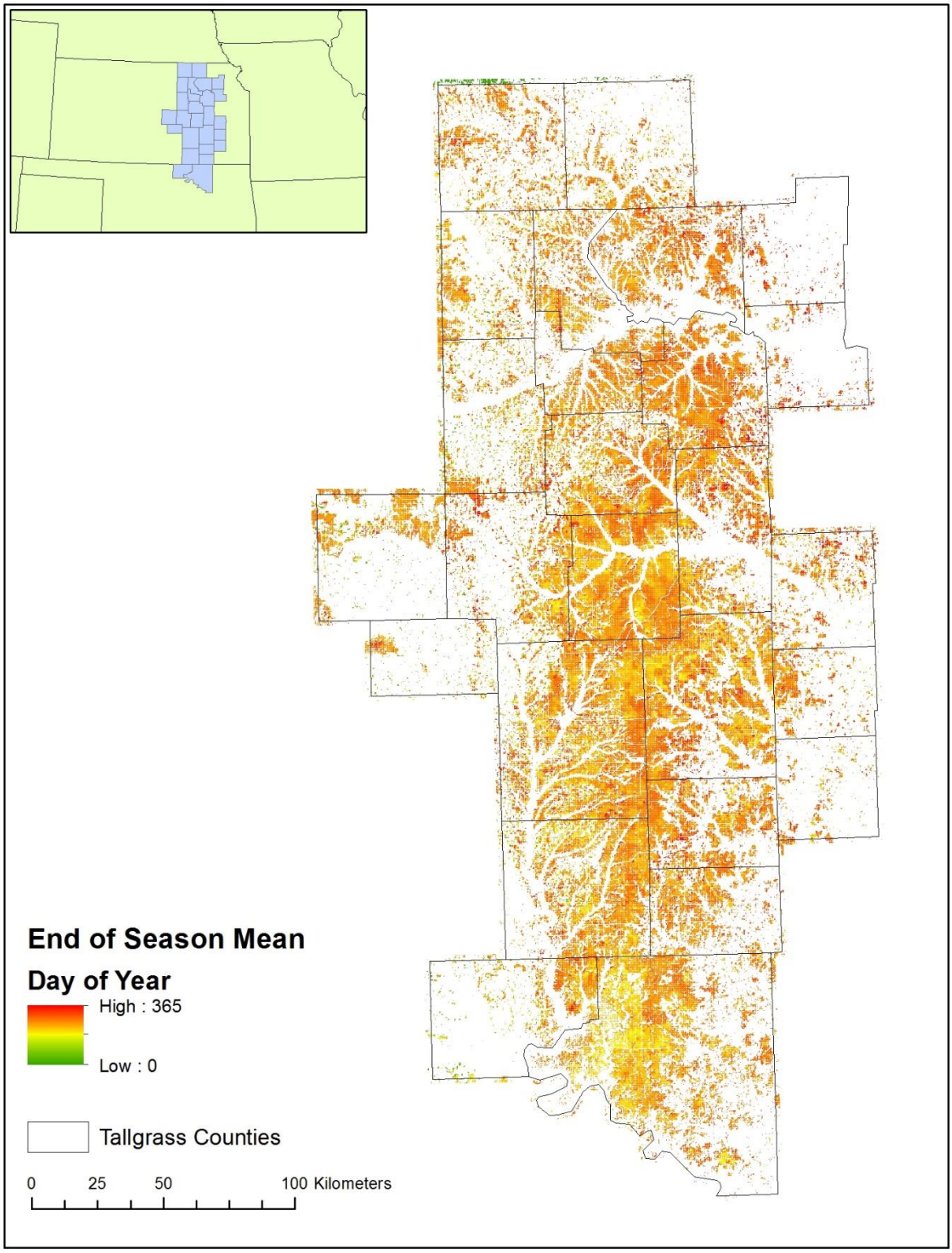

Figure D-37. Map of Tukey HSD test results for the growing season phenometric.

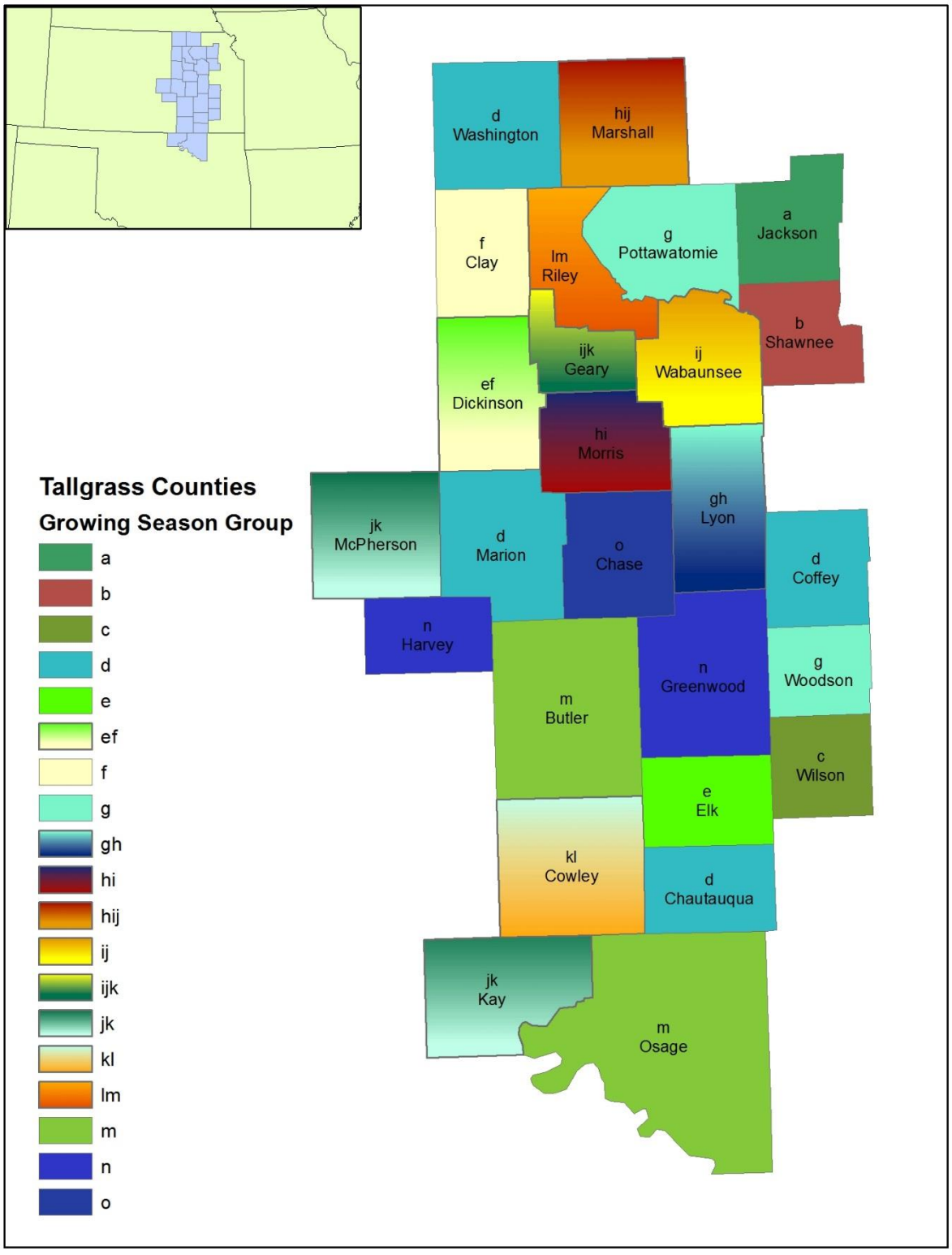

Figure D-38. Map of Tukey HSD test results for the left derivative phenometric.

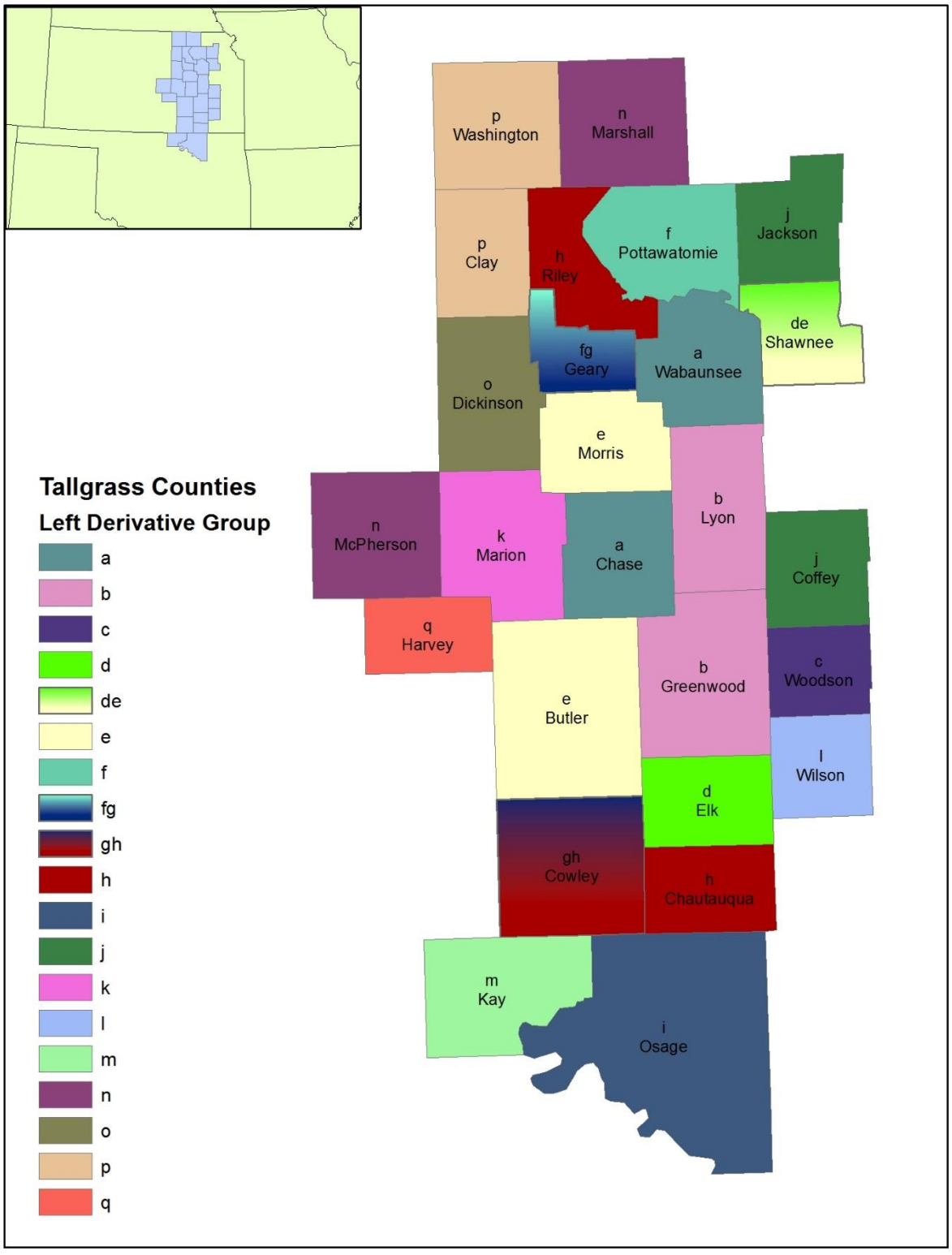

Figure D-39. Map of Tukey HSD test results for the Maximum NDVI phenometric.

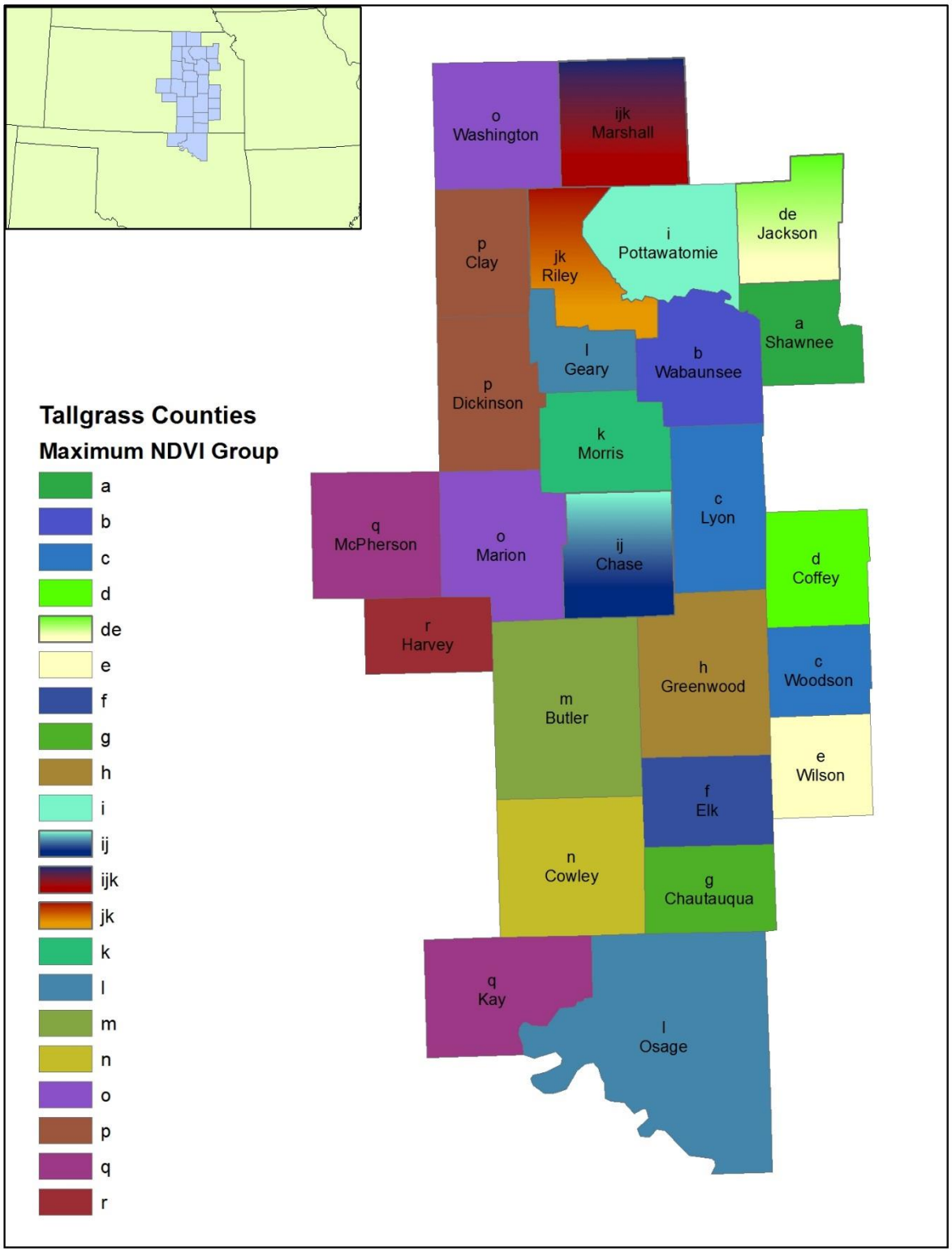

Figure D-40. Map of Tukey HSD test results for the middle of season phenometric.

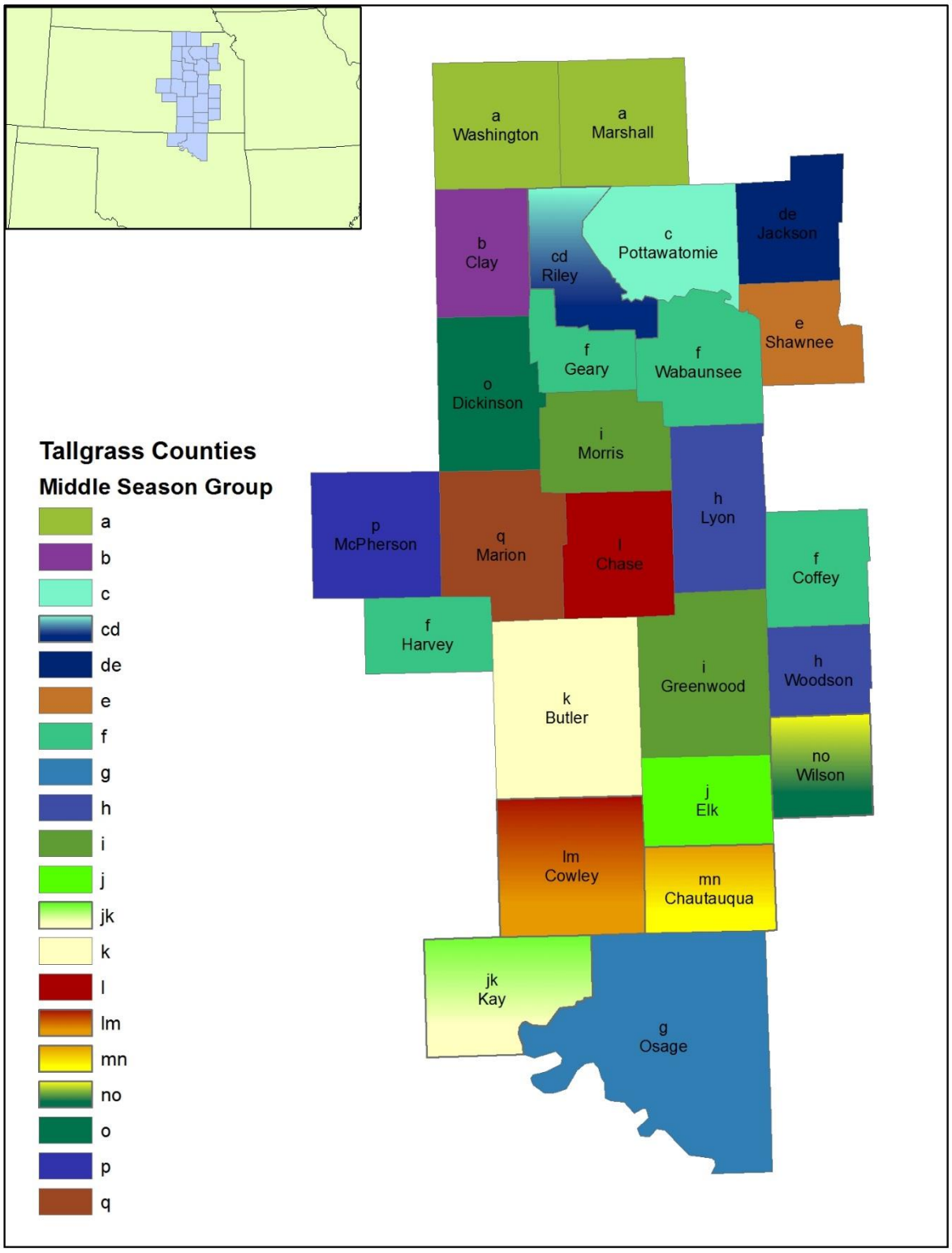

Figure D-41. Map of Tukey HSD test results for the right derivative phenometric.

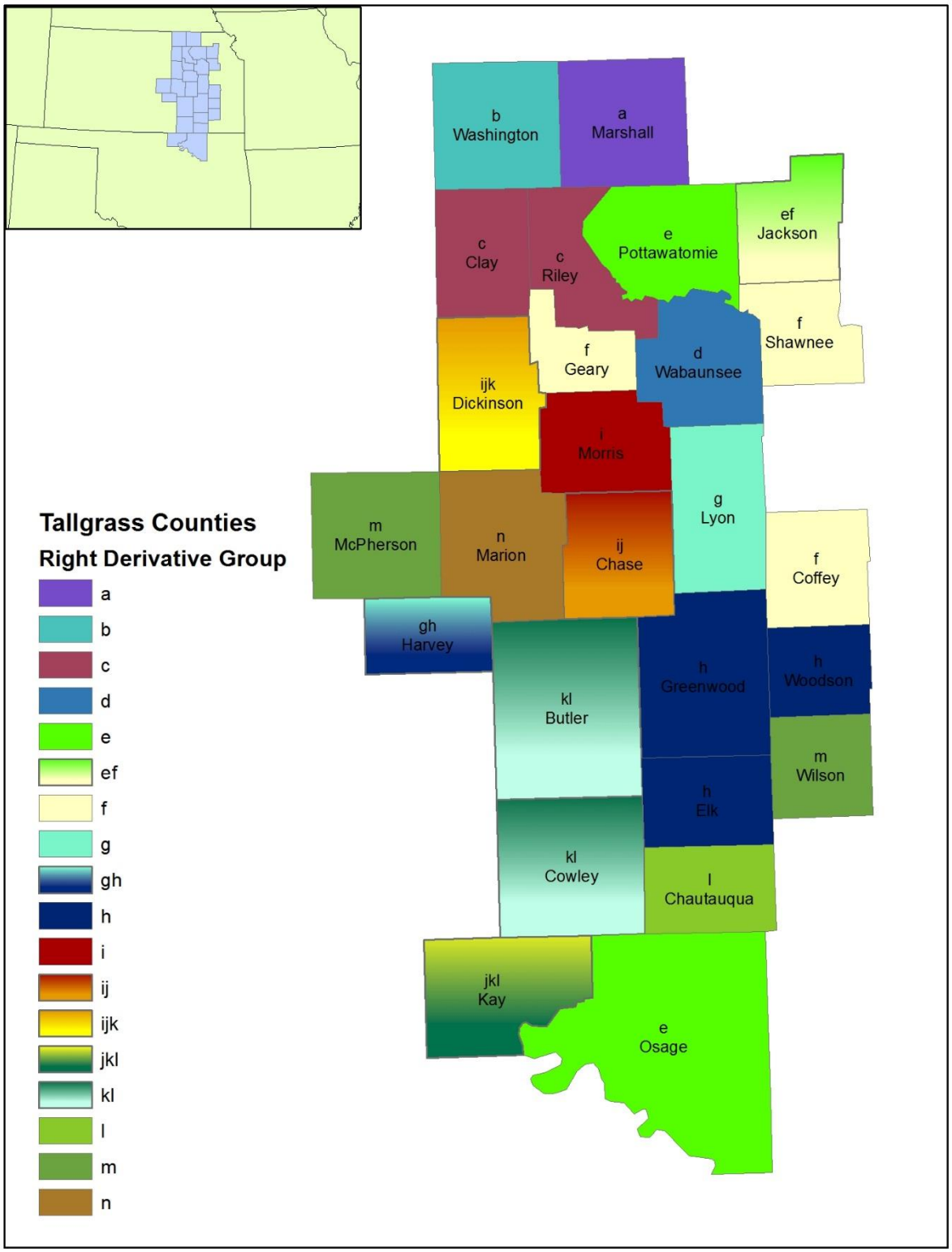

Figure D-42. Map of Tukey HSD test results for the small integral phenometric.

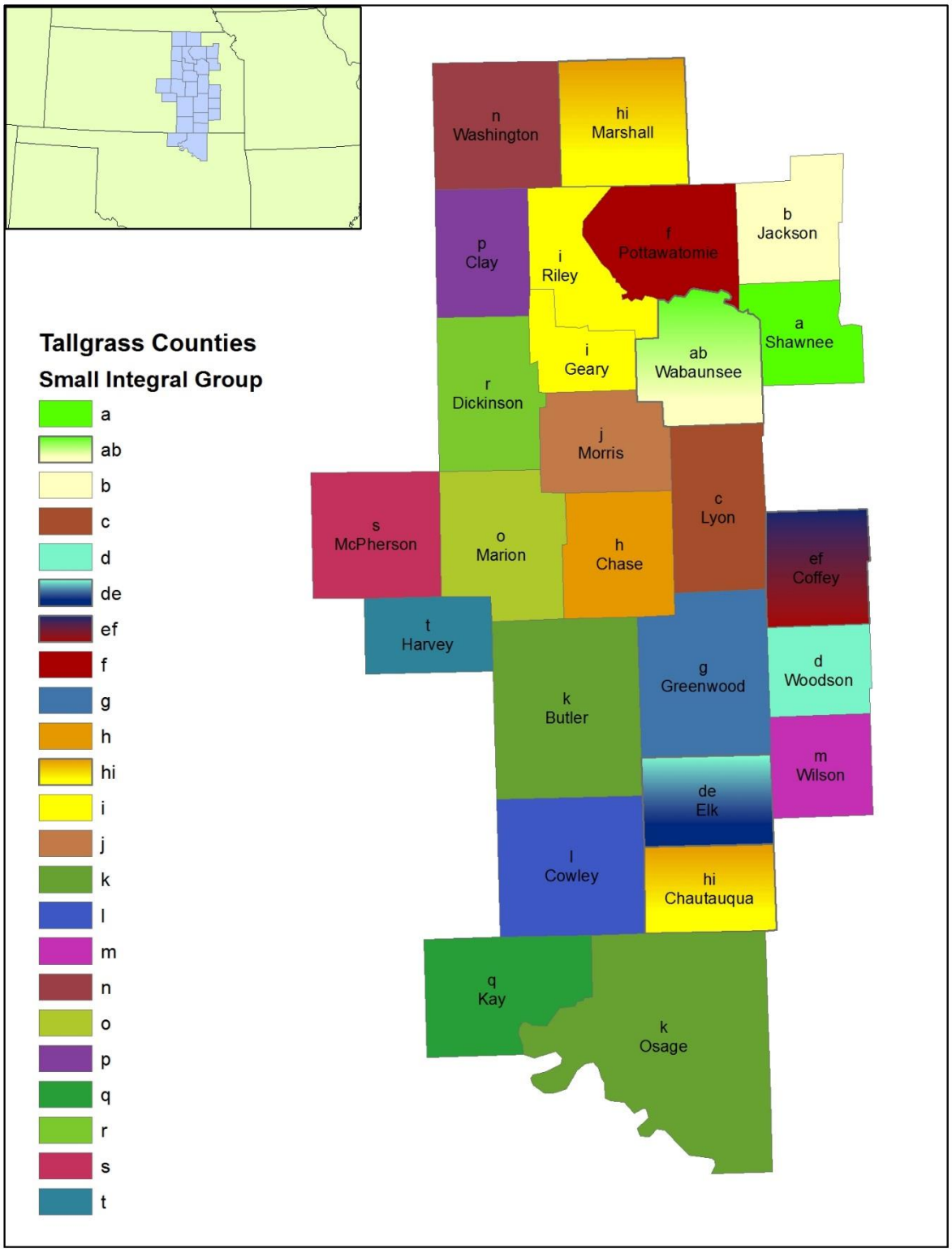

Figure D-43. Map of Tukey HSD test results for the start of season phenometric.